Dissertation

submitted to the
Combined Faculty of Natural Sciences and Mathematics
of the Ruperto Carola University Heidelberg, Germany
for the degree of
Doctor of Natural Sciences

presented by
M.Sc. Sara Haghani
born in Tehran, Iran
Oral examination: 19 of March 2024

Characterization of the regulatory role of cysteine synthase complex in *Arabidopsis thaliana*

Referees:

Prof. Dr. Rüdiger Hell

Prof. Dr. Thomas Rausch

Dedicated to the noble souls who, in 2022, devoted themselves to the cause of freedom for Iran.

Table of Contents

Summary

In plants, the synthesis of cysteine occurs via a two-step process catalyzed by serine acetyltransferase (SERAT) and *O*-acetylserine(thiol)lase (OAS-TL) enzymes. The two enzymes can interact reversibly, thereby forming the cysteine synthase (CS) complex, which is present in the cytosol, mitochondria, and plastids. This research aimed to investigate the cytosolic and mitochondrial CS complexes in *Arabidopsis thaliana* to determine whether there are any compartment-specific differences in their regulation. Moreover, the significance of SERAT in the regulatory function of the CS complex and cysteine synthesis was explored. Therefore, a specific mutation in a conserved serine was implemented, localized in S102 and S210 in cytosolic *At*OAS-TL A and mitochondrial *At*OAS-TL C, respectively. The mutation had been previously studied in rice and represented a stable CS complex, which *O*-acetylserine (OAS) could not dissociate.

Earlier findings have demonstrated that substituting Ser102 with Asn in the OAS-TL A protein results in complete inactivation of the corresponding mutant OAS-TL A^{S102N} protein. The findings of this study also indicated a significant reduction in enzymatic activity of the OAS-TL C^{S210N} compared to the wild-type OAS-TL C. Comparative *in vitro* analysis indicated that the CS complex composed of cytosolic *At*OAS-TL A^{S102N} and either cytosolic *At*SERAT1;1 or mitochondrial *At*SERAT2;2 displayed a notably higher level of resistance to OAS dissociation. Nonetheless, even though the interaction between mitochondrial *At*OAS-TL C^{S210N} and mitochondrial *At*SERAT2;2 seemed inseparable, it was observed that mitochondrial *At*OAS-TL C^{S210N} was unable to establish a non-dissociable complex with cytosolic *At*SERAT1;1. Upon subsequent *in vivo* analysis, it was observed that both *oastla* and wild-type (WT) plants, which were complemented with cytosolic *At*OAS-TL A^{S102N}, exhibited increased levels of OAS, cysteine, and glutathione. This finding confirms the formation of a stable CS complex, which results in constant stimulation of the SERAT within the complex. However, upon complementing the *serat1;1* or *a1;1* mutants with *At*OAS-TL A^{S102N}, no noticeable increase in the levels of OAS or thiols was observed in comparison to the control condition. The findings in the absence of SERAT1;1 confirm that it is indeed the CS complex formation through mutated AtOAS-TL A^{S102N} within the cytosolic environment leads to the observed synthesis of OAS and thiols in the wildtype background. Moreover, upon investigation of the metabo-

lite content in transformants that were complemented with mutated mitochondrial *At*OAS-TL C^{S210N}, it was discovered that both WT (*At*OAS-TL C^{S210N}) and *oastlc* (*At*OAS-TL C^{S210N}) transformants exhibited an increase in OAS steady-state level. Additionally, the cysteine content in the WT (*At*OAS-TL C^{S210N}) and the glutathione content in *oastlc* (*At*OAS-TL C^{S210N}) indicated a notable increase. In conclusion, the findings suggest that the modified version of mitochondrial *At*OAS-TL C^{S210N} is capable of generating a stable CS complex in Arabidopsis, leading to an increase in OAS production as it consistently activates SERAT2;2.

Finally, the effects of cadmium stress on the root growth of the transformants were assessed as an indirect approach to evaluate the levels of flux of OAS and thiols compared to their steady-state levels. Under cadmium treatment, the *oastla* (*At*OAS-TL A) transformants exhibited a comparable root length to that of the control condition. This finding suggests that the transformants resist high concentrations of cadmium, which is attributed to the higher quantity of phytochelatins. Correspondingly, both *serat1;1* (*At*OAS-TL A^{S102N}) and *a1;1* (*At*OAS-TL A^{S102N}) displayed a significant reduction in root length under cadmium treatment, implying the critical role of functional endogenous SERAT to uninterrupted synthesis of OAS and thiols.

Taken together, the findings in this study suggest that the CS complex within the chloroplast of the monocotyledonous rice system demonstrates comparable functionality to various cellular compartments in the dicotyledonous Arabidopsis model. The identified mutation in *At*OAS-TL consistently yields a stabilized CS complex within the cell. Nevertheless, this process is contingent upon an active and functional SERAT.

Zusammenfassung

In Pflanzen erfolgt die Synthese von Cystein über einen zweistufigen Prozess, der durch die Enzyme Serinacetyltransferase (SERAT) und *O*-Acetylserin(thiol)lase (OAS-TL) katalysiert wird. Die beiden Enzyme können reversibel interagieren und bilden so den Cysteinsynthase (CS)-Komplex, der sowohl im Zytosol als auch in den Mitochondrien und Plastiden vorliegt. Ziel dieser Untersuchung war es, die zytosolischen und mitochondrialen CS-Komplexe in *Arabidopsis thaliana* zu analysieren, um mögliche kompartimentspezifische Unterschiede in ihrer Regulation festzustellen. Zudem wurde die Rolle von SERAT für die regulatorische Funktion des CS-Komplexes und der Cysteinsynthese genauer erforscht. Hierzu wurde eine spezifische Mutation an einer konservierten Serinposition implementiert, die sich in S102 und S210 im zytosolischen *At*OAS-TL A bzw. im mitochondrialen *At*OAS-TL C befindet. Diese Mutation wurde zuvor an Reis untersucht und führte zu einem stabilen CS-Komplex, der nicht durch *O*-Acetylserin (OAS) dissoziiert werden konnte.

Frühere Erkenntnisse haben gezeigt, dass die Substitution von Ser102 durch Asn im OAS-TL A-Protein zu einer vollständigen Inaktivierung des entsprechenden mutierten OAS-TL A^{S102N} Proteins führt. Die Ergebnisse dieser Studie zeigten darüber hinaus eine signifikante Reduktion der enzymatischen Aktivität des OAS-TL C^{S210N} Proteins im Vergleich zum Wildtyp-OAS-TL C. Im Vergleich ging aus *in vitro*-Analysen hervor, dass der CS-Komplex aus dem zytosolischen *At*OAS-TL A^{S102N} und entweder dem zytosolischen *At*SERAT1;1 oder dem mitochondrialen *At*SERAT2;2 Protein einen deutlich erhöhten Widerstand gegen die OAS-Dissoziation aufwies. Der mitochondriale CS-Komplex aus *At*OAS-TL C^{S210N} und SERAT2;2 ist ebenfalls resistent gegenüber OAS. Überaschenderweise konnte der Komplex aus zytosolischer SERAT1;1 mit *At*OAS-TL C^{S210N} durch OAS dissoziiert werden. Dies deutet Proteoform-spezifische Unterschiede hinsichtlich der Komplexinteraktion an. In der nachfolgenden *in vivo*-Analyse wurde beobachtet, dass sowohl *oastla*- als auch Wildtyp-(WT)-Pflanzen, die mit zytosolischem *At*OAS-TL A^{S102N} Protein ergänzt wurden, erhöhte Werte von OAS, Cystein und Glutathion aufwiesen. Diese Ergebnisse bestätigen die Bildung eines stabilen CS-Komplexes, der zu einer kontinuierlichen Stimulation von SERAT innerhalb des Komplexes führt. Im Gegensatz dazu wurde bei der Ergänzung von *serat1;1*- oder *a1;1*-Mutanten mit *At*OAS-TL A^{S102N} kein signifikanter Anstieg der

OAS- oder Thiolspiegel im Vergleich zur Kontrollbedingung beobachtet. Die Ergebnisse bestätigen, dass die CS-Komplexbildung durch die *At*OAS-TL A^{S102N} Mutation im Zytosol tatsächlich für die beobachtete Synthese von OAS und Thiolen verantwortlich ist. Des Weiteren wurde bei der Analyse der Metabolitengehalte in Transformanten festgestellt, die mit dem mutierten mitochondrialen *At*OAS-TL C^{S210N} ergänzt wurden, dass sowohl WT (*At*OAS-TL C^{S210N}) als auch *oastlc* (*At*OAS-TL C^{S210N})-Transformanten einen Anstieg des OAS-Steady-State-Spiegels aufwiesen. Darüber hinaus wiesen der Cysteingehalt im WT (*At*OAS-TL C^{S210N}) und der Glutathiongehalt in *oastlc* (*At*OAS-TL C^{S210N}) auf einen deutlichen Anstieg hin. Zusammenfassend lässt sich aufgrund der vorliegenden Ergebnisse ableiten, dass die modifizierte Version des mitochondrialen *At*OAS-TL C^{S210N} die Fähigkeit aufweist einen stabilen CS-Komplex in Arabidopsis zu bewirken. Dies führt zu einer erhöhten Produktion von OAS, da SERAT2;2 kontinuierlich aktiviert ist. Abschließend wurden die Auswirkungen von Cadmiumstress auf das Wurzelwachstum der Transformanden als indirekter Ansatz zur Beurteilung des Flussniveaus von OAS und Thiolen im Vergleich zu ihren Steady-State-Niveaus bewertet. Unter Cadmiumbehandlung zeigten die *oastla* (*At*OAS-TL A)-Transformanden eine vergleichbare Wurzellänge wie unter Kontrollbedingungen, während die erhöhten Cd Konzentration das Wurzelwachstum des Wildtyps behinderten.

Dieses Ergebnis deutet darauf hin, dass die transformierten *oastla* (*At*OAS-TL A) Pflanzen hohe Cadmiumkonzentrationen erfolgreich bewältigen können, was auf die erhöhte Produktion von Phytochelatinen zurückzuführen ist. Im Gegensatz dazu zeigten sowohl *serat1;1* (*At*OAS-TL A^{S102N}) als auch *a1;1* (*At*OAS-TL A^{S102N}) unter Cadmiumbehandlung eine signifikante Reduktion der Wurzellänge, was auf die entscheidende Rolle von funktionellem endogenem SERAT für die kontinuierliche Synthese von OAS und Thiolen hindeutet.

Zusammenfassend ergibt sich aus den Ergebnissen dieser Studie, dass der chloroplastidäre CS-Komplex in der Monokotyle Reis, eine vergleichbare Funktionalität aufweist wie der CS-Komplex in verschiedenen Zellkompartimenten der Dikotyle Arabidopsis. Die identifizierte Mutation in *At*OAS-TL führt konsequent zu einem stabilisierten CS-Komplex innerhalb der Zelle. Dennoch ist dieser Prozess von einem aktiven und funktionsfähigen SERAT abhängig. Die erfolgreiche Übertragung auf die Modellpflanze Arabidopsis eröffnet nun die Möglichkeit der gezielten Optimierung von Cystein- und Glutathion-abhängigen Stressresistenz-Mechanismen.

1 Introduction

1.1 Sulfur assimilation and cysteine biosynthesis

1.1.1 The importance of sulfur in plant nutrition

In nature, sulfur can be found in both organic and inorganic forms. Plants and microorganisms reduce sulfate, the most oxidized form of the sulfur present as a divalent anion in aqueous solution, to sulfide and incorporate it into a wide variety of organic metabolites (Norici et al. 2005; Leustek et al. 2000; Saito 2004). The presence of sulfur in major cellular components and diversified biological activities of the sulfur-containing metabolite indicates its importance (Crawford 2000; Leustek et al. 2000; Saito 2000; Saito 2004). Moreover, sulfur is present in the functional moieties of sulfur-containing amino acids, i.e., cysteine and methionine. Notably, the disulfide bonds formed through the thiol residue of cysteine are essential for the structure of proteins. Reduced sulfur is also involved in redox control in thiols of proteins and peptides (Foyer et al. 2009) and is likewise present in vitamins and cofactors such as biotin, thiamine, and coenzyme A (Mildvan et al. 1966; Bowen et al. 1968; Sigel et al. 1969).

1.1.2 Sulfur uptake and reduction in higher plants

Sulfate is absorbed into the roots by sulfate transporters (SULTR). Multiple isoforms of sulfate transporters are present in the higher plants with different localization and affinities. For example, in *Arabidopsis thaliana*, there are 14 members of sulfate transporter categorized into four distinct groups, including functional and putative isoforms (Takahashi 2010). *At*SULTR1;1 and *At*SULTR1;2 constitute the high-affinity sulfate root membrane transporter. *At*SULTR1;2 is the major sulfate uptake contributor expressed in the root epidermal and cortical plasma membranes, and the root apex (Shibagaki et al. 2002; Yoshimoto et al. 2002). The

*At*SULTR1;1 transporter is much less expressed as compared to *At*SULTR1;2 (Rouached et al. 2008); however, the transcript accumulation of both genes and in particular of *At*SULTR1;2 is stimulated under sulfur limitation (El Kassis et al. 2007; Yoshimoto et al. 2002).

Moreover, SULTR1;1 has a lower K_m value and is more intensely stimulated by sulfur deprivation compared to SULTR1;2, proposing SULTR1;1 as a more specialized component for the uptake of trace sulfate (Takahashi et al. 2000; Yoshimoto et al. 2002). The high-affinity SULTR1;3 transporter also contributes to sulfur translocation of sulfate from source to sink organs (Yoshimoto et al. 2003). SULTR2;1 and SULTR2;2, low-affinity sulfate transporters, promote sulfate translocation from roots to shoots (Kataoka et al. 2004a; Takahashi et al. 2000). SULTR1;1 has been identified as the regulator of sulfate transfer to developing seeds (Awazuhara et al. 2005). The sulfate transporter members of group three in Arabidopsis are the least characterized, and their activity to transfer sulfate still needs to be verified. SULTR3;5, which is not functioning as a sulfate transporter itself, has been reported to co-facilitate the sulfate influx through SULTR2:1 (Kataoka et al. 2004a). However, Chen et al. 2019 showed that all five members of the SULTR3 family localize to the chloroplast envelope and function in sulfate import into the organelle. SULTR4;1 and SULTR4;2, the tonoplast-localized sulfate transporters release sulfate from vacuoles and their transcription increases under the sulfur limitation (Kataoka et al. 2004b).

Sulfate requires to be reduced to enter the assimilation pathway. Sulfate reduction occurs in the plastids of all photosynthetic except *Euglena gracilis*, in which the sulfate-reducing enzymes locate in mitochondria (Brunold et al. 1976; Patron et al. 2008). Sulfate is activated before reduction by ATP sulfurylase (ATPS) (EC: 2.7.7.4) to create adenosine 5'-phosphosulfate (APS). The APS is further reduced by APS reductase (APR) (EC: 1.8.99.2) to sulfite following the reduction to sulfide, catalyzed by sulfite reductase (SiR) (EC: 1.8.7.9) (Lunn et al. 1990; Koprivova et al. 2001). The produced sulfide is an immediate substrate for cysteine biosynthesis (Figure. 1.1).

1.1.3 Assimilation of reduced sulfide into cysteine

The final step of sulfur assimilation in plants is the synthesis of cysteine, an almost exclusive entry of reduced inorganic sulfur into organic compounds. In contrast, most fungi and animals use methionine as the source of reduced sulfur (Takahashi et al. 2011). Moreover,

although animals are not able to fix sulfide in the form of cysteine, they gain sulfide as a by-product of cysteine catabolism (Gadalla et al. 2010).

Cysteine synthesis is achieved by integrating sulfide into the carbon skeleton *O*-acetylserine (OAS), and it is accomplished by two sequential steps, which are conserved in plants, archaea, and eubacteria (Hell et al. 2008). First, the acetyl moiety of acetyl coenzyme A is transferred to amino acid serine, catalyzed by serine acetyltransferase (SERAT; SAT) (EC:2.3.1.30), leading to the activation of serine and production of *O*-acetylserine (OAS). In the next step, *O*-acetylserine (thiol) lyase (OAS-TL) (EC:2.5.1.47) exchanges the acetyl moiety of OAS by sulfide in a β-replacement reaction to form cysteine (Wirtz et al. 2006). Both SERAT and OAS-TL have been found in the cytosol, plastid, and mitochondria of various plants, suggesting the requirement of the three cellular compartments that carry out protein biosynthesis to the incorporation of sulfide into cysteine (Lunn et al. 1990; Rolland et al. 1992; Ruffet et al. 1994) (Figure. 1.1).

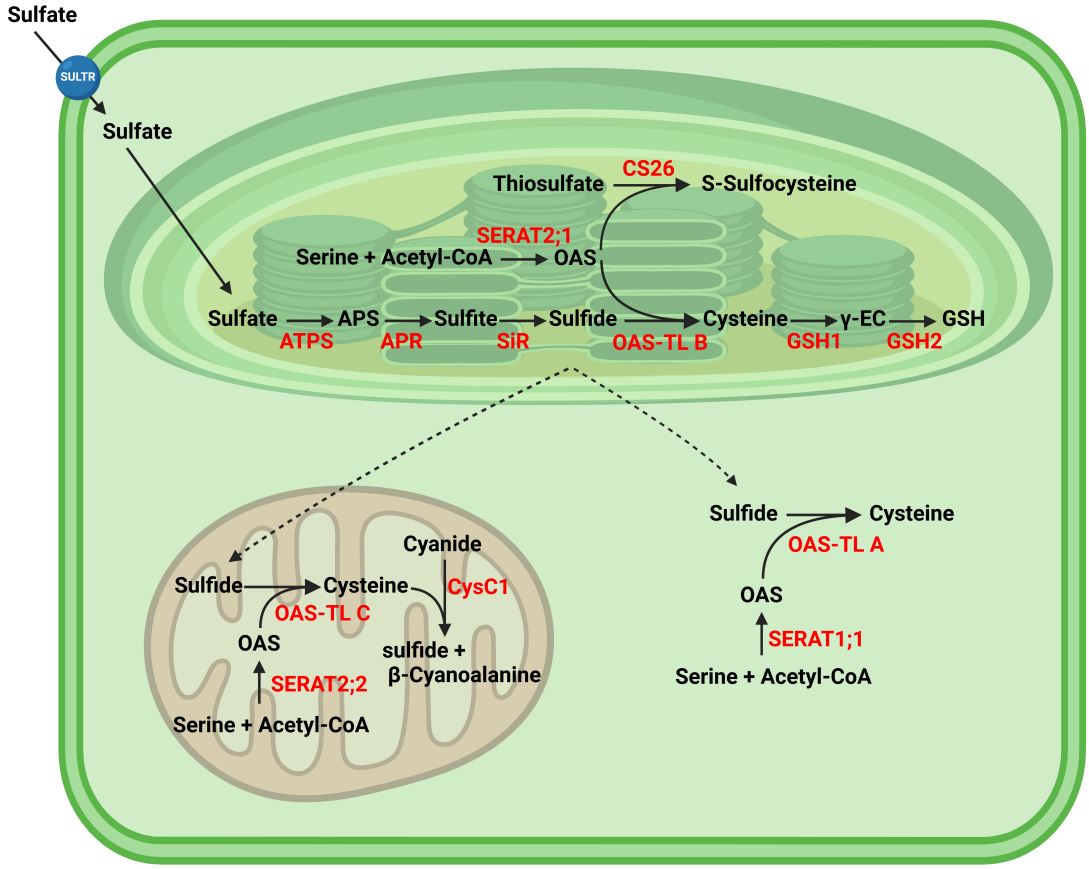

Figure 1.1: **Schematic overview of sulfate assimilation pathway and compartmentation of cysteine synthesis in *Arabidopsis thaliana*.** Explanations regarding the individual reactions of sulfate uptake and reduction and the subsequent fixation of reduced sulfide into the amino acid cysteine and glutathione biosynthesis in different cellular compartments are provided in the text. Enzymes are indicated in red characters. Dashed lines indicate putative pathways for metabolite transport. APR: APS reductase; APS: adenosine-5'-phosposulfate; ATPS: ATP sulfurylase; CS26: cysteine synthase 26; CysC1: cysteine synthase C1; GSH: reduced glutathione; GSH1: γ-glutamylcysteine ligase; GSH2: glutathione synthetase; OAS: *O*-acetylserine; OAS-TL: *O*-acetylserine(thiol)lyase; SERAT: serine acetyltransferase; SiR: sulfite reductase; SULTR: sulfate transporter; γ-EC: γ-glutamylcysteine.

1.2 The cysteine synthase (CS) complex

The CS complex consists of one SERAT hexamer and two OAS-TL dimers and was first discovered in *S. typhimurium* (Kredich et al. 1966; Kredich et al. 1969). In bacteria and plants, SERAT and OAS-TL are connected via a hetero-oligomeric CS complex (Hell et al. 2008; Kredich 2008; Saito 2004; Wirtz et al. 2006). According to evidence from analyses of bacterial and Arabidopsis SERATs and OAS-TLs, free homohexameric SERAT is a dimer consisting of two trimers (Pye et al. 2004) that probably serves as the complex's core with two OAS-TL dimers bound at the hexamer's opposing ends (Feldman-Salit et al. 2009; Wirtz et al. 2010). SERAT interacts with OAS-TL via its highly flexible C-terminus and binds to the catalytic grove of OAS-TL (Bogdanova et al. 1997; Jost et al. 2000). Interestingly mitochondrial SERAT2;2 can form a CS complex with OAS-TL proteins even after losing the activity by mutation of a histidine residue in the catalytic center (Wirtz et al. 2001).

Although OAS-TL is inactive in the cysteine synthase complex, the excess of free and active OAS-TL in the surrounding convert produced OAS to cysteine (Cook et al. 1978; Droux et al. 1998). However, high concentrations of OAS that compete for binding with the C-terminus of SERAT can cause the block of enzymatic activity to be removed (Francois et al. 2006; Huang et al. 2005). Although OAS dissociates the CS complex, it was revealed that sulfide stabilizes the complex (Wirtz et al. 2006).

Despite abundant free and active OAS-TL homodimers, all SERAT activity in protein extracts has been discovered in conjunction with OAS-TL. The activity of SERAT is about 10 nmol mg^{-1} min^{-1} whereas OAS-TL represents about 600 nmol mg^{-1} min^{-1} activity; therefore, SERAT activity is assumed the rate-limiting for cysteine biosynthesis (Heeg et al. 2008). For the optimal production of cysteine, a molar excess of OAS-TL to SERAT is required (Droux 2003; Wirtz et al. 2006; Hell et al. 2008).

1.2.1 The serine acetyltransferase (SERAT) gene family in Arabidopsis

SERAT and OAS-TL are ubiquitously expressed in plant cells, and almost all plant species can produce cysteine in their cytosol, plastids, and mitochondria (Hell et al. 2008). In Arabidopsis, the SERAT protein family possesses five members. The encoding gene of each protein is located on one of the five chromosomes; therefore, each SERAT protein was initially

named after the chromosome number by which it is encoded. SERAT2;1 (SAT1, AT1G55920) and SERAT2;2 (SAT3, AT3G13110) are targeted to the plastid and mitochondrial, respectively, whereas SERAT3;1 (SAT2, AT2G17640), SERAT3;2 (SAT4, AT4G35640), and SERAT1;1 (SAT5, AT5G56760) are localized to the cytosol (Kawashima et al. 2005; Wirtz et al. 2006).

The three major isoforms are SERAT2;1, SERAT2;2, and SERAT1;1, which have a K_M for serine between 1-3 mM (Davidian et al. 2010). Moreover, when disregarding the organellar transit peptides, they represent the most similarities in sequence (Hell et al. 2011; Kawashima et al. 2005). In comparison, SERAT3;1 and SERAT3;2 exhibit low affinities to serine and acetyl coenzyme A and show lower amino acids sequence similarities compared to the other isoforms and thus are assumed to not contribute considerably to OAS synthesis (Noji et al. 1998; Kawashima et al. 2005; Watanabe et al. 2008b). Moreover, the latter isoforms represented 10-100 times less transcript levels than the other three isoforms (Kawashima et al. 2005; Wirtz et al. 2006). It has been revealed that although SERAT3;1 and SERAT3;2 have enzymatic activity, they are unable to interact with cytosolic OAS-TL to form the CS complex due to their long C-terminal extensions (Kawashima et al. 2005; Watanabe et al. 2008b; Birke et al. 2012). Nonetheless, the knockout mutants lacking either SERAT3;1 or SERAT3;2 showed strong growth retardation suggesting the involvement of these two isoforms in other or additional metabolic functions (Watanabe et al. 2008b).

The activity of SERAT is differently distributed to the three compartments. It has been revealed that around 80-90% of the total SERAT activity is located in mitochondria, whereas cytosol and plastid are each responsible for 5-10% (Ruffet et al. 1995; Droux 2003). This determination was reinforced when the complete loss of function of mitochondrial SERAT2;2 due to an insertional mutation led to a 70-80% decline in total SERAT activity (Watanabe et al. 2008b), and slight growth retardation (Watanabe et al. 2008b; Haas et al. 2008). Additionally, down-regulation of SERAT2;2 due to a gene-specific artificial miRNA resulted in stunted growth, reduction of the transcription level of the target gene, and a strong decrease in the flux of ^{35}S-sulfate into cysteine (Haas et al. 2008). SERAT activity is inhibited by allosteric feedback of cysteine. However, this inhibitory effect which is a crucial way to regulate the activity of SERAT depends on its subcellular localization. In Arabidopsis, plastidic SERAT2;1 and cytosolic SERAT3;1 showed no feedback inhibition effect by cysteine. However, cytosolic SERAT3;2 and SERAT1;1 showed a 50% Inhibition Constant (IC_{50}) at 0.8 µM and 1.8 µM cys-

teine, respectively. The highest cysteine concentration (IC_{50}= 53 μM) for having an inhibition effect was demonstrated for free mitochondrial SERAT2;2 (Noji et al. 1998; Kawashima et al. 2005; Wirtz et al. 2006).

Different approaches were employed to augment cysteine and glutathione production to enhance stress tolerance by increasing SERAT activity or implementing feedback-insensitive SERAT. An earlier study has demonstrated that constitutive overexpression of active *E. coli* SERAT (CYS E) in tobacco and potato can significantly boost the cysteine and glutathione (GSH) steady-state levels in leaves by 2-3 times (Blaszczyk et al. 1999; Harms et al. 2000). Likewise, tobacco plants were transformed with the mutated *E. coli cysE** encoding insensitive SERAT to feedback inhibition by cysteine (Denk et al. 1987), indicating a comparable increase in cysteine and GSH levels in both cytosol and mitochondria, although they showed several-fold higher SERAT activity than the control plant. Nonetheless, these transgenic plants exhibited a remarkable increase in their resistance to oxidative stress caused by hydrogen peroxide (Clarkson et al. 1993). In pursuit of enhancing cysteine production in both bacterial and plant systems, Wirtz and Hell 2003 showed that the expression of an insensitive *SERAT* gene from *Nicotiana tabacum* (*SAT4*) in an *E. coli* host strain lacking endogenous SERAT activity led to a significant accumulation of cysteine. Similarly, transgenic tobacco plants expressing an insensitive SERAT2;2 from *A. thaliana* (Noji et al. 1998; Wirtz et al. 2001) exhibited increased levels of cysteine by up to 3- and 6-fold in cytosol and plastids, respectively, and GSH levels up to 3-fold (Wirtz et al. 2003), suggesting the effectiveness of this approach to enhance cysteine levels in transgenic tobacco plants. SERAT2;2 was the preferred isoform due to its low sensitivity to feedback inhibition by cysteine, suggesting that it is not affected by cellular cysteine concentrations (Wirtz et al. 2003). To elucidate the regulatory role of the cysteine synthase complex in plants, a mutagenized inactive SERAT2;2 from *Arabidopsis thaliana* under the control of the cauliflower mosaic virus 35S promoter could bind to OAS-TL within the cytosol of transgenic tobacco plants, leading to an elevation in cysteine (up to 30-fold), glutathione (2.3-fold), and total sulfur (36%) levels (Wirtz et al. 2007). Interestingly, a recent study across the three subcellular compartments in *Brassica napus* revealed that the constitutive overexpression of the feedback-insensitive SERAT isoform from tobacco (*Nt*SAT4) using different transit peptides under the control of the 35S promoter resulted in a concurrent 2.5 to 3.5-fold increase in free cysteine levels and a 2.2 to 5.3-fold increase in GSH levels in leaves compared to nontransformed plants. Addition-

ally, the overexpression of *Nt*SAT4 provided plants with improved tolerance against oxidative stress from hydrogen peroxide and the heavy metal cadmium (Rajab et al. 2020).

1.2.2 The *O*-acetylserine(thoil)lyase (OAS-TL) gene family in Arabidopsis

OAS-TL belongs to the superfamily of pyridoxal phosphate-dependent enzymes and is responsible for the β-substitution of the acetyl group of OAS by sulfide (Hatzfeld et al. 2000; Watanabe et al. 2008a). In Arabidopsis, there are, in total, nine *Oastl*-like genes encoding for the proteins OAS-TL A1 (AT4G14880), OAS-TL A2 (AT3G22460), CysD1 (AT3G04940), CysD2 (AT5G28020), CS-like (AT5G28030) localized in the cytosol, OAS-TL B (AT2G43750) and CS26 (AT3G03630) localized in the plastid, and OAS-TL C (AT3G59760) and CysC1 (AT3G61440) localized in mitochondria (Hell et al. 2002; Heeg et al. 2008; Watanabe et al. 2008a; Alvarez et al. 2010; Bermúdez et al. 2010). OAS-TL A2, however, is a pseudogene that is expressed but encodes for a truncated and non-functional protein (Jost et al. 2000); therefore, OAS-TL A refers to OAS-TL A1 in this thesis.

There is a correlation between the gene transcription pattern of OASTLs reported in Genevestigator, and the protein intensities observed in the 2-dimensional gels (Zimmermann et al. 2004). OAS-TL A, OAS-TL B, and OAS-TL C are the three most highly expressed genes encoding the major isoenzymes in the cytosol, plastids, and mitochondria, respectively. After analyzing the amino acid sequences of these three *A. thaliana* OAS-TLs, it was found that they have a significantly high level of identity (Bonner et al. 2005). Specifically, OAS-TL A and OAS-TL B exhibit a shared identity of 71.12%, OAS-TL A and OAS-TL C share a 70.19% identity, and OAS-TL B and OAS-TL C demonstrate a 79.74% identity (Supplementary Fig. S49). Previous research has demonstrated that the crystal structures of cytosolic OAS-TL A (Bonner et al. 2005), mitochondrial OAS-TL C (Feldman-Salit et al. 2012), and OAS-TL B (Wang 2018) are quite similar. However, upon further analysis, it has been determined that a significant difference exists between plastidic OAS-TL B and the other two variants. Specifically, the last α-helices found at the C-terminus of both plastidic OAS-TL B monomers were observed to be uniquely oriented outward from the protein body. Conversely, the last α-helices of cytosolic OAS-TL A and mitochondrial OAS-TL C remained in close proximity to the protein bodies (Wang 2018).

The low abundant CysD1 and CysD2 proteins, together with OAS-TL A, OAS-TL B, and OAS-

TL C, are enzymatically true OAS-TLs that are assumed to associate with SERAT in the CS complex (Yamaguchi et al. 2000; Wirtz et al. 2004; Heeg et al. 2008). The analyses of several T-DNA knock-out lines showed that OAS-TL A, OAS-TL B, and OAS-TL C contribute 55%, 45%, and 5% of the total activity in leaves, respectively (Heeg et al. 2008; Watanabe et al. 2008a). CysC1, however, has been demonstrated to express strongly and catalyze the formation of β-cyanoalanine from the cysteine and cyanide substrates in mitochondria rather than catalyzing cysteine synthase in vivo (Hatzfeld et al. 2000; Jost et al. 2000; Yamaguchi et al. 2000). Among CysD1 and CysD2 showing weak expression levels (Yamaguchi et al. 2000), only CysD2 displayed low OAS-TL activity (Rabeh et al. 2004). Nonetheless, purification of both CysD1 and CysD2 by SERAT affinity chromatography indicated the ability of these proteins to form a CS complex (Heeg et al. 2008). CysD2 has an exchange of a conserved serine at position 88, which is part of the catalytic center (Rabeh et al. 2004). Mutation of serine 88 in OAS-TL A resulted in the elimination of catalytic activity (Bonner et al. 2005), excluding the contribution of CysD2 to enzyme synthesis in Arabidopsis. Likewise, the other two members of the OAS-TL-like protein family, cytosolic CS-like and plastid CS26, indicated substitutional serine at position 88. However, after exchanging the serine in the catalytic center, CS-like protein exhibited no OAS-TL activity yet was able to cleave cysteine to form sulfide (Hatzfeld et al. 2000; Alvarez et al. 2010). In contrast to CS-like, CS26 isoform act as a S-sulfocysteine synthase yielding cysteine by utilizing thiosulfate as a donor of reduced sulfur instead of sulfide (Bermúdez et al. 2010).

OAS-TL overproduction upon non-stressed conditions has a comparatively minor impact on the level of non-cellular thiols compared to the overproduction of SERAT. Nonetheless, the same transformants under stress conditions exhibit an increased abundance of thiols and are more stress-tolerant than control plants (Sirko et al. 2004). The overexpression of the bacterial *cysK* gene encoding cysteine synthase in the cytosol and chloroplast of tobacco plants (Liszewska et al. 2001; Liszewska et al. 2003; Liszewska et al. 2005) resulted in an elevated OAS-TL activity and non-protein thiols. In the case of bacterial OAS-TL targeting to plastids, the occurrence of bleaching color in older leaves and, in some cases, the entire plant suggests a potentially harmful effect associated with increased OAS-TL activity on chlorophyll contents and/or plant metabolism. On the other hand, cytosolic transformants appear to exhibit a slightly greater degree of tolerance to cadmium when compared to control plants (Liszewska et al. 2005).

Several independent research groups have successfully obtained and analyzed transgenic tobacco lines that produce various isoforms of plant OAS-TL. The transformation of tobacco plants by *Cys1* cDNA obtained from wheat (*Triticum aestivum*) that encodes for OAS-TL (Youssefian et al. 1993) indicated a significant increase in OAS-TL activity, slight elevation of thiol levels and increasing the resistance of the transgenic plants to H_2S and SO_2 fumigation and oxidative damage caused by methyl viologen (Youssefian et al. 2001). Likewise, the tobacco plants were transformed with cytosolic OAS-TL A from spinach (*Spinacia oleracea*) targeted in the cytosol or chloroplast (Saito et al. 1994), revealing increased OAS-TL activity and slight elevation of cysteine and glutathione. Nonetheless, the formation of cysteine was significantly enhanced in chloroplastic transformants upon feeding with OAS and sulfite, resulting in more tolerance against sulfite toxicity. Interestingly, the double-transgenic tobacco plants overproducing spinach OAS-TL in both chloroplast and cytosol showed similar content of cysteine and glutathione. However, they were more resistant to SO_2 and methyl viologen than the single transformants (Noji et al. 2002). Similarly, the transgenic tobacco plants that were transformed with the cytosolic cysteine synthase gene (*RCS1*) from rice (*Oryza sativa*) demonstrated more cadmium tolerance than the control plants, probably due to detoxifying of cadmium by the higher concentration of sulfur-containing compounds (Harada et al. 2001). The increase of cysteine and more tolerance to cadmium due to the overproducing OAS-TL was also demonstrated in transgenic Arabidopsis plants. Their finding suggest that a high rate of cysteine biosynthesis is necessary for the plant detoxification mechanism under heavy metal stress. This is required for the synthesis of GSH and phytochelatins, which play crucial roles in the detoxification process (Dominguez-Solis et al. 2001).

1.3 Compartmentation of cysteine biosynthesis

In most higher plants, both consecutively acting enzymes, SERAT and OAS-TL, are present in three cellular compartments; cytosol, plastids, and mitochondria (Lunn et al. 1990; Ruffet et al. 1995; Birke et al. 2012). In Arabidopsis, both enzymes contain a protein family with several isoforms; each of the three subcellular compartments, which host their protein biosynthesis, utilize different isoforms of SERAT and OAS-TL, as explained in sections 1.2.1 and 1.2.2. Investigation of SERAT mutants and measurement of the component distribution revealed that

OAS and cysteine are predominantly synthesized in mitochondria and cytosol, respectively (Haas et al. 2008; Watanabe et al. 2008b; Krueger et al. 2009), whereas plastids are the central organelle for sulfate reduction (Clarkson et al. 1993; Leustek et al. 2000).

The extensive analysis of mutants lacking OAS-TL or SERAT in different subcellular compartments and some of their combinations implied that sulfide, OAS, and cysteine might cross organellar membranes. For example, plastids and potentially mitochondria are able to supply the required cysteine for the cytosol since mutants lacking cytosolic OAS-TL A remained fully viable (Heeg et al. 2008; López-Martín et al. 2008; Watanabe et al. 2008a). The *oastlAB* double mutant, depending exclusively on mitochondrial OAS-TL C for cysteine synthesis, also showed only 25% growth retardation and a high amount of OAS, cysteine, and glutathione. This result suggested that OAS-TL C, with the lowest activity among the three isoforms, can partially compensate for the total cysteine requirement in the cell and reinforce the cysteine's ability to leave the mitochondria and enter cytosol and plastids. Additionally, it proposed a more increased flow of sulfide from chloroplasts to mitochondria compared to wild-type plants. The accumulation of sulfide concentration in the mitochondria resulted in a higher activity of SERAT and OAS production (Heeg et al. 2008). Consistently, the viability of mutants deficient in plastid OAS-TL B indicated that sulfide could leave the plastid and enter the cytosol and, indeed, mitochondria, as revealed in the mutant lacking both cytosolic OAS-TL A and plastid OAS-TL B. Correspondingly, analysis of mutants lacking either one SERAT isoform or a combination of SERATs demonstrated that OAS could transport into or out of the organelles (Watanabe et al. 2008b; Krueger et al. 2009).

1.4 Regulatory role of cysteine synthase complex

1.4.1 Regulation of sulfur homeostasis by the CS complex

CS complex acts as a sensor to maintain sulfur homeostasis in plants (Kredich 2008). This concept is based on the reversible protein-protein interaction between SERAT and OASTL. A sufficient sulfide supply stabilizes the CS complex leading to a higher activity of SERAT and OAS production (Heeg et al. 2008). Since OAS-TL is inactive in the CS complex, the OAS is released into the surrounding solution (Droux et al. 1998; Berkowitz et al. 2002) and is used by free OAS-TL for cysteine synthesis. Besides the role of OAS in metabolic functions, i.e.,

cysteine synthesis, it also serves regulatory functions, such as the dissociation effect of CS complex and induction of sulfur metabolism genes. It was reported that in *E. coli*, OAS could induce the responsible genes encoding enzymes of the sulfate-to-sulfide reduction pathway, whereas cysteine and sulfide suppress the expression of these genes (Jones-Mortimer et al. 1968). Moreover, Kredich demonstrated in 1969 that 1 mM of OAS was sufficient to dissociate the CS complex to SERAT and OAS-TL *in vitro*, proposing the ability of OAS to induce the sulfate reduction pathway *in vivo* may be due to its effect on the dissociation of CS complex (Kredich et al. 1969).

During sulfur deprivation in plants, accumulated OAS provokes dissociation of the CS complex and induces the sulfur-deficiency related genes. For example, an ambient concentration of 50-70 µM OAS concentration is sufficient to induce the dissociation of 50% of the CS complex. The concentration above this range provokes complete dissociation of the CS complex, whereas a lower concentration fails to dissociate the complex (Berkowitz et al. 2002). On the other hand, the dissociation of the CS complex results in free and less active SERAT and stops the OAS production. After restoring the sulfide supply, the CS complex is re-associated, and SERAT activity resumes (Hell et al. 2001; Wirtz et al. 2006). OAS-feeding experiments on the other hand consistently revealed the sulfate transporter mRNA's accumulation and raised the sulfate absorption rate in barley roots (Smith et al. 1997).

1.4.2 Regulation of cysteine biosynthesis by the CS complex

The CS complex regulates the rate of cysteine synthesis based on the concentrations of OAS and sulfide. Besides, it has a regulatory function on SERAT enzymatic activity. Indeed, a common feature in controlling the SERAT activity and the flux of reduced sulfur into cysteine is the modification of feedback sensitivity of SERAT induced by cysteine (Hell et al. 2011). Kredich and Tomkins (1966) demonstrated that in bacteria, a very low concentration of L-cysteine has a feedback inhibitory effect on serine transacetylase (UniProt: P29847), although its synthesis is not subjected (Kredich et al. 1966). In bacteria, SERAT regulates cysteine biosynthesis via feedback control. Additionally, the SERAT-produced OAS, which serves as substrates for cysteine synthesis, gives rise to the spontaneously formed derivative N-acetylserine that functions as the inducer of the bacterial cysteine regulon (Kredich 1996). However, such a function has not been observed in plants.

The feedback sensitivity of SERAT to cysteine decreases inside the complex (Kumaran et al. 2009; Wirtz et al. 2010). Furthermore, under cysteine limitation, the restriction of SERAT activity caused by the feedback inhibitory action of cysteine is lowered. Raising the SERAT activity further results in OAS production required for cysteine biosynthesis and possibly, in a so far unknown mechanism, for the induction of the gene expression of genes of cysteine biosynthesis enzymes (Noji et al. 1998). SERAT isoforms localized in different cellular compartments display various levels of sensitivity to cysteine concentration. For instance, the cytosolic SERAT1;1 depicts high sensitivity to the feedback inhibitory effect of cysteine. In contrast, organellar SERAT2;1 and SERAT2;2 possess low or no sensitivity suggesting the cytosol as the major regulatory site, at least in Arabidopsis (Noji et al. 1998).

1.5 Glutathione and its role in plants

GSH is the principal low-molecular-weight thiol functioning in plants' primary and secondary metabolism, defense and detoxification, and redox signaling (Noctor et al. 2012). It is also central to animal defense metabolism since selenium-dependent glutathione peroxidase (GPX) is a central pillar of animal antioxidant metabolism (Meister 1994). In plants, like animals, GSH is synthesized in two ATP-dependent steps. First, dipeptide γ-glutamyl cysteine (γ-GC) is produced from L-glutamate and L-cysteine catalyzed by γ-glutamylcysteine synthetase (EC 6.3.2.2), also called glutamate cysteine ligase (GCL; GSH1, AT4G23100). Then, glycine is added to the C-terminal site of the γ-glutamylcysteine to produce glutathione catalyzed by glutathione synthetase (EC 6.3.2.3) (Rennenberg 1980; Meister et al. 1983; Meister 1988; Noctor et al. 2002; Mullineaux et al. 2005). The activity of GSH1 is typically regulated by feedback inhibition from glutathione to regulate the accumulation of GSH within physiological limits, indicating the rate-limiting role of GSH1 in GSH biosynthesis. This mechanism prevents the excessive accumulation of GSH, which holds significant physiological importance (Richman et al. 1975). Although GSH1 is exclusively localized in plastids, the second enzyme, glutathione synthetase (GS; GSH2, AT5G27380), is concluded to be mainly in the cytosol, based on the abundance of mRNA splice variants, and in the plastid (Wachter et al. 2005). In Arabidopsis, the knockout of the synthetic enzymes renders a lethal phenotype (Pasternak et al. 2008). Although extensive research has been conducted on the physiological functions of GSH in various organisms, including human

and animal tissues, plant cells, and microbial cells (Carmel-Harel et al. 2000; Penninckx et al. 1993; Penninckx 2000; Penninckx 2002), there is a scarcity of reviews that discuss the biotechnological production of this medically significant tripeptide. GSH was first discovered in the ethanol extract of baker's yeast in 1888, and its molecular structure was later established in 1921 (Penninckx et al. 1993). Subsequent research found this molecule present in various living organisms. However, extracting GSH from animal and plant tissues using solvents proved challenging due to limited raw materials and the relatively low amount of GSH within cells. Consequently, the resulting product was expensive and not widely applicable (Li et al. 2004). In 1935, Harington and Mead demonstrated a chemical method for synthesizing glutathione that involved introducing and removing sulfhydryl protective agents on a cysteine residue (Harington et al. 1935). Although commercially available since the 1950s, chemically synthesized GSH consisted of a mixture of D- and L-isomers, with only the L-form being biologically active. In order to use GSH effectively, an optical resolution process was necessary to separate the physiologically active L-form from the inactive D-isomer (Li et al. 2004).

The enzymatic approach is a well-studied method for producing GSH. The process requires several crucial components, including GSH1 and GSH2 enzymes, precursor amino acids such as L-glutamic acid, L-cysteine, and glycine, ATP, essential cofactors like Mg^{2+}, and the maintenance of an appropriate pH level, typically around pH 7.5. Although enzymatic production of GSH offers the advantage of achieving high concentrations of up to 9 g/l, using three precursor amino acids increases production costs (Li et al. 2004). As a result, researchers have extensively studied the fermentative production of glutathione using sugar materials as substrates, which has emerged as the primary commercial method. The most common selection method was to disrupt or release the feedback inhibition of GSH on GSH1 (Li et al. 2004). Mutants have been found to yield a GSH content of 3-5%, while a significantly elevated level of 9.5% was detected in *S. cerevisiae* (Ishii et al. 1989). The genes responsible for encoding GSHI (Murata et al. 1981) and GSHII (Murata et al. 1983), namely *gshA* and *gshB*, respectively, were cloned and sequenced. GSHI desensitized to feedback inhibition of GSH, originated from the *E. coli* B strain, was screened, and the responsible coding gene (*gshA**) was cloned (Murata et al. 1983). The recombinant plasmid containing the *gshA** and *gshB* genes was introduced into *E. coli* RC912, resulting in a concurrent increase in the activities of GSHI and GSHII to 10.0- and 14.5-fold, respectively (Gushima et al. 1983). Despite only

a 1.3-fold increase in intracellular GSH concentration in *E. coli* RC912 cells compared to the wild type, the recombinant *E. coli* cells remain an exceptional system for GSH biosynthesis. These cells produced 5 g/l GSH when exposed to three precursor amino acids and ATP. A similar study was conducted in *S. cerevisiae*, wherein the expression of GSHI and GSHII raised by 1,039-fold and 33-fold, respectively, while the intracellular GSH content observed a 2-fold increase (Ohtake et al. 1988; Ohtake et al. 1989). Further, transgenic approaches have been employed to enhance the glutathione (GSH) content in various plant species. These strategies have predominantly entailed the ectopic expression of either *E. coli* GCL or GS and explicitly targeted the cytosol (Noctor et al. 1996) or the chloroplast (Noctor et al. 1998a; Zhu et al. 1999) compartment. By implementing this approach, the GSH content in plants has increased by two- to sixfold.

Increased GSH production is connected with the up-regulation of the cysteine synthesis pathway (Queval et al. 2009). GSH has a critical role in response to high levels of heavy metals because it is the precursor for phytochelatins ([g-Glu-Cys]nGly), chelating compounds produced in reaction to cadmium and other heavy metals. The metal is sequestered by phytochelatins forming a complex that is subsequently carried into the vacuole (Grill et al. 1987; Grill et al. 1989; Cobbett et al. 2002; Rea et al. 2004). In addition to serving as a precursor in synthesizing phytochelatin, glutathione may also play an antioxidant role in developing heavy metal resistance. Many heavy metals are assumed to cause disturbances in cellular redox homeostasis through various mechanisms, such as the displacement of redox-active metals from bound sites. Increased glutathione production in transgenic lines has been shown to increase heavy metal tolerance (Zhu et al. 1999; Lee et al. 2003). However, such a precise effect was not observed by overexpressing PCS itself (Peterson et al. 2006; Picault et al. 2006). Moreover, protein S-glutathionylation forms a persistent bond between glutathione and a cysteine residue, which can modify the target protein's conformation, stability, or activity (Butt et al. 1991). Correspondingly, arsenite [As(III)] complexation by thiol compounds, such as glutathione (GSH) and phytochelatins (PCS), and subsequent isolation within vacuoles is a critical strategy of As detoxification in plants (Ha et al. 1999; Song et al. 2010; Song et al. 2014; Clemens et al. 2016; Yang et al. 2016). Importantly, synthesis of GSH and PCS challenged by metalloid stress is limited by the cysteine (Cys) availability in plants (Cobbett et al. 1998; Pasternak et al. 2008; Khan et al. 2010). A specific mutation identified in chloroplast-localized OAS-TL in rice elevated the physical interaction of OAS-TL and SERAT

proteins in the CS complex. It inactivated the catalytic activity of OAS-TL by inhibiting OAS binding, forming a non-dissociable CS complex, and permanently stimulating endogenous SERAT. The higher activity of SERAT in the CS complex resulted in more sulfate and selenium uptake and higher production of cysteine, glutathione, and phytochelatins. Consequently, the tolerance to arsenic was promoted, and the arsenic translocation to grains was reduced (Sun et al. 2021).

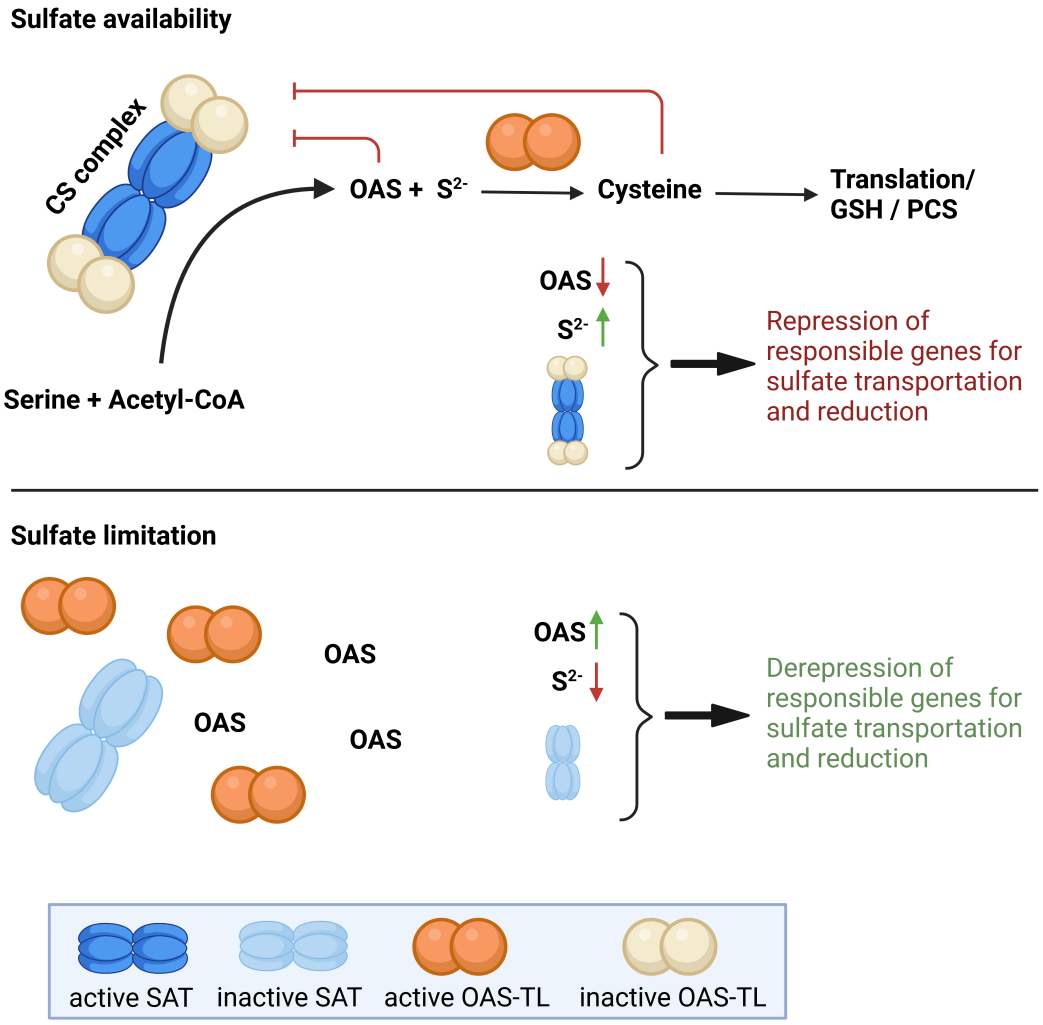

Figure 1.2: **Model for regulation of the cysteine synthase complex in the cytosol.** Serine acetyltransferase (SERAT) transfers the acetyl moiety of acetyl coenzyme A to the amino acid serine leading to O-acetylserine (OAS) production. Under sulfate availability, OAS incorporates reduced sulfide catalyzed by O-acetylserine (thiol) lyase (OAS-TL), leading to cysteine production. Accumulation of OAS and limitation of sulfide due to the sulfate deprivation induce the dissociation of the CS complex. The activity of free SERAT out of the complex diminishes since free SERAT hexamers are sensitive to the inhibitory effect caused by cysteine. Accumulation of OAS and dissociation of the CS complex serve as signals for the derepression of the responsible genes for sulfate transportation and reduction and resupplying of sulfide.

1.6 Aim of the project

Cysteine synthase (CS) complex is hetero-oligomeric consisting of SERAT and OAS-TL, regulating cysteine biosynthesis and sensing the supply of OAS and sulfide precursors. Although it has been known that in *Arabidopsis thaliana*, the CS complex is present in different cellular compartments, the importance of compartmentation still needs to be investigated. *In vitro* studies have shown that ambient concentrations of OAS and H_2S can antagonistically drive the equilibrium of CS complex association and thus determine the activation state of SERAT providing OAS for cysteine and GSH synthesis. However, evidence for this model *in vivo* is scarce.

The primary objective of this study was to examine the CS complex in both the cytosol and mitochondria and to demonstrate whether there are any compartment-specific variations in the regulation of the CS complexes. In a previous study in rice, a specific point mutation in chloroplast localized OAS-TL caused a non-dissociable CS complex. Through my research, I aimed to utilize the same mutation as the biological tool to explore the CS complex across different cellular compartments in Arabidopsis. The objective was to ascertain discrepancies between these compartments and determine whether the CS complex in the chloroplast of the monocotyledonous rice system operates comparably to the different cellular compartments of the dicotyledonous Arabidopsis model. Accordingly, before rebuilding the CS complex with the exact biochemical characterization in Arabidopsis plants, I first analyzed the specific mutation in cytosolic and mitochondrial *At*OAS-TL *in vitro*. Then, I transformed mutant plants lacking the endogenous cytosolic and mitochondrial *At*OAS-TL with the construct containing the target mutation, i.e., as a dominant-negative mutation.

The secondary objective of the investigation was to ascertain the significance of SERAT in the regulatory function of the CS complex. Based on my hypothesis, the constitutive formation of the complex would trigger the activation of SERAT, leading to the production of OAS in a heightened manner within an *in vivo* setting. Therefore, mutated plants lacking the functional endogenous cytosolic SERAT were transformed with the same construct, i.e., the construct containing the target mutation in cytosolic *At*OAS-TL A (35S::*At*OAS-TL A^{S102N}). If the observed mutation in rice leads to a similar outcome in Arabidopsis, specifically, a stable CS complex formation, the absence of this outcome in plants lacking the endogenous SERAT

will support the proposed hypothesis.

Finally, the effectivity of OAS and subsequent cysteine and glutathione formation was tested by challenging plants with sublethal doses of cadmium since plants containing a higher amount of cysteine and glutathione are less sensitive to heavy metals. Therefore, the transgenic plants carrying a confirmed higher concentration of cysteine and glutathione were examined under a growth-inhibiting cadmium concentration.

2 | Materials and methods

2.1 Technical equipment and material

Table 2.1: Technical equipment

Equipment	**Manufacturer**
Autoclave Sanoclav	Sanoklav, Bad Überkingen-Hausen
Camera DSC-RX100 M3	Sony Deutschland, Cologne
Centrifuge 5417R	Eppendorf, Hamburg
Centrifuge Mikro200R	Hettich Zentrifugen, Tuttlingen
Centrifuge Rotanta 460R	Hettich Zentrifugen, Tuttlingen
Centrifuge Sorvall LYNX 6000	Thermo Fisher Scientific, Waltham (USA)
Centrifuge Sorvall RC5C, Rotor SCA-1500	DuPont, Bad Homburg
Confocal microscope A1R	Zeiss, Jena
Confocal microscope: Axiovert 200M LSM510 Meta	Zeiss, Jena
Confocal microscope Leica TCS SP5II	Leica, Wetzlar
DNA Gel Chamber 40-1214	PeqLab, Erlangen
Electrophoresis chamber PerfectBlue Twin ExW	PeqLab, Erlangen
Electrophoresis chamber Mini Preotean III	Bio-Rad, Feldkirchen
Electrophoresis chamber Mini Preotean Tetra	Bio-Rad, Feldkirchen

Continued on next page

Table 2.1 – Technical equipment

Equipment	**Manufacturer**
Electroporator MicroPulser	BioRad, München
ElgaPurelab Classic VWS	Marlow, Bucks (UK)
Gas burner gasprofi 2 accu	WLD-Tec GmbH, Arenshausen
Gel Jet Imager 2000	Intas, Göttingen
Growth chambers	Waiss, Gießen
Heater (80 °C) B6120	Heraeus Instruments, Hanau
Heatblock HBT-2 132	Labor Consult HLC, Bovenden
HLC Block Thermostat HTMR 133 Haep	Labor Consult HLC, Bovenden
Horizontal shaker The Belly Dancer	Stovall, Greensboro, NC (USA)
Ice machine	Ziegra Eis Maschinen, Isernhagen
ImageQuant LAS 4000	GE Healthcare GmbH, Freiburg
Incubators (28 °C / 37 °C)	Heraeus Instruments, Hanau
Laminar flow hood: Lamin Air 2448/HB 2472	Heraeus Instruments, Osterode
Magnetic stirrer MR 3001	Heidolph Instruments, Schwabach
Mastercycler Gradient 5531	Eppendorf, Hamburg
Mastercycler Personal 5332	Eppendorf, Hamburg
Microscope Leica DM IRB	Leica, Bensheim
Multitron incubator	Inforst HT, Switzerland
NanoDrop ND-2000	Peqlab, Erlangen
Orbital Shaker Rotamax 120	Heidolph Instruments, Schwabach
PCR cycler Biometra T-Gradient	Analytik Jena, Jena
PCR cycler Mastercycler Gradient 5531	Eppendorf, Hamburg
PCR cycler Mastercycler Personal 5332	Eppendorf, Hamburg
Percival Intellus Control System CLF	Laborgeräte GmbH, Emersacker
Peristaltic pump	behr Labor-Technik, Düsseldorf
Photometer UvikonXL	Secoman, Kandsberg
Plate Reader Fluostar Omega	BMG, Offenburg
PowerPac 300	BioRad, München
Precision balance AUW120D	Shimadzu, Griesheim
PURELAB Classic water purification system	ELGA LabWater, Celle

Continued on next page

Table 2.1 – Technical equipment

Equipment	**Manufacturer**
Rotor-Gene 6000	Qiagen, Hilden
Spectral photometer Ultraspec III	Pharmacia, Freiburg
Stereomicroscope Leica MZ FLIII	Leica, Bensheim
Table Centrifuge 5415 C	Eppendorf, Hamburg
Ultrasonic homogeniser UW70	Bandelin Electronic, Berlin
Ultra-low temperature freezer C660-86	Brunswick Scientific, Nürtingen
Vortex Genie 2	Scientific Instruments, Ringoes (USA)
Zeiss Confocal Microscope LSM 510 Meta	Zeiss, Jena
HiLoad 16/600 Superdex 75 prep grade	GE Healthcare GmbH, Freiburg
ÄKTAexplorer	GE Healthcare GmbH, Freiburg
Column Nova-Pak®C18, 4 μm, 60 Å 3,9 × 150mm	Waters, Milford (USA)
Column Nova-Pak®C18 4,6 × 250mm	Waters, Milford (USA)
W600 controller	Waters, Milford (USA)
W600E pump	Waters, Milford (USA)
W717 plus autosampler	Waters, Milford (USA)
FP-920 fluorescence detector	Jasco, Groß-Umstadt
ICS-5000+ DC	Dionex, Thermo Scientific, Walldorf

Table 2.2: List of consumables

Consumables	**Manufacturer**
12-well plates	Greiner Bio-One, Frickenhausen
96-well plates	Greiner Bio-One, Frickenhausen
Cover glass	Menzel, Braunschweig
Dialysis membrane standard RC tubing (MWCO: 6-8 kDa)	Spectrum, US
Immobilon-P PVDF transfer membrane, 0.45 μm	Merck Millipore, Darmstadt
HiTrap Chelating High Performance Column (1 ml)	GE Healthcare, München
Microscope slides	Marienfeld, Laude-K¨onigshofen

Continued on next page

Table 2.2 – List of consumables

Consumables	**Manufacturer**
PD SpintrapTM G-25 columns	GE Healthcare, München
Petri dishes (round, 94 x 16 mm)	Greiner Bio-One, Frickenhausen
Petri dishes (square, 120 x 120 x 17 mm)	Greiner Bio-One, Frickenhausen
Rotilabo syringe filter (0.45 μm, 0.22 μm)	Roth, Karlsruhe
Semi-micro cuvettes (10 x 4 x 45 mm)	Sarstedt, N¨umbrecht
Single-use syringe Luer-Look (10 ml)	BD Biosciences, Heidelberg
Strep-Tactin XT Superflow gravity flow columns (0.2ml)	IBA Lifesciences, Göttingen
Streptavidin-coated sepharose beads	Cytvia, Chalfont St. Gilles (UK)
STRIP Tubes & caps 0.1 ml for Rotor-Gene	LTF-Labortechnik GmbH

Table 2.3: List of chemicals

Chemicals	**Manufacturer**
2-log-DNA-Marker	New England Biolabs, Beverly (USA)
3H-acetylCoA	Hartmann Analytic, Braunschweig
Abscisic acid (ABA)	Sigma-Aldrich, Steinheim
AccQ−Tag^{TM}	Waters, Milford (USA)
Acetic acid	Fluka Biochemika, Fuchs
Acetonitrile	Sigma-Aldrich, Steinheim
Acetosyringone	Sigma-Aldrich, Steinheim
Agar	FlukaBiochemika, Fuchs
Agarose	Biozym Scientific GmbH, Oldendorf
Albumin fraction V (BSA)	Roth, Karlsruhe
Ammonium persulfate (APS)	Serva, Heidelberg
Ampicillin	Roth, Karlsruhe
β -Mercaptoethanol	Merck, Darmstadt
BactoTM Tryptone	BD Biosciences, Heidelberg
BactoTM Yeast Extract	BD Biosciences, Heidelberg
BlueStar Prestained Protein Marker	NIPPON Genetics, Düren

Continued on next page

Table 2.3 – List of chemicals

Chemicals	**Manufacturer**
Boric acid	Merck, Darmstadt
Bromophenol blue	Kallies Feinchemie, Sebnitz
CaCl2	AppliChem, Darmstadt
Ca(NO3)2 ·4H2O	Fluka Biochemika, Fuchs
Carbenicillin	Duchefa, Haarlem (Netherlands)
Cellulase Onozuka R-10	Duchefa, Haarlem (Netherlands)
CelLytic P	Sigma-Aldrich, Steinheim
Citric acid	AppliChem, Darmstadt
CoCl2	Duchefa, Haarlem (Netherlands)
Comassie brilliant blue G250	Merck, Darmstadt
cOmplete protease inhibitor cocktail	Roche, Mannheim
CuCl2 ·2H2O	Roth, Karlsruhe
CuSO4	Merck, Darmstadt
Cycloheximide	Sigma-Aldrich, Steinheim
Deoxynucleotide Solution Mix (dNTP)	New England Biolabs, Beverly (USA)
Dimethylformamide (DMF)	Sigma-Aldrich, Steinheim
Dimethyl sulfoxide (DMSO)	Roth, Karlsruhe
Dithiothreitol (DTT)	AppliChem, Darmstadt
Ethanol	Merck, Darmstadt
Ethidium bromide	Sigma-Aldrich, Steinheim
Ethylene glycol-bis (-aminoethyl ether)	Fluka Biochemika, Fuchs
-N,N,N',N'-tetraacetic acid (EGTA)	Fluka Biochemika, Fuchs
Ethylenediaminetetraacetic acid (EDTA)	Roth, Karlsruhe
Fe-EDTA	Duchefa, Haarlem (Netherlands)
Gentamicin	Duchefa, Haarlem (Netherlands)
Glucose	Merck, Darmstadt
Glufosinat-ammonium (Basta)	Bayer, Leverkusen
Glycerine	Merck, Darmstadt
H3BO3	Merck, Darmstadt
HCl	Sigma-Aldrich, Steinheim

Continued on next page

Table 2.3 – List of chemicals

Chemicals	**Manufacturer**
Hepes	Roth, Karlsruhe
Hygromycin	Sigma-Aldrich, Steinheim
Imidazole	Sigma-Aldrich, Steinheim
IPTG	Sigma-Aldrich, Steinheim
Isopropanol	Roth, Karlsruhe
Kanamycin	Duchefa, Haarlem (Netherlands)
KCl	Merck, Darmstadt
KH2PO4	Merck, Darmstadt
KNO3	Roth, Karlsruhe
KOH	Sigma-Aldrich, Steinheim
Lithium dodecyl sulfate	AppliChem, Darmstadt
Macerozyme R-10	Duchefa, Haarlem (Netherlands)
Mannitol	VWR International, Darmstadt
MES	AppliChem, Darmstadt
Methanol	Fisher Scientific, Schwerte
Micro agar	Duchefa, Haarlem (Netherlands)
MgCl2 x 6H2O	AppliChem, Darmstadt
MgSO4	Merck, Darmstadt
MnCl2 ·4H2O	AppliChem, Darmstadt
Monobromobimane (MBB)	Sigma-Aldrich, Steinheim
MOPS Run Buffer	Expedeon, San Diego (USA)
Murashige Skoog (MS) incl. vitamins	Duchefa, Haarlem (Netherlands)
Murashige Skoog (MS) basal salts	Duchefa, Haarlem (Netherlands)
Na2MoO4	AppliChem, Darmstadt
NaCl	AppliChem, Darmstadt
NaOH	AppliChem, Darmstadt
(NH4)6Mo7O24 ·4H2O	AppliChem, Darmstadt
Nitrotetrazolium blue (NBT)	Roche, Mannheim
Phenol	Riedel-de Haen, Seelze
Phenol red	Sigma-Aldrich, Steinheim

Continued on next page

Table 2.3 – List of chemicals

Chemicals	**Manufacturer**
Phenylmethanesulfonylfluoride (PMSF)	Serva, Heidelberg
Phytagel	Sigma-Aldrich, Steinheim
Polyethylenglycol (PEG) 6000	Roth, Karlsruhe
Protein Standard Mark12TM	Invitrogen, Karlsruhe
Quick Coomassie® Stain	Serva, Heidelberg
Rifampicin	Duchefa, Haarlem (Netherlands)
Rotiphorese® Gel 30	Roth, Karlsruhe
Roti®-Quant Bradford reagent	Roth, Karlsruhe
Salicylic acid	Sigma-Aldrich, Steinheim
Silwet Gold	Spiess-Urania Chemicals, Hamburg
Sodium citrate	Riedel-de Haen, Seelze
Sodium dodecyl sulfate (SDS)	Fluka Biochemika, Seelze
Sodium hypochlorite	Fluka Biochemika, Seelze
Spectinomycin	Sigma-Aldrich, Steinheim
Streptomycin	AppliChem, Darmstadt
Sucrose	Roth, Karlsruhe
Sulfadiazine	Sigma-Aldrich, Steinheim
TEMED	Roth, Karlsruhe
Trishydroxymethylaminomethane (Tris)	Roth, Karlsruhe
Triton X-100	Sigma-Aldrich, Steinheim
Tween 20	Sigma-Aldrich, Steinheim
Western blocking reagent	Roche, Mannheim
Z-Leu-Leu-Leu-al (MG132)	Sigma-Aldrich, Steinheim
Z-Leu-Leu-Leu-AMC Proteasome Substrate I	Sigma-Aldrich, Steinheim
ZnCl2	Merck, Darmstadt
ZnSO4	Riedel-de Haen, Seelze

Table 2.4: List of Buffers and solutions

Buffer/Solution	**Component**
1/2 Hoagland medium	2.5 mM $Ca(NO_3)_2 \cdot 4H_2O$; 0.5 mM $MgSO_4$; 2.5 mM KNO_3; 0.5 mM KH_2PO_4; 4 μM Fe-EDTA; 25 μM H_3BO_3; 2.25 μM $MnCl_2 \cdot 4H_2O$; 1.9 μM $ZnCl_2$; 0.15 μM $CuCl_2 \cdot 2H_2O$; 0.05 μM $(NH_4)6Mo_7O_{24} \cdot 4H_2O$; pH 5.8 (with KOH)
1/2 MS medium	2.21 g/l MS; 0.4 g/l MES; 1% (w/v) sucrose; pH 5.8; 0.8% (w/v) microagar
1x blotting buffer	1.44% (w/v) glycin; 0.5% (w/v) Tris; 0.1% (w/v) SDS; 20% (v/v) methanol
1x SDS running buffer	25 mM Tris; 192 mM glycin; 0.1% (w/v) SDS; pH 8.3
1x TAE buffer	90 mM Tris; 90 mM H_3BO_3; 0.5 mM EDTA
1x TBS-T buffer	20 mM Tris; 137 mM NaCl; 0.1% Tween 20; pH 7.6
3x loading buffer	100 mM Tris; 3% (w/v) SDS; 30% (v/v) glycerine; 75 mM DTT; pH 6.8
5x Lämmli buffer	10% (w/v) SDS; 20% (v/v) glycerine; 100 mM Tris, pH 7; 0.1% (w/v) bromophenol blue; 25% (v/v)-mercaptoethanol
6x loading dye	30% (v/v) glycerine; 0.12% (w/v) xylencyanol FF; 0.12% (w/v) bromophenol blue
3.5x Bis-Tris buffer	52.32 g Bis-Tris in 200 ml H_2O; pH 6.5 to 6.8 with HCl
AP buffer	100 mM Tris; 100 mM NaCl; 5 mM $MgCl_2$; pH 8.8
AT medium	5 mM KNO_3, 2.5 mM KH_2PO_4, 2 mM $MgSO_4$, 2 mM $Ca(NO_3)_2$, 0.05 mM Fe-EDTA, 0.01 μM $CoCl_2$, 0.02 μM Na_2MoO_4, 0.5 μM $CuSO_4$, 1 μM $ZnSO_4$, 10 μM NaCl, 14 μM $MnCl_2$; pH 5.8
Amido black staining	0.1% amido black, 45% ethanol, 10% acetic acid
BCIP	16.5% (w/v) 5-bromo-4-chloro-3-indolyl-phosphate in 100% dimethylformamid
Buffer B	50 mM Tris, pH 8.0; 250 mM NaCl; 20 mM imidazol

Continued on next page

Table 2.4 – List of buffers and solution

Buffer/Solution	**Component**
Buffer BXT	100 mM Tris-HCl, pH 8.0; 150 mM NaCl; 1 mM EDTA; 50 mM biotin
Buffer E	50 mM Tris, pH 8.0; 250 mM NaCl; 400 mM imidazole
Buffer W	50 mM Tris, pH 8.0; 250 mM NaCl; 80 mM imidazol
Citrate buffer	0.172 g/l citric acid; 14.41 g/l sodium citrate; 1 mM EDTA; pH 7
Coomassie Brilliant Blue staining	50% (v/v) ethanol; 1% (v/v) acetic acid; 0.1% (w/v) Coomassie; Brilliant Blue G-250
Edwards buffer	0.2 M Tris; 250 mM NaCl; 25 mM EDTA; 0.5% (w/v) SDS; pH 7.5
Enzyme solution	0.4 M mannitol; 10 mM $CaCl_2$; 20 mM KCl; 20 mM MES; pH 5.7 (with KOH or HCl)
Extraction buffer	4 M urea; 100 mM DTT; 1% (v/v) Triton X-100 (v/v)
Incubation buffer	10 mM MES/KOH, pH 6.15; 30 mM KCl
LB medium	1% (w/v) BactoTM Tryptone; 0.5% (w/v) BactoTM Yeast Extract; 1% (w/v) NaCl
MMg solution	0.4 M mannitol; 15 mM $MgCl_2$; 4 mM MES; pH 5.7 (with KOH or HCl) (1.5% microagar for plates)
NBT	16.5% (w/v) nitrotetrazolium blue in 70% (v/v) dimethylformamid
NuPAGE sample buffer	106 mM Tris-HCl, pH 8.5; 141 mM Tris; 2% (w/v) lithium dodecyl sulfate; 0.51 mM EDTA; pH 8.0; 10% (v/v) glycerine; 0.22 mM Coomassie Blue G-250; 0.166 mM Phenol Red; 50mM DTT
PEG solution	40% (w/v) PEG; 0.1 M $CaCl_2$; 0.2 M mannitol
Protein extraction buffer	50 mM Hepes; 10 mM KCl;

Continued on next page

Table 2.4 – List of buffers and solution

Buffer/Solution	**Component**
	1 mM EDTA; 1 mM EGTA; 10\% (v/v) glycerine; 10 mM DTT; 0.5 mM PMSF; pH 7.4
Resolving gel buffer	1.5 M Tris; 0.4% (w/v) SDS; pH 8.8
RIPA buffer	50 mM HEPES-KOH, 100 mM KCl, 5 mM EDTA, 5 mM EGTA, 50 mM NaF, 10% (v/v) glycerol, 1% (v/v) IGEPAL, 0.5 % (w/v) deoxycholate, 0.10 % (w/v) SDS, 1 mM Na4VO3, 1 mM PMSF; pH 7.8 supplemented with 1 × protease inhibitor cocktail (Roche)
Stacking gel buffer	0.5 M Tris; 0.4% (w/v) SDS; pH 6.8
TB buffer	10 mM HEPES; 15 mM $CaCl_2$; 250 mM KCl; 55 mM $MgCl_2$; pH 6.7 sterile filtration with 0.22 μm filter
Transformation medium	50 g/l saccharose; 200 μl/l Silwet Gold
W5 solution	154 mM NaCl; 125 mM $CaCl_2$; 5 mM KCl; 5 mM glucose; 2 mM MES; pH 5.7 (with KOH or HCl)

Table 2.5: List of enzymes and kits

Enzyme/Kit	**Manufacturer**
CloneJET PCR Cloning Kit	Thermo Scientific, Waldorf
E.Z.N.A. Plasmid Midi Kit	Omega Biotek, Norcross (USA)
EZQ® Protein Quantitation Kit	Thermo Scientific, Waldorf
Fast Gene Scriptase II cDNA Synthesis Kit	NIPPON Genetics, D¨uren
FastGene® TAQ Ready Mix	NIPPON Genetics, Düren
Gateway® BP clonase II enzyme mix	Invitrogen, Karlsruhe
Gateway® LR clonase II enzyme mix	Invitrogen, Karlsruhe
NucleoSpinTM Gel and PCR Clean-up Kit	Macherey-Nagel, Düren
NucleoSpinTM Plasmid Kit	Macherey-Nagel, Düren
NucleoSpin Plasmid Kit	Macherey-Nagel, Düren
PCRBIO HiFi Polymerase & Buffer	PCR Biosystems, London (UK)

Continued on next page

Table 2.5 – List of enzymes and kits

Enzyme/Kit	Manufacturer
peqGOLD total RNA kit	Peqlab, Erlangen
peqGOLD DNase I Digest Kit	Peqlab, Erlangen
PierceTM ECL Western Blotting Substrate	ThermoFisher
PlusOne Silver Staining Kit	GE Healthcare, Freiburg
Phusion® High-Fidelity DNA Polymerase	New England Biolabs, Beverly (USA)
qPCRBIO SyGreen Mix Lo-ROX	PCR Biosystems, London (UK)
Restriction enzymes	New England Biolabs, Beverly (USA)
RevertAid H Minus First Strand cDNA Synthesis Kit	Thermo Scientific, Walldorf
SuperSignal West Dura Extended Duration Substrate	Thermo Scientific, Walldorf
T4 DNA Ligase & Buffer	New England Biolabs, Beverly (USA)

Table 2.6: List of antibodies

No.	Antibody	Dilution	Incubation	Reference
19	α OAS-TL A	1:1000 1% BSA	overnight/ 4 °C	H.Birke et al., 2013
20	α OAS-TL C	1:1000 1% BSA	overnight/ 4 °C	C.Heeg et al., 2008
139	α 6x-His tag	1:3000 1% BSA	overnight/ 4 °C	
22	α SAT3 (SERAT2;2)	1:2000 1% BSA	overnight/ 4 °C	
23	α SAT5 (SERAT1;1)	1:500 1% BSA	overnight/ 4 °C	
19	Goat α-Rabbit IgG (H&L), HRP conjugated	1:20 000 1% BSA	1h/ RT	secondary antibody

Table 2.7: List of softwares

Software	License
ApE (A plasmid Editor)	by M. Wayne Davis c
EndNote X9	Thomson Reuters, New York (USA)
Fiji (based on ImageJ)	Schindelin et al., 2012, Schindelin et al., 2015
GraphPad Prism 8	USA
Image Studio Lite	LI-COR, USA
ImageQuant TL 8.1	GE Helathcare, München
Jalview	
Millenium32 Waters	Waters, Milford MA, USA
MS Office 365	Microsoft, Redmond (USA)
NanoDrop ND-2000	Peqlab, Erlangen
Photoshop CS5	Adobe Systems, San Jose (USA)
Rotor-Gene Q Series Software	Qiagen, Hilden
Sigma Plot 14.5	SPPS Inc, München
SnapGene	GSL Biotech LLC

Table 2.8: Web based software tools and websites

Web page	Web address
Brainarray	http://brainarray.mbni.med.umich.edu/Brainarray/Database/CustomCDF/genomic_curated_CDF.asp
eFP Browser	bbc.botany.utoronto.ca/efp/cgi-bin/efpWeb.cgi
Esprint	https://espript.ibcp.fr/ESPript/ESPript/
ExPASY	http://web.expasy.org
Gene Investigator	www.genevestigator.com
GSEA	www.broadinstitute.org/gsea/index.jsp
MASCOT	http://www.matrixscience.com
Primer calc	www.basic.northwestern.edu/biotools/oligocalc.htm
R	www.r-project.org
TAIR	www.arabidopsis.org

2.2 Microbiological methods

2.2.1 Bacterial strains

The list of bacterial strains used in this study is provided in the table 2.9.

Table 2.9: Bacterial strains

Strain	Manufacturer	Genotype
E. coli XL1-blue	Stratagene	*rec*A1 endA1 gyrA96 thi-1 hsdR17 supE44 relA1 lac F'[::Tn10 proAB+ lacIq Δ (lacZ) M15 Tetr]
E. coli DB3.1	Invitrogen	F-gyrA462 endA1 glnV44 (sr1-recA) mcrB mrr hsdS20(rB-, mB-) ara14 galK2 lacY1 proA2 rpsL20(Smr) xyl5 leu mtl1
E. coli BL21 (DE3)	Stratagene	F–ompT galdcm lon hsdSB(rB-, mB-) [malB+]K-12(λS)
A. tumefaciens GV3101	Novagen	pMP90pTiC58δT-DNA, Gentr,Rifr

2.2.2 Preparation of chemocompetent *E. coli* XL1 Blue cells

Chemically competent *E. coli* XL1-Blue cells were added to 10 ml liquid LB medium (Table 2.4) without antibiotic and cultivated at 37 °C and 120 rpm overnight. Next, 500 ml LB medium (Table 2.4) was inoculated with the overnight culture of chemocompetent bacteria and incubated at 37 °C and 120 rpm until the OD_{600} reached 0.5-1. After the cell suspension was incubated on ice for 10 min, it was pelleted at 4 °C and 6000 rpm for 10 min. Next, the pellet was resuspended in 100 ml pre-cooled TB buffer (Table 2.4) following by incubation on ice for 10 min. The bacteria were pelleted at 4 °C and 6000 rpm for 10 min. Then, the cells were resuspended in an 18.6 ml pre-cooled TB buffer (Table 2.4). 1.4 mL DMSO was added to the bacteria. Finally, the cells were transferred to 1.5 mL microcentrifuge tubes in 100 μl aliquots. The aliquots were frozen in liquid nitrogen and stored at -80 °C.

2.2.3 Preparation of chemocompetent *A. tumefaciens* GV3101 cells

Chemically competent *Agrobacterium tumefaciens* GV3101 cells were added to 5 ml liquid LB medium (Table 2.4), supplemented with gentamycin (25 g ml^{-1}) and rifampicin (50 g

ml^{-1}), and cultivated for two days at 28 °C and 120 rpm. Next, 250 ml LB medium (Table 2.4) containing gentamycin and rifampicin was inoculated with 5 ml of an overnight culture of chemocompetent bacteria and incubated at 28 °C and 120 rpm overnight. When the cell culture reached OD_{600} of 0.5-1, it was incubated on ice for 10 min. Then, the cell suspension was pelleted at 4 °C and 6000 rpm for 10 min. The pellet was resuspended in 50 ml pre-cooled autoclaved 150 mM NaCl solution and pelleted at 4 °C and 6000 rpm for 10 min. Then, the cells were resuspended in 10 ml pre-cooled 20 mM $CaCl_2$ solution. Finally, the cells were transferred to 1.5 ml microcentrifuge tubes in 200 μl aliquots, frozen in liquid nitrogen, and stored at -80 °C.

2.2.4 Transformation of *E. coli* by heat shock

The deep-frozen competent cells, either XL1 Blue or BL21 (DE3) (Table 2.9), thawed on ice. Then, 5 μl of the vector DNA was added to 50 μl of the bacteria. The mixture was incubated on ice for 1 hour. Next, bacteria were heat-shocked in a heater at 42 °C for 30 sec and placed on ice for 1 min. Finally, 1 ml LB medium (Table 2.4) was added, and the bacteria were incubated at 37 °C and 120 rpm for 1h.

2.2.5 Transformation *A. tumefaciens* by heat shock

The deep-frozen competent cells, GV3101, thawed on ice. Then, 1 μg of the vector DNA was added to 200 μl of the bacteria. The mixture was inverted twice, incubated on ice for 10 min, and put into liquid nitrogen for 5min. Next, bacteria were heat-shocked in a heater at 37 °C for 5 min. Finally, 1 ml LB medium (Table 2.4) was added, and the bacteria were incubated at 28 °C and 120 rpm for 3 h.

2.2.6 Cultivation of bacteria

After transformation (2.2.4 and 2.2.5), the bacteria were centrifuged at 6000 rpm for 2 min. Then, the supernatant was removed, and only 100 μl of the supernatant over the pellet was kept. Next, the pellet was resuspended with the remaining supernatant by pipetting and plated onto plates with LB medium (Table 2.4) supplemented with 1% agar and corresponding antibiotics (ampicillin: 100 μg ml^{-1}; gentamycin: 30 μg ml^{-1}; kanamycin: 50 μg ml^{-1}; rifampicin: 20 μg ml^{-1}; hygromycin: 50 μg ml^{-1}) for selection. *E. coli* were incubated at 37 °C for 16 h, and *A. tumefaciens* were incubated at 28 °C for 48 hours. Some colonies on the

plates were further grown in liquid LB medium (Table 2.4) supplemented with corresponding antibiotics under the same shaking condition.

2.2.7 Bacterial cultures stored in glycerin

500 μl of bacterial culture was mixed with 500 μl autoclaved 50% glycerol (v/v), snap-frozen in liquid nitrogen, and stored at -80 °C until further usage.

2.3 Molecular biology methods

2.3.1 Extraction of genomic DNA from plant tissue

Extraction of the genomic DNA from *A. thaliana* was performed according to (Edwards et al. 1991). First, a small leaf of *Arabidopsis* (20-30 mg) was excised and placed into a 1.5 ml microcentrifuge tube. The tissue was ground with a plastic pestle for 10-15 seconds, and then 400 μl of Edward buffer (Table 2.4) was added to the ground tissue. Samples were vortexed for 10 seconds and centrifuged at 15000 rpm for 5 min. Next, 300 μl of supernatant were collected and mixed with an equal volume of 100% isopropanol by inversion of the reaction tube several times. After 2 min incubation at RT, samples were centrifuged at 15000 rpm for 10 min to precipitate the DNA. The supernatant was removed, and the pellet was washed with 70 % (v/v) ethanol. Samples were centrifuged at 15 000 rpm for another 2 min. Ethanol was discarded, and the DNA pellet was dried on air for 1 hour at RT. The dried pellet was resuspended in 25 μl sterile ddH_2O and stored at -20 °C until further usage.

2.3.2 Isolation of plasmid from *E. coli* for cloning

Plasmid DNA was extracted from 4 ml *E. coli* overnight culture using the NucleoSpin Plasmid kit® (Macherey Nagel) (Table 2.5) according to the manufacturer's instructions. Finally, extracted plasmids were eluted in 50 μl ddH_2O and stored at -20 °C until further usage.

2.3.3 Primer design and listing

Primers for cloning, genotyping, and qRT-PCR (Table 2.10) were synthesized by Sigma-Aldrich. The melting temperature was kept between 55 °C and 65 °C whenever possible. Lyophilized primers were resuspended in ddH_2O to a stock concentration of 100 μM and kept at -20 °C until further usage to dilute as necessary.

Table 2.10: List of primers

No.	Sequence (5' to 3')	Description	Gene locus
	Primers used for cloning		
5202	AAGGCCATGGATGGCTGTTAAGCGCGAGACTGGA	OAS-TLC_NcoI_fwd	AT3G59760
5203	CCAAGGATCCTTAACCGCTGACTCTCTCAGGC	OASTLC_BamHI_rev	AT3G59760
5248	AATTGGATCCATGGCCATGGCTCTTCGAAG	SHMT_BamHI_fwd	
5249	AAGGGGCGCGCCATCTTGTACAGCTCGTCCATGC	GFP_AscI_rev	
5259	GGCGCGCCGGGACAGCTTCACTGGGC	SHMT_AscI_rev	
5421	AAGGCATATGATGGCTGTTAAGCGCGAGACTGGA	OASTLC_NdeI_fwd	AT3G59760
	Primers used for genotyping		
1639	GGATGCTTTTGAGCACTTTTG	SERAT1;1_fwd	AT5G56760
1640	TGCGCCTAATTCAAATTCAAC	SERAT1;1_rev	AT5G56760
1401	ATTTTGCCGATTTCGGAAC	SERAT1;1_LB	AT5G56760
2318	GGTCACAAGTCGCCGCCACTTC	SERAT2;2_fwd	AT3G13110
2319	CCGTCTCACCGATCACAATAGCCG	SERAT2;2_rev	AT3G13110
1635	AAGAAAATGCCGATACTTCATTGGC	SERAT2;2_LB	AT3G13110
302	CTCACAAGATTCAAGGGATAGGA	OAS-TLA_fwd	AT4G14880
653	GTCATGGCTTCCGCTTCTTTC	OAS-TLA_rev	AT4G14880
1225	GAACATCGGTCTCAATGCAAAAGGGGAAC	OAS-TLA_LB	AT4G14880
325	CGATGATCATGGCTTCAAGG	OAS-TLC_fwd	AT3G59760
922	CGATGAATGCTAGGCCAATACCCGTG	OAS-TLC_rev	AT3G59760
309	GACCGCTTGCTGCAACTCTCTCAGG	OAS-TLC_LB	AT3G59760
4890	GTACCTTGAAGCTTGCTAATCCTA	TUB9_fwd	AT4G20890
4891	GTTCTGGACGTTCATCATCTGTTC	TUB9_rev	AT4G20890

continued on next page

Table 2.10 – List of primers

No.	Sequence (5' to 3')	Description	Gene locus
5301	CTCACGATGCCGGCCTCCCTGA	ASTOL1-DdeI_fwd	
5302	TCCCAGTATGAGTCCACAGAACACA	ASTOL1-DdeI_rev	
	Primers used for qRT-PCR		
5332	GAAACCGCAAAGCAACTAGC	OAS-TLC_fwr	AT3G59760
5333	GAAGCTCGGGAAAACAACAG	OAS-TLC_rev	AT3G59760
2457	GATGAGGCACCAACTGTTCTTCGTG	TIP41_fwd	AT4G34270
2458	CTGACTGATGGAGCTCGGGTCG	TIP41_rev	AT4G34270
4632	GATTGGTTTTAGCATGATTTCTGAT	OAS-TLA_fwd	AT4G14880
4633	TAACCCAACTCCAGTGTTTCC	OAS-TLA_rev	AT4G14880
2459	CTTCTCGCTCCAGTAATGGGATCC	PP2A_fwd	AT1G13320
2460	GCTTGGTCGACTATCGGAATGAGAG	PP2A_rev	AT1G13320

2.3.4 Polymerase chain reaction (PCR)

For the genotyping, the FastGene® TAQ Ready Mix PCR Kit (Table 2.5) was employed. For the PCR reaction, 2 μl gDNA, 1 μM each primer, 10 μl FastGene® TAQ Ready Mix PCR, and 6 μl sterile ddH_2O (total volume 20 μl) were mixed. The reaction mix was treated according to the PCR program presented in Table 2.11.

Cycle	Step	Temperature	Time
1	Initial denaturation	95 °C	3 min
35	Denaturation	95 °C	30 sec
35	Annealing	55-68 °C	30 sec
35	Extension	72 °C	1 min/kb
1	Final extension	72 °C	5 min
1	Hold	16 °C	Infinite

Table 2.11: PCR program using FastGene polymerase

PCRBIO HiFi Polymerase kit (Table 2.5) was employed to amplify DNA fragments for cloning. For PCR reaction, 1 μl template (plasmid or cDNA), 10 μl 5x PCRBIO HiFi buffer, 2 μl each primer (10 μM), 0.5 μl PCRBIO HiFi Polymerase, and 34.5 μl sterile ddH_2O (total volume 50 μl) were mixed in 200 μl PCR tube. The PCR program in Table 2.12 was used. The annealing temperature was determined with the help of OligoCalc and adjusted to 60 °C whenever possible. The result of the PCR amplification was validated by agarose gel electrophoresis (2.3.5) and sequencing (2.3.10).

Cycle	Step	Temperature	Time
1	Initial denaturation	95 °C	30 sec
35	Denaturation	95 °C	10 sec
35	Annealing	55-68 °C	30 sec
35	Extension	72 °C	30 sec/kb
1	Final extension	72 °C	2 min
1	Hold	16 °C	Infinite

Table 2.12: PCR program for the PCRBIO HiFi polymerase

2.3.5 Agarose gel electrophoresis

Amplified PCR products (2.3.4) or digested DNA fragments (2.3.7) were separated by agarose gel electrophoresis. For this purpose, the required amount of agarose (0.8-2 % (w/v)) was melted in 1x TAE buffer (Table 2.4). After cooling down, ethidium bromide was added in the concentration of 0.7 μg ml^{-1}, and the mixture was poured into a gel chamber equipped with a gel comb. Next, the DNA samples were either directly loaded onto the gel (e.g., when a pre-stained reaction mix had been used for PCR) or mixed with 6 x loading dye (Table 2.4). The 2-Log DNA Ladder (New England Biolabs) was used as a size standard. The electrophoresis was carried out at 120 V in 1x TAE buffer (Table 2.4) until the fragments were separated. The result was documented on the Gel Jet Imager 2000 (INTAS) under UV light.

2.3.6 Extraction of DNA from agarose gels

NucleoSpin® Gel and PCR Clean-up kit (Macherey and Nagel) (Table 2.5) were used to extract DNA fragments from agarose gel according to the manufacturer's protocol. Finally, extracted DNA fragments were eluted in 20 μl ddH_2O.

2.3.7 Restriction endonuclease digestion of DNA

Restriction enzymes (New England Biolabs, NEB) (Table 2.5) were used for restriction digestion of DNA either for further test-digest of the ligated purified vector (2.3.9) or to digest the PCR product (2.3.4) and the target vector for subsequent ligation. For test digestion, 5 μl DNA, 1 μl of each restriction enzyme, 2 μl buffer, and ddH_2O to 20 μl were mixed and left to incubate for 1 h at 37 °C. For the digestion of PCR fragments and target vectors for subsequent cloning, 12 μl target vector or PCR fragment, 1.5 μl of each restriction enzyme, 5 μl buffer, and ddH_2O to 50 μl were mixed and left to incubate for 3 h at 37 °C. The resulting DNA fragments were separated on agarose gel electrophoresis (2.3.5) and extracted from the gel (2.3.6).

2.3.8 Ligation of DNA fragments

The CloneJET PCR Cloning Kit (Thermo Scientific, Waldorf) (Table 2.5) was used to ligate blunt-end PCR products into the pJET1.2 vector according to the manufacturer's instructions. This step was performed for PCR products obtained in low concentrations to be am-

plified once again before attempting a restriction digest. In all other cases, T4 DNA Ligase (New England Biolabs, NEB) (Table 2.5) was used to ligate the linearized vector and the PCR fragments with compatible ends. 2 μl 10x T4 buffer, 1 μl T4 DNA Ligase, up to 300 ng DNA (3:1 molar ratio insert:vector), and ddH_2O to 20 μl were mixed and incubated for up to 1 h or overnight at 16 °C. Finally, the ligation mix was inactivated by incubation at 65 °C for 10 min and used directly to transform chemocompetent *E. coli* (2.2.4).

2.3.9 Cloning using restriction sites

The amplified PCR product and cloning vector were digested with the corresponding restriction enzymes (Table 2.5). The resulting fragments were separated on agarose gel electrophoresis (2.3.5), cut out of the gel, and purified (2.3.6). Then, the purified fragment was ligated (2.3.8) into the vector. *E. coli* was transformed by the construct. Overnight culture of *E. coli* was prepared, followed by purification of the plasmids (2.3.2). Finally, the presence of the insert was proved by a test digest (2.3.7) and sequencing (2.3.10). The constructs used in this thesis are presented in supplemented Figures 5.4.

2.3.10 Sequencing

The sequencing of the cloned constructs was ordered and performed by Eurofins Genomics (Ebersberg). The samples were prepared according to the instructions on the Eurofins Genomics (50-100 ng μl^{-1} plasmid DNA or up to 10 ng μl^{-1} of purified PCR fragment based on the size in ddH_2O). The sequencing results were analyzed with either ApE (M. Wayne Davis) or SnapGene (GSL Biotech LLC) (Table 2.7).

2.3.11 Isolation of total RNA from plant tissue

RNA was isolated from 50 mg plant leaf material with peqGOLD Total RNA Kit (Peqlab, Erlangen), the Universal RNA Kit (Roboclon, Berlin), or the RNA Extraction Kit (VWR, Radnor) (Table 2.5). Leaf material was snap-frozen in liquid nitrogen and ground in a Retsch mill with stainless steel beads (QIAGEN) at 20 Hz for 30 sec. The following steps were done according to the manufacturer's protocols. The optional DNA digestion step was always carried out. Finally, RNA was eluted with up to 50 μl sterile RNAase-free ddH_2O. The concentration of the resulting RNA was measured with the Nanodrop ND-2000 (Peqlab, Erlangen) (Table 2.1).

2.3.12 cDNA synthesis

cDNA was synthesized using FastGene Scriptase II cDNA Synthesis Kit (NIPPON Genetics) (Table 2.5). 0.5-2 μg RNA was mixed with 0.5 μl oligo dT Primer and 1 μl of dNTP and DEPC-treated ddH_2O to a final volume of 6.25 μl. The pre-mix was incubated in the PCR Cycler at 65 °C for 5 min and subsequently cooled down on the ice and spun down. Then, 2 μl 5x FastGene Scriptase II buffer, 1 μl 0.1 M DTT, and 0.25 μl RNase inhibitor were added, and the mixture was incubated at 42 °C for 2 min. The RNA mixture was kept on ice then, and 0.5 μl FastGene Scriptase II was added. The reaction mix was incubated at 42 °C for 50 min. Finally, the reaction was inactivated by incubation at 70 °C for 15 min. The resulting cDNA was diluted in a 1:10 ratio and stored at -80 °C until further usage.

2.3.13 Quantitative real-time polymerase chain reaction (qRT-PCR)

2 μl of diluted cDNA (2.3.12) was mixed with 6.25 μl qPCRBIO SyGreen Mix Lo-ROX (PCR Biosystems), 0.5 μl primer mix (each 5 μM), 3.75 μl ddH_2O to perform gene expression analysis via quantitative real-time PCR. The PCR program was adjusted according to the manufacturer's instructions. All samples were measured in duplicates, and one control sample was employed as a reference. The diluted cDNA of the reference sample (1:10 and 1:00) served to calculate the standard curve. The expression of the genes of interest was calculated with the help of a standard curve and normalized to the housekeeping genes *TIP41* (AT4G34270) and *PP2A* (AT1G69960).

2.4 Protein biochemical methods

2.4.1 Extraction of soluble proteins from plant tissue

Soluble proteins were extracted from 50-100 mg of snap-frozen plant leaves ground with mortar and pestle. First, 250-350 μl of protein extraction buffer (Table 2.4) was added to the ground material. The mixture was vortexed on ice for 15 min and then centrifuged at maximum speed at 4 °C for 10 min. Then the supernatant was transferred into a new Eppendorf tube. Centrifugation was repeated until the supernatant was clear. Extracted proteins were kept on ice for further usage and at -80 °C for long-term storage.

2.4.2 Determination of protein concentration according to Bradford

In order to measure the concentration of proteins, extracts (2.4.1) were diluted at 1:10 in ddH_2O. 10 μl of the dilution was mixed with 250 μl 1x Roti®Quant (Roth) (Table 2.3) in a 96 well plate. The absorption at 595 nm was measured on the FLUOStar Optima Microplate Reader (BMG Labtech) (Table 2.1) in duplicates. ddH_2O was performed as a blank. The concentration of samples was quantified using a standard curve calculated from 0.1, 0.2, and 0.4 $\mu g\,\mu l^{-1}$ BSA (Bradford 1976).

2.4.3 SDS-polyacrylamide gel electrophoresis (SDS-PAGE)

Proteins were separated according to size utilizing polyacrylamide gel electrophoresis (PAGE). To set up the SDS-PAGE, either Mini-PROTEAN II-System (Bio-Rad) or PerfectBlue Twin ExW S-System (peqlab) (Table 2.1) systems were utilized. Each SDS gel consists of resolving gel and stacking gel. The polyacrylamide concentration in the resolving and stacking gels was adapted according to the target protein's size and gel system (Tables 2.13; 2.14; 2.15). Samples (2.4.1) were denatured by heating up to 95 °C for 5-10 min, and 10-25 μl of each sample were loaded depending on the gel system and protein concentration. In addition, 10 μl of BlueStar Prestained Protein Marker (NIPPON Genetics) (Table 2.3) was utilized as a protein molecular size reference. The PAGE was performed in 1x SDS running buffer (Table 2.4) at 80 V for the first 15 min, followed by an increasing voltage to 150-180 V for 1.5 h. The separated proteins in the gel were then stained with Quick Coomassie Stain (Table 2.3) or transferred onto a PVDF membrane for the immunological detection of target proteins (2.4.4).

PAGE (%)	**ddH_2O (ml)**	**Resolving gel (ml)**	**Rotigel 30 (ml)**	**10% APS (µl)**	**TEMED (µl)**
10	5.55	3.3	4.5	90	16
12.5	4.5	3.3	5.55	90	16
15	3.37	3.3	6.68	90	16
PAGE (%)	**ddH_2O (ml)**	**Stacking gel (ml)**	**Rotigel 30 (ml)**	**10% APS (µl)**	**TEMED (µl)**
7.5	2.61	0.72	1.13	45	9

Table 2.13: Composition of SDS-PAGE gels for the Mini Protean system.

PAGE (%)	ddH_2O (ml)	Resolving gel (ml)	Rotigel 30 (ml)	10% APS (µl)	TEMED (µl)
10	3.82	2.84	3.34	50	14
12	3.16	2.84	4	50	14
15	2.16	2.84	5	50	14
PAGE (%)	**ddH_2O (ml)**	**Stacking gel (ml)**	**Rotigel 30 (ml)**	**10% APS (µl)**	**TEMED (µl)**
4	2.04	1	0.46	40	20

Table 2.14: Composition of SDS-PAGE gels (Bis-Tris) for the Mini Protean system.

PAGE (%)	ddH_2O (ml)	Resolving gel (ml)	Rotigel 30 (ml)	10% APS (µl)	TEMED (µl)
10	16.65	9.9	13.5	270	48
12.5	13.5	3.3	16.65	270	48
15	10.11	3.3	20.04	270	48
PAGE (%)	**ddH_2O (ml)**	**Stacking gel (ml)**	**Rotigel 30 (ml)**	**10% APS (µl)**	**TEMED (µl)**
7.5	7.83	2.16	3.39	90	18

Table 2.15: Composition of SDS-PAGE gels for the Perfect Blue Twin ExW system.

2.4.4 Western blotting

Separated proteins via SDS-PAGE (2.4.3) were transferred to the PVDF membrane (Immobilon-P Transfer Membrane, 0.45 μm; Millipore) (Table 2.2) activated in methanol for 10 sec. Mini Trans-Blot Cell systems (Bio-Rad) were used to transfer proteins from small gels, and blotting was performed at 360 mA for 1.5 h at 4 °C or 60 mA for 16 h at 4 °C. For transfer proteins from the big gels, Trans-Blot Cell systems (Bio-Rad) were employed. Blotting for the big gels was performed at 200 mA for 16 h at 4 °C. Both blotting systems were filled with 1x blotting buffer (Table 2.4) and an ice block for cooling.

2.4.5 Immunological detection of proteins

After blotting, the target protein was detected and quantified by doing immunodetection. All the following steps were carried out in a Petri dish on The Belly Dancer orbital shaker (IBI Scientific) (Table 2.1). First, the membrane was washed with 1x TBS-T buffer (Table 2.4) and blocked with 5 % BSA in TBS-T for 1 h at RT. The blocked membrane was then washed 5x for 3

min with 1x TBS-T buffer and incubated in a specific primary antibody (Table 2.6) in 1 % BSA (w/v) in 1x TBS-T buffer for 1.5 h at RT or 16 h at 4 °C. Afterward, the membrane was rewashed 5x for 3 min with 1x TBS-T buffer and incubated in the secondary antibody (Anti-Rabbit IgG, HRP-Conjugate) (Table 2.6) in 1 % BSA (w/v) in 1x TBS-T buffer for 1 h at RT. Finally, the membrane was rewashed 5x for 3 min and developed with PierceTM ECL Western Blotting Substrate (ThermoFisher) (Table 2.5) for 2 min. The membrane was covered with a plastic bag, and signal intensity was captured with ImageQuant LAS 4000 (GE Healthcare) (Table 2.1).

2.4.6 Determination of signal intensity

Developed membranes after immunological detection (2.4.5), stained membranes (2.4.7), and stained gels (2.4.8) were captured with ImageQuant LAS 4000 (GE Healthcare) (Table 2.1), and signal intensities of the protein bands were determined with Image Studio Lite (LI-COR) (Table 2.7) and normalized to the loading control.

2.4.7 Visualization of proteins by amido black staining

After developing the membrane (2.4.5) and capturing the signal intensities (2.4.6), the membrane was incubated in the amido black staining solution (Table 2.4) for 10 min and destained with ddH_2O until the desired contrast of the stained protein bands had been achieved. Finally, the membrane was covered with a plastic bag, and signal intensities were captured with ImageQuant LAS 4000 (GE Healthcare) (Table 2.1).

2.4.8 Visualization of proteins by Coomassie Brilliant Blue staining

After SDS-PAGE, separated protein bands in the polyacrylamide gel (2.4.3) were visualized by Coomassie Brilliant Blue staining (Table 2.4). For that purpose, the gel was incubated in staining on an orbital shaker (The Belly Dancer®; IBI Scientific) for 0.5-1 h, then incubated in ddH_2O until the background of the gel was completely destained. Finally, the gels were covered in a plastic bag and visualized in ImageQuant LAS 4000 (GE Healthcare) (Table 2.1).

2.4.9 Expression of recombinant proteins in *E. coli*

Transformed *E. coli* BL21 (DE3) cells (2.2.4) were grown in 10 ml liquid LB medium (Table 2.4) supplemented with ampicillin (100 μg ml^{-1}) at 37 °C and 180 rpm for 16 hours. The

grown culture was transferred to an Erlenmeyer flask filled with 300 ml LB medium (Table 2.4) supplemented with ampicillin (100 μg ml^{-1}) and incubated under the same condition until OD_{600} reached 0.6-0.8. IPTG to a final concentration of 1 mM was added to induce the protein expression, and the culture was then incubated at 37 °C and 180 rpm for 4 hours. Bacteria were pelleted by centrifugation at 7 °C and 10 000 rpm for 10 min. The supernatant was removed, and the pellet was frozen in liquid nitrogen and then stored at -80 °C until further usage.

2.4.10 Purification of recombinant SERAT expressed in *E. coli*

*At*SERAT2;2 (*At*SAT3) and *At*SERAT1;1 (*At*SAT5) were expressed in *E. coli* with an N-terminal fusion to a hexahistidine tag (His-tag) using the vectors pET28a*At*SAT3 and pET28a*At*SAT5 (Figure S19), respectively. HiTrap Chelating High-Performance Column (GE Healthcare) (Table 2.2) connected to a peristaltic pump (Behr Labor-Technik) (Table 2.1) was used to purify recombinant proteins from *E. coli*. The flow rate was adjusted to 1 ml min^{-1}. First, the column was washed with 10 mM EDTA and ddH_2O for 5 min and then loaded with $NiCl_2$ for 5 min. Next, the column was equilibrated with buffer B (Table 2.4) until the sample was ready to be loaded. Meanwhile, the bacterial pellet (Table 2.9) was resuspended in buffer B (Table 2.4) and was sonicated in a centrifuge tube at 40 % activity for 5 min, followed by sonication for 4 min (Sonopuls GM70, Bandelin Electronic) (Table 2.1). The lysate was centrifuged at 13000 g and 4 °C for 10 min, and the supernatant (crude extract) was transferred into a conical centrifuge tube. To eliminate cell debris, the crude extract was filtered with a 45 μm syringe filter (Table 2.2). 500 μl of the crude extract was transferred to a reaction tube and kept on ice until further usage, and the rest was loaded onto the column, where it circulated for 0.5-1 h. 500 μl of flowthrough was collected and kept on ice until further usage. Then, the column was washed with buffer W (Table 2.4) for 5-10 min to elute unspecifically bound proteins. The fraction of the washing step was collected to verify the success of this step and kept on ice until further usage. Finally, the specifically bound proteins were eluted with 5 ml buffer E (Table 2.4) in 10 fractions, each 500 μl. The column was cleaned with 10 mM EDTA loading for 5 min, 250 mM NaOH for 2 min, ddH_2O until pH was 7, and 0.02 % NaN_3 for 2 min. The column was sealed with parafilm and stored at 4 °C until further usage. Protein concentration in all fractions was measured by Bradford assay (2.4.2), and the presence of the purified protein was detected via SDS-PAGE (2.4.3), followed by western blotting (2.4.4)

and immunodetection (2.4.5).

2.4.11 Purification of recombinant OAS-TL expressed in *E. coli*

The affinity of OAS-TL to SERAT was used to purify the OAS-TL protein. For that purpose, the recombinant His-tagged *At*SERAT was first coupled to a HiTrapTM column, as described in 2.4.10. Then, the bacterial OAS-TL was removed from the column by loading 10 mM OAS, followed by the washing step with buffer W (Table 2.4). Next, the bacterial extract containing recombinant *At*OAS-TL expressed in *E. coli* (2.4.9) was loaded to the column and circulated for 30 min leading to the binding of the recombinant *At*OAS-TL to the column-bound *At*SERAT. The column was washed with buffer W (Table 2.4) for 10 min. Finally, to elute the whole complex containing *At*SERAT and *At*OAS-TL, the column was loaded directly with buffer E (Table 2.4), and followthrough was collected. However, to test if the *At*OAS-TL can make a stable complex with *At*SERAT, 10 mM OAS was loaded into the column, and the followthrough was collected. If the complex containing *At*SERAT and *At*OAS-TL dissociates, the recombinant *At*OAS-TL is separated from the complex and washed out in this step. Finally, the column was washed with buffer W (Table 2.4) for 10 min and loaded with buffer E (Table 2.4) to collect the *At*SERAT. The column was cleaned as described in 2.4.10.

2.4.12 Determination of OAS-TL activity

Determination of OAS-TL (EC 2.5.1.47) enzymatic activity was acquired by photometric detection of the reaction product cysteine. 1-2 μl of protein crude extract (for recombinant protein diluted 1:100) was mixed with 5 μl of 1 M HEPES/KOH pH 7.5, 10 μl of 100 mM OAS, 5 μl of 100 mM DTT and added ddH_2O to the total 100 μl. The reaction mix was incubated for 5 min at 25 °C. Then, 10 μl of 50 mM Na_2S was added to start the reaction and incubated for 10 min at 25 °C. Then, 50 μl 20% TCA was added to the mixture to stop the reaction and precipitation of proteins, followed by centrifugation for 5 min at maximum speed at RT. Alternatively, 200 μl ninhydrin, which reacts with the primary amino group of cysteine, was mixed with 100 μl 100% acetic acid, added to the mixture, and incubated for 10 min at 99.9 °C. Finally, the reaction was cooled down on the ice for 1-2 min and mixed with 550 μl 100% ethanol. The absorbance was measured at 560 nm in a plastic cuvette. The specific activity was calculated according to the formula below:

1 OD_{560} = 36.6 nmol Cysteine

Specific activity = amount of cysteine * $(\text{time})^{-1}$ * $(\text{amount of protein})^{-1}$

2.4.13 Determination of SERAT activity

Determination of SERAT (EC:2.3.1.30) enzymatic activity was acquired by coupling the SERAT reaction to the OAS-TL reaction and production of cysteine. The entire OAS generated by SERAT was converted to cysteine by excess OAS-TL activity. Then, the reaction product cysteine was detected, as described in 2.4.13. For a 100 μl reaction volume, 5 μl of 1M HEPES/KOH pH 7.5, 10 μl of 100 mM serine, 10 μl of 100 mM Na_2S, 5μl of 100mM DTT, 2μl of OAS-TL A added to protein crude extract and ddH_2O. Usually, up to 58 μl of the protein crude extract is used to determine specific SERAT activity. First, the reaction mix was incubated for 5 min at 25 °C. Then, 10 μl of 10 mM Acetyl-CoA was added to the mixture to start the reaction and incubate for 30 min at 25 °C. Then, 50 μl 20% TCA was added to the mix to stop the reaction and precipitation of proteins, followed by centrifugation for 5 min at maximum speed at RT. Alternatively, 200 μl ninhydrin, which reacts with the primary amino group of cysteine, was mixed with 100 μl 100% acetic acid, added to the mixture, and incubated for 10 min at 99.9 °C. Finally, the reaction was cooled down on the ice for 1-2 min and mixed with 550 μl 100% ethanol. The absorbance was measured at 560 nm in a plastic cuvette, and the activity was calculated as described in 2.4.12.

2.5 Methods of plant work

2.5.1 Plant material

All experiments used Arabidopsis thaliana ecotype Col-0 (Columbia) as the model organism and wild-type (WT) control. First, all seeds were verified for homozygosity of the corresponding T-DNA insertion by genotyping (Table 2.11) before the transformation. Then, a series of mutants were complemented with wild-type and mutated cytosolic and mitochondrial *At*OAS-TLs (Table 2.16) under the control of the maize *Ubiquitin* promoter (Clough et al. 1998). The constructs used for the transformation were provided by Dr. Shengkai Sun, Centre for Orgnaismal Studies Heidelberg.

GVO*	GVO**	Name	Gene locus	Accession line	Reference	Description
#13	#1794	*oastla* (*At*OAS-TL A)	AT4G14880	SP1960	Heeg et al. 2008	T-DNA; KO; Co *At*OAS-TL A
#13	#1795	*oastla* (*At*OAS-TL A^{S102N})	AT4G14880	SP1960	Heeg et al. 2008	T-DNA; KO; Co *At*OAS-TL A^{S102N}
#504	#1794	*serat1;1* (*At*OAS-TL A)	AT5G56760	SALK_050213	Watanabe et al. 2008b	T-DNA; KO; Co *At*OAS-TL A
#504	#1795	*serat1;1* (*At*OAS-TL A^{S102N})	AT5G56760	SALK_050213	Watanabe et al. 2008b	T-DNA; KO; Co *At*OAS-TL A^{S102N}
#1210	#1794	*oastla*serat1;1* (*At*OAS-TL A)	AT4G14880 AT5G56760	SP1960 SALK_050213	Haas et al. 2010	Double KO; Co *At*OAS-TL A
#1210	#1795	*oastla*serat1;1* (*At*OAS-TL A^{S102N})	AT4G14880 AT5G56760	SP1960 SALK_050213	Haas et al. 2010	Double KO; Co *At*OAS-TL A^{S102N}
	#1794	WT (*At*OAS-TL A)	AT4G14880			WT; Co *At*OAS-TL A
	#1795	WT (*At*OAS-TL A^{S102N})	AT4G14880			WT; Co *At*OAS-TL A^{S102N}
#15	#1798	*oastlc* (*At*OAS-TL C)	AT3G59760	SALK_000860	Heeg et al. 2008	T-DNA; KO; Co *At*OAS-TL C
#15	#1799	*oastlc* (*At*OAS-TL C^{S210N})	AT3G59760	SALK_000860	Heeg et al. 2008	T-DNA; KO; Co *At*OAS-TL C^{S210N}
#15	#2047	*oastlc* (SHMT-*At*OAS-TL A)	AT3G59760	SALK_000860	Heeg et al. 2008	T-DNA; KO; Co SHMT-*At*OAS-TL A
#15	#2048	*oastlc* (SHMT-*At*OAS-TL A^{S102N})	AT3G59760	SALK_000860	Heeg et al. 2008	T-DNA; KO; Co SHMT-*At*OAS-TL A^{S102N}
	#1798	WT (*At*OAS-TL C)				WT; Co *At*OAS-TL C
	#1799	WT (*At*OAS-TL C^{S210N})				WT; Co *At*OAS-TL C^{S210N}

Table 2.16: List of transformants used in this dissertation. T-DNA: T-DNA insertion; WT: wild type; KO: knock-out; Co: complement with; GVO*: GVO number of plants; GVO**: GVO number of bacteria.

2.5.2 Cultivation on soil and seed production

The seeds were sowed on humid soil (Tonsubstrat from Ökohum, Herbertingen supplemented with 10% (v/v) vermiculite and 2% (v/v) quartz sand) and stratified for two days at 4 °C in darkness. After two weeks in the growth chamber under short-day conditions (8.5 h day/15.5 h night, 50-60 % relative humidity, 70 – 100 μmol $m^{-2}s^{-1}$ light intensity, and 22 °C during the light periods and 18 °C in the dark), plants were separated to individual pots with humid soil and further grown under short-day condition until they had an age of six to nine weeks. For propagation of seeds, plants were moved to long-day conditions (16 h day/8 h night, other conditions remained the same as described for the short day) after eight weeks of growth. Later, plant stems were fastened to wooden sticks and covered with a paper bag to ensure the collection of all seeds. Watering was stopped when leaves started to senescence. Seeds were harvested when plants were completely dry, using a sieve, and stored in a dry and dark place.

2.5.3 Cultivation under sterile conditions on plates

For cultivation of *Arabidopsis thaliana* under sterile conditions, seeds were surface-sterilized 2x 3 min with 70% (v/v) ethanol and then washed 3x 3 min with ddH_2O. Then, seeds were distributed onto Petri dishes filled with 1/2 MS medium (Table 2.4) and were stratified for 2 days at 4 °C in the darkness. Later, they were transferred onto the climate chambers (Percival Intellus, Laborgeräte GmbH) under short-day conditions (8 h day/16 h night, light intensity: 120 μmol $m^{-2}s^{-1}$, day temperature: 22 °C, night temperature: 18 °C).

2.5.4 Stable transformation of *A. thaliana*

The stable transformation of Arabidopsis plants was carried out as described by Clough and Bent (Clough et al. 1998). For this purpose, plants were grown for 8 weeks under short-day growth conditions (2.5.2) and then transferred to the long-day conditions (2.5.2) to produce flowers. First, the primary bold was cut off to produce more flowers. The transformation was done when the secondary bolds were 2-10 cm with few open flowers. Any siliques present before transformation were snipped off. 100 ml LB medium (Table 2.4) containing the corresponding antibiotics was inoculated with an overnight culture of *A. thaliana* cells containing the plasmid of interest and left to incubate at 28 °C and 180 rpm for two days. When the

OD_{600} of the culture reached 0.8-1.2, the bacteria suspension was centrifuged at 6000 g at 4 °C for 15 min. Then, the supernatant was removed, and the pellet was resuspended in the transformation medium (20 g l-1 Sucrose and 80 μl l^{-1} Silwet 77 in 400 ml ddH_2O) to an OD_{600} of 0.8 – 1.2. Next, the flowering stalks of *A. thaliana* were dipped into the suspension medium, bringing the flowers into direct contact with the bacteria. Plants were covered then with a plastic bag, laid horizontally on the tray, and kept under the darkness at RT for 24 h. After one week, the procedure was repeated to increase the transformation efficiency. Finally, plants were kept under long-day conditions (2.5.2) until seed maturation.

2.5.5 Selection of transformants

Seeds were sterilized (2.5.3) and germinated on AT medium (Table 2.4) supplemented with hygromycin (10 μg ml^{-1}) to select positive transformants of T1 generation containing the transgene and hygromycin-resistance gene from the plasmid. After 4-5 weeks of growth under short-day conditions (2.5.2) in the Percival chamber, the surviving seedlings were transferred to pots containing humid soil (2.5.2). The presence of the transgene of interest was verified by PCR-based genotyping (Table 2.11).

2.5.6 Plants on plates exposed to cadmium

Sterilized seeds (2.5.3) were germinated on ½ AT medium (Table 2.4) supplemented with 100 μM $CdCl_2$ in the short-day condition for five weeks. Then, the root length of the seedlings was measured using Fiji (based on ImageJ).

2.6 Metabolomics

2.6.1 Metabolite extraction from plant tissue

Plant metabolites were extracted from 50 ±10 mg of ground frozen leaf samples in 300 ml 0.1 M HCl (Table 2.3) and incubated on ice for 15 min while vortexed every 30 sec. Then, the mixtures were centrifuged at maximum speed and 4 °C for 5 min. The supernatant containing the soluble metabolites was then transfered into new microcentrifuge tubes. The centrifugation step was repeated until the lysate was clear. Finally, the supernatant was flash-frozen in liquid nitrogen and stored at -80 °C for further usage.

2.6.2 Derivatization and determination of OAS and amino acids

For OAS derivatization, 50 μl of the fresh metabolite extraction (2.6.1) was mixed with 30 μl of 0.8 M borate buffer (Table 2.3) and immediately supplemented with 20 μl of fluorescent dye AccQ-Tag™ reagent (Table 2.3). First, the mixture was mixed thoroughly by pipetting and incubated for 1 min at RT. Then, the mixture was incubated for 10 min at 55 °C, followed by centrifuging at maximum speed for 15 min at RT. Finally, the supernatant was transferred into the vials. For amino acid derivatization, 5 μl of the fresh metabolite extraction (2.6.1) was mixed with 35 μl of 0.8 M borate buffer (Table 2.3) and immediately supplemented with 20 μl of fluorescent dye AccQ-Tag™ reagent (Table 2.3). After mixing with pipetting and incubation for 1 min at RT, the mixture was incubated for 10 min at 55 °C. Then, the mixture was centrifuged at maximum speed for 2 sec at RT and added with 440 μl ddH_2O. The final diluted mixture was centrifuged at maximum speed for 15 min at RT and transferred into the vial. Derivatized metabolites were separated by high-performance liquid chromatography using a Nova-Pak® C18-column (Table 2.1) as described in (Hartmann et al. 2004). They were detected with the Jasco FP-920 Fluorescence-Detector (Table 2.1) at 395 nm after they were excited at 250 nm. Quantification was performed using the Waters LC control- and analysis software Millenium (Table 2.7). Standardization was carried out by co-derivatized external standards for OAS and each amino acid.

2.6.3 Derivatization and determination of thiols

For thiol derivatization, 25 μl of metabolite extract (2.6.1) was mixed with 270 μl of the reduction buffer containing 190 μl ddH2O, 20 μl 1 M Tris pH 8.3, 10 μl 10 mM DTT and 25 μl 0.08 M NaOH. After 1 h incubation in the darkness, the reduced thiols were conjugated with 25 μl 10 mM monobromobimane (Table 2.3), mixed by inverting the tube, and spun down. The mixture was incubated for 15 min at RT in the darkness. Then, 705 μl 5 % (v/v) acetic acid was added to stop the reaction, stabilize the thiol-bimane-derivatives and mix by inverting the tube. Precipitates were removed by centrifugation at 4 °C for 45 min. The reaction is then stored either at 4 °C for short-term storage or -80 °C for long-term storage for further usage. Finally, derivatized thiols were separated by reversed-phase HPLC with a Nova-Pak® C18-column (Table 2.1) as described in (Wirtz et al. 2003). The separated thiol derivatives were detected with the Jasco FP-920 Fluorescence-Detector (Table 2.1) at 480 nm after they were

excited at 380 nm. Quantification was performed using the Waters LC control- and analysis software Millenium (Table 2.7). Standardization was carried out by co-derivatized external standards for thiols.

2.6.4 Determination of anions

The metabolite extract (2.6.1) was diluted 10-fold with ddH_2O and centrifuged for 45 min at 4 °C to quantify anions. Anion exchange chromatography with an IonPac® AS9-HC column (2 × 250 mm; Dionex) and an Ion-PAC® AG9-HC pre-column (Dionex) connected to a Dionex - HPLC system ICS 1000 composed of ICS-1000 (pump and conductivity detector) and AS-50 (autosampler) was used to separate the anions. Separated ions were detected with a conductivity detector (Dionex) and quantified based on standard calibration curves for each ion utilizing the manufacturer's Chromeleon 7.1 software (Dionex).

2.7 Statistical analysis

For the statistical analysis, the software Prism 8 was used. An unpaired two-tailed Student's t-test was used to compare the average values of two genotypes/treatments. Significant differences are indicated with asterisks (* $p<0.05$, ** $p<0.01$, and *** $p<0.001$). To compare more than two genotypes/treatments, Holm-Sidak one-way ANOVA or RM ANOVA was used, followed by Tukey post-host statistical analysis test, and the significant differences are indicated with different letters. In addition, the constant variance and normal distribution of data were checked before statistical analysis. The Mann-Whitney rank sum test was used to analyze samples that did not follow normal Gaussian distribution. Asterisks in all figures indicate the significance.

3 | Results

3.1 The dissociation effect of OAS on cysteine synthase complex

Cysteine biosynthesis in plants is restricted by the supply of OAS, which is exclusively produced by SERAT (Heeg et al. 2008; Wirtz et al. 2004; Saito et al. 1994). The prevalent mechanism for regulating SERAT activity is forming the CS complex, which facilitates the activation of SERAT. Upon accumulation of OAS, it binds into the active site of OAS-TL, leading to the dissociation of the CS complex (Hell et al. 2011). Interestingly, a specific point mutation was found in the rice mutant *astol1* in which serine 189 (S189) was replaced by asparagine in the OAS-TL enzyme localized within the chloroplast. This alteration formed a stable and non-dissociable CS complex (Sun et al. 2021). The S189 in this gene is highly conserved in all analyzed OAS-TLs and localized in S102 and S210 in *At*OAS-TL A and *At*OAS-TL C, respectively (Fig. S48). Therefore, to assess the biochemical impact of the same mutation in the conserved serine in Arabidopsis and whether the mutation yields comparable *in vitro* outcomes as in rice, a two-step affinity column-based pull-down analysis (2.4.10 and 2.4.11) was conducted.

To achieve this, 288 amino acid residues from *At*OAS-TL A and 300 amino acid residues from *At*OAS-TL C were deleted to eliminate the encoding transit peptides. S102 and S210 in *At*OAS-TL A and *At*OAS-TL C were replaced by Asp using site-directed mutagenesis of cDNAs (carried out by Dr. S. Sun, COS). Then, the remaining mature polypeptide chains of wild type and mutant *At*OAS-TLs were expressed in *E. coli*, followed by purification (2.4.9 and 2.4.11). The well-characterized cytosolic *At*SERAT1;1 and mitochondrial *At*SERAT2;2 proteins labeled with His-tag in N-terminus were applied as the bait proteins and were similarly expressed in *E. coli*, and purified (2.4.9 and 2.4.10). Subsequently, the HiTrap Chelating

High-Performance Column (GE Healthcare) (Table 2.2) was used to purify the recombinant proteins and study the association of the CS complex.

The recombinant His-tagged *At*SERAT was first coupled to a HiTrapTM column (2.4.10). Then, the bacterial extract containing recombinant *At*OAS-TL expressed in *E. coli* was loaded to the column leading to the binding of the recombinant *At*OAS-TL to the column-bound *At*SERAT. After the formation of the CS complex, the column was loaded by OAS to test whether S102N mutation in *At*OAS-TL A and S210N mutation in *At*OAS-TL C protein affect their association with *At*SERAT proteins in the CS complex (2.4.11). If the complex containing *At*SERAT and *At*OAS-TL dissociates, the recombinant *At*OAS-TL is separated from the complex and washed out in this step, whereas in a non-dissociable complex, recombinant *At*OAS-TL washed out in the final elution in conjugation with *At*SERAT. After collecting the fraction in each step and measuring the amount of proteins by Bradford assay (2.4.2), an equal amount of protein (2 μg) was loaded in the SDS-PAGE gel (2.4.3), followed by western blotting (2.4.4) and immunological detection (2.4.5) of proteins using a polyclonal antibody against the *At*OAS-TL C (1:1000) (Jost et al. 2000). The cross-reactivity of this antibody with all OAS-TL isoforms from Arabidopsis allowed the simultaneous detection of these proteins. The result depicted that the application of OAS dissociated the CS complex consisting of wild-type *At*OAS-TL A and His-*At*SERAT1;1 (Fig. 3.1, a). In contrast, the CS complex consisting of *At*OAS-TL A^{S102N} and His-*At*SERAT1;1 indicated remarkable stability even when subjected to 10 mM OAS (Fig. 3.1, b). Based on this feature, we defined this CS complex as stable.

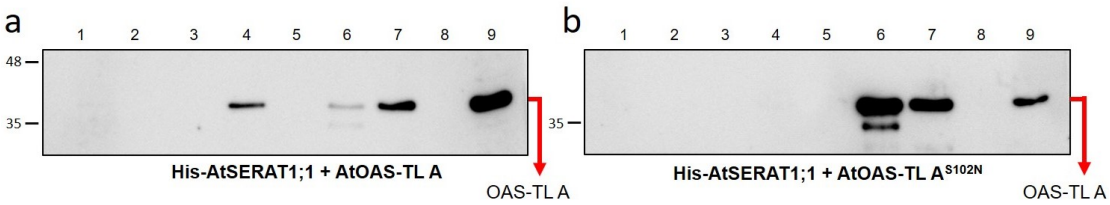

Figure 3.1: ***In vitro* pull-down analysis of the dissociation effect of OAS on CS complex consisting of recombinant cytosolic *At*SERAT1;1 and cytosolic *At*OAS-TL A.** Immunological detection of *At*OAS-TL A in elution fractions of a two steps affinity column-based pull-down analysis. 2 μg of protein from each elution fraction was loaded in the SDS-PAGE gel (2.4.3), followed by western blotting (2.4.4) and immunological detection (2.4.5). The presence of *At*OAS-TL A was detected by a polyclonal antibody against the *At*OAS-TL C (1:1000), able to detect all three OAS-TL isoforms simultaneously. Lane 1: crude extract of His-*At*SERAT1;1; lane 2: flow-through of His-*At*SERAT1;1; lane 3: washing buffer (80mM imidazole); lane 4: OAS elution (10mM OAS + 80mM imidazole); lane 5: washing buffer (80mM imidazole); lane 6: final elution (400mM imidazole); lane 7: crude extract of **a)** *At*OAS-TL A, **b)** *At*OAS-TL A^{S102N}; lane 8: washing buffer (80mM imidazole); lane 9: final elution (400mM imidazole). The uncropped versions of these western blots are depicted in Fig. S1, a,b.

Upon examination of the recombinant CS complex containing mitochondrial His-*At*SERAT2;2 and cytosolic *At*OAS-TL A, a similar outcome was observed. OAS dissociated the CS complex consisting of wild-type *At*OAS-TL A and His-*At*SERAT2;2 (Fig. 3.2, a), whereas it failed to dissociate the CS complex consisting of *At*OAS-TL A^{S102N} and His-*At*SERAT2;2 (Fig. 3.2, b). These results indicated that mutated cytosolic *At*OAS-TL A could make a non-dissociable complex with either cytosolic or mitochondrial *At*SERATs. The weak, low molecular weight signal observed (e.g., in lane six) is likely attributed to the presence of the *E. coli* cycK protein, which is an expected by-product of the co-purification process during the isolation of the recombinant protein (Wirtz et al. 2001).

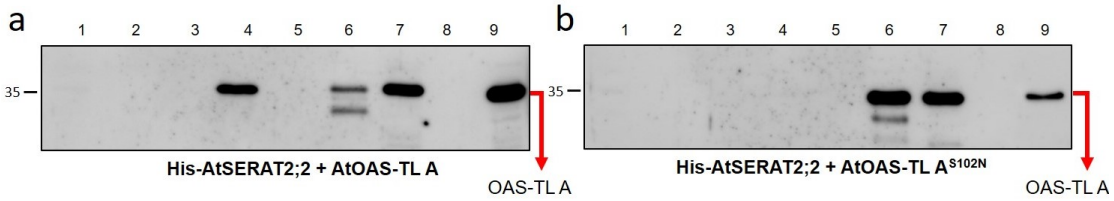

Figure 3.2: ***In vitro* pull-down analysis of the dissociation effect of OAS on CSC consisting of recombinant mitochondrial *At*SERAT2;2 and cytosolic *At*OAS-TL A.** Immunological detection of *At*OAS-TL A in elution fractions of a two steps affinity column-based pull-down analysis. 2 μg of protein from each elution fraction was loaded in the SDS-PAGE gel (2.4.3), followed by western blotting (2.4.4) and immunological detection (2.4.5). The presence of *At*OAS-TL A was detected by a polyclonal antibody against the *At*OAS-TL C (1:1000), able to detect all three OAS-TL isoforms simultaneously. Lane 1: crude extract of His-*At*SERAT2;2; lane 2: flow-through of His-*At*SERAT2;2; lane 3: washing buffer (80mM imidazole); lane 4: OAS elution (10mM OAS + 80mM imidazole); lane 5: washing buffer (80mM imidazole); lane 6: final elution (400mM imidazole); lane 7: crude extract of **a)** *At*OAS-TL A, **b)** *At*OAS-TL A^{S102N}; lane 8: washing buffer (80mM imidazole); lane 9: final elution (400mM imidazole). The uncropped versions of these western blots are depicted in Fig. S2, a,b.

However, the result of the recombinant CS complex containing mutated mitochondrial *At*OAS-TL C^{S210N} differed from the mutated cytosolic *At*OAS-TL A^{S102N}. Although OAS dissociated the complex consisting of cytosolic His-*At*SERAT1;1 and either *At*OAS-TL C or *At*OAS-TL C^{S210N} (Fig. 3.3, a and b), it failed to dissociate the complex containing mitochondrial His-*At*SERAT2;2 and *At*OAS-TL C^{S210N} (Fig. 3.4, b). In summary, it has been ascertained that the mutated mitochondrial *At*OAS-TL C^{S210N} can form a stable complex with mitochondrial *At*SERAT2;2. However, it has been observed that it lacks the capacity to do so with cytosolic *At*SERAT1;1.

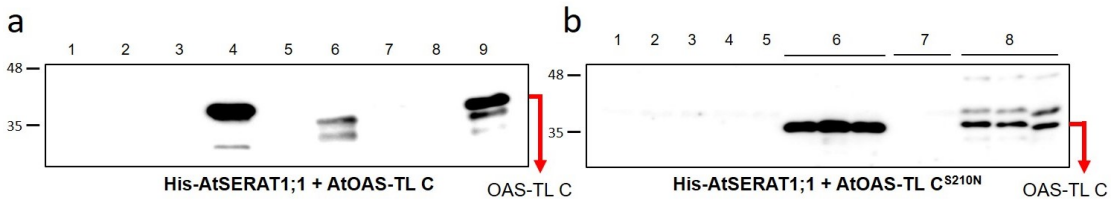

Figure 3.3: ***In vitro* pull-down analysis of the dissociation effect of OAS on CSC consisting of recombinant cytosolic *At*SERAT1;1 and mitochondrial *At*OAS-TL C.** Immunological detection of *At*OAS-TL C in elution fractions of a two steps affinity column-based pull-down analysis. 2 μg of protein from each elution fraction was loaded in the SDS-PAGE gel (2.4.3), followed by western blotting (2.4.4) and immunological detection (2.4.5). The presence of *At*OAS-TL C was detected by a polyclonal antibody against the *At*OAS-TL C (1:1000), able to detect all three OAS-TL isoforms simultaneously. **a)** lane 1: crude extract of His-*At*SERAT1;1; lane 2: flow-through of His-*At*SERAT1;1; lane 3: washing buffer (80mM imidazole); lane 4: OAS elution (10mM OAS + 80mM imidazole); lane 5: washing buffer (80mM imidazole); lane 6: final elution (400mM imidazole); lane 7: crude extract of His-*At*SERAT1;1; lane 8: washing buffer (80mM imidazole); lane 9: final elution (400mM imidazole). **b)** lane 1: crude extract of His-*At*SERAT1;1; lane 2: flow-through of His-*At*SERAT1;1; lane 3: washing buffer (80mM imidazole); lane 4: OAS elution (10mM OAS + 80mM imidazole) to get rid of bacterial OAS-TL (this step is done before loading the *At*OAS-TL C^{S210N} in the column); lane 5: washing buffer (80mM imidazole); lane 6: OAS elution (10mM OAS + 80mM imidazole) (this step is done after loading the *At*OAS-TL C^{S210N} in the column); lane 7: washing buffer (80mM imidazole); lane 8: final elution (400mM imidazole). The uncropped versions of these western blots are depicted in Fig. S3, a,b.

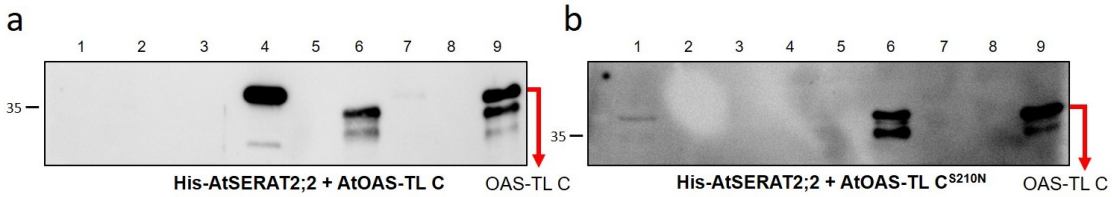

Figure 3.4: ***In vitro* pull-down analysis of the dissociation effect of OAS on CSC consists of recombinant mitochondrial *At*SERAT2;2 and mitochondrial *At*OAS-TL C.** Immunological detection of *At*OAS-TL C in elution fractions of a two steps affinity column-based pull-down analysis. 2 μg of protein from each elution fraction was loaded in the SDS-PAGE gel (2.4.3), followed by western blotting (2.4.4) and immunological detection (2.4.5). The presence of *At*OAS-TL C was detected by a polyclonal antibody against the *At*OAS-TL C (1:1000), able to detect all three OAS-TL isoforms simultaneously. Lane 1: crude extract of His-*At*SERAT2;2; lane 2: flow-through of His-*At*SERAT2;2; lane 3: washing buffer (80mM imidazole); lane 4: OAS elution (10mM OAS + 80mM imidazole); lane 5: washing buffer (80mM imidazole); lane 6: final elution (400mM imidazole); lane 7: crude extract of His-*At*SERAT2;2; lane 8: washing buffer (80mM imidazole); lane 9: final elution (400mM imidazole). The uncropped versions of these western blots are depicted in Fig. S4, a,b.

3.2 Introducing mutated cytosolic and mitochondrial *At*OAS-TL into *Arabidopsis*

To introduce the specific point mutation in S102 in cytosolic *At*OAS-TL A and S210 in mitochondrial *At*OAS-TL C proteins, different single/double mutants of Arabidopsis were utilized. Selected mutants lacked the functional endogenous *At*OAS-TL A in the cytosol (*oastla*) or *At*OAS-TL C in the mitochondria (*oastlc*); therefore, the impact of the specific point mutation can be studied across multiple cellular locations without the interference of endogenous *At*OAS-TLs. Moreover, to study the importance of the SERAT activity in the CS complex regulatory role, plants lacking the functional endogenous cytosolic *At*SERAT1;1 were likewise transformed with recombinant cytosolic *At*OAS-TL A. Additionally, to eliminate the effect of endogenous *At*OAS-TL A in transformed *At*SERAT1;1, double mutants lacking both, functional endogenous cytosolic *At*OAS-TL A and *At*SERAT1;1, were similarly transformed with recombinant cytosolic *At*OAS-TL A. Exclusive details of the utilized mutants and the constructs they were complemented with are provided in Table 2.16.

The phenotype, localization of T-DNA insertion, and the primer binding sites used for the molecular characterization of the respective mutants are illustrated in Fig. 3.5. The *oastla*, *oastlc*, *serat1;1*, and *oastla*serat1;1* (abbreviated *a1;1*) mutants had been previously characterized (Heeg et al. 2008; Watanabe et al. 2008b; Haas et al. 2008). Although *oastla* displayed a phenotype similar to wild-type plants, *oastlc*, *serat1;1*, and *a1;1* plants were smaller than wild-type plants (Fig. 3.5).

The constructs (Fig. S20) for Agrobacterium-mediated gene transfer using floral dip transformation of wild type and mutant *A. thaliana* (Col-0) were provided kindly by Dr. S. Sun (COS). The seeds of T0 transformed plants (Table 2.16) were collected and selected first on plates containing 1/2 MS medium (Table 2.4) supplemented with 10 μg ml^{-1} hygromycin (Table 2.3). The efficiency of the transformation was about 2%. Then, the four-week-old survival seedlings were transferred to the soil and grew under short-day conditions until T1 seeds could be harvested (2.5.2). The presence of the T-DNA insertion and homozygosity of T0 plants was confirmed by PCR (Table 2.11) using the primer pairs (Table 2.10) shown in Figure 3.5 (data are not provided).

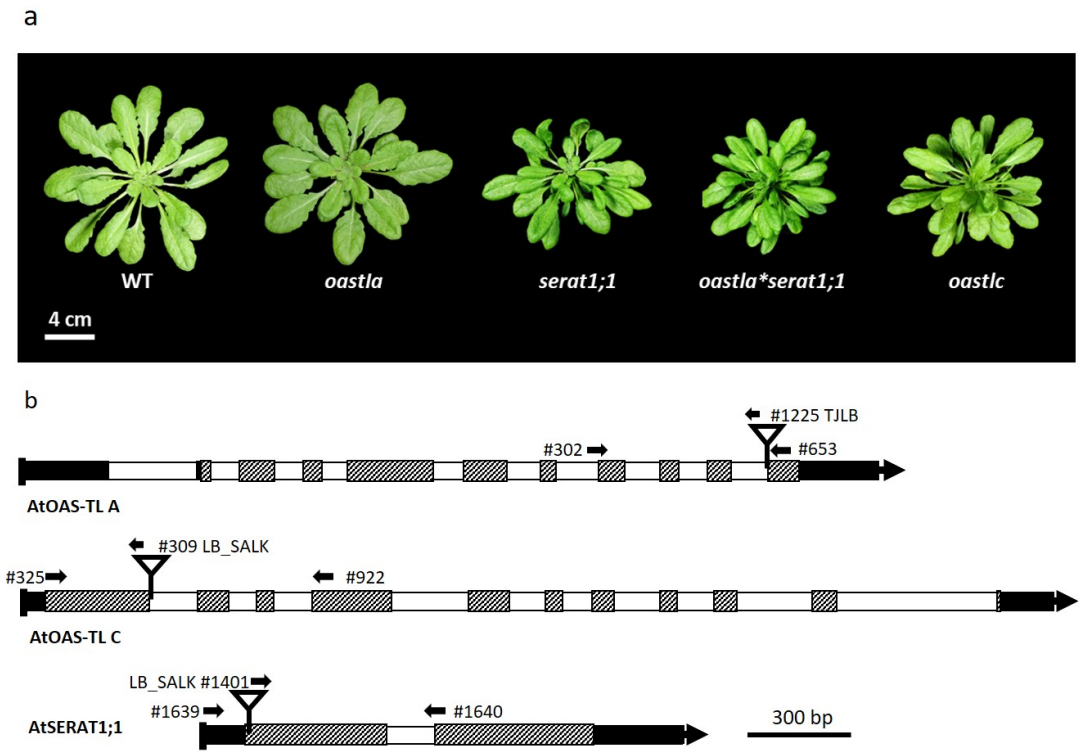

Figure 3.5: **Growth phenotype and localization of T-DNA insertion of the single/double mutants used in this study. a)** The phenotype of the eight-week-old wild-type (WT), *oastla*, *serat1;1*, *oastla*serat1;1* (*a1;1*), and *oastlc* plants. **b)** Gene model of the *Arabidopsis thaliana* gene *At*OAS-TL A (AT4G14880), *At*OAS-TL C (AT3G59760), and *At*SERAT1;1 (AT5G56760). Black, cross-hatching, and white rectangles represent UTRs, exons, and introns, respectively. Triangles define the T-DNA insertions. Black arrows and appendant numbering indicate the used primers; sequences are given in Table 2.10.

3.3 Characterization of T1 transformants

3.3.1 Genotyping of T1 transgenes to confirm the presence of insertion

Approximately 15-18 of four-week-old T1 transformants surviving on plates containing 1/2 MS medium (Table 2.4) supplemented with 10 μg ml^{-1} hygromycin (Table 2.3) were translocated to the soil and grew under the short-day conditions (2.5.2). Including three transformed lines within each group of transformants is considered the minimum number for establishing the reliability of the observed target effect. However, given the specific objectives of this study, which encompassed the characterization of the CS complex, the dominant effect of the mutation, and practical considerations regarding the handling of plants in the T2 generation, a total of five lookalike T1 individuals were selected from each group. This

decision ensured continuity into the subsequent generation in case of line loss or the emergence of aberrant traits in any particular line. Genotyping of these plants allowed us to verify the presence of the transgene in the transformants for further analysis. The genotyping was continued until a minimum of five positive candidates in each group were identified. For this purpose, DNA (2.3.1) was extracted first from the six-week-old soil-grown plants under the short-day condition (2.5.2). Then, PCR (Table 2.11) was performed using primer pairs (Table 2.10) aligned to the wild-type gene. Therefore, in each gel, the larger signal represents the gDNA, while the smaller signal represents the cDNA of the transgene (Fig. 3.6).

The *oastla* and *a1;1* plants complemented with either *At*OAS-TL A or *At*OAS-TL A^{S102N} represented 298bp signal corresponding to the cDNA in the transgene, whereas complemented wild-type plants displayed both 600bp and 298bp signals related to gDNA and cDNA of *AtOAS-TL A*, respectively (Fig. 3.6, a and c). Similarly, the *oastlc* complemented with either SHMT-*At*OAS-TL A or SHMT-*At*OAS-TL A^{S102N}, *serat1;1* (*At*OAS-TL A), and *serat1;1* (*At*OAS-TL A^{S102N}) represented both 600bp and 298bp signals related to gDNA and cDNA of *AtOAS-TL A*, respectively (Fig. 3.6, b-c). Likewise, *oastlc* (*At*OAS-TL C) and *oastlc* (*At*OAS-TL C^{S210N}) indicated the 573bp signal related to the cDNA in the transgene, while WT (*At*OAS-TL C) and WT (*At*OAS-TL C^{S210N}) demonstrated both 950bp and 573 bp signals correspond to the gDNA and cDNA of *AtOAS-TL C* gene (Fig. 3.6, d). The complete list of all transformants' names and abbreviations is provided in Table 2.16.

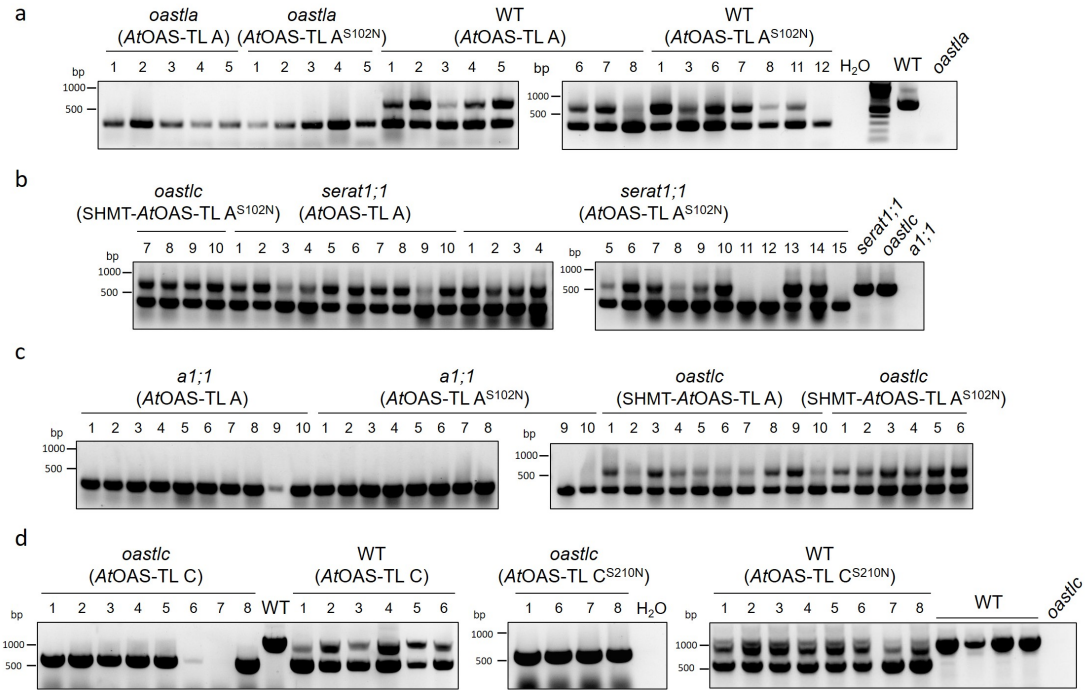

Figure 3.6: **Confirmation of insertion into the genome of T1 transformants by genotyping.** Representative pictures illustrate genomic screening of T1 plants complemented with either *At*OAS-TLA and *At*OAS-TLC or the mutated versions *At*OAS-TL A^{S102N} and *At*OAS-TL C^{S210N}. The genomic DNA of six-week-old individual plants was extracted (2.3.1), and the presence of the respective transgene was detected by PCR (Table 2.11) using primer combinations of 302+653 for **a)** *oastla* and wild-type plants complemented with *At*OAS-TLA and *At*OAS-TL A^{S102N}, **b-c)** *serat1;1* and *a1;1* complemented with *At*OAS-TLA and *At*OAS-TL A^{S102N}, and *oastlc* complemented with SHMT-*At*OAS-TLA and SHMT-*At*OAS-TL A^{S102N}, and 325+922 primer combination for **d)** *oastlc* and wild-type plants complemented with *At*OAS-TLC and *At*OAS-TL C^{S210N}. Wild type (WT), *oastla*, *serat1;1*, *a1;1*, *oastlc*, and H_2O served as control samples. The uncropped versions of these gel pictures are depicted in Fig. S5 and Fig. S6.

3.3.2 Transcript analysis of T1 transformants of *oastl* mutants

Having confirmed the presence of the T-DNA insertion in five selected lines of each transformation experiment, the expression levels of the respective OAS-TL variants were analysed in order to identify suitable lines for further experiments towards protein levels and physiological repsonses. The CaMV 35S promoter had been used to control the expression of the OAS-TL variants in the constructs used for transformation of wild-type, *oastla*, *oastlc*, *serat1;1* and *a1;1* mutants; hence, it was expected to observe a high transcript level of *AtOAS-TL* in the knock-out mutant for the same gene. Therefore, quantitative expression analysis for the *AtOAS-TL* transcript was performed by operating qRT-PCR (2.3.13) to assess the expression of the *OAS-TL* variants in T1 individuals. Accordingly, the total RNA (2.3.11) was extracted

from the leaves of six-week-old plants, followed by cDNA synthesis (2.3.12), and the relative abundance of the designated expressed genes was determined by qRT-PCR (2.3.13).

The *oastla* and wild-type plants that were complemented or transformed, with either *At*OAS-TL A or *At*OAS-TL A^{S102N}, depicted a 66-361 and a 54-311 fold increase, respectively, in *AtOAS-TL A* transcript level compared to the WT control (Fig. 3.7, a). The increase was slighter in *serat1;1* and *a1;1* transformants transformed by similar constructs. Nonetheless, they demonstrated a 19-100 and a 14-56 fold increase in *AtOAS-TL A* transcript level, respectively, compared to the WT control (Fig. 3.7, b-c). The *oastlc* mutant and wild-type plants transformed by either *At*OAS-TL C or *At*OAS-TL C^{S210N} likewise showed a 9-32 and a 6-89 fold increase in *AtOAS-TL C* transcript level, respectively, compared to the WT control (Fig. 3.8, a). Similarly, *oastlc* mutant transformed by cytosolic *At*OAS-TL A and *At*OAS-TL A^{S102N} indicated a 19-133 fold increase in *AtOAS-TL A* transcript level compared to the control plants(Fig. 3.8, b). According to the findings, there was a noticeable increase in the expression of the *At*OAS-TL genes in the transformed samples compared to the control group.

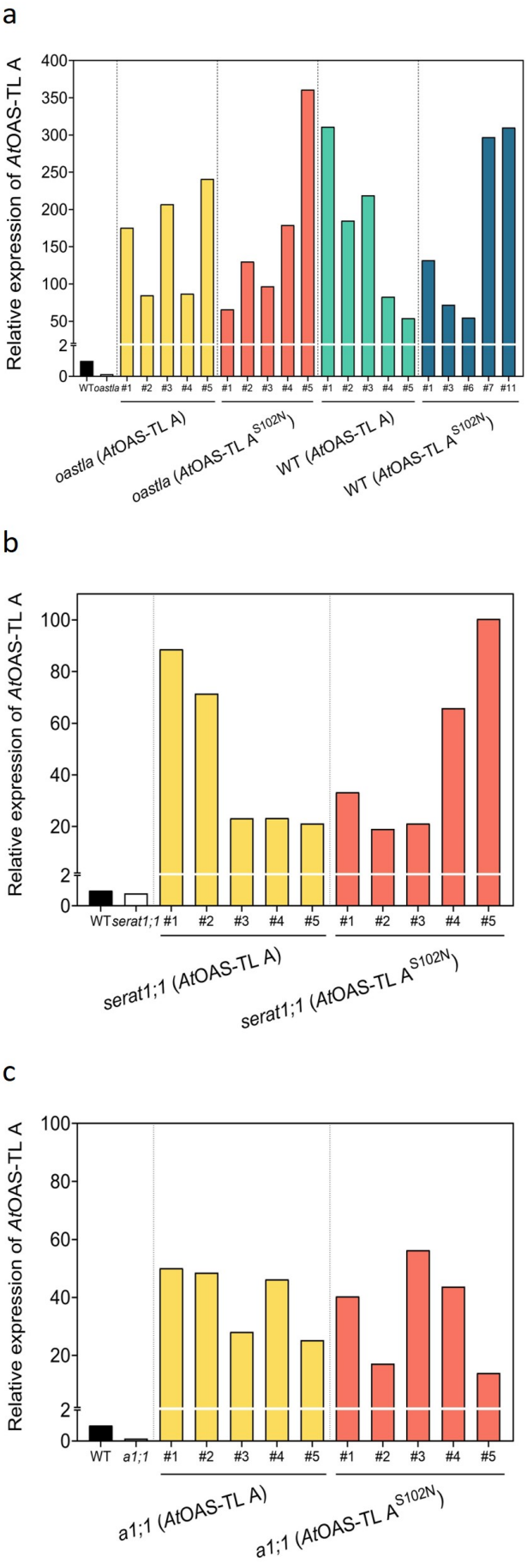

Figure 3.7: **The expression level of *AtOAS-TL A* in T1 transformants.** The transcript level of *AtOAS-TL A* in **a**) *oastla* and wild-type complemented with *At*OAS-TL A/*At*OAS-TL A^{S102N} **b**) *serat1;1* complemented with *At*OAS-TL A/*At*OAS-TL A^{S102N} and **c**) *a1;1* complemented with *At*OAS-TL A/*At*OAS-TL A^{S102N} was determined by qRT-PCR (2.3.13) using 4632+4633 primer pairs (Table 2.10) in the leaves of 6-week-old soil-grown plants cultivated under short-day conditions (2.5.2). Five individuals in every group of transformants were chosen. Values were normalized to *TIP41* (AT4G34270) and are presented relative to WT control. WT transcript level was set to one.

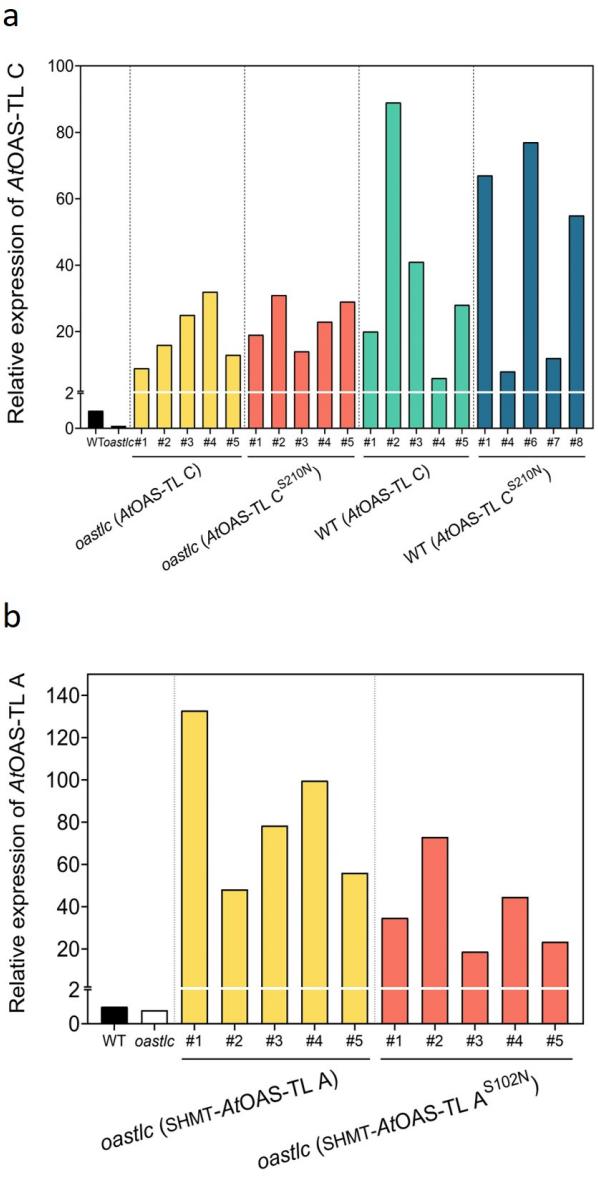

Figure 3.8: **The expression level of *AtOAS-TL C* and *AtOAS-TL A* in T1 transformants.** The transcript level of *AtOAS-TL C* in **a**) *oastlc* and wild-type complemented with *At*OAS-TL C/*At*OAS-TL C^{S210N} and *AtOAS-TL A* in **b**) *oastlc* complemented with SHMT-*At*OAS-TL A/SHMT-*At*OAS-TL A^{S102N} was determined by qRT-PCR (2.3.13) using 5332+5333 primer pairs (Table 2.10) in the leaves of 6-week-old soil-grown plants cultivated under short-day conditions (2.5.2). Five individuals in every group of transformants were chosen. Values were normalized to *TIP41* (AT4G34270) and are presented relative to WT control. WT transcript level was set to one.

3.4 Phenotype of T2 plants of complemented *oastl*, *serat*, and *a1;1* mutants

Figure 3.9 shows the phenotype of T2 transformants that represent the selected five lines of each transformation experiment. The growth retardation and later flowering in *oastlc* mutants compared to WT, *oastla*, *serat1;1*, and *a1;1* (Heeg et al. 2008; Watanabe et al. 2008b; Khan et al. 2010) were likewise observed in these transformants. However, complementing these mutants with wild-type or mutated *At*OAS-TLs did not further change their growth phenotype or flowering time (Fig. 3.9).

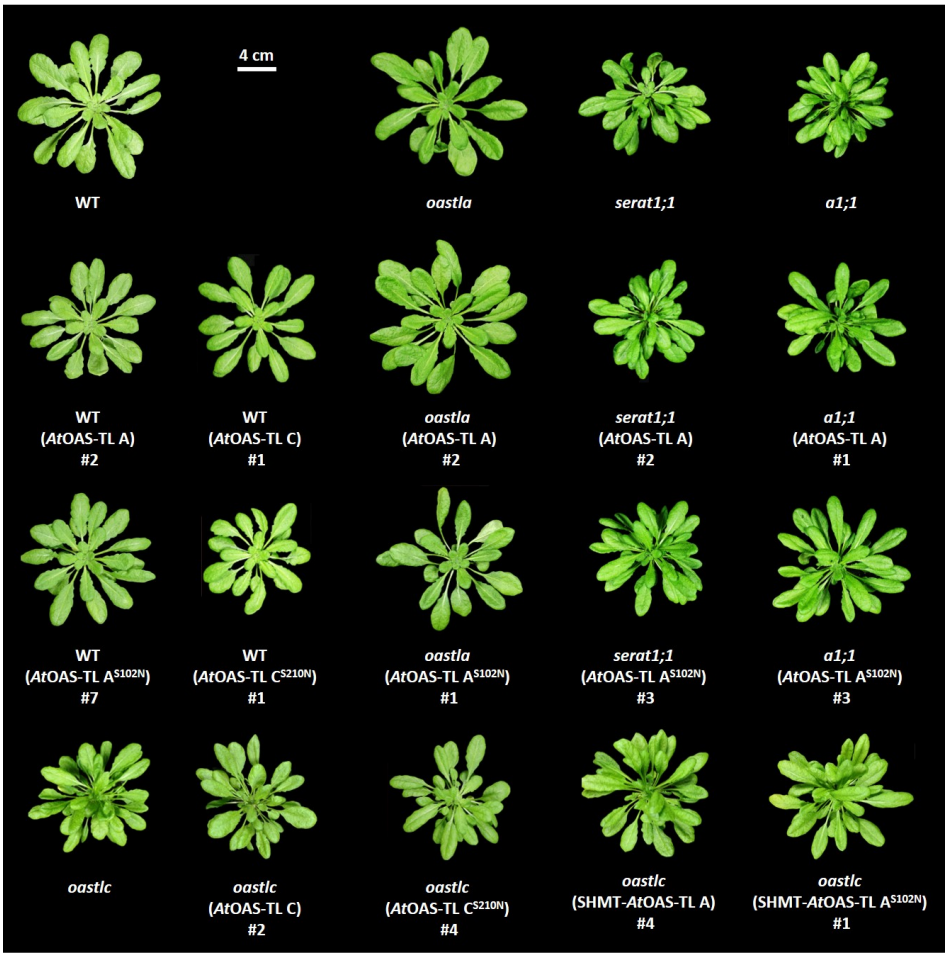

Figure 3.9: **Growth phenotype of the T2 transformants complemented with cytosolic and mitochondrial *At*OAS-TL.** The phenotype of the eight-week-old wild-type (WT), *oastla*, *serat1;1*, *a1;1*, *oastlc* complemented with either *At*OAS-TL A or AtAOS-TL A^{S102N}, and WT and *oastlc* complemented with either *At*OAS-TL C or AtAOS-TL CS^{210N} plants.

3.5 Characterization of T2 transformants

3.5.1 Genotyping of T2 transgenes

Five phenotypically similar T1 individuals were selected from each group and subsequently characterized to follow in the T2 generation. However, some individuals exhibited limited seed production or poor germination rates in T2, resulting in less than five lines generated in certain T2 groups. Nevertheless, the T2 seeds were selected again on plates containing 1/2 MS medium (Table 2.4) supplemented with 10 μg ml^{-1} Hygromycin (Table 2.3). Then, the four-week-old survival seedlings were translocated to the soil and grew under short-day conditions (2.5.2). The presence of the transgene in T2 individuals was confirmed by genotyping. The methodology employed for genotyping was consistent with that described for T1

plants, as previously elucidated in detail (3.3.1); therefore, this section will not address the specific procedural details to maintain conciseness and avoid redundancy.

Five individuals were selected and genotyped from each line of complemented *oastla* (3.10, a-b) and *a1;1* (S9, a-b) with either *At*OAS-TL A or *At*OAS-TL A^{S102N}, all of which exhibited the 298bp signal related to the cDNA in the transgene. In addition, at least five individuals were also selected and genotyped from three lines of WT (*At*OAS-TL A) and four lines of WT (*At*OAS-TL A^{S102N}), all of which showed 600bp and 298bp signals corresponding to gDNA and cDNA of *AtOAS-TL A*, respectively (3.10, b-c). The *serat1;1* (*At*OAS-TL A), *serat1;1* (*At*OAS-TL A^{S102N}), *oastlc* (SHMT-*At*OAS-TL A), and *oastlc* (SHMT-*At*OAS-TL A^{S102N}) likewise represented 600bp and 298bp signals corresponding to gDNA and cDNA of *AtOAS-TL A*, respectively (S9, b-e).

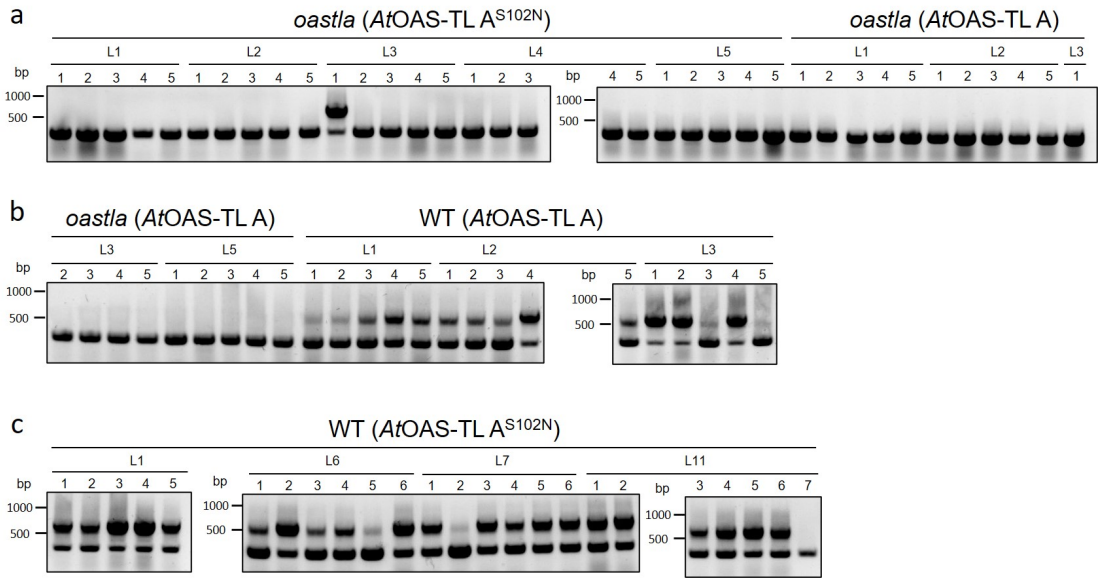

Figure 3.10: **Confirmation of insertion into the genome of T2 transformants by genotyping.** Representative pictures of agarose gels detecting the presence of the transgene. To perform PCR (Table 2.11), DNA was extracted (2.3.1) from 6-week-old plants grown under short-day conditions on soil (2.5.2). Then, PCR was performed with 302+653 primer pairs (Table 2.10). The smaller signal with 298bp is related to the cDNA of *AtOAS-TL A*, and the bigger one with 600bp is related to the gDNA. WT and *oastla* served as the control sample shown in S9. The uncropped versions of these gel pictures are depicted in Fig. S7.

Likewise, five individuals were selected from each T2 line of plants that had undergone complementation with mitochondrial *At*OAS-TL C to examine the presence of the transgene through genotyping. The *oastlc* mutants were complemented with either *At*OAS-TL C or

*At*OAS-TL C^{S210N} indicated the 573bp signal related to the cDNA of the *AtOAS-TL C* gene inserted in the construct, whereas the complemented wild-type plants demonstrated 573bp and 950bp signals related to the cDNA and gDNA of the gene of interest, respectively (Fig. 3.11).

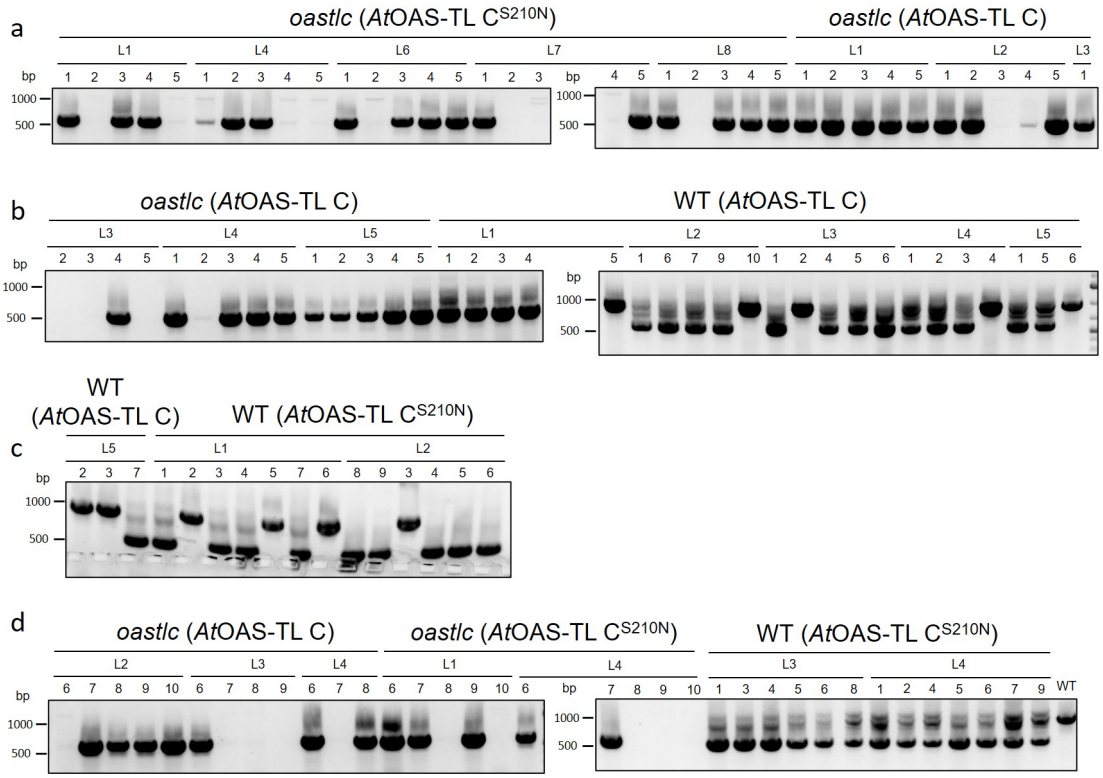

Figure 3.11: **Confirmation of insertion into the genome of T2 transformants by genotyping.** Representative pictures of agarose gels detecting the presence of the transgene. To perform PCR (Table 2.11), DNA was extracted (2.3.1) from 6-week-old plants grown under short-day conditions on soil (2.5.2). Then, PCR was performed with 325+922 primer pairs (Table 2.10). The smaller signal with 573bp is related to the cDNA of *At*OAS-TL C, and the bigger one with 950bp is related to the gDNA. WT and *oastlc* served as the control sample shown in S9. The uncropped versions of these gel pictures are depicted in Fig. S8.

3.5.2 Transcript analysis of T2 transformants

Quantitative expression analysis for the T2 transformants was performed to investigate the transcript level of the *AtOAS-TL A* and *AtOAS-TL C*. Accordingly, the total RNA (2.3.11) was extracted from the leaves of six-week-old soil-grown plants (2.5.2), followed by cDNA synthesis (2.3.12). The relative abundance of the designated expressed genes was determined with qRT-PCR (2.3.13) using 4632+4633 primer pairs for *AtOAS-TL A* and 5332+5333 primer

pairs for *AtOAS-TL C* (Table 2.10). The *oastla* and wild-type plants were complemented with either *At*OAS-TL A or *At*OAS-TL A^{S102N}, depicting a 2-117 and 11-241 fold increase compared to the WT control, respectively (Fig. 3.12, a). This increase was slighter in mitochondrial transformants. The *oastlc* and WT plants complemented with mitochondrial *At*OAS-TL C representing a 1-112 and 3-125 fold increase in *AtOAS-TL C* transcript level, respectively, compared to the WT control (Fig. 3.12, b).

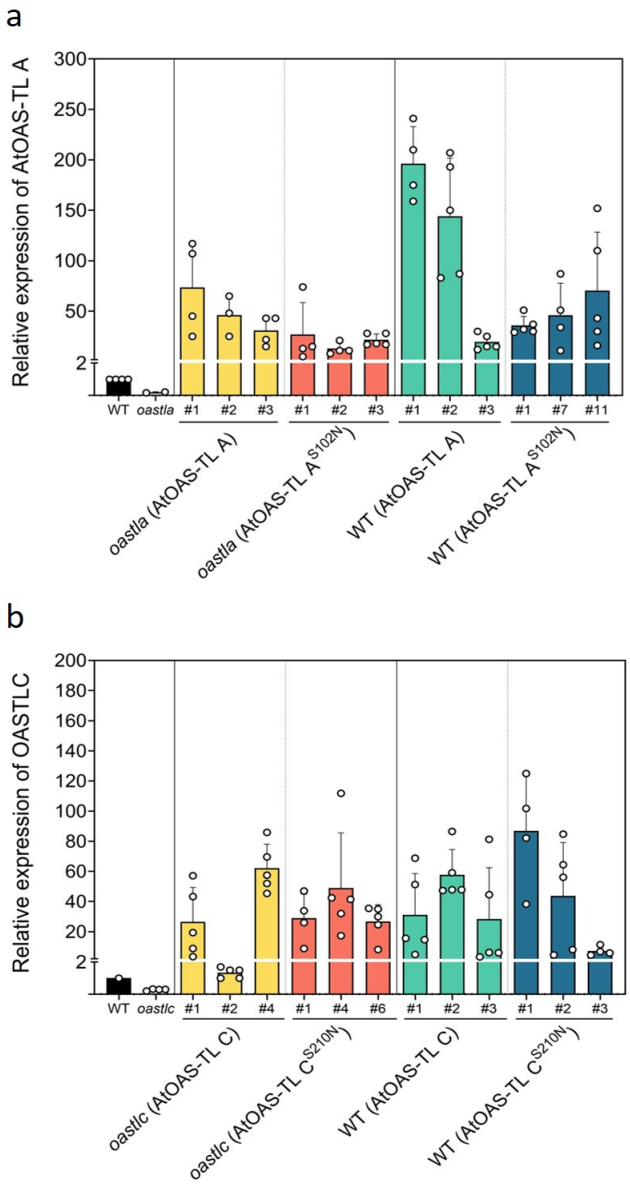

Figure 3.12: **The mRNA expression level of *AtOAS-TL* in T2 transformants.** The transcript level of **a)** *AtOAS-TL A* (Table 2.10; 4632+4633 primer pairs) and **b)** *AtOAS-TL C* (Table 2.10; 5332+5333 primer pairs) was determined by qRT-PCR (2.3.13) in the leaves of 6-week-old soil-grown plants cultivated under short-day conditions (2.5.2). Values were normalized to TIP41 (AT4G34270) and are presented relative to WT control. Each bar represented the mean ± SE of three to five biological replicates in each line.

3.5.3 Biochemical analysis of T2 transformants

qRT-PCR results demonstrated a specific up-regulation of *AtOAS-TL A* and *AtOAS-TL C*; therefore, immunoblot analysis (2.4.5) was performed for the T2 generation plants to investigate if the higher transcript level of *AtOAS-TL A* and *AtOAS-TL C* in the transformants would result in a higher OAS-TL A and OAS-TL C protein amount. Therefore, total soluble proteins (2.4.1) were extracted from the leaves of six-week-old soil-grown plants under short-day conditions (2.5.2). The concentration of proteins was measured by Bradford assay (2.4.2), and an equal amount of protein of each sample was separated by performing SDS-PAGE gel (2.4.3), followed by western blotting (2.4.4) and immunological detection (2.4.5). Immunosignals of leaf protein extracts were detected with a polyclonal antibody against Arabidopsis OAS-TL C (Jost et al. 2000). Cross-reaction with OAS-TL isoforms, giving rise to the detection of three different isoforms using the same antibody. In order to verify the mutant lines used and the identity of immunosignals the whole leaf exracts of *oastla*, *oastlb* and *oastlc* mutants were analysed. The first (small), second (middle), and third (large) signals with >35 kDa protein size belong to OAS-TL A, OAS-TL B, and OAS-TLC, respectively (Fig. 3.13). For the loading control, either amido black or ponceau staining was used to stain the large subunit of ribulose-1,5-bisphosphate carboxylase/oxygenase protein.

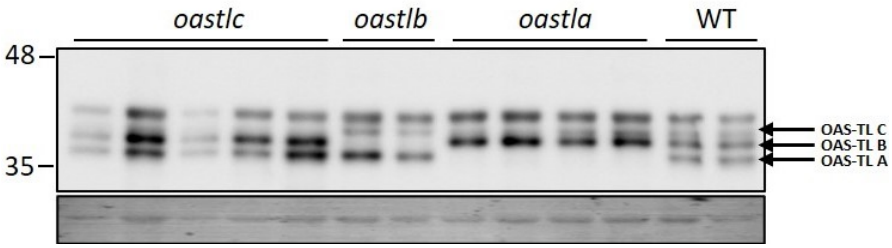

Figure 3.13: **Immunological detection of different Arabidopsis *At*OAS-TL isoforms.** Soluble proteins were extracted (2.4.1) from the leaves of six-week-old plants grown on soil under short-day conditions (2.5.2). Separated proteins (10 μg per lane) by SDS-PAGE (2.4.3) were immunologically detected (2.4.4 and 2.4.5) with the polyclonal antibody against Arabidopsis OAS-TLC in 1:1000 dilution. Cross-reaction with OAS-TL isoforms causes the detection of three signals. The first signal from the bottom (the smallest one) is OAS-TL A, the second one (middle) is OAS-TL B, and the third one (larger) is OAS-TL C. The fourth signal (the largest one on top) is a non-specific signal caused by cross-reaction. The Loading control (LC) represents the intensities of the large subunit of ribulose-1,5-bisphosphate carboxylase/oxygenase protein in the samples stained with ponceau staining (Table 2.3) used for quantification of the signals. The complete membrane pictures are depicted in Fig. S10.

3.5.3.1 Immunoblot analysis of *oastla* and wild-type T2 plants complemented with cytosolic *At*OAS-TL A

Based on the results of the immunoblotting analysis, it appears that the majority of T2 transformants exhibited a significant increase in the expression of OAS-TL A and OAS-TL C proteins, though the intensities of this increase varied. Interestingly, the presence of OAS-TL A protein was confirmed in the complemented *oastla* (*At*OAS-TL A) (Fig. 3.14, a-c), *oastla* (*At*OAS-TL A^{S102N}) (Fig. 3.14, d-e), WT (*At*OAS-TL A) (Fig. 3.14, f-g), and WT (*At*OAS-TL A^{S102N}) (Fig. 3.14, h) plants, which served to validate the transcript analysis (as described in section 3.5.2). Notably, the upregulation of OAS-TL A protein expression was more pronounced in complemented *serat1;1* (*At*OAS-TL A^{S102N}) transformants (Fig. 3.15, c-d) as compared to *serat1;1* (*At*OAS-TL A) transformants (Fig. 3.15, a-b). Similarly, *a1;1* (*At*OAS-TL A^{S102N}) transformants showed greater upregulation of OAS-TL A protein expression than *a1;1* (*At*OAS-TL A) transformants (Fig. 3.15, e-h). Overall, these findings provide valuable insights into the differential expression of OAS-TL A and OAS-TL C proteins in various transformants, which could prove useful for future research in this area.

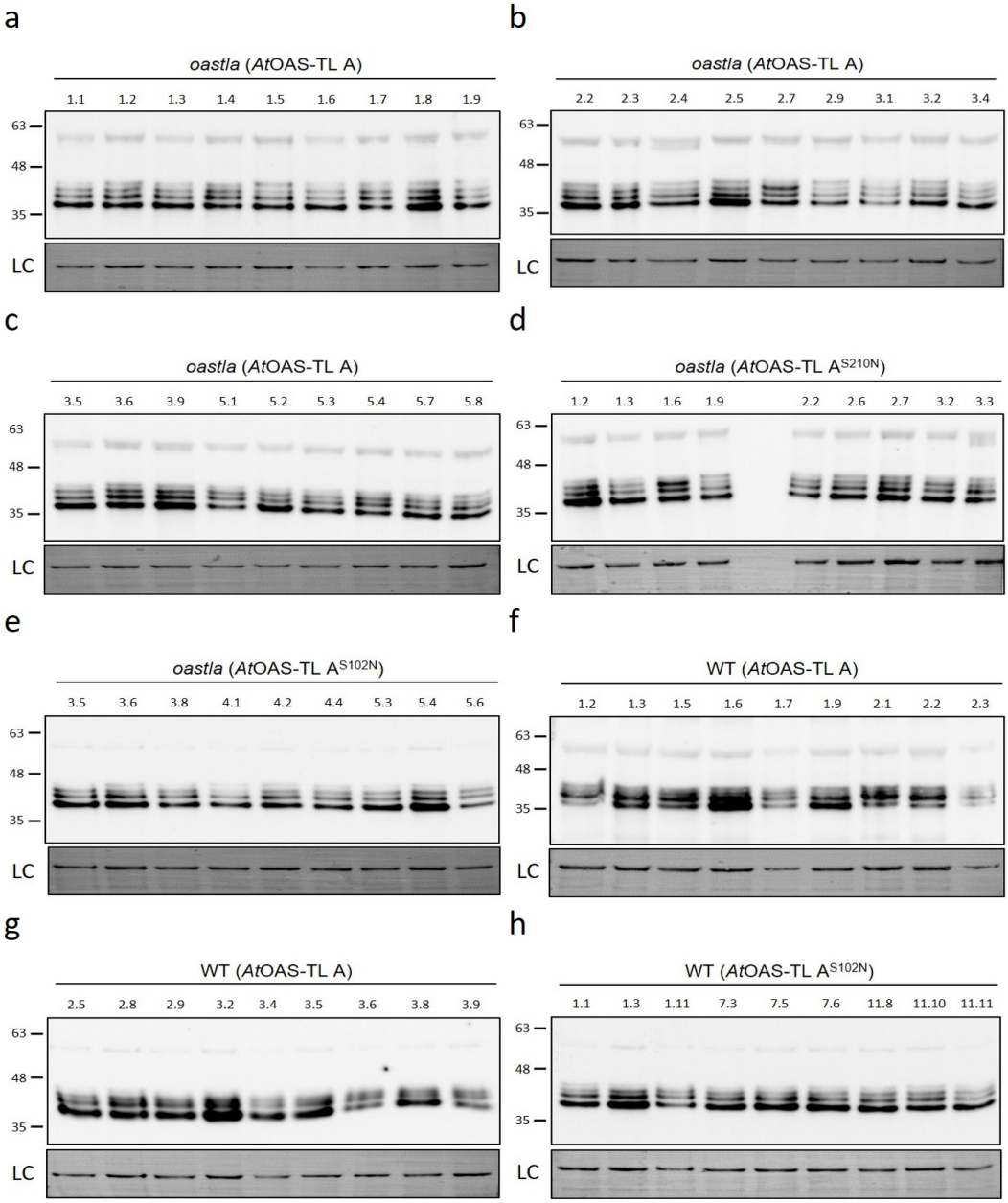

Figure 3.14: **Immunoblot analysis of *At*OAS-TL A protein in T2 plants. a-h)** Immunological detection of OAS-TL A on T2 generation. Soluble proteins were extracted (2.4.1) from the leaves of six-week-old plants grown on soil under short-day conditions (2.5.2). Separated proteins (10 μg per lane) by SDS-PAGE (2.4.3) were immunologically detected (2.4.4 and 2.4.5) with the polyclonal antibody against Arabidopsis OAS-TLC in 1:1000 dilution. Cross-reaction with OAS-TL isoforms causes the detection of three signals, of which the first signal from the bottom (the smallest one) is OAS-TL A, the second one (middle) is OAS-TL B, and the third one (larger) is OAS-TL C. The fourth signal (the largest one on top) is a non-specific signal caused by cross-reaction. The Loading control (LC) represents the intensities of the large subunit of ribulose-1,5-bisphosphate carboxylase/oxygenase protein in the samples stained with amido black (Table 2.3). Controls are represented in 3.13.The complete membrane pictures are depicted in Fig. S11 and S12.

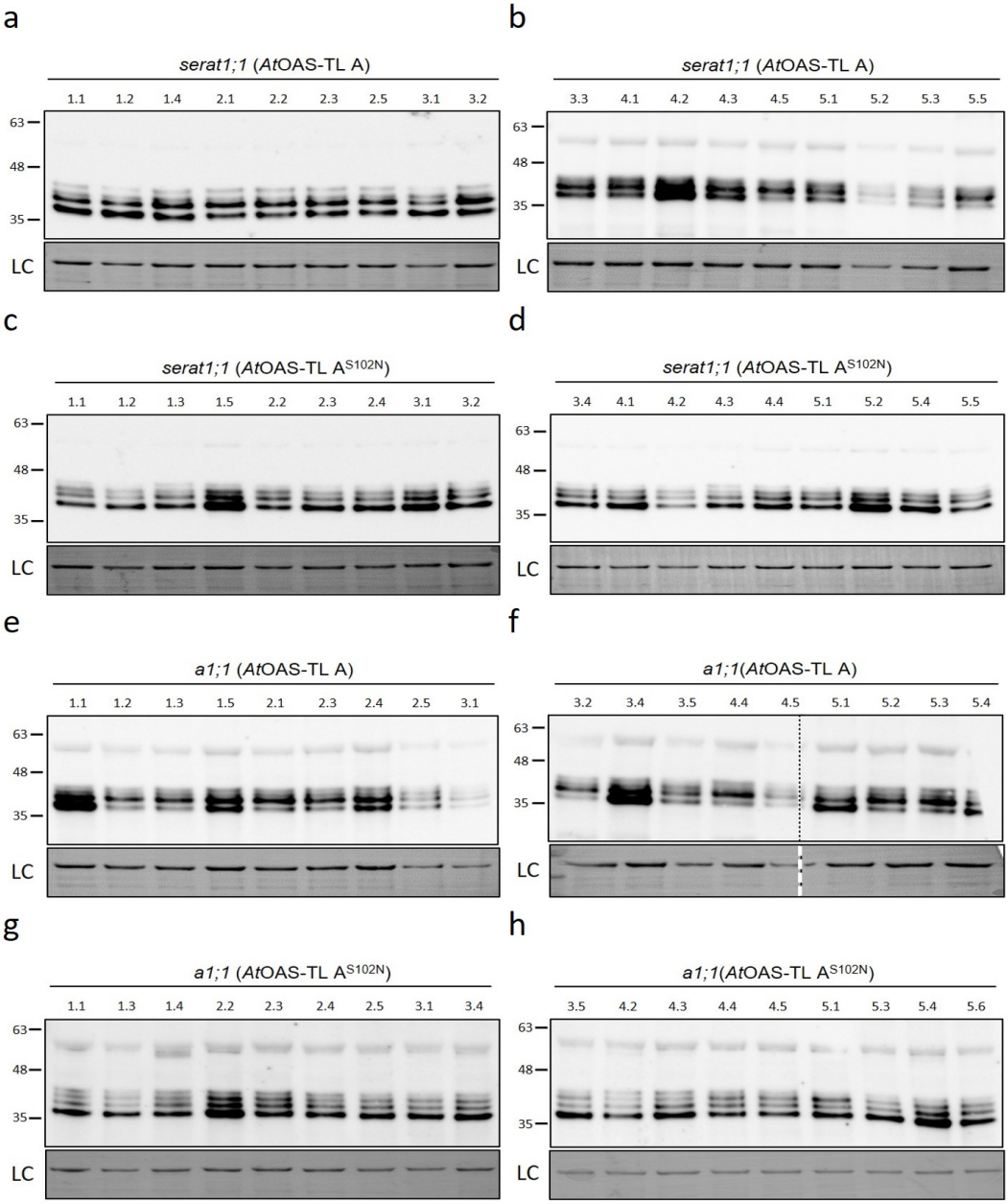

Figure 3.15: **Immunoblot analysis of *At*OAS-TL A protein in T2 plants. a-h)** Immunological detection of OAS-TL A on T2 generation. Soluble proteins were extracted (2.4.1) from the leaves of six-week-old plants grown on soil under short-day conditions (2.5.2). Separated proteins (10 μg per lane) by SDS-PAGE (2.4.3) were immunologically detected (2.4.4 and 2.4.5) with the polyclonal antibody against Arabidopsis OAS-TLC in 1:1000 dilution. Cross-reaction with OAS-TL isoforms causes the detection of three signals, of which the first signal from the bottom (the smallest one) is OAS-TL A, the second one (middle) is OAS-TL B, and the third one (larger) is OAS-TL C. The fourth signal (the largest one on top) is a non-specific signal caused by cross-reaction. The Loading control (LC) represents the intensities of the large subunit of ribulose-1,5-bisphosphate carboxylase/oxygenase protein in the samples stained with amido black (Table 2.3). Controls are represented in 3.13. The complete membrane pictures are depicted in Fig. S13 and S14.

3.5.3.2 Immunoblot analysis of *oastlc* and wild-type T2 plants complemented with mitochondrial *At*OAS-TL C

The outcomes of the immunoblot analysis conducted on *oastlc* and wild-type plants, which were complemented with *At*OAS-TL C and *At*OAS-TL C^{S210N}, were found to be analogous to those observed in *oastla* and wild-type transformants explained in 3.5.3.1. However, the intensity of the OAS-TL C protein was comparatively lower. In the *oastlc* group, individuals from lines four and five of *oastlc* (*At*OAS-TL C) and line eight of *oastlc* (*At*OAS-TL C^{S210N}) displayed higher OAS-TL C protein intensity in comparison to the other lines in their respective groups. Conversely, in complemented wild-type plants, the majority of individuals demonstrated enhanced expression of OAS-TL C protein (Fig. 3.16, d-f).

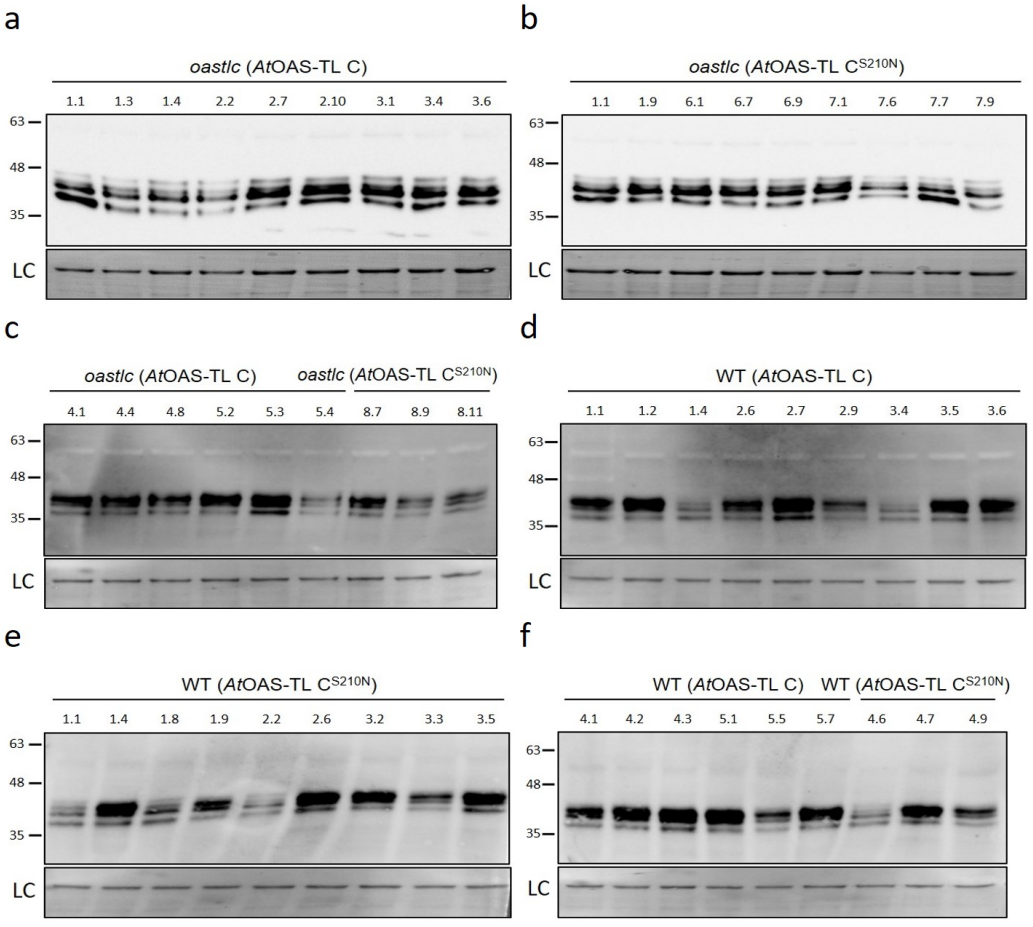

Figure 3.16: **Immunoblot analysis of *At*OAS-TL C protein in T2 plants. a-f)** Immunological detection of OAS-TL C in T2 generation. Soluble proteins were extracted (2.4.1) from the leaves of six-week-old plants grown on soil under short-day conditions (2.5.2). Separated proteins (10 μg per lane) by SDS-PAGE (2.4.3) were immunologically detected (2.4.4 and 2.4.5) with the polyclonal antibody against Arabidopsis OAS-TLC in 1:1000 dilution.

Figure 3.16: **Immunoblot analysis of *At*OAS-TL C protein in T2 plants.** Cross-reaction with OAS-TL isoforms causes the detection of three signals, of which the first signal from the bottom (the smallest one) is OAS-TL A, the second one (middle) is OAS-TL B, and the third one (larger) is OAS-TL C. The fourth signal (the largest one on top) is a non-specific signal caused by cross-reaction. The Loading control (LC) represents the intensities of the large subunit of ribulose-1,5-bisphosphate carboxylase/oxygenase protein in the samples stained with amido black (Table 2.3). Controls are represented in 3.13. The complete membrane pictures are depicted in Fig. S15 and S16.

3.5.3.3 Immunoblot analysis of *oastlc* T2 plants complemented with cytosolic *At*OAS-TL A

Finally, *oastlc* plants complemented with cytosolic OAS-TL A fused with the serine hydroxymethyltransferase (SHMT) transit peptide for mitochondrial targeting were investigated by immunoblotting to test the OAS-TL A protein amount. The background of this group is a knockout in the *At*OAS-TL C gene; therefore, the third signal responsible for the OAS-TL C isoform (explained in 3.5.3) is missing. Nevertheless, the result showed a higher OAS-TL A protein expression level in these transformants compared to the wild-type (Fig. 3.17, a-d).

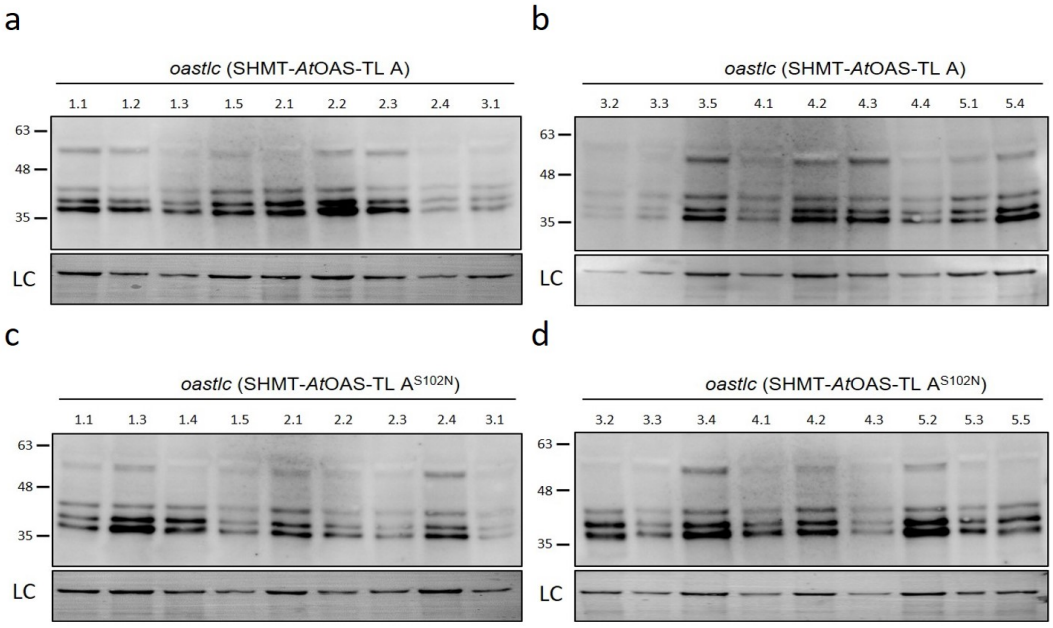

Figure 3.17: **Immunoblot analysis of *At*OAS-TL A protein in T2 plants. a-d)** Immunological detection of OAS-TL A on T2 generation. Soluble proteins were extracted (2.4.1) from the leaves of six-week-old plants grown on soil under short-day conditions (2.5.2). Separated proteins (10 μg per lane) by SDS-PAGE (2.4.3) were immunologically detected (2.4.4 and 2.4.5) with the polyclonal antibody against Arabidopsis OAS-TLC in 1:1000 dilution. Cross-reaction with OAS-TL isoforms causes the detection of three signals, of which the first signal from the bottom (the smallest one) is OAS-TL A, the second one (middle) is OAS-TL B, and the third one (larger) is OAS-TL C. The fourth signal (the largest one on top) is a non-specific signal caused by cross-reaction. The Loading control (LC) represents the intensities of the large subunit of ribulose-1,5-bisphosphate carboxylase/oxygenase protein in the samples stained with amido black (Table 2.3). Controls are represented in 3.13. The complete membrane pictures are depicted in Fig. S17 and S18.

To sum up, most of the T2 transformants demonstrated a notable increase in the level of OAS-TL protein compared to the wild-type control. Among the plants that underwent transformation via cytosolic *At*OAS-TL A, *oastla* (*At*OAS-TL A/*At*OAS-TL A^{S102N}) and *a1;1* (*At*OAS-TL A^{S102N}) exhibited the highest quantity of OAS-TL A proteins. Although *serat1;1* and the wild-type transformants in this group, as well as *oastlc* mutants, complemented with cytosolic *At*OAS-TL A possess the active *At*OAS-TL A gene, express OAS-TL A protein to a lesser extent than *oastla* and *a1;1*, yet more than wild-type control plants. In contrast, wild-type plants complemented with mitochondrial *At*OAS-TL C presented a greater amount of OAS-TL C protein than *oastlc* transformants.

3.6 Investigation of the OAS-TL C enzymatic activity

The replacement of the S102 with asparagine (S102N) in *At*OAS-TL A had been shown to fully inactivate the OAS-TL A^{S102N} mutated protein (Sun et al. 2021). Subsequently, analysis of OAS-TL enzymatic activity was performed *in vitro* for the purified mature *At*OAS-TL C, and the corresponding mutated protein *At*OAS-TL C^{S210N} to examine whether S210N mutation in OAS-TL C protein impact on its activity. To accomplish this, the 100 amino acid residues encoding the transit peptide were removed, and the peptide was then expressed in *E. coli* (2.4.9) and purified (2.4.10 and 2.4.11), followed by the determination of OAS-TL enzymatic activity (2.4.12). The result demonstrated that although OAS-TL C^{S210N} displayed some activity, it was 42 times lower than the activity in OAS-TL C wild-type protein (Fig. 3.18). These findings suggest that the asparagine replacement in *At*OAS-TL C significantly impacts the protein's activity and may have implications for future research in this area.

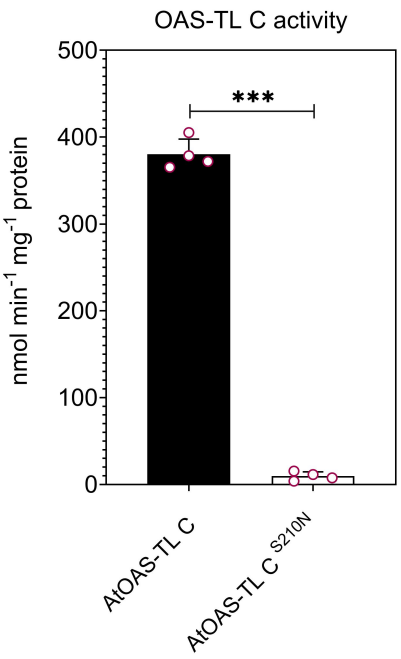

Figure 3.18: ***In vitro* OAS-TL enzyme activity of purified mature *At*OAS-TL C and the corresponding mutant protein *At*OAS-TL C^{S210N}.** Data are shown as means ± SD and n = 4 technical replicates. Asterisks indicates significant difference by two-sided Student's t test: ***P < 0.001.

3.7 Investigation of the SERAT enzymatic activity

To analyze whether the endogenous SERAT activity was stimulated by the presence of mutated *At*OAS-TL A^{S102N} and *At*OAS-TL C^{S210N} proteins *in planta*, the total SERAT activities in the crude protein extracts of wild-type, *oastla*, complemented *oastla* with *At*OAS-TL A

/ *At*OAS-TL A^{S102N}, *oastlc*, and complemented *oastlc* with *At*OAS-TL C / *At*OAS-TL C^{S210N} were measured and compared (Fig. 3.19). Complemented *oastla* mutant with either *At*OAS-TL A or *At*OAS-TL A^{S102N} represented a similar SERAT activity compared to the *oastla* and wild-type plants (Fig. 3.19, a), suggesting that mutated textitAtOAS-TL A^{S102N} has no significant effect on endogenous SERAT activity in *oastla* mutants. However, total SERAT activity in *oastlc* mutants complemented with *At*OAS-TL C^{S210N} displayed a significant two- to three-fold increases compared to *oastlc* (*At*OAS-TL C), *oastlc*, and wild-type plants (Fig. 3.19, b). This implies that mutated *At*OAS-TL C^{S210N}, may stimulate endogenous SERAT activity in *oastlc* mutants as desired.

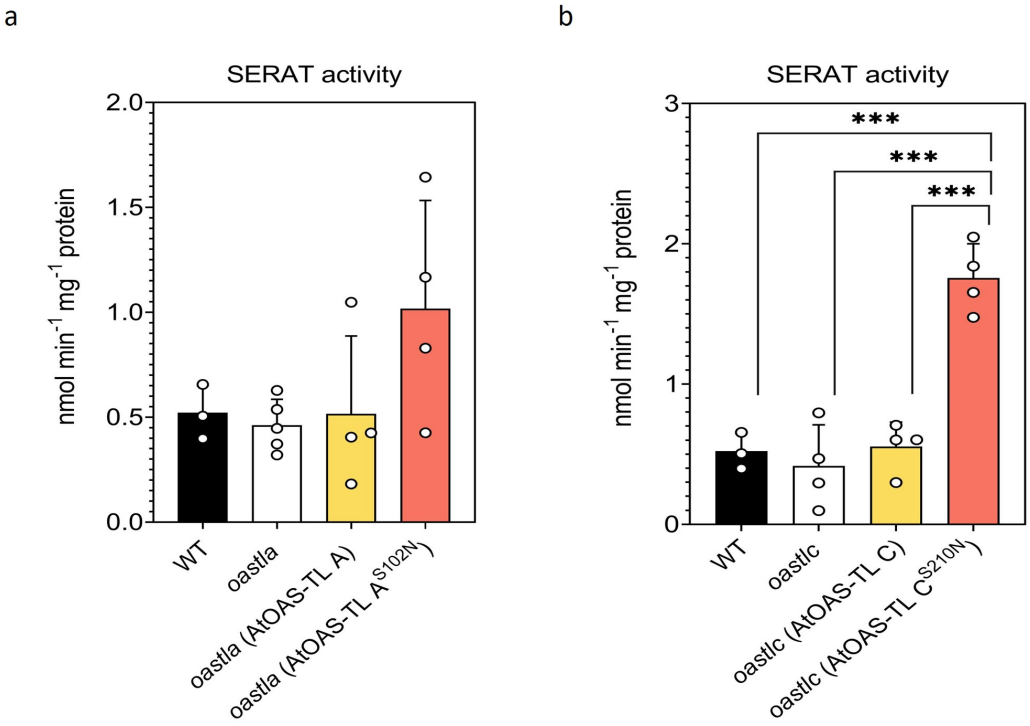

Figure 3.19: ***In vivo* SERAT enzyme activity in complemented cytosolic and mitochondrial *At*OAS-TL mutants in the T2 generation.** Total SERAT enzyme activity in whole soluble protein extract of the shoot of six weeks old **a)** WT, *oastla*, and *oastla* complemented with wild-type and mutated *At*OAS-TL A protein and **b)** WT, *oastlc*, and *oastlc* complemented with wild-type and mutated *At*OAS-TL C protein. Data are shown as means ± SD and n =3-5 technical replicates. Significant differences are marked with asterisks and were determined using one-way ANOVA followed by Tukey's test. The threshold for significance was set at $P < 0.001$.

3.8 Determination of metabolites in the transgenic lines

The results of the transcript (3.5.2) and immunoblot analysis (3.5.3.1 and 3.5.3.2) indicated a substantial increase in OAS-TL A and OAS-TL C expression in mRNA and protein abundance in the transformants. Additionally, it was observed that *At*OAS-TL A^{S102N} and *At*OAS-TL C^{S210N} formed a non-dissociable complex with SERAT *in vitro* (3.1), leading to the envisaged higher activity of SERAT in the CS complex. This increase in the total SERAT activity was observed in complemented *oastlc* lines (Fig. 3.19). Since SERAT activity is considered the rate-limiting step in cysteine synthesis and thiols, the consequent next step was to investigate whether the steady state levels of OAS, cysteine, and glutathione of the transformants were affected. For this purpose, metabolites were extracted (2.6.1) from rosette leaves of six weeks old plants grown under short-day conditions on soil (2.5.2). At least three biological replicates were employed from each line. After fluorescence derivatization (2.6.2 and 2.6.3), the OAS, cysteine, and glutathione were determined by HPLC.

3.8.1 Determination of OAS and thiols in the leaves of T2 cytosolic mutants complemented with modified cytosolic *At*OAS-TL A

Upon comparing the OAS concentration in the leaves of *oastla* and wildtype plants complemented with wild-type cytosolic *At*OAS-TL A, it was observed that there was no significant difference when compared to the control group. However, *oastla* (*At*OAS-TL A^{S102N}) demonstrated a 5.8-12.5 fold increase compared with complemented *oastla* with *At*OAS-TL A, and controls. Likewise, the OAS concentration in wild-type (*At*OAS-TL A^{S102N}) represented a 6.4-10.6 fold accumulation compared to WT (*At*OAS-TL A) (Fig. 3.20, a) and controls. The evaluation of the low molecular thiols cysteine and glutathione depicted an equivalent trend. Specifically, in the case of *oastla* (*At*OAS-TL A^{S102N}), the concentration of cysteine and glutathione has increased by 3-5.4 and 1.9-2.6 fold, respectively, in comparison to *oastla* (*At*OAS-TL A). The same trend has been observed in (*At*OAS-TL A^{S102N}), with a 2.2-4 and 1.9-2.5 fold increase in cysteine and glutathione levels, respectively, compared to WT (*At*OAS-TL A) (Fig. 3.20, b-c).

In contrast, the results obtained from OAS and thiol analysis of the complemented *serat1;1* plants revealed some remarkable findings. Based on the outcome of the OAS analysis conducted on the *serat1;1* plants, there was a notable difference compared to the wild-type

plants. This result is inconsistent with the previous study (Watanabe et al. 2008b) and may be attributed to technical errors considering the high standard deviation within the *serat1;1* group. Further, the analysis demonstrated no significant shifts in the steady-state level of either OAS (Fig. 3.21, a) or downstream thiols cysteine (Fig. 3.21, b) and glutathione (Fig. 3.21, c) in *serat1;1* (*At*OAS-TL A^{S102N}) or *serat1;1* (*At*OAS-TL A) compared to wild-type and *serat1;1* control plants. Likewise, the *a1;1* (*At*OAS-TL A) and *a1;1* (*At*OAS-TL A^{S102N}) transformants indicated no significant changes in the steady state levels of OAS (Fig. 3.22, a), cysteine (Fig. 3.22, b) and glutathione (Fig. 3.22, c) compared to wild-type and *a1;1* control plants.

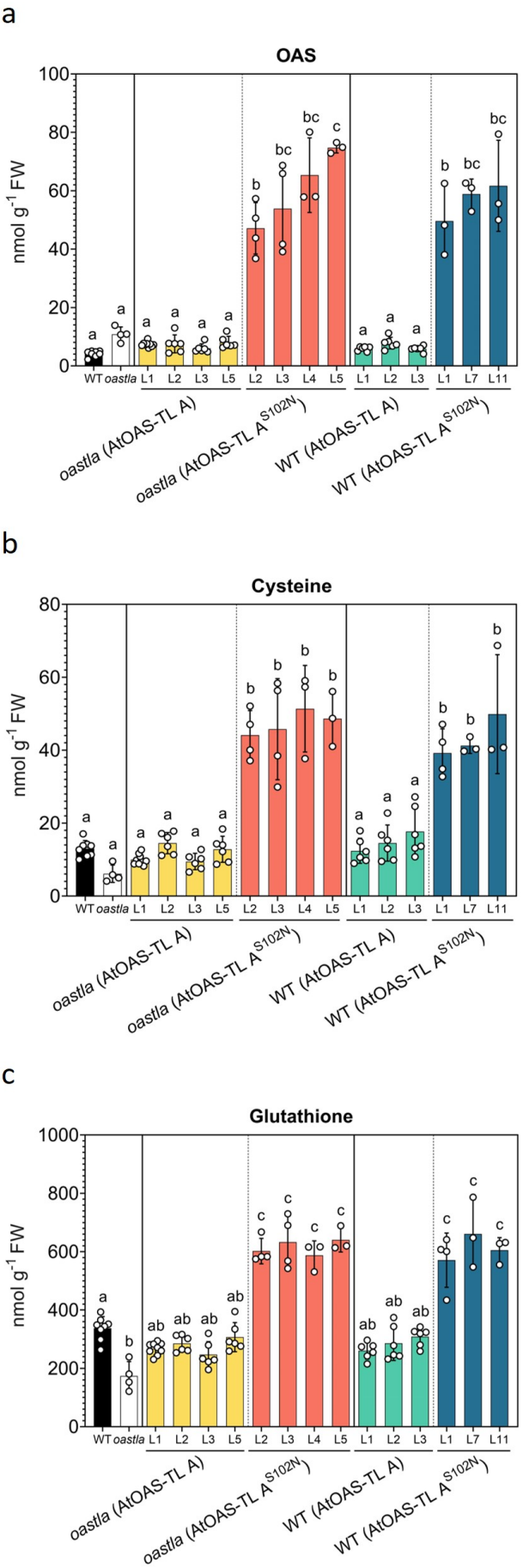

Figure 3.20: **Steady-state levels of OAS and low molecular thiols cysteine and glutathione in the leaves of complemented *oastla* and wild-type lines.** Metabolites were extracted using 0.1 M HCl (2.6.1) from the leaf tissue of six-week-old plants grown on soil under short-day conditions (2.5.2). **a)** OAS was derivatized using AccTaq (2.6.2). **b)** cysteine and **c)** glutathione were derivatized using monobromobimane (2.6.3). Derivatized samples were separated and quantified using HPLC. Data are shown as means ± SD, n=3-8 biological replicates; each biological replicate represents an individual plant. Different letters indicate significant differences ($p<0.05$) using one-way ANOVA followed by Tukey's test.

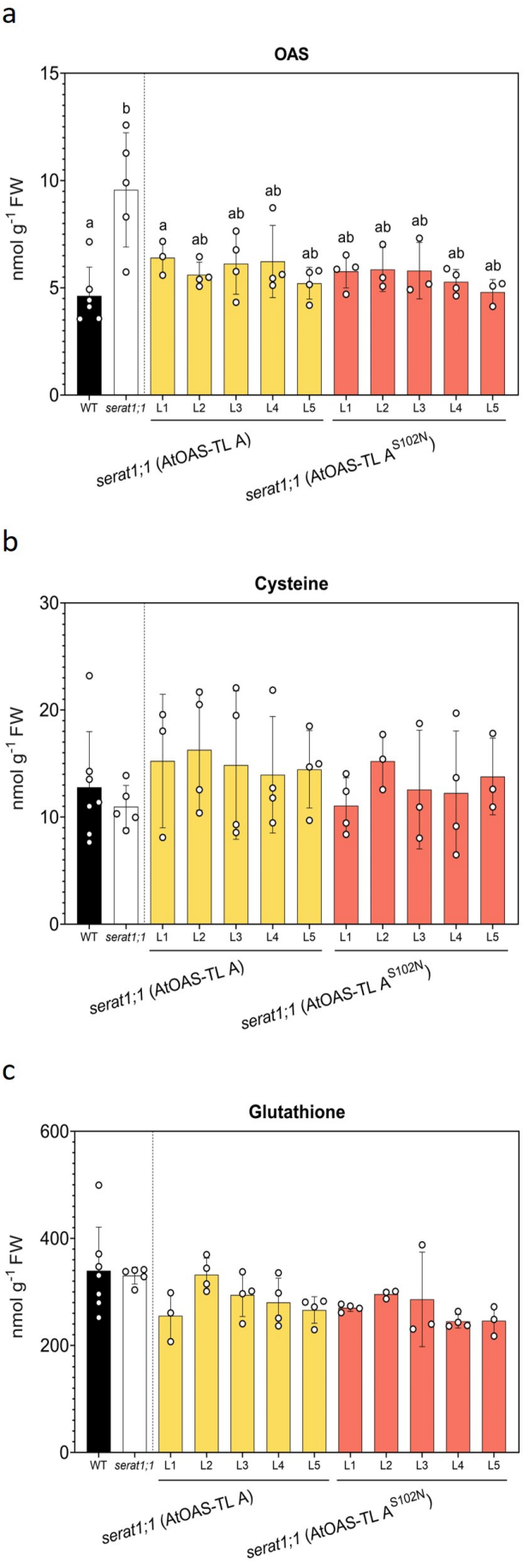

Figure 3.21: **Steady-state levels of OAS and low molecular thiols cysteine and glutathione in the leaves of complemented *serat1;1* lines.** Metabolites were extracted using 0.1 M HCl (2.6.1) from the leaf tissue of six-week-old plants grown on soil under short-day conditions (2.5.2). **a)** OAS was derivatized using AccTaq (2.6.2). **b)** cysteine and **c)** glutathione were derivatized using monobromobimane (2.6.3). Derivatized samples were separated and quantified using HPLC. Data are shown as means ± SD, n=3-6 biological replicates; each biological replicate represents an individual plant. Different letters indicate significant differences ($p<0.05$) using one-way ANOVA followed by Tukey's test.

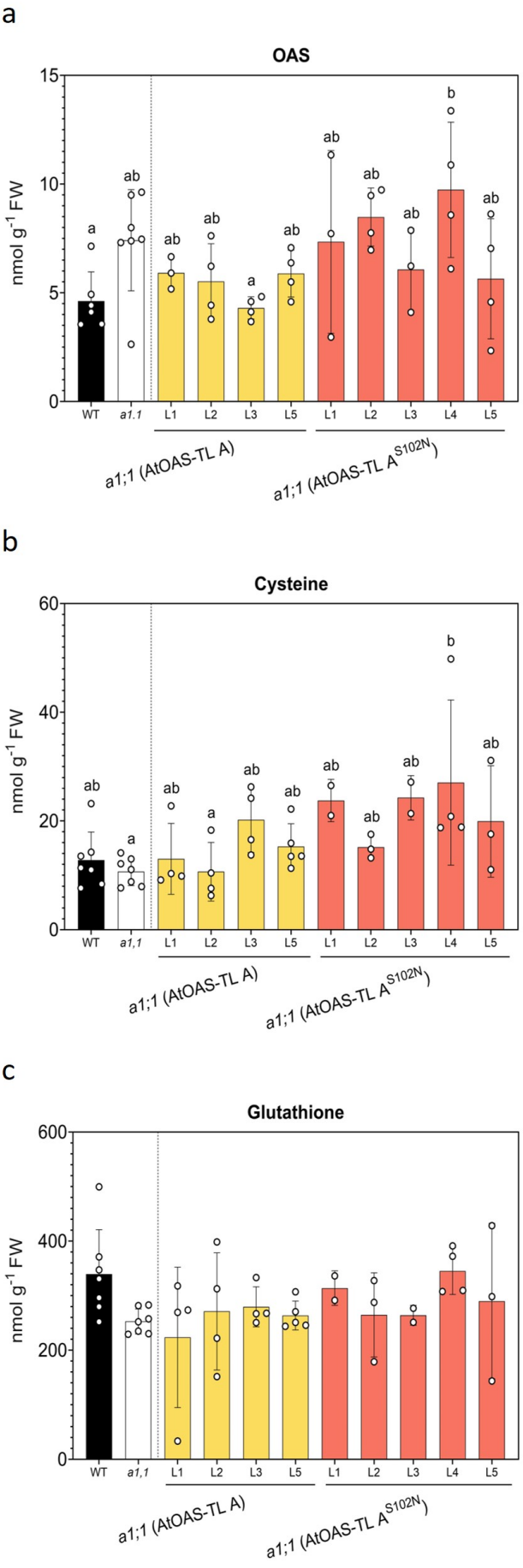

Figure 3.22: **Steady-state levels of OAS and low molecular thiols cysteine and glutathione in the leaves of complemented *a1;1* lines.** Metabolites were extracted using 0.1 M HCl (2.6.1) from the leaf tissue of six-week-old plants grown on soil under short-day conditions (2.5.2). **a)** OAS was derivatized using AccTaq (2.6.2). **b)** cysteine and **c)** glutathione were derivatized using monobromobimane (2.6.3). Derivatized samples were separated and quantified using HPLC. Data are shown as means ± SD, n=3-7 biological replicates; each biological replicate represents an individual plant. Different letters indicate significant differences ($p<0.05$) using one-way ANOVA followed by Tukey's test.

3.8.2 Determination of anions in the leaves of T2 transgenic lines complemented with cytosolic *At*OAS-TL

Analysis of OAS and low molecular thiols cysteine and glutathione in the complemented *oastla* and wild-type plants revealed an intense increase. This prompted further investigation into examining the content of sulfate and other anions, especially those needed for protein biosyntheses, such as nitrate and phosphate. Accordingly, the separated quantified anions (2.6.4) were determined by HPLC using the 1:10 dilution of the same metabolite extract (2.6.1). The sulfate content in the wild-type plants was around 13 nmol mg^{-1} FW, whereas in *oastla*, it was slightly reduced to 9 nmol mg^{-1} FW. Although the sulfate content in *oastla* (*At*OAS-TL A^{S102N}) did not indicate a significant change compared to *oastla* (*At*OAS-TL A), a general rise in the sulfate content up to 14 nmol mg^{-1} FW was observed in the complemented *oastla* lines compared to *oastla* (Fig. 3.23, a). In contrast, the sulfate content in wild-type plants complemented with either *At*OAS-TL A or *At*OAS-TL A^{S102N} indicated no differences compared to the control (Fig. 3.23, a).

The nitrate concentration of wild-type and *oastla* control plants indicated no significant differences. Among the transformants, except for one line (#3) in the *oastla* (*At*OAS-TL A) and two lines (#2 and #3) in the *oastla* (*At*OAS-TL A^{S102N}) group, the rest of the complemented *oastla* lines demonstrated no significant differences compared to the *oastla* control. Furthermore, complemented WT (*At*OAS-TL A^{S102N}) showed a significantly lowered nitrate accumulation, whereas WT (*At*OAS-TL A) indicated no significant differences compared to the wild-type control (Fig. 3.23, b). The analysis of nitrite concentration revealed that only one line (#1) of *oastla* (*At*OAS-TL A^{S102N}) contains a high accumulation of nitrite. In contrast, the rest of the complemented *oastla* plants indicated no significant differences in nitrite concentration compared to the *oastla* control (Fig. 3.23, c).

Analysis of the phosphate content revealed no differences between the transformants and respected control plants (Fig. 3.23, d). Likewise, the analysis of the acetate content illustrated a similar pattern except for one line (#11) in WT (*At*OAS-TL A^{S102N}), in which the acetate content was significantly lower than the wild-type control plants (Fig. 3.24, b). Ultimately, the analysis of other anions revealed no significant differences in the citrate (Fig. 3.24, a) and oxalate (Fig. 3.24, c) content in the complemented *oastla* lines compared to the *oastla* control plants. Nevertheless, all of the complemented wild-type plants displayed a reduction in the

same anion's content compared to the wild-type control plants but not among themselves (Fig. 3.24, a, c-d). The supplemented Figures S21 and S22 represent the other anions in the same lines.

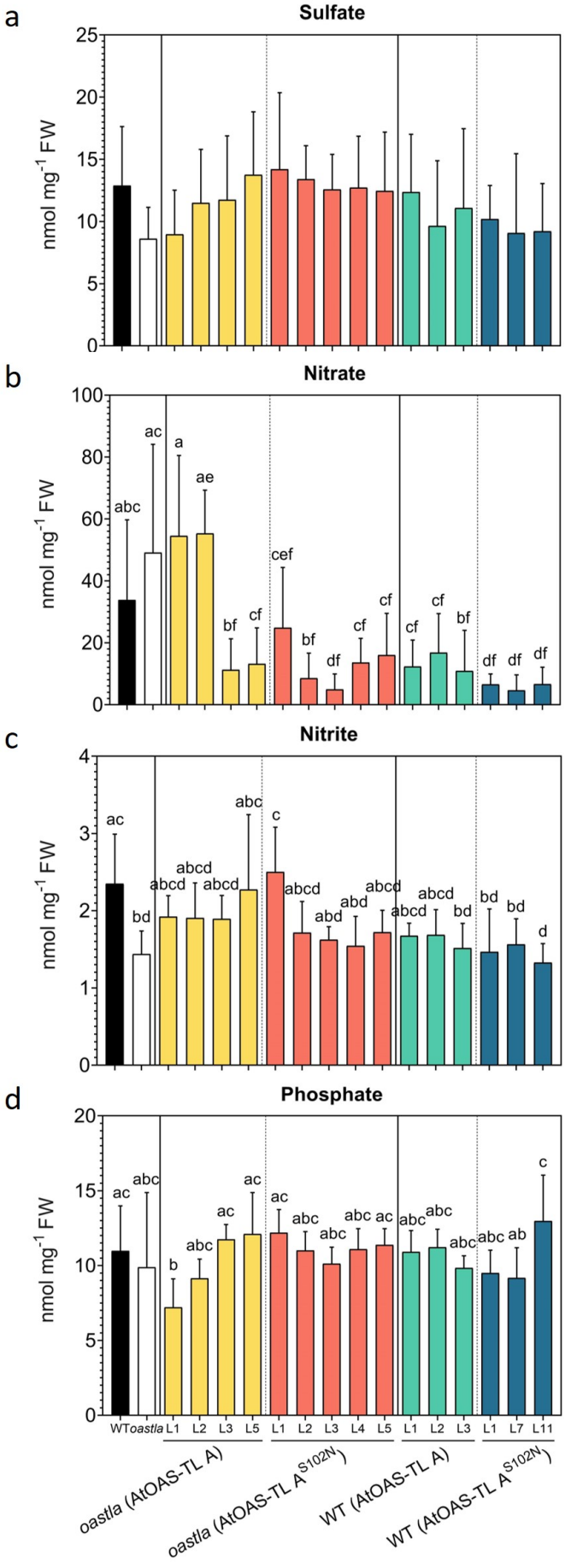

Figure 3.23: **Steady-state levels of anions in the leaves of complemented *oastla* and wild-type lines.** To analyze **a)** sulfate, **b)** nitrate, **c)** nitrite and **d)** phosphate, metabolites were extracted from the leaf tissue of six-week-old plants grown on soil under short-day conditions (2.5.2). The HCl extract was diluted 1:10 using ddH_2O; otherwise, the chloride ions from the HCl extract would overload the column and interfere with the run. Diluted samples were separated and quantified using HPLC. Data are shown as means ± SD, n=6-9 biological replicates; each biological replicate represents an individual plant. Different letters indicate significant differences ($p<0.05$) using one-way ANOVA followed by Tukey's test.

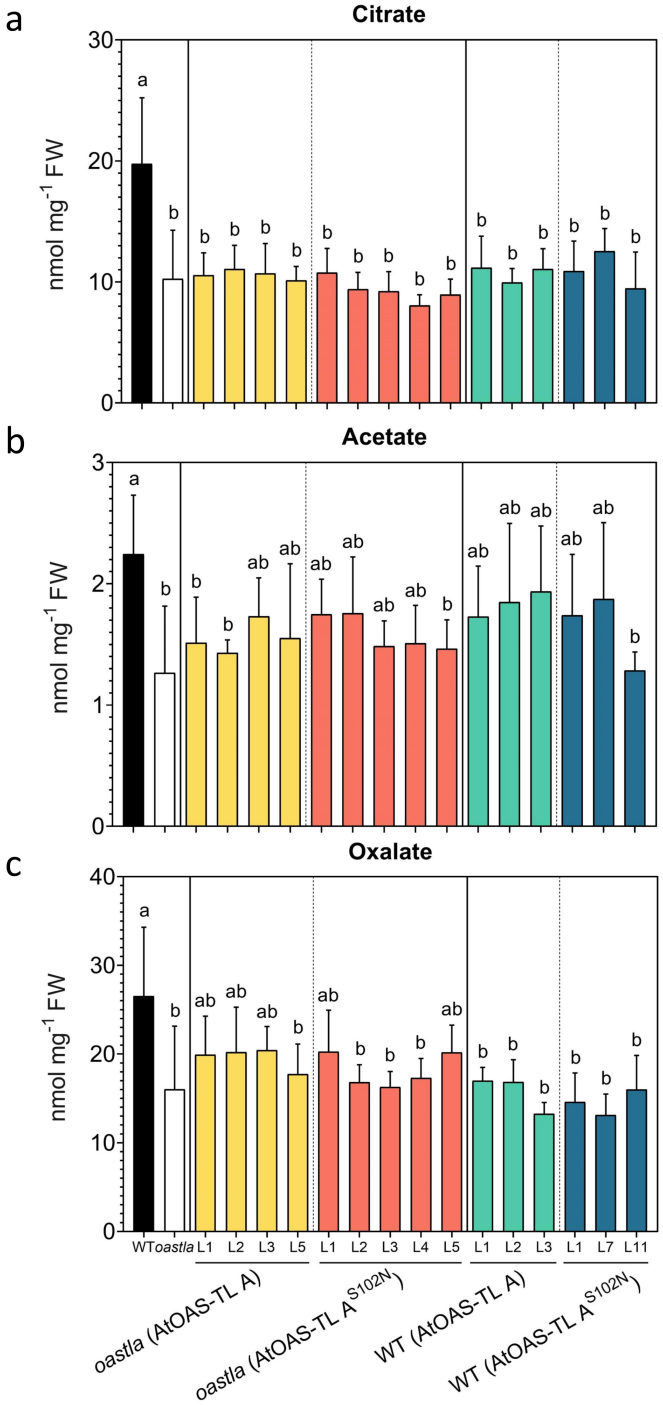

Figure 3.24: **Steady-state levels of anions in the leaves of complemented *oastla* and wild-type lines.** To analyze **a)** citrate, **b)** acetate and **c)** oxalate, metabolites were extracted from the leaf tissue of six-week-old plants grown on soil under short-day conditions (2.5.2). The HCl extract was diluted 1:10 using ddH_2O; otherwise, the chloride ions from the HCl extract would overload the column and interfere with the run. Diluted samples were separated and quantified using HPLC. Data are shown as means ± SD, n=6-9 biological replicates; each biological replicate represents an individual plant. Different letters indicate significant differences ($p<0.05$) using one-way ANOVA followed by Tukey's test.

According to the anion analysis of complemented *serat1;1*, the sulfate content in two lines (#1 and #3) of *serat1;1* (*At*OAS-TL A) depicted a significant decrease compared to the *serat1;1* control plants. Likewise, all the *serat1;1* (*At*OAS-TL A^{S102N}) lines, except line #4, demonstrated a lowered sulfate accumulation compared to the control (Fig. 3.25, a). However, the nitrite content in most of the *serat1;1* (*At*OAS-TL A) lines displayed no differences compared to the *serat1;1* control plants, whereas three lines in complemented *serat1;1* (*At*OAS-TL A^{S102N}) plants depicted a significantly lowered nitrite accumulation (Fig. 3.25, c). The other anions consist of nitrate (Fig. 3.25, b), phosphate(Fig. 3.25, d), citrate(Fig. 3.26, a), acetate (Fig. 3.26, b) and oxalate (Fig. 3.26, c) in the complemented *serat1;1* demonstrated no significant difference compared to the *serat1;1* control plants. The supplemented Figures S23 and S24 represent the other anions in the same lines.

The result of the anion analysis in the complemented *a1;1* transformants indicated no changes in the sulfate (Fig. 3.27, a), nitrite (Fig. 3.27, c), phosphate (Fig. 3.27, d) and oxalate (Fig. 3.28, c) accumulation compared to the control *a1;1* and wild-type plants. Analysis of the nitrate (Fig. 3.27, b) and citrate (Fig. 3.28, a) showed that only line #5 in *a1;1* (*At*OAS-TL A^{S102N}) group indicated a significantly lower concentration than the control plants, whereas the rest of the transformants showed similar contents. Finally, the acetate content in all four lines of *a1;1* (*At*OAS-TL A) and three lines of *a1;1* (*At*OAS-TL A^{S102N}) did not show any significant changes compared to the control *a1;1* plants (Fig. 3.28, b). The representation of the other anions in the complemented *a1;1* plants are provided in the supplemented Figures S25 and S26.

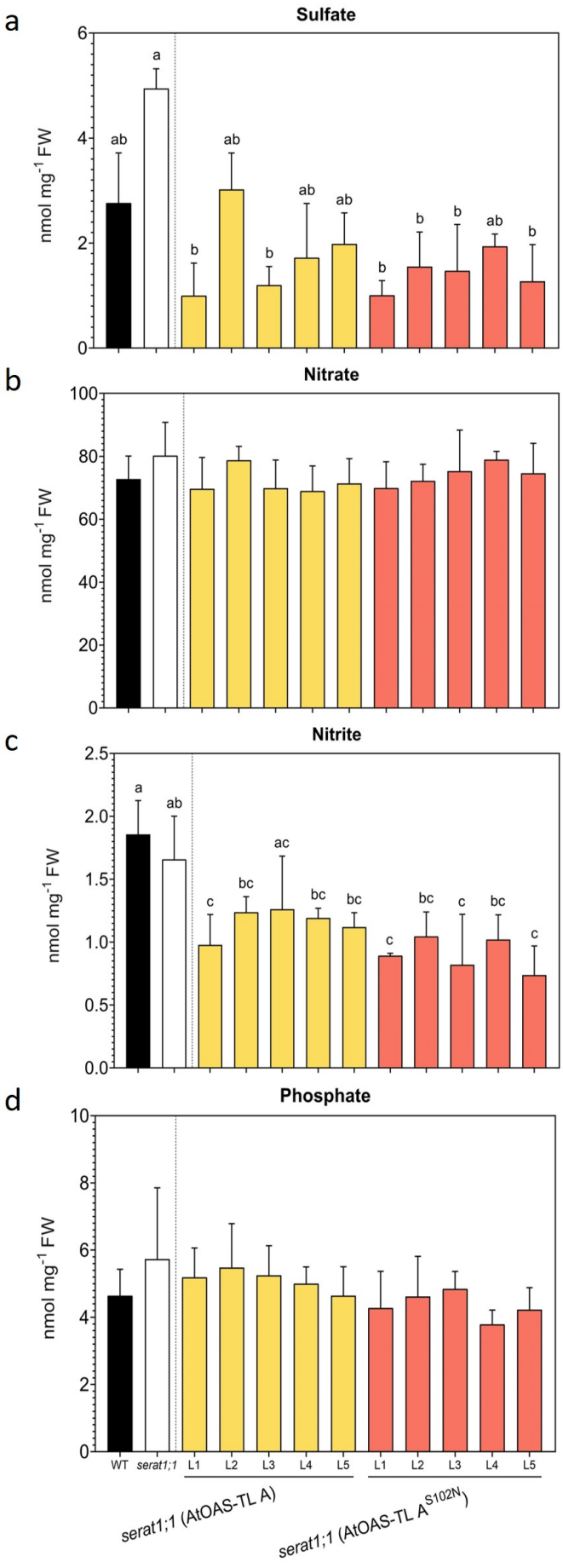

Figure 3.25: **Steady-state levels of anions in the leaves of complemented *serat1;1* lines.** To analyze **a)** sulfate, **b)** nitrate, **c)** nitrite and **d)** phosphate, metabolites were extracted from the leaf tissue of six-week-old plants grown on soil under short-day conditions (2.5.2). The HCl extract was diluted 1:10 using ddH_2O; otherwise, the chloride ions from the HCl extract would overload the column and interfere with the run. Diluted samples were separated and quantified using HPLC. Data are shown as means ± SD, n=3-5 biological replicates; each biological replicate represents an individual plant. Different letters indicate significant differences ($p<0.05$) using one-way ANOVA followed by Tukey's test.

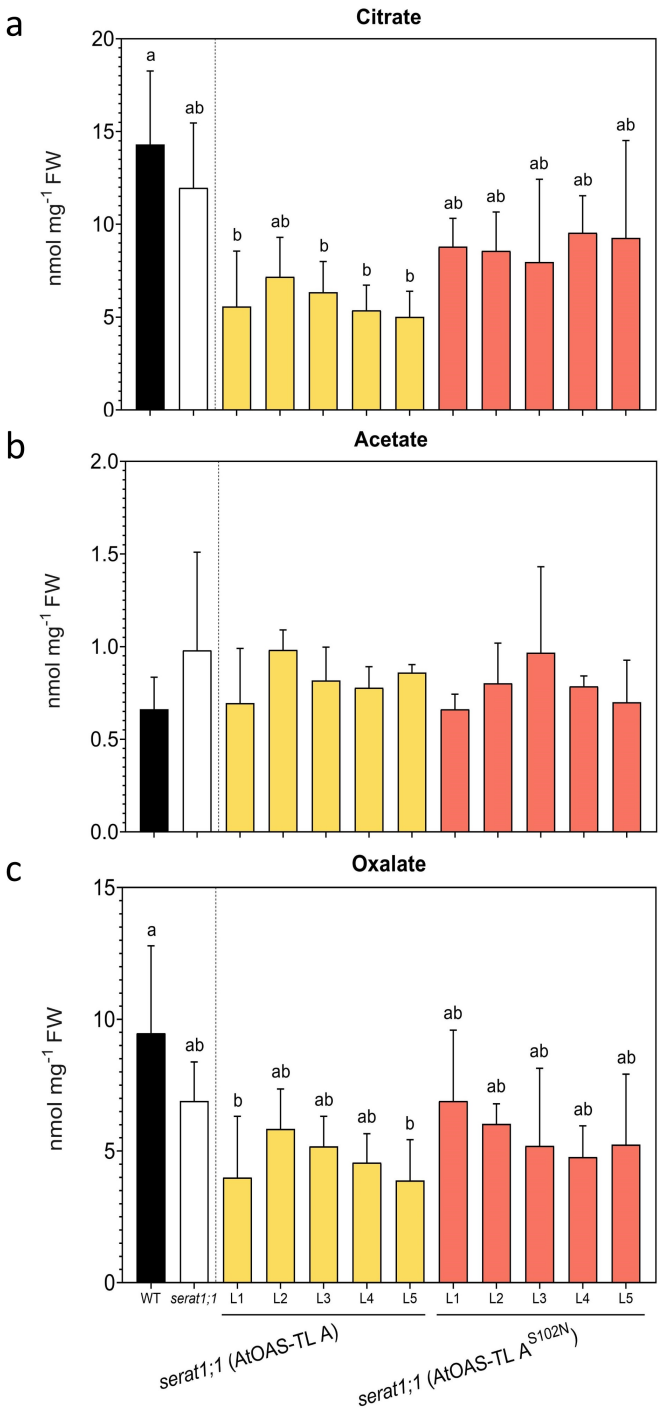

Figure 3.26: **Steady-state levels of anions in the leaves of complemented *serat1;1* lines.** To analyze **a)** citrate, **b)** acetate and **c)** oxalate, metabolites were extracted from the leaf tissue of six-week-old plants grown on soil under short-day conditions (2.5.2). The HCl extract was diluted 1:10 using ddH_2O; otherwise, the chloride ions from the HCl extract would overload the column and interfere with the run. Diluted samples were separated and quantified using HPLC. Data are shown as means ± SD, n=3-5 biological replicates; each biological replicate represents an individual plant. Different letters indicate significant differences ($p<0.05$) using one-way ANOVA followed by Tukey's test.

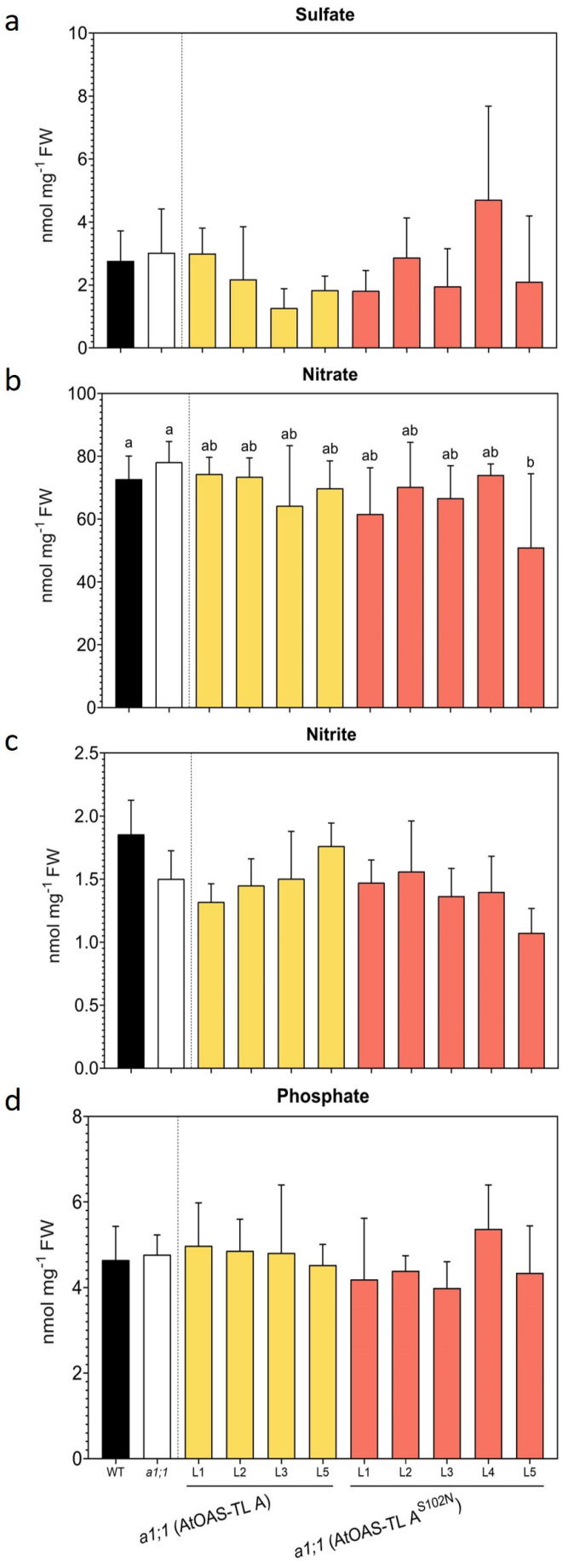

Figure 3.27: **Steady-state levels of anions in the leaves of complemented *a1;1* lines.** To analyze **a)** sulfate, **b)** nitrate, **c)** nitrite and **d)** phosphate, metabolites were extracted from the leaf tissue of six-week-old plants grown on soil under short-day conditions (2.5.2). The HCl extract was diluted 1:10 using ddH_2O; otherwise, the chloride ions from the HCl extract would overload the column and interfere with the run. Diluted samples were separated and quantified using HPLC. Data are shown as means ± SD, n=3-5 biological replicates; each biological replicate represents an individual plant. Different letters indicate significant differences ($p<0.05$) using one-way ANOVA followed by Tukey's test.

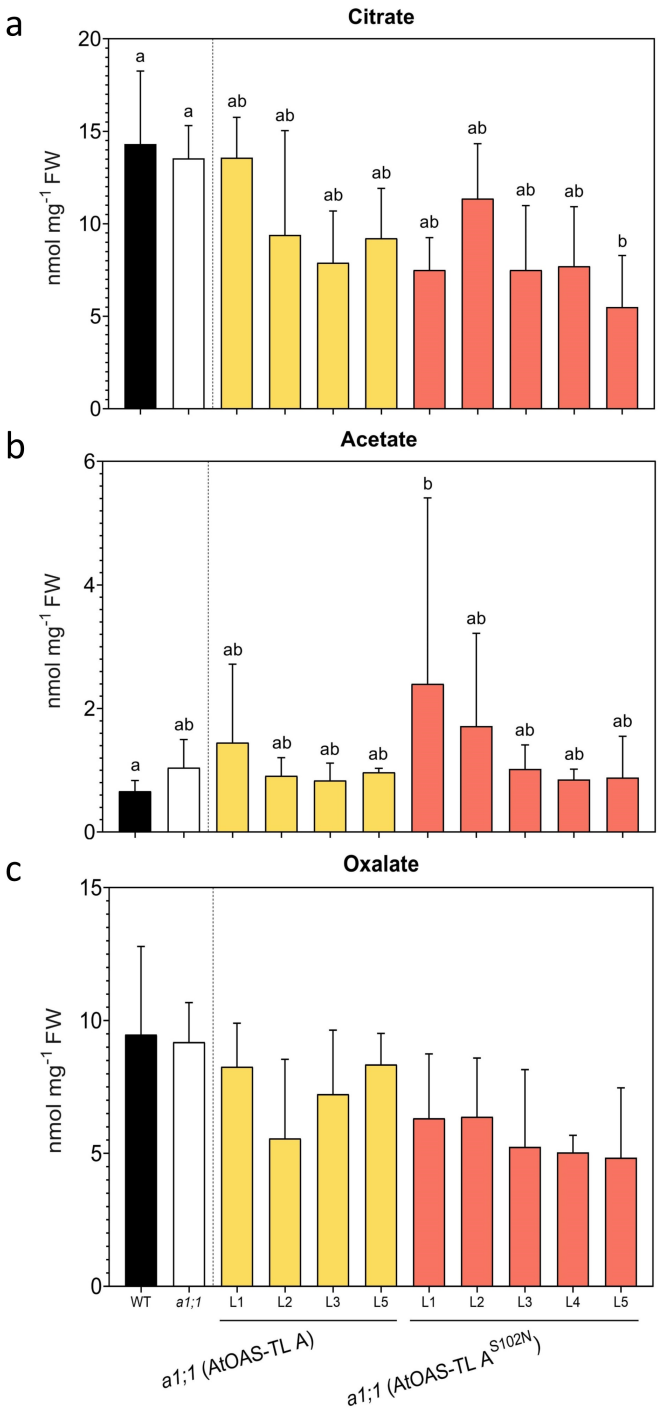

Figure 3.28: **Steady-state levels of anions in the leaves of complemented *a1;1* lines.** To analyze **a)** citrate, **b)** acetate and **c)** oxalate, metabolites were extracted from the leaf tissue of six-week-old plants grown on soil under short-day conditions (2.5.2). The HCl extract was diluted 1:10 using ddH_2O; otherwise, the chloride ions from the HCl extract would overload the column and interfere with the run. Diluted samples were separated and quantified using HPLC. Data are shown as means ± SD, n=3-5 biological replicates; each biological replicate represents an individual plant. Different letters indicate significant differences ($p<0.05$) using one-way ANOVA followed by Tukey's test.

3.8.3 Determination of amino acids in the leaves of T2 transgenic lines complemented with cytosolic *At*OAS-TL

In order to test whether the specific point mutations of cytosolic and mitochondrial *At*OAS-TLs in the complemented plants influence the amino acid content, the steady state level of different amino acids was determined in the same samples. After derivatization (2.6.2), the amino acids were determined by HPLC. The *oastla* (*At*OAS-TL A) and *oastla* (*At*OAS-TL A^{S102N}) indicated no significant differences in methionine (Fig. 3.29, a), serine (Fig. 3.29, c), and threonine (Fig. 3.29, d) compared to the *oastla* control. However, *oastla* (*At*OAS-TL A^{S102N}) transformants in all three experimented lines displayed a significant accumulation of tyrosine (Fig. 3.29, b) compared to *oastla* control, yet similar to the tyrosine content of *oastla* (*At*OAS-TL A). Further analysis revealed no changes in the content of histidine (Fig. 3.30, a), asparagine (Fig. 3.30, b), and glutamine (Fig. 3.30, c) between complemented *oastla* and controls. Nevertheless, only one line in *oastla* (*At*OAS-TL A) group indicated a significant accumulation of glycine compared to the *oastla* control plants, whereas the rest of the transformants displayed similar glycine accumulation (Fig. 3.30, d).

The complemented wild-type plants with either *At*OAS-TL A or *At*OAS-TL A^{S102N} indicated comparable levels of methionine (Fig. 3.29, a) tyrosine (Fig. 3.29, b) and histidine (Fig. 3.30, a) content as those observed in the wild-type control plants. Moreover, although the serine (Fig. 3.29, c) and threonine (Fig. 3.29, d) content in some of the complemented lines showed a decrease compared to the control wild-type plants, there were no significant differences among the complemented lines. Likewise, upon examining the content of asparagine (Fig. 3.30, b), glutamine (Fig. 3.30, c), and glycine (Fig. 3.30, d), no noteworthy differences were observed between the WT (*At*OAS-TL A) and WT (*At*OAS-TL A^{S102N}) lines. However, the analysis indicated a decrease in some of the complemented lines compared to the wild-type control. Further details regarding the remaining amino acids are provided in the supplemented Figures S31, S32, and S33.

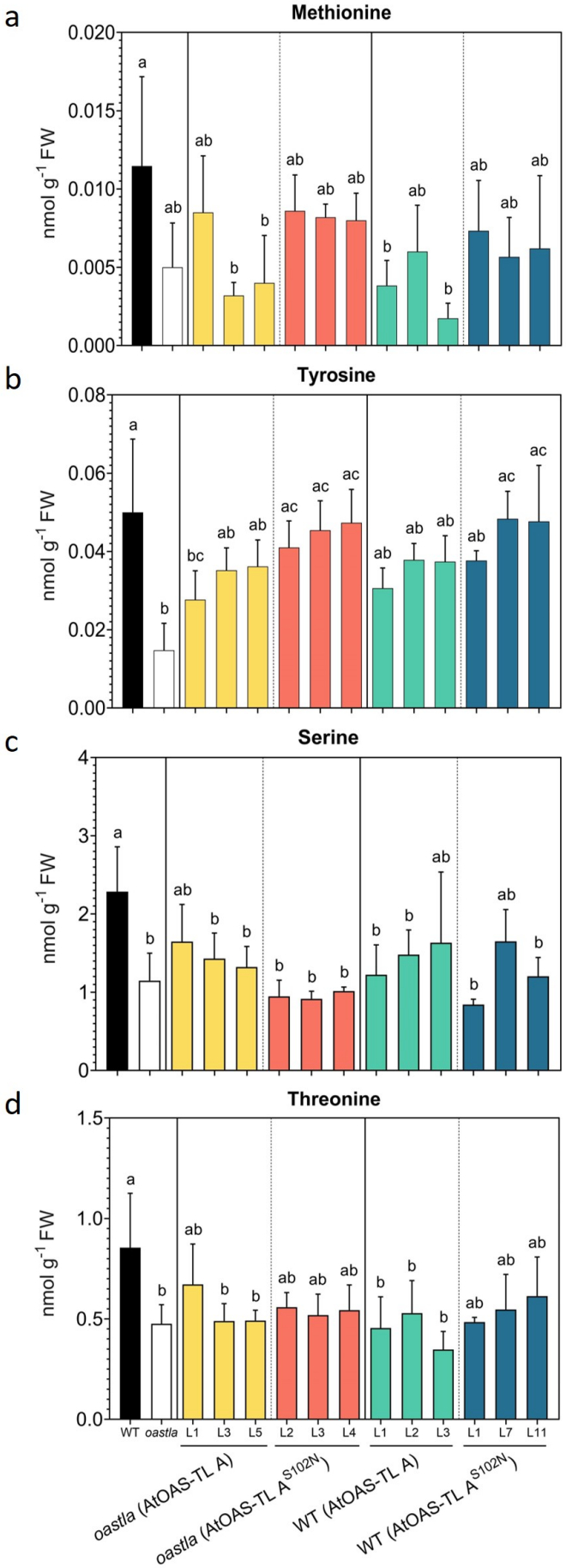

Figure 3.29: **Steady-state levels of amino acids in the leaves of complemented *oastla* and wild-type lines.** To analyze amino acids **a)** methionine, **b)** tyrosine and **c)** serine, and **d)** threonine, metabolites were extracted using 0.1 M HCl (2.6.1) from the leaf tissue of six-week-old plants grown on soil under short-day conditions (2.5.2). Then, the amino acids were derivatized using AccTaq (2.6.2). Derivatized samples were separated and quantified using HPLC. Data are shown as means ± SD, n=3-6 biological replicates; each biological replicate represents an individual plant. Different letters indicate significant differences ($p<0.05$) using one-way ANOVA followed by Tukey's test.

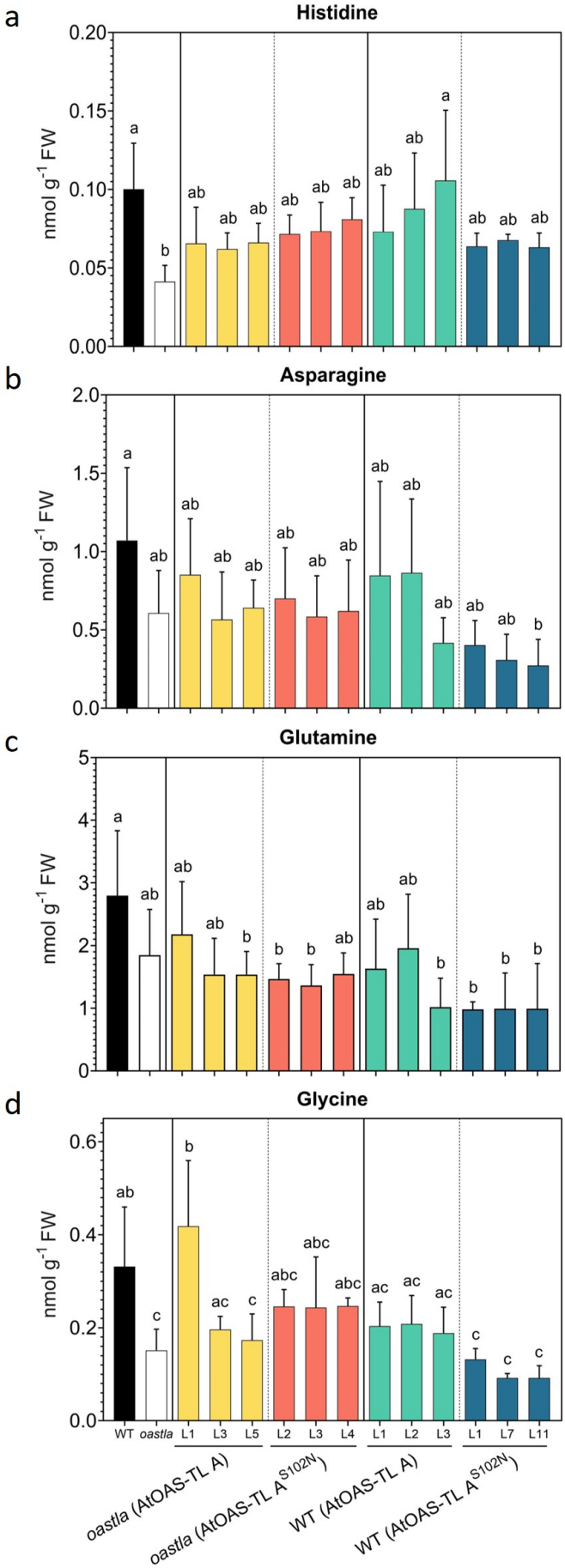

Figure 3.30: **Steady-state levels of amino acids in the leaves of complemented *oastla* and wild-type lines.** To analyze amino acids **a)** histidine, **b)** asparagine and **c)** glutamine, and **d)** glycine, metabolites were extracted using 0.1 M HCl (2.6.1) from the leaf tissue of six-week-old plants grown on soil under short-day conditions (2.5.2). Then, the amino acids were derivatized using AccTaq (2.6.2). Derivatized samples were separated and quantified using HPLC. Data are shown as means ± SD, n=3-6 biological replicates; each biological replicate represents an individual plant. Different letters indicate significant differences ($p<0.05$) using one-way ANOVA followed by Tukey's test.

Nevertheless, the amino acid analysis of *serat1;1* (Fig. 3.31 and 3.32) and *a1;1* (Fig. 3.33 and 3.34) complemented with *At*OAS-TL A and *At*OAS-TL A^{S102N} indicated no differences compared to the controls. The further results of the other amino acids are present in the supplemented Figures S34, S35, S36 for complemented *serat1;1*, and Figures S37, S38, and S39 for *a1;1* plants.

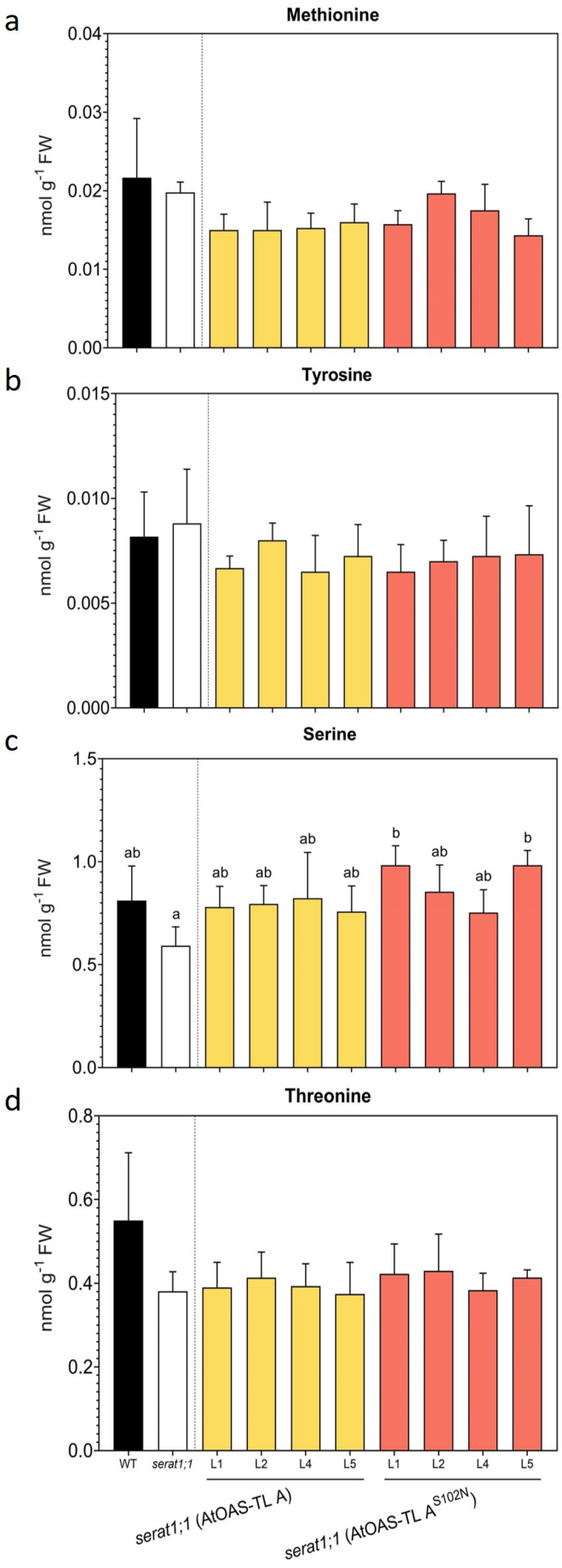

Figure 3.31: **Steady-state levels of amino acids in the leaves of complemented *serat1;1*.** To analyze amino acids **a)** methionine, **b)** tyrosine and **c)** serine, and **d)** threonine, metabolites were extracted using 0.1 M HCl (2.6.1) from the leaf tissue of six-week-old plants grown on soil under short-day conditions (2.5.2). Then, the amino acids were derivatized using AccTaq (2.6.2). Derivatized samples were separated and quantified using HPLC. Data are shown as means ± SD, n=3-6 biological replicates; each biological replicate represents an individual plant. Different letters indicate significant differences ($p<0.05$) using one-way ANOVA followed by Tukey's test.

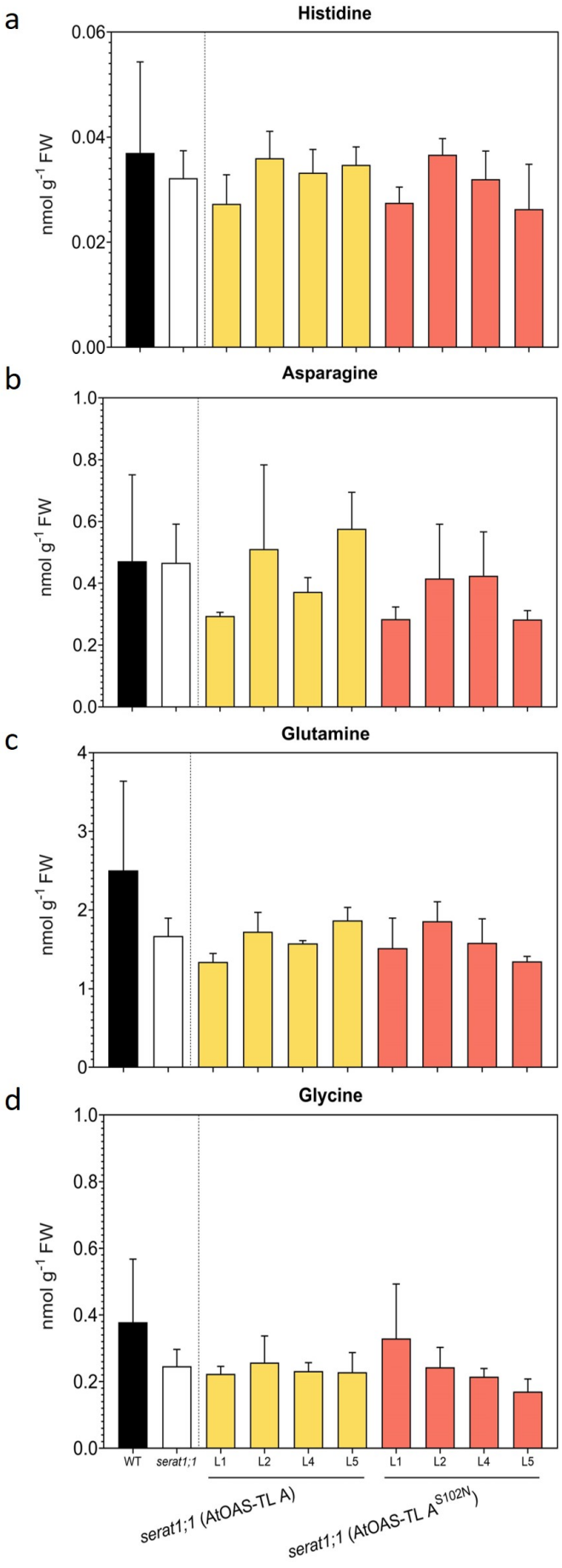

Figure 3.32: **Steady-state levels of amino acids in the leaves of complemented *serat1;1*.** To analyze amino acids **a)** histidine, **b)** asparagine and **c)** glutamin, and **d)** glycine, metabolites were extracted using 0.1 M HCl (2.6.1) from the leaf tissue of six-week-old plants grown on soil under short-day conditions (2.5.2). Then, the amino acids were derivatized using AccTaq (2.6.2). Derivatized samples were separated and quantified using HPLC. Data are shown as means ± SD, n=3-6 biological replicates; each biological replicate represents an individual plant. Different letters indicate significant differences ($p<0.05$) using one-way ANOVA followed by Tukey's test.

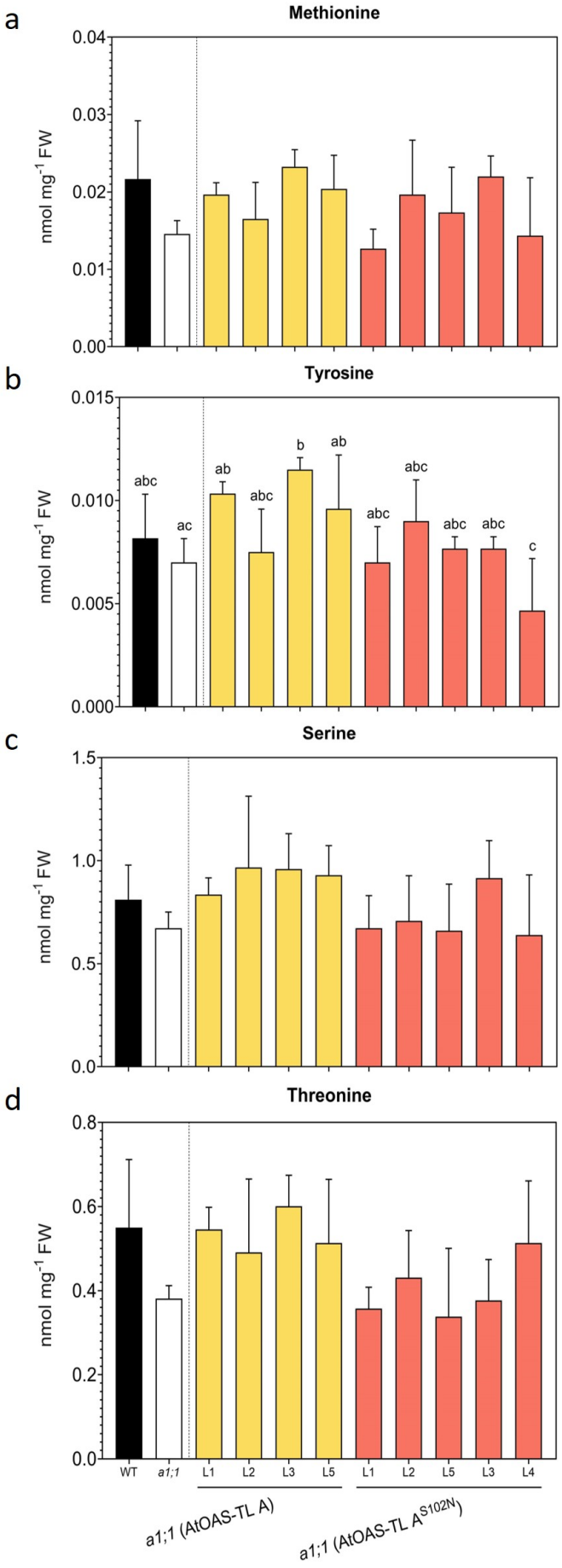

Figure 3.33: **Steady-state levels of amino acids in the leaves of complemented *a1;1*.** To analyze amino acids **a)** methionine, **b)** tyrosine and **c)** serine, and **d)** threonine, metabolites were extracted using 0.1 M HCl (2.6.1) from the leaf tissue of six-week-old plants grown on soil under short-day conditions (2.5.2). Then, the amino acids were derivatized using AccTaq (2.6.2). Derivatized samples were separated and quantified using HPLC. Data are shown as means ± SD, n=3-6 biological replicates; each biological replicate represents an individual plant. Different letters indicate significant differences ($p<0.05$) using one-way ANOVA followed by Tukey's test.

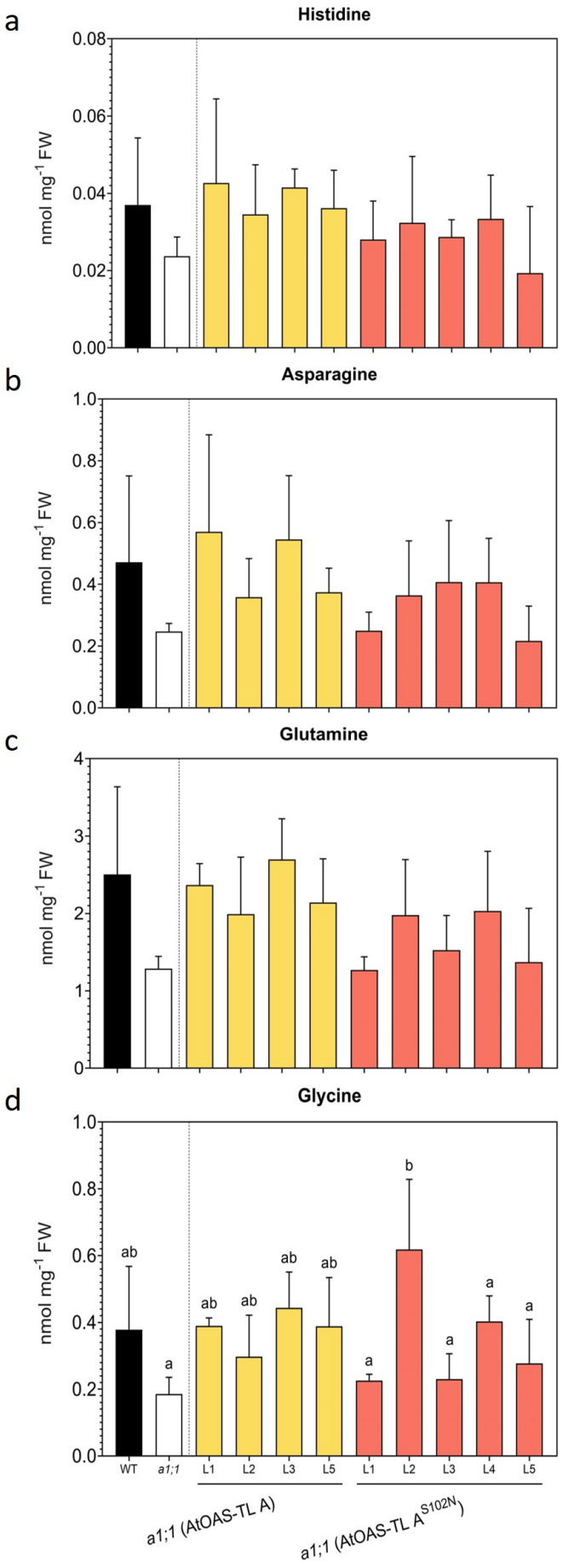

Figure 3.34: **Steady-state levels of amino acids in the leaves of complemented *a1;1*.** To analyze amino acids **a)** histidine, **b)** asparagine and **c)** glutamin, and **d)** glycine, metabolites were extracted using 0.1 M HCl (2.6.1) from the leaf tissue of six-week-old plants grown on soil under short-day conditions (2.5.2). Then, the amino acids were derivatized using AccTaq (2.6.2). Derivatized samples were separated and quantified using HPLC. Data are shown as means ± SD, n=3-6 biological replicates; each biological replicate represents an individual plant. Different letters indicate significant differences ($p<0.05$) using one-way ANOVA followed by Tukey's test.

3.8.4 Determination of OAS and thiols in the leaves of T2 mitochondrial mutants complemented with modified mitochondrial *At*OAS-TL C

The steady-state levels of OAS and downstream metabolites, cysteine and glutathione, in the leaves of *oastlc* and wild-type plants complemented with wild-type/mutated mitochondrial *At*OAS-TL C were likewise determined. OAS concentration in the leaves of *oastlc* (*At*OAS-TL C) and WT (*At*OAS-TL C) plants indicated no differences compared to the controls. However, there was up to 2.1-3.8 fold accumulation in the OAS concentration of *oastlc* (*At*OAS-TL C^{S210N}) compared to *oastlc* (*At*OAS-TL C). Likewise, the OAS analysis of WT (*At*OAS-TL C^{S210N}) depicted a 1.6-7.1 fold increase compared to WT (*At*OAS-TL C) (Fig. 3.35, a).

Nevertheless, the result of the downstream metabolite thiols, cysteine (Fig. 3.35, b), and glutathione (Fig. 3.35, c) in *oastlc* (*At*OAS-TL C^{S210N}) indicated a slighter increase up to 0.9-1.9 and 1.1-2.6 fold, respectively. Similarly, WT (*At*OAS-TL C^{S210N}) represented accumulation in cysteine (Fig. 3.35, b) and glutathione (Fig. 3.35, c) up to 1.2-2.9 and 0.8-1.5 fold, respectively, compared to complemented wild-type plants with *At*OAS-TL C.

3.8.5 Determination of OAS and thiols in the leaves of T2 mitochondrial mutants complemented with modified cytosolic *At*OAS-TL A

Unlike *oastlc* transformants complemented with mitochondrial *At*OAS-TL C^{S210N}, only a few individuals of *oastlc* (SHMT-*At*OAS-TL A^{S102N}) transformants represented a significant rise in OAS concentration (Fig. 3.36, a). However, the steady-state levels of cysteine (Fig. 3.36, b) and glutathione (Fig. 3.36, c) in *oastlc* (SHMT-*At*OAS-TL A^{S102N}) indicated no differences from *oastlc* (SHMT-*At*OAS-TL A).

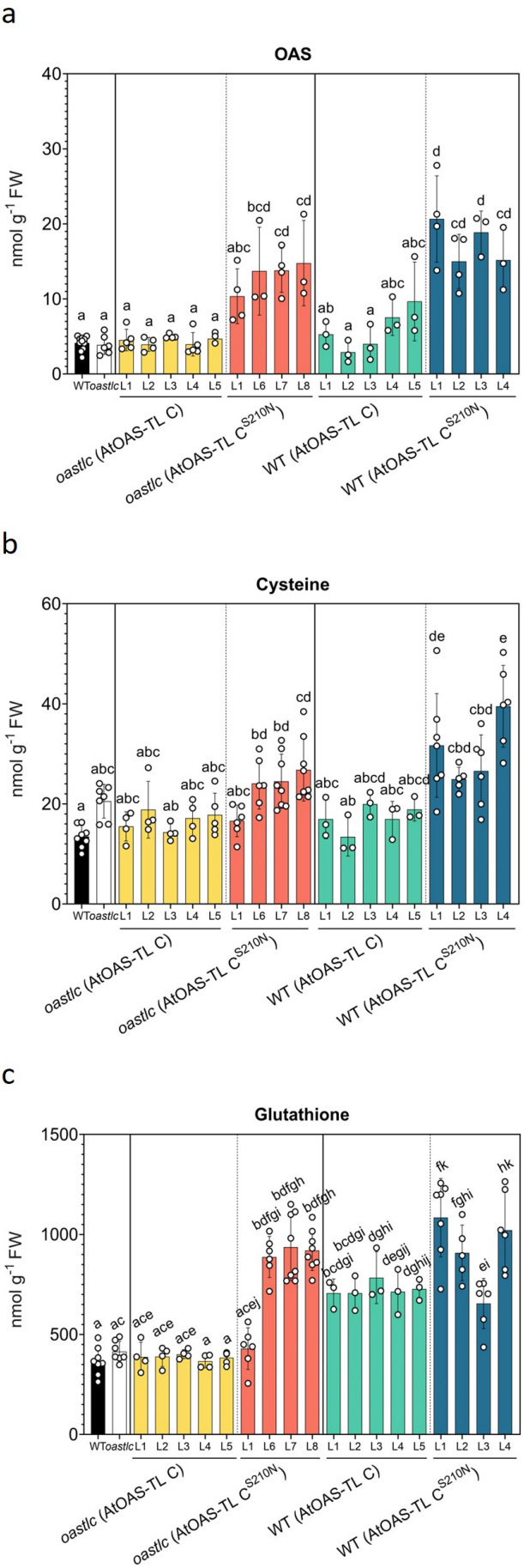

Figure 3.35: **Steady-state levels of OAS and low molecular thiols cysteine and glutathione in the leaves of complemented *oastlc* and wild-type lines.** Metabolites were extracted using 0.1 M HCl (2.6.1) from the leaf tissue of six-week-old plants grown on soil under short-day conditions (2.5.2). **a)** OAS was derivatized using AccTaq (2.6.2). **b)** cysteine and **c)** glutathione were derivatized using monobromobimane (2.6.3). Derivatized samples were separated and quantified using HPLC. Data are shown as means ± SD, n=3-6 biological replicates; each biological replicate represents an individual plant. Different letters indicate significant differences ($p<0.05$) using one-way ANOVA followed by Tukey's test.

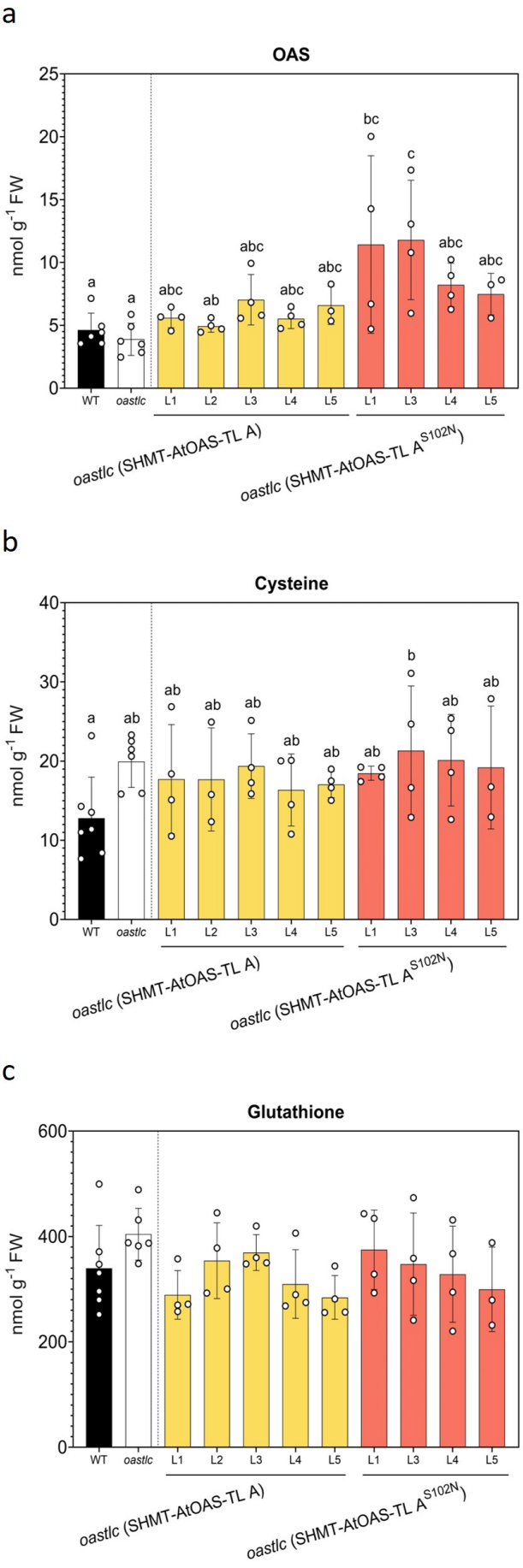

Figure 3.36: **Steady-state levels of OAS and low molecular thiols cysteine and glutathione in the leaves of complemented *oastlc* lines.** Metabolites were extracted using 0.1 M HCl (2.6.1) from the leaf tissue of six-week-old plants grown on soil under short-day conditions (2.5.2). **a)** OAS was derivatized using AccTaq (2.6.2). **b)** cysteine and **c)** glutathione were derivatized using monobromobimane (2.6.3). Derivatized samples were separated and quantified using HPLC. Data are shown as means ± SD, n=3-6 biological replicates; each biological replicate represents an individual plant. Different letters indicate significant differences ($p<0.05$) using one-way ANOVA followed by Tukey's test.

3.8.6 Determination of anions in the leaves of T2 mitochondrial mutants complemented with modified mitochondrial *At*OAS-TL C

The anions were determined for *oastlc* and wild-type T2 plants complemented with mitochondrial *At*OAS-TL C and *At*OAS-TL C^{S210N}. The sulfate content in two lines of *oastlc* (*At*OAS-TL C^{S210N}) group displayed a reduction compared to the *oastlc* control, whereas the rest of the transformants indicated no differences (Fig. 3.37, a). The nitrate content in *oastlc* (*At*OAS-TL C) represented a significant reduction compared to the control *oastlc* plants. The oastlc (*At*OAS-TL C^{S210N}), however, showed an intense increase in nitrate content in most of the transformants yet did not show a statistical difference due to the high standard deviation among the samples (Fig. 3.37, b). Moreover, the analysis of the nitrite (Fig. 3.37, c), phosphate (Fig. 3.37, d), acetate (Fig. 3.38, b) and oxalate (Fig. 3.38, c) revealed identical concentrations in almost all the complemented lines and control plants. Finally, the citrate concentration in all the complemented lines was identical; however, they indicated a general decline compared to the control plants (Fig. 3.38, a). Analyses of the rest of the anions are demonstrated in Figures S27 and S28.

The wild-type plants complemented with *At*OAS-TL C^{S210N} indicated an increase in the sulfate content compared to the WT (*At*OAS-TL C), yet no difference with the control plants (Fig. 3.37, a). The analysis of nitrate (Fig. 3.37, b), phosphate (Fig. 3.37, d) and acetate (Fig. 3.38, b) showed comparable concentrations in almost all the complemented lines and the control plants. Moreover, the complemented wild-type plants displayed no changes in the concentration of nitrite (Fig. 3.37, c) and citrate (Fig. 3.38, a), yet showed a general reduction compared to the wild-type control plants. A similar result was observed in the oxalate concentration. Although some of the complemented lines declined compared to wild-type control plants, there was no difference among them (Fig. 3.38, c). Analyses of the rest of the anions are demonstrated in Figures S27 and S28.

3.8.7 Determination of anions in the leaves of T2 mitochondrial mutants complemented with modified cytosolic *At*OAS-TL A

The anion analysis of the complemented *oastlc* plants with the cytosolic SHMT-*At*OAS-TL A and SHMT-*At*OAS-TL A^{S102N} revealed no differences compared to the control condition (Fig. 3.39 and 3.40). Analyses of the rest of the anions are demonstrated in Figures S29 and S30.

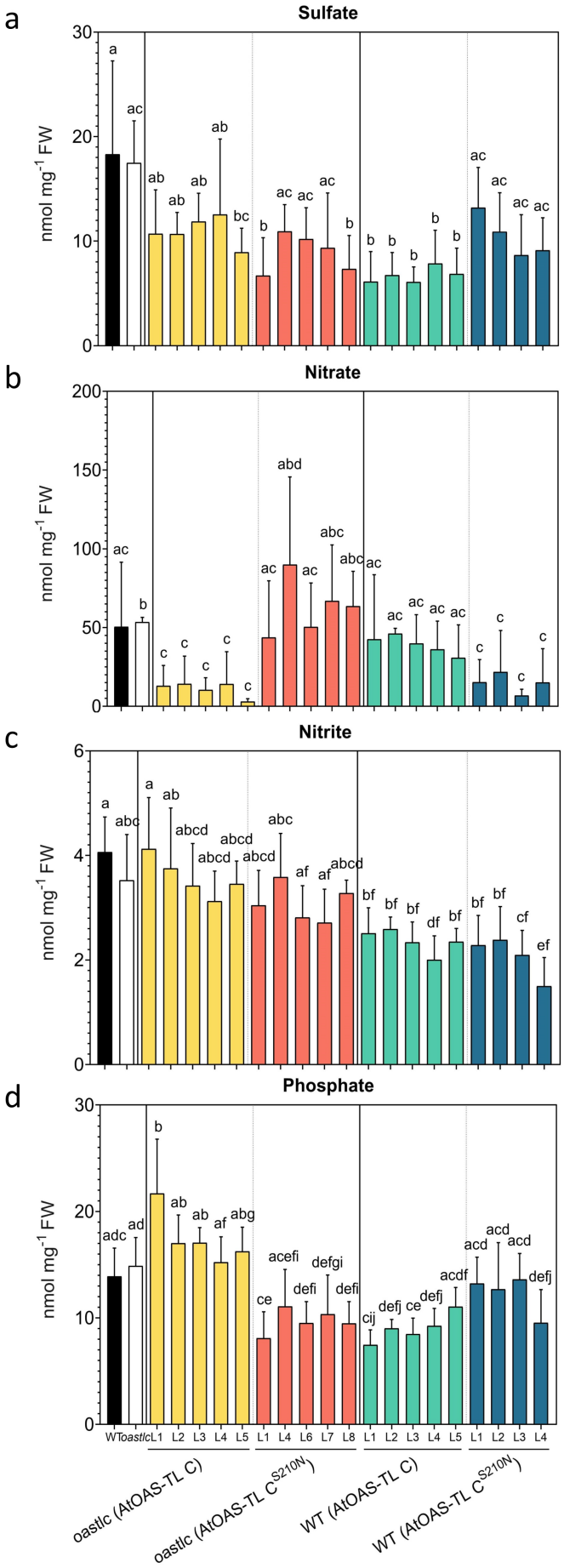

Figure 3.37: **Steady-state levels of anions in the leaves of complemented *oastlc* and wild-type lines.** To analyze **a)** sulfate, **b)** nitrate, **c)** nitrite and **d)** phosphate, metabolites were extracted from the leaf tissue of six-week-old plants grown on soil under short-day conditions (4.5.2). The HCl extract was diluted 1:10 using ddH_2O; otherwise, the chloride ions from the HCl extract would overload the column and interfere with the run. Diluted samples were separated and quantified using HPLC. Data are shown as means ± SD, n=4-5 biological replicates; each biological replicate represents an individual plant. Different letters indicate significant differences ($p<0.05$) using one-way ANOVA followed by Tukey's test.

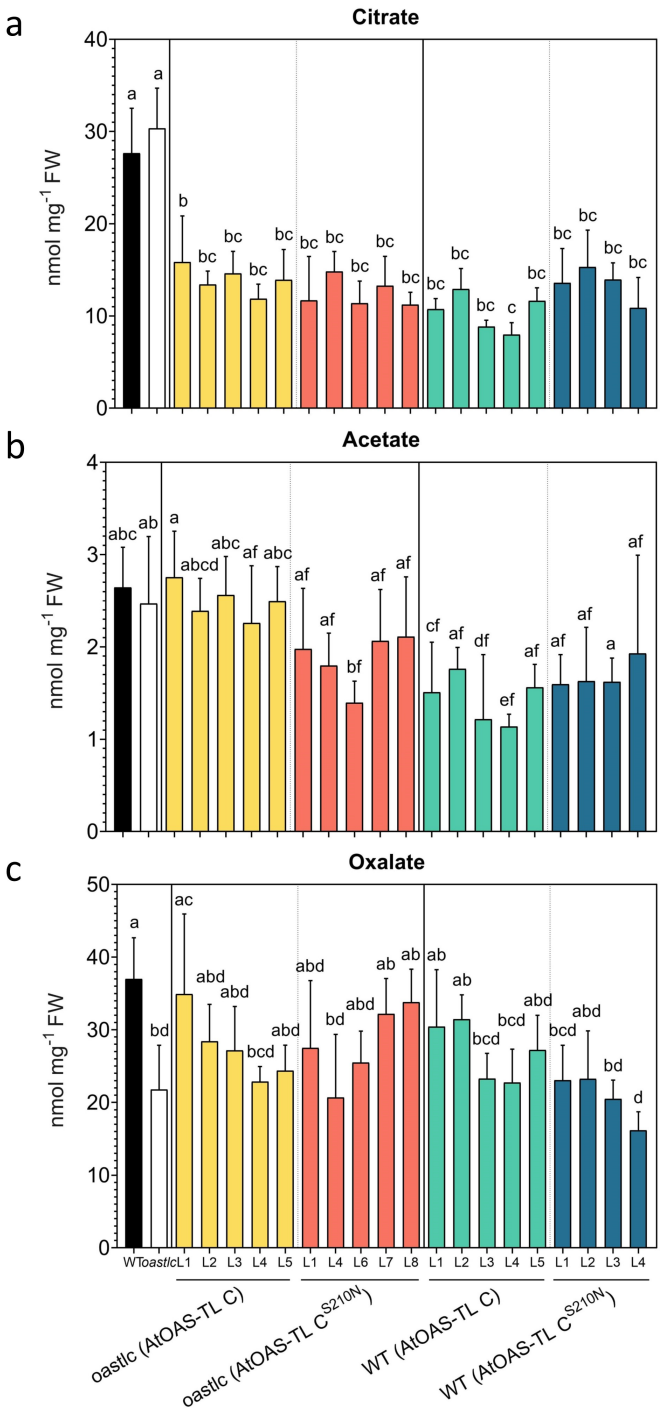

Figure 3.38: **Steady-state levels of anions in the leaves of complemented *oastlc* and wild-type lines.** To analyze **a)** citrate, **b)** acetate and **c)** oxalate, metabolites were extracted from the leaf tissue of six-week-old plants grown on soil under short-day conditions (4.5.2). The HCl extract was diluted 1:10 using ddH_2O; otherwise, the chloride ions from the HCl extract would overload the column and interfere with the run. Diluted samples were separated and quantified using HPLC. Data are shown as means ± SD, n=4-5 biological replicates; each biological replicate represents an individual plant. Different letters indicate significant differences ($p<0.05$) using one-way ANOVA followed by Tukey's test.

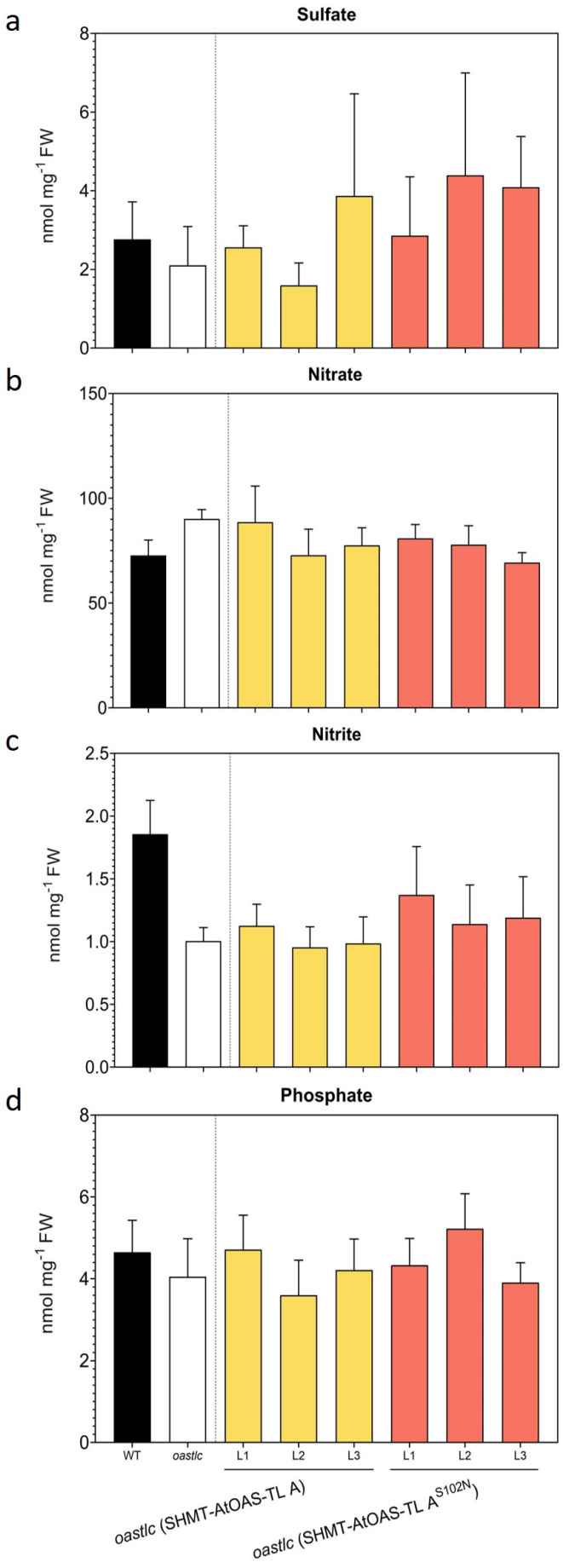

Figure 3.39: **Steady-state levels of anions in the leaves of complemented *oastlc* lines.** To analyze **a)** sulfate, **b)** nitrate, **c)** nitrite and **d)** phosphate, metabolites were extracted from the leaf tissue of six-week-old plants grown on soil under short-day conditions (4.5.2). The HCl extract was diluted 1:10 using ddH_2O; otherwise, the chloride ions from the HCl extract would overload the column and interfere with the run. Diluted samples were separated and quantified using HPLC. Data are shown as means ± SD, n=3-5 biological replicates; each biological replicate represents an individual plant.

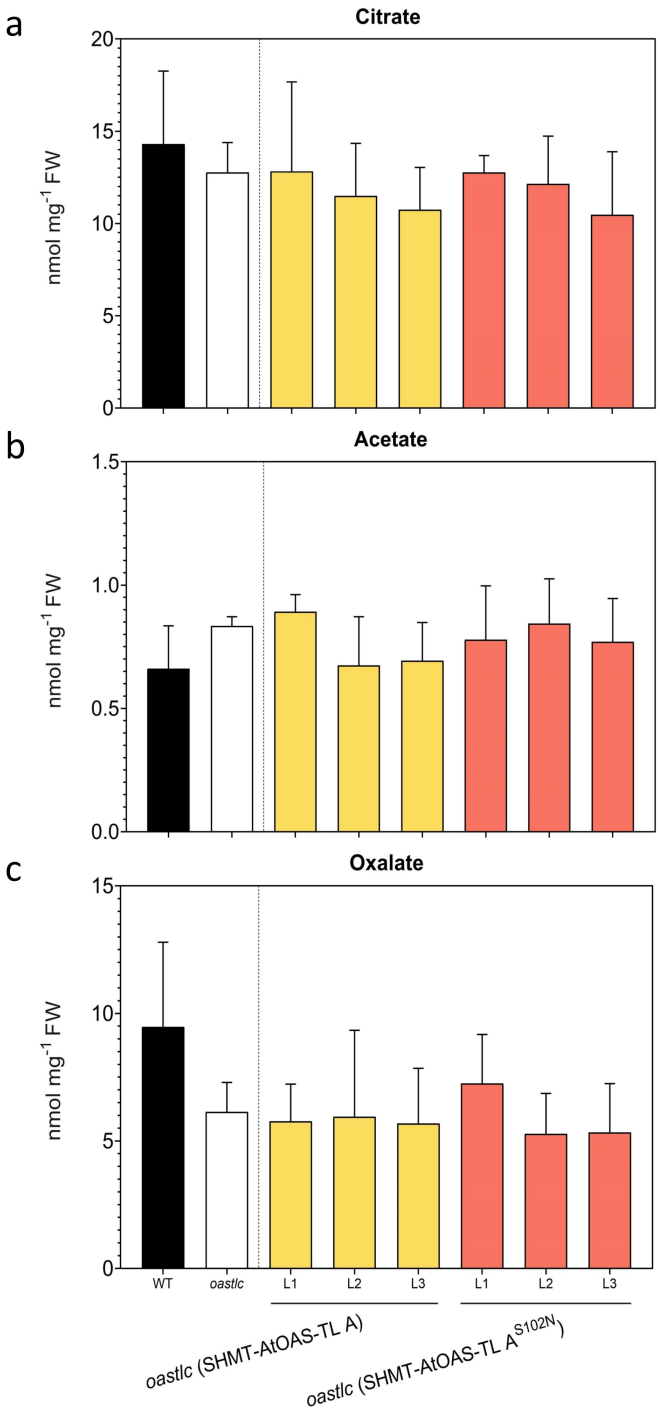

Figure 3.40: **Steady-state levels of anions in the leaves of complemented *oastlc* lines.** To analyze **a)** citrate, **b)** acetate and **c)** oxalate, metabolites were extracted from the leaf tissue of six-week-old plants grown on soil under short-day conditions (4.5.2). The HCl extract was diluted 1:10 using ddH_2O; otherwise, the chloride ions from the HCl extract would overload the column and interfere with the run. Diluted samples were separated and quantified using HPLC. Data are shown as means ± SD, n=3-5 biological replicates; each biological replicate represents an individual plant.

3.8.8 Determination of amino acids in the leaves of T2 mitochondrial mutants complemented with modified mitochondrial *At*OAS-TL C

The amino acid analysis was likewise accomplished for the complemented *oastlc* and wild-type plants. The result indicated no significant differences in the content of most amino acids of complemented plants compared to the controls (Fig. 3.41 and 3.42). Nevertheless, the concentration of isoleucine (Fig. S41, a), leucine (Fig. S41, b), phenylalanine (Fig. S41, d), and valine (Fig. S42, b) in some of the complemented lines showed a reduction compared to the control plants but not with each other. The results of the rest of the amino acids are displayed in the supplemented Figures S40, S41, and S42.

3.8.9 Determination of amino acids in the leaves of T2 mitochondrial mutants complemented with modified cytosolic *At*OAS-TL A

Nevertheless, the amino acid analysis of *oastlc* plants complemented with (SHMT-*At*OAS-TL A) and (SHMT-*At*OAS-TL A^{S102N}) indicated no differences compared to the control plants (Fig. 3.43 and 3.44). Further results of the other amino acids in this group of transformants are presented in the supplemented Figures S43, S44, and S45.

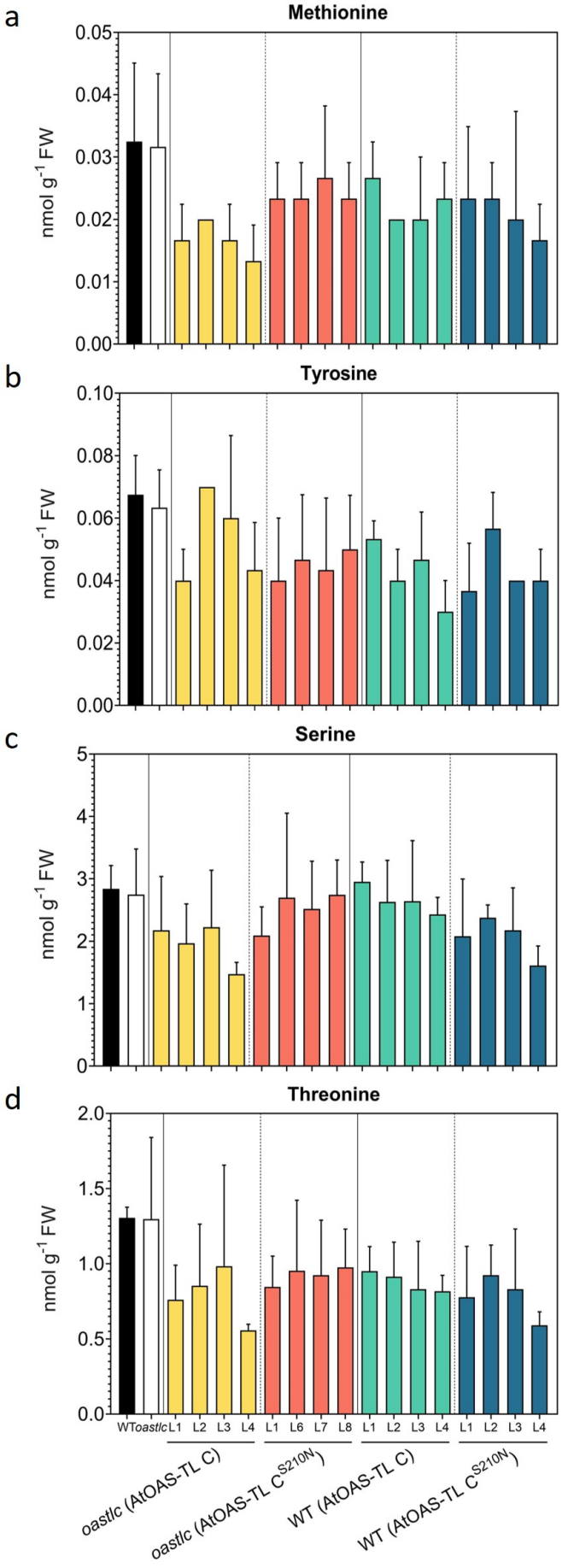

Figure 3.41: **Steady-state levels of amino acids in the leaves of complemented *oastlc* and wild-type lines.** To analyze amino acids **a)** methionine, **b)** tyrosine and **c)** serine, and **d)** threonine, metabolites were extracted using 0.1 M HCl (2.6.1) from the leaf tissue of six-week-old plants grown on soil under short-day conditions (2.5.2). Then, the amino acids were derivatized using AccTaq (2.6.2). Derivatized samples were separated and quantified using HPLC. Data are shown as means ± SD, n=3-6 biological replicates; each biological replicate represents an individual plant. Different letters indicate significant differences ($p<0.05$) using one-way ANOVA followed by Tukey's test.

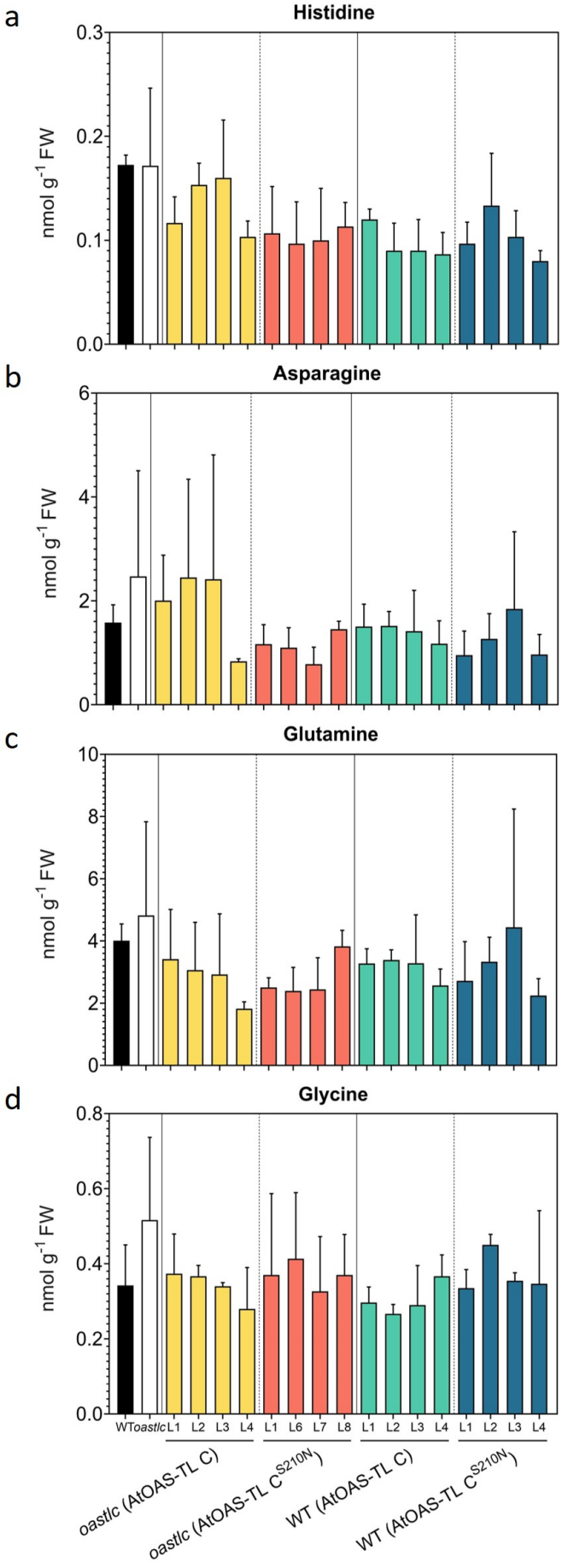

Figure 3.42: **Steady-state levels of amino acids in the leaves of complemented *oastlc* and wild-type lines.** To analyze amino acids **a)** histidine, **b)** asparagine and **c)** glutamin, and **d)** glycine, metabolites were extracted using 0.1 M HCl (2.6.1) from the leaf tissue of six-week-old plants grown on soil under short-day conditions (2.5.2). Then, the amino acids were derivatized using AccTaq (2.6.2). Derivatized samples were separated and quantified using HPLC. Data are shown as means ± SD, n=3-6 biological replicates; each biological replicate represents an individual plant. Different letters indicate significant differences ($p<0.05$) using one-way ANOVA followed by Tukey's test.

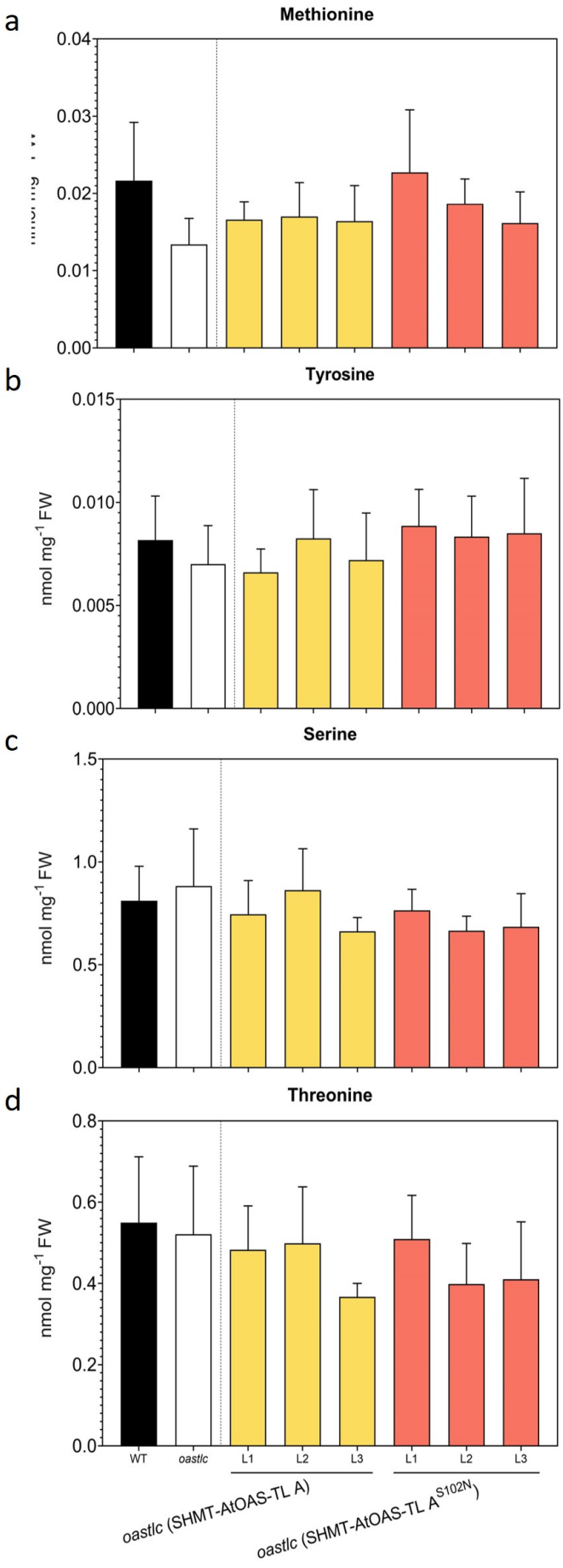

Figure 3.43: **Steady-state levels of amino acids in the leaves of complemented *oastlc*.** To analyze amino acids **a)** methionine, **b)** tyrosine and **c)** serine, and **d)** threonine, metabolites were extracted using 0.1 M HCl (2.6.1) from the leaf tissue of six-week-old plants grown on soil under short-day conditions (2.5.2). Then, the amino acids were derivatized using AccTaq (2.6.2). Derivatized samples were separated and quantified using HPLC. Data are shown as means ± SD, n=3-6 biological replicates; each biological replicate represents an individual plant. Different letters indicate significant differences ($p<0.05$) using one-way ANOVA followed by Tukey's test.

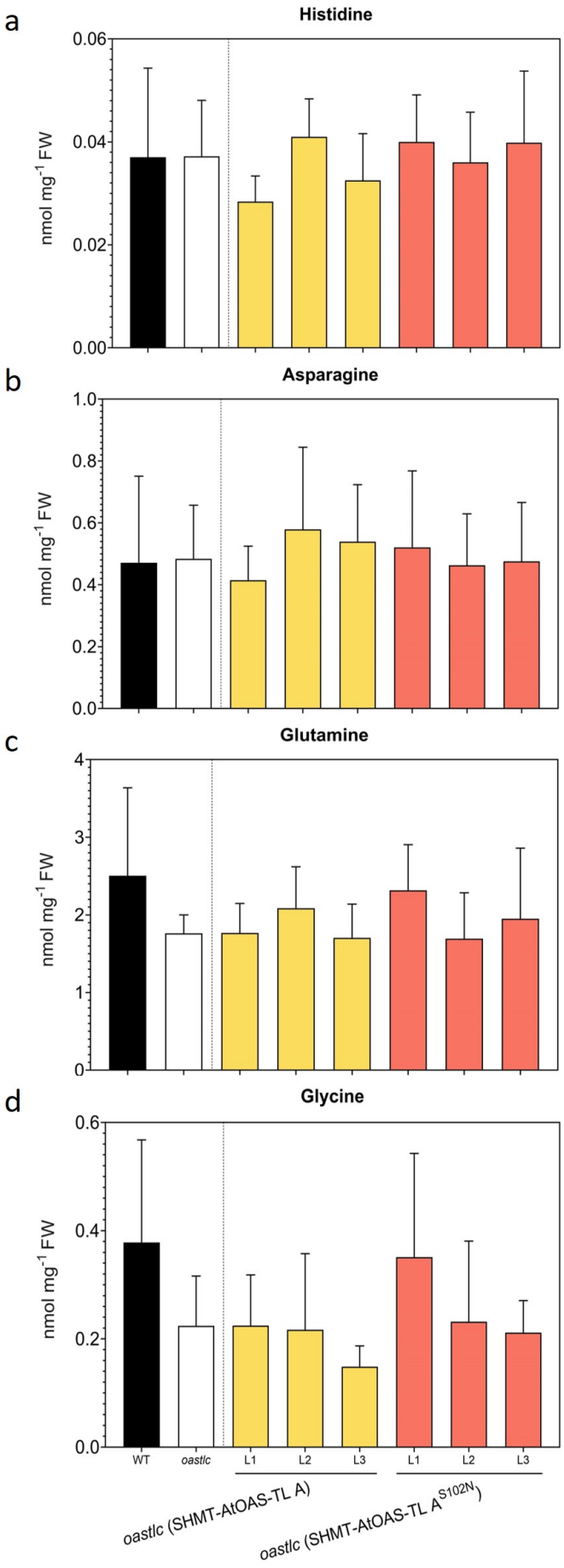

Figure 3.44: **Steady-state levels of amino acids in the leaves of complemented *oastlc*.** To analyze amino acids **a)** histidine, **b)** asparagine and **c)** glutamin, and **d)** glycine, metabolites were extracted using 0.1 M HCl (2.6.1) from the leaf tissue of six-week-old plants grown on soil under short-day conditions (2.5.2). Then, the amino acids were derivatized using AccTaq (2.6.2). Derivatized samples were separated and quantified using HPLC. Data are shown as means ± SD, n=3-6 biological replicates; each biological replicate represents an individual plant. Different letters indicate significant differences ($p<0.05$) using one-way ANOVA followed by Tukey's test.

3.9 Characterization of transformants under cadmium treatment

Phytochelatins are synthesized from cysteine and are essential for detoxifying heavy metals (Cobbett 2000). The precursor of cysteine synthesis OAS might also be in high demand under heavy metal stresses such as cadmium. The results in this study demonstrated the higher steady-state concentration of cysteine, as a component of phytochelatins, and OAS in the mutants complemented with specific-mutated cytosolic and mitochondrial OAS-TL. However, exposure to sub-lethal doses of cadmium has been shown to create a sink for reduced sulfur due to the demand for cysteine in phytochelatins (Yamaguchi et al. 2017). Stressing transgenic Arabidopsis plants with cadmium consequently allows to indirectly assess the potential dynamics of cysteine formation beyonf steady-state levels via deposition into phytochelatins. Therefore, the root growth performance of these transgenic plants under cadmium treatment was measured to examine the response under stress.To determine the best cadmium concentration for the experiment, wild-type and *oastla* seeds were germinated and grown on AT medium with varying levels of $CdCl_2$, ranging from 0 to 250 μM (i.e., 0, 50, 100, 150, 200, 250 μM) to assess growth impairment under these conditions. This process is illustrated in Figure S46. Then, *oastla*, *serat1;1*, and *a1;1* complemented with *At*OAS-TL A or *At*OAS-TL A^{S102N} as well as wild-type, *oastla*, *serat1;1*, and *a1;1* as controls were grown on ½ AT medium (Table 2.4) plates containing 100 μM $CdCl_2$ for five weeks under short-day conditions (2.5.3) as this cadmium concentration allowed for phenotypes under sub-lethal stress. The root length of 30-40 five-week-old seedlings in each group was determined and compared against wild-type seedlings of the same age (Fig. 3.45). The wild-type and *oastla* seedlings under control conditions and cadmium treatment indicated comparable root lengths. However, both showed a significantly lower root length under cadmium treatment (+Cd) than the control condition (Ctrl) (Fig. 3.45, a). The complemented *oastla* plants with either *At*OAS-TL A or *At*OAS-TL A^{S102N} indicated a general reduction in the root length compared to the *oastla*. Nevertheless, *oastla* (*At*OAS-TL A^{S102N}) represented identical root length in cadmium treatment (+Cd) and control condition (Ctrl), whereas the root length of *oastla* (*At*OAS-TL A) reduced significantly under cadmium treatment (Fig. 3.45, a). Thus, transgenic plants expressing modified AtOAS-TLA S102N were able to maintain root length under cadmium stress, suggesting that enhanced cysteine synthesis may have provided more phytochelatins resulting in less stress and growth reduction. Nonetheless, the

results of complemented *serat1;1* and *a1;1* were rather different. The average root length of *serat1;1* was significantly lower than wild-type plants in general. Moreover, it indicated a reduction in root length when treated with cadmium. Interestingly, both complemented *serat1;1* (*At*OAS-TL A) and *serat1;1* (*At*OAS-TL A^{S102N}) displayed a significant decline in root length under cadmium treatment compared to the controls (Fig. 3.45, b). Likewise, control *a1;1* seedlings represented much lower root length than wild-type plants, almost as lowered as the root length of wild-type plants under cadmium treatment. Similar to the result of complemented *serat1;1* plants, the root length of both *a1;1* (*At*OAS-TL A) and *a1;1* (*At*OAS-TL A^{S102N}) showed a significant reduction compared to the control condition (Fig. 3.45, c). The results support the importance of SERAT for the production of cysteine via the CSC.

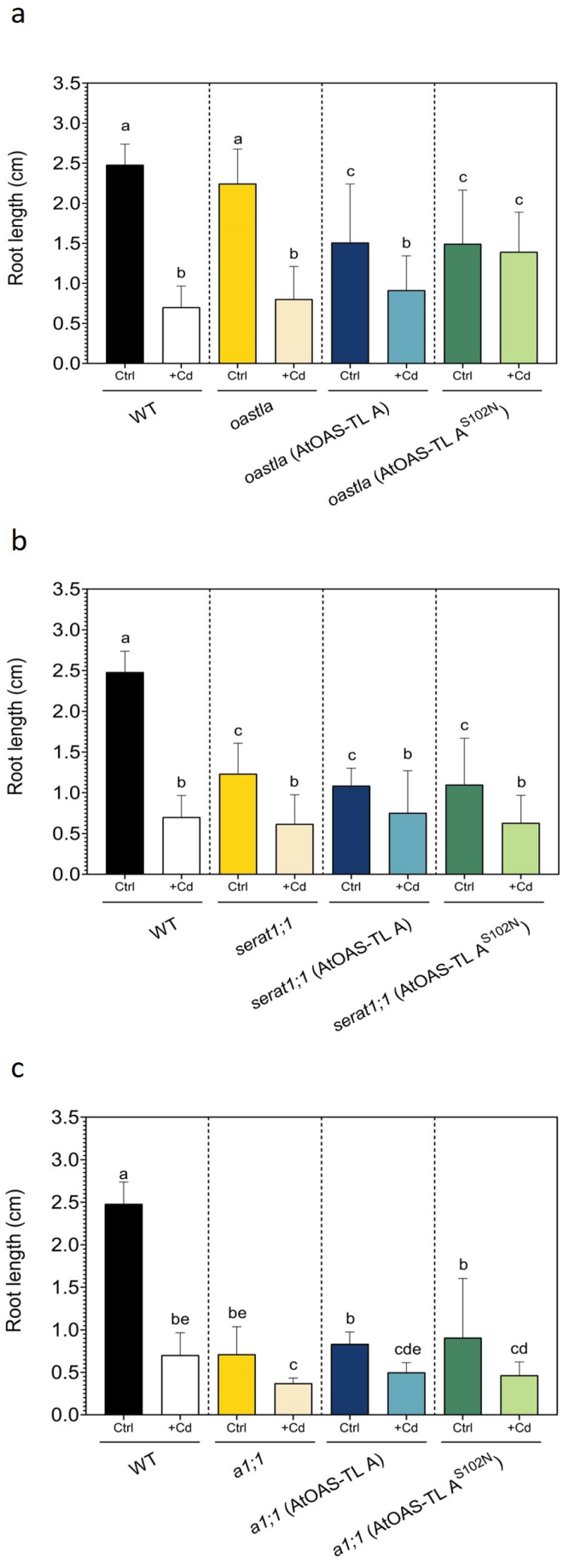

Figure 3.45: **Root growth of complemented T2 transgenic plants under cadmium treatment.** Seeds of different T2 transgenes and wild-type were germinated in ½ Hoagland agar (Table 2.4) containing 100 µM $CdCl_2$ and incubated for five weeks under short-day conditions (2.5.2). Data are shown as means ± SD, n=30-40 biological replicates; each biological replicate represents an individual seedling. Different letters indicate significant differences ($p<0.05$) using one-way ANOVA followed by Tukey's test.

4 | Discussion

Cysteine is a sulfur-containing amino acid and is an integral component in numerous biological processes. For example, it is involved in protein synthesis, redox signaling, and producing vital biomolecules like GSH. The biosynthesis of cysteine in plants and bacteria is catalyzed by the cysteine synthase complex, which consists of two subunits: O-acetylserine (thiol) lyase (OAS-TL) and serine acetyltransferase (SERAT). The complex regulates the cysteine biosynthesis pathway and manages sulfur assimilation and metabolism (Hell et al. 2011). The cysteine synthase complex has been extensively studied in plants, where it is known to be regulated by various environmental cues such as nutrient availability. However, the molecular mechanisms underlying this regulation remain largely unknown. Therefore, recent studies have focused on the cysteine synthase complex's structural and functional characterization, aiming to understand its catalytic mechanism and regulation better (Wirtz et al. 2006; Wirtz et al. 2010).

This research aimed to examine the cysteine synthase complex in two distinct subcellular compartments of *Arabidopsis thaliana*. To achieve a better understanding of the complex's functionality in these areas, I intended to employ a mutation that has been previously examined in rice. The mutation involves substituting serine with asparagine at position 189 in the *OsASTOL1*, which has been shown to affect the stability and activity of the cysteine synthase complex in rice (Sun et al. 2021). However, before proceeding with the experiments, I aimed to ascertain whether the target mutation demonstrates analogous characteristics in Arabidopsis as in rice. The second objective was to investigate the role of SERAT in regulating the CS complex. To test if SERAT activity affects cysteine synthesis in the complex, the specific mutation was introduced likewise into plants that lacked functional endogenous cytosolic SERAT. Finally, an analysis was conducted on transgenic plants to evaluate their response to elevated levels of heavy metals.

4.1 *At*OAS-TL A^{S102N} and *At*OAS-TL C^{S210N} make a stable cysteine synthase complex *in vitro*

Notably, the occurrence of OAS, a compound exclusively synthesized by SERAT, could challenge the interaction with the C-terminus of SERAT and bind with it effectively, mainly when it is present in substantial amounts. Such a scenario could result in the dissociation of the CS complex, comprising SERAT and OAS-TL (Kredich et al. 1969; Huang et al. 2005; Francois et al. 2006), making CS complex unstable and challenging to study. Through analysis of the amino acid sequences of three *A. thaliana* OAS-TLs, it was determined that the level of identity between them is notably high (Bonner et al. 2005). Moreover, rice *Os*ASTOL1 displays considerable sequence similarity to the mentioned *At*OAS-TLs, despite additional amino acid residues at the N-terminus responsible for the transit peptide (Fig. S48 S49).

A specific mutation in serine 189 in *Os*ASTOL1 in rice elevated the physical interaction of chloroplast-localized OAS-TL and SERAT proteins and led to formation of a non-dissociable CS complex (Sun et al. 2021). This specific serine is highly conserved and observed in residue S102 in *At*OAS-TL A and S210 in *At*OAS-TL C. Upon completion of a pull-down analysis, it has been ascertained that the CS complex, comprising *At*OAS-TL A^{S102N} and cytosolic *At*SERAT1;1, exhibited a markedly elevated resistance level towards OAS dissociation. Likewise, it must be emphasized that the association between cytosolic *At*OAS-TL A^{S102N} and mitochondrial *At*SERAT2;2 also exhibited non-dissociative characteristics. Nevertheless, although the interaction between mitochondrial *At*OAS-TL C^{S210N} and mitochondrial *At*SERAT2;2 appeared inseparable, mitochondrial *At*OAS-TL C^{S210N} failed to form a non-dissociable complex with cytosolic *At*SERAT1;1.

The specificity of protein-protein interactions may be influenced by subtle differences in their binding domains, which may vary based on their subcellular localization. For instance, the ability of OAS-TL A to interact with cytosolic SERAT1;1 and mitochondrial SERAT2;2 proteins suggests that it may have a more promiscuous binding site capable of recognizing multiple targets. Conversely, the failure of OAS-TL C to form a non-dissociable complex with cytosolic SERAT1;1 indicates that its binding site is more specific to mitochondrial SERAT2;2. Furthermore, the weaker or less specific binding interactions between mitochondrial OAS-TL C protein and cytosolic SERAT1;1 may make their complex easier to dissoci-

ate. Nevertheless, it should be noted that *in vitro* results do not necessarily correspond to *in vivo* studies, where proteins exist in their natural cellular environment and are subject to post-translational modifications and fluctuations in protein concentrations. In conclusion, the findings suggest that the desired results, which were forming a stable complex between SERAT and either mutated cytosolic or mitochondrial OAS-TL, were supported by the *in vitro* analysis, resembling the findings observed in the prior study (Sun et al. 2021). The outcomes of the *in vitro* experiments are encouraging and lay the groundwork for further investigations in the *in vivo* setting.

4.2 S210 of *At*OAS-TL C is essential for OAS-TL activity

Based on empirical evidence from *in vitro* experiments, replacing the amino acid residue Ser102 with Asn in the OAS-TL A protein resulted in the complete inactivation of the mutant OAS-TL A^{S102N} protein (Sun et al. 2021). Consistent with prior research, the *in vitro* analysis of the enzymatic activity in this study confirms that the mutated OAS-TL C^{S210N} exhibits significantly diminished activity relative to the wild-type OAS-TL C.

Even though SERAT has a lower cellular activity compared to OAS-TL by 100-300 folds (Ruffet et al. 1994), its activity within the CS complex is significantly higher than OAS-TL activity due to the aforementioned binding in the catalytic centre of OAS-TL. Consequently, the amount of SERAT inside the complex defines the rate of OAS production and cysteine synthesis (Droux et al. 1998). The formation of a non-dissociable CS complex is anticipated to result in the permanent stimulation of SERAT, which will subsequently increase its activity. Therefore, a comparison was made between the SERAT activity observed in crude plant protein extracts of the WT, *oastla*, *oastla* (*At*OAS-TL A), *oastla* (*At*OAS-TL A^{S102N}), *oastlc*, *oastlc* (*At*OAS-TL C), and *oastlc* (*At*OAS-TL C^{S210N}) samples to assess the ability of the mutated *At*OAS-TL protein to stimulate endogenous SERAT activity. Based on the results, the *oastlc* (*At*OAS-TL C^{S210N}) plants exhibit a notably elevated activity level of SERAT activity compared to the *oastlc* (*At*OAS-TL C), *oastlc*, and wild-type plants. However, the complementation of the *oastla* mutant with either *At*OASTL A or *At*OAS-TL A^{S102N} exhibited a comparable level of SERAT activity to that of the *oastla* and wild-type plants. It must be considered that although SERAT isoforms in Arabidopsis have different subcellular localizations (Noji et al. 1998), the activity of the SERAT enzyme is not uniform throughout the cell but instead varies depend-

ing on its location. Specifically, most of its activity has been observed to occur within the mitochondria (Ruffet et al. 1995; Droux 2003), highlighting the importance of mitochondria in OAS production (Wirtz et al. 2007). Therefore, it can be hypothesized that forming a non-dissociable complex between the mutated *At*OAS-TL CS210N and SERAT2;2 in the mitochondria would result in a significantly higher SERAT activity compared to forming a non-dissociable complex between the mutated *At*OAS-TL AS102N and SERAT1;1 in the cytosol, and the result in this study support this hypothesis.

4.3 Characterization of the complemented transformants with cytosolic and mitochondrial *At*OAS-TLs

The phenotype of the *oastla* plants was comparable to that of the wild-type plants, whereas the *oastlc* mutant plants exhibited a noticeable reduction in their overall size (Heeg et al. 2008). According to the previous studies, there were no apparent phenotypic alterations observed in any of the individual *serat* mutants when compared to the wild type, regardless of whether they were cultivated in germination growth agar (Watanabe et al. 2008b) or in soil (Watanabe et al. 2018). Nonetheless, *oastlc*, *serat1;1*, and *a1;1* plants used in this study were smaller than wild-type and *oastla* plants (Fig. 3.5). Moreover, the complementation of mentioned mutants and wild-type plants with cytosolic *At*OAS-TL A and mitochondrial *At*OAS-TL C did not result in any evident changes to the physical characteristics of the plants (Fig. 3.9).

During the genotyping process, primers were aligned with genomic DNA and complementary DNA of the gene of interest. As a result, transformants containing the endogenous gene, such as wild-type plants complemented with either *At*OAS-TL A or *At*OAS-TL A^{S102N}, displayed two distinct signals of varying sizes. The larger signal corresponded to genomic DNA, while the smaller signal corresponded to complementary DNA. Occasionally, there were instances where the signal strength for either genomic DNA or complementary DNA was lower. This may attribute to the copy number variation of transgene and the endogenous gene within the genome of the transformants, leading to a more or lower intense signal when amplified by PCR (Ingham et al. 2001; Kong et al. 2009). Other important factors in this context include the integration site of the transgene (Palmiter et al. 1986) and transgene rearrangement (DuBose et al. 2013).

4.4 Transcriptome analysis of transformants

Through the examination and analysis of mRNA levels in transformants, valuable insights can be acquired into the expression of the introduced transgene. Such analysis offers a means of assessing the efficacy of the 35S promoter in driving transgene expression, as well as comprehending the transcriptional activity of the transgene and its potential impact on downstream cellular processes. Therefore, to assess the expression of the OAS-TL variants in T1 and T2 individuals and to select suitable lines for further investigation, a quantitative expression analysis of the AtOAS-TL transcript was carried out using qRT-PCR (2.3.13).

Upon analyzing individuals in T1, it has been observed that the transcript level of *AtOAS-TL A* and *AtOAS-TL C* has increased, albeit to varying degrees. After transforming with either *At*OAS-TL A or *At*OAS-TL A^{S102N}, complemented *oastla* and wild-type plants showed a significant increase in *AtOAS-TL A* transcript level, exceeding in some cases 300-fold. However, in *serat1;1* (*At*OAS-TL A / *At*OAS-TL A^{S102N}) and *oastlc* (SHMT-*At*OAS-TL A / SHMT-*At*OAS-TL A^{S102N}), the increase was only up to 100-fold, and in *a1;1* (*At*OAS-TL A / *At*OAS-TL A^{S102N}) plants, up to 56-fold. Additionally, the *AtOAS-TL C* transcript level in complemented *oastlc* and wild-type plants with either *At*OAS-TL C or *At*OAS-TL C^{S210N} increased up to 32- and 89-fold, respectively. Likewise, the transcript levels of both *AtOAS-TL A* and *AtOAS-TL C* increased significantly in the T2 transformants. The *oastla* and wild-type complemented with either *At*OAS-TL A or *At*OAS-TL A^{S102N} represented up to 117- and 241-fold increases in *AtOAS-TL A*, respectively. However, the magnitude of this increase was not as substantial as in T1 plants. On the other hand, the *oastlc* and wild-type plants complemented with either *At*OAS-TL C or *At*OAS-TL C^{S210N} represented up to 112- and 125-fold increases, respectively, in *AtOAS-TL C* transcript level which is relatively higher compare to the same group of transformants in T1. Several variables contributing to the variance in mRNA expression levels of a transgene between the T1 and T2 generations were exemplified earlier, such as integration site and position-dependent effect, transgene copy numbers, epigenetic modification, and transgene silencing. Additionally, it is critical to note that in the T1 generation, the transgene expression may exhibit discrepancies due to genetic segregation. This phenomenon arises from the fact that the T1 generation is generally derived from a single transformed plant, and the transgene can segregate in subsequent generations, resulting in variations in both the copy number and expression levels of the transgene in the T2 generation.

4.5 Protein analysis of transformants

Once the presence of the transgene in transformants was confirmed through genotyping, the mRNA analysis was conducted to determine if the transgene was being expressed and to measure transcriptional activity. However, it's important to note that mRNA levels may not always align with protein expression levels due to factors such as post-transcriptional regulation, mRNA stability, and translation efficiency. Furthermore, relying solely on mRNA analysis may not provide insight into post-translational modifications or protein function. In order to gain precise insight into the presence and abundance of the transgene-encoded protein, western blotting was conducted for the transformants. This approach provides a comprehensive assessment of the functional impact resulting from the transgene expression.

The result of the western blotting analysis revealed distinct protein bands corresponding to the OAS-TL A and OAS-TL C proteins. The intensity of these bands varied among the experimental groups, indicating potential differences in protein expression levels. In certain instances, comparable signal intensities were noted. However, there were also cases where only one isoform of OAS-TL was selectively overexpressed, displaying the highest intensity and distinct band differences. This observation emphasizes the successful enrichment of either OAS-TL A or C as the desired objective. Transformed *oastla* and *a1;1* with either *At*OAS-TL A or *At*OAS-TL A^{S102N}, lacking the endogenous *At*OAS-TL A, exhibited robust signals corresponding to the OAS-TL A protein. Nevertheless, wild-type (*At*OAS-TL A / *At*OAS-TL A^{S102N}), *serat1;1* (*At*OAS-TL A / *At*OAS-TL A^{S102N}), and *oastlc* (SHMT-*At*OAS-TL A / SHMT-*At*OAS-TL A^{S102N}) plants, possessing endogenous *At*OAS-TL A, indicated comparable signal intensity for the same protein. These results indicate that introducing *At*OAS-TL A and *At*OAS-TL A^{S102N} constructs into the plants that either possess or lack the endogenous OAS-TL A protein results in equivalent levels of expressed OAS-TLA protein in both groups of transformants. Besides possible experimental artifacts, various factors could account for this outcome. First, the 35s promoter utilized in the construct is a robust promoter that can elevate gene expression levels in diverse plant tissues. It is plausible that the potent 35s promoter compensated for the lack of the endogenous OAS-TL gene in the *oastla* and *a1;1* mutant, resulting in comparable levels of OAS-TLA protein expression in these transformants compared to the complemented plants containing the endogenous OAS-TL A protein. Second, the western blotting methodology poses certain limitations in accurately assessing protein

levels, e.g., due to the saturation of the detected signal. When there is significant protein expression, as in this example for complemented plants possessing the endogenous OAS-TL A with either *At*OAS-TL A or *At*OAS-TL A^{S102N}, the signal on the Western blot can reach saturation levels. The saturation can pose difficulties in accurately determining the absolute or relative levels of the highly expressed protein, as it may overwhelm the detection system. Likewise, complemented *oastlc* and wild-type plants with either *At*OAS-TL C or *At*OAS-TL C^{S102N} depicted the signal corresponding to the OAS-TL C protein. Nonetheless, the intensity of the signal in the complemented wild-type plants with AtOAS-TL C / AtOAS-TL C^{S102N} was higher.

4.6 Sulfur-related metabolites in complemented transformants with cytosolic and mitochondrial *At*OAS-TL

Thiols are a class of organic compounds with a sulfhydryl (-SH) group and play a crucial role in various cellular processes, including redox regulation, antioxidant defense, and protein structure stabilization (Noctor et al. 1998b; Buchanan et al. 2005). In-depth research on thiols has been conducted on *Arabidopsis thaliana*, a plant species that contains a diverse set of thiols, including GSH, which is the most abundant thiol in Arabidopsis, phytochelatins (PCs), and thioredoxins (TRXs). The biosynthesis of thiols in Arabidopsis is regulated through the control of *O*-acetylserine (OAS), which regulates cysteine production (Droux 2004). Cysteine is a crucial precursor for synthesizing glutathione (GSH) and phytochelatins (PCs) (Foyer et al. 2011). Extensive research has revealed that OAS plays a vital role in regulating the production of thiols by controlling the activity of SERAT (serine acetyltransferase). Elevated levels of OAS inhibit SERAT activity, leading to a decrease in cysteine and thiol production. Conversely, decreased levels of OAS stimulate SERAT activity, increasing cysteine and thiol production (Wirtz et al. 2006; Heeg et al. 2008; Hell et al. 2011).

According to the findings of *in vitro* analysis in this study, it has been observed that the mutated cytosolic *At*OAS-TL A^{S102N} could generate a stable CS complex that exhibits resistance to dissociation in the presence of OAS accumulation. Therefore, the steady-state level of OAS should be raised because of the constant stimulation of SERAT in the CS complex. In order to validate this concept *in vivo*, an analysis was conducted on the steady-state levels of OAS, cysteine, and glutathione in transgenic plants under investigation in this study. Upon initial

observation, it was observed that *oastla* plants that lacked the functional endogenous *At*OAS-TL A exhibited similar OAS levels to those of the wild-type plants. This was an anticipated outcome, as the synthesis of OAS primarily takes place within the mitochondria rather than the cytosol (Haas et al. 2008; Watanabe et al. 2008b; Krueger et al. 2009). Furthermore, upon the comparison of *oastla* and wild-type plants that were transformed with the *At*OAS-TL A to the control group, it was observed that there were no significant differences in the concentrations of OAS and thiols. This outcome is consistent with the current models of the CS complex, wherein the accumulation of OAS triggers the dissociation of the CS complex, thereby hindering subsequent OAS production (Wirtz et al. 2006). Moreover, the findings demonstrated that wild-type plants that were complemented with *At*OAS-TL A^{S102N} displayed elevated levels of OAS up to 10.6-fold. Likewise, the *oastla* (*At*OAS-TL A^{S102N}) plants exhibited a similarly high concentration of OAS up to 12.5 fold. Further analysis revealed that, in comparison to the control plants, the complemented wild-type (*At*OAS-TL A^{S102N}) and *oastla* (*At*OAS-TL A^{S102N}) plants contained elevated levels of cysteine up to 4- and 5.4-fold and glutathione up to 2.5- and 2.6-fold, respectively. These findings strengthen the possibility that mutated cytosolic *At*OAS-TL A^{S102N} can form a stable CS complex in Arabidopsis. As a result, permanent stimulation of SERAT would lead to increased OAS production and a greater level of thiols. These findings are in concordance with the previous investigation conducted on rice (Sun et al. 2021).

However, complementing the *serat1;1* mutant with either *At*OAS-TL A or *At*OAS-TL A^{S102N} did not result in increased levels of OAS, cysteine, or glutathione compared to the control condition. Furthermore, it should be noted that the *a1;1* (*At*OAS-TL A^{S102N}) plants devoid of both endogenous OAS-TL A and SEART1;1 demonstrated comparable outcomes regarding OAS and thiol levels compared to the transformed *serat1;1* plants. Based on the findings, it has been observed that the mutated *At*OAS-TL A^{S102N} can generate a stable CS complex within the cytosolic environment. However, to ensure the uninterrupted synthesis of OAS and thiols, the functional endogenous SERAT1;1 is imperative.

Investigating the steady-state level of OAS in both wild-type and *oastlc* plants complemented with mutated mitochondrial *At*OAS-TL C^{S210N} likewise demonstrated an increase up to 7.1- and 3.8-fold, respectively. However, the accumulation of OAS in these transformants was found to be slighter compared to wild-type and *oastla* plants transformed with the mutated

cytosolic *At*OAS-TL A^{S102N}. Upon comparison, it was observed that two out of four transformed lines from the WT (*At*OAS-TL C^{S210N}) group showed a significant increase in cysteine and glutathione levels up to 2.9- and 1.5-fold compared to WT (*At*OAS-TL C). Further, the *oastlc* (AtOAS-TL C^{S210N}) displayed a substantial elevation in glutathione concentrations up to 2.6-fold compared to the control group. In conclusion, it appears that a modified variant of mitochondrial *At*OAS-TL C^{S210N} has the potential to generate a stable CS complex within the Arabidopsis, increasing OAS production as it continuously activates SERAT2;2.

In the supplementary analysis, the OAS and thiol levels were examined in the *oastlc* transformant, which was complemented with cytosolic *At*OAS-TL A^{S102N}. Within these transformed organisms, the cytosolic *At*OAS-TL A^{S102N} protein targeted to the mitochondria facilitated by the SHMT (serine hydroxymethyltransferase) transit peptide. Surprisingly, OAS, cysteine, and glutathione concentrations in these transformants exhibited no significant variations. This result implies that while cytosolic *At*OAS-TL A^{S102N} successfully formed a stable CS complex with mitochondrial *At*SERAT2;2 *in vitro*, the CS complex comprising these two proteins does not exhibit the same biochemical impact in living organisms.

Various studies have demonstrated that the accumulation of OAS dissociates the CS complex that constitutes SERAT and OAS-TL, impeding the activity of SERAT and ultimately leading to a reduction in thiol biosynthesis (Kredich et al. 1969; Huang et al. 2005; Francois et al. 2006). The results of this study indicate that mutated cytosolic *At*OAS-TL A^{S102N} and mitochondrial *At*OAS-TL C^{S210N} can establish a stable CS complex in the respective cytosolic and mitochondrial environments of Arabidopsis. Consequently, continuous stimulation of the corresponding SERAT in the cytosol would boost OAS production and lead to elevated levels of thiols. Nonetheless, having the functional endogenous SERAT is crucial to maintaining the continuous synthesis of OAS and thiols. These findings suggest that the elevated physical interaction of OAS-TL and SERAT proteins in the CS complex in rice due to the specific mutation identified in chloroplast-localized OAS-TL is transferable to Arabidopsis, highlighting its versatility. Furthermore, the formation of stable CS complex observed in cytosol and mitochondria by employing the cytosolic *At*OAS-TL A^{S102N} and mitochondrial *At*OAS-TL C^{S210N}, respectively, indicating that this effect is not limited to chloroplast localized OAS-TL isoform, implying the transferability of the effect to other compartments. It is important to note that the outcome observed *in vitro* was only partially consistent with the *in vivo* results. Specifi-

cally, *At*OAS-TL A^{S102N} and *At*OAS-TL C^{S210N} demonstrated the ability to form a stable complex with cytosolic SERAT1;1 and mitochondrial SERAT2;2, respectively, *in vitro*. The same outcome was observed *in vivo*. However, the formation of a stable complex between *At*OAS-TL A^{S102N} and mitochondrial SERAT2;2 *in vitro* yielded a different result *in vivo*. The results from the *oastlc* (SHMT-*At*OAS-TL A^{S102N}) indicate that the mutated cytosolic *At*OAS-TL A^{S102N} is incapable of forming a stable complex in mitochondria.

Numerous research studies have been conducted utilizing various methodologies to elevate cysteine and glutathione levels in plant organisms. For instance, the overexpression of γ-glutamylcysteine synthetase (γ-EC), a crucial enzyme involved in GSH biosynthesis, from *E. coli* has been found to increase GSH content in poplar by four-fold (Arisi et al. 1997), in tobacco leaves by three-fold (Creissen et al. 1999), in Brassica juncea by 2.5-fold (Zhu et al. 1999), and in Arabidopsis by three-fold (Li et al. 2006). Following the overexpression of enzymes involved in the biosynthesis of cysteine, a notable increase of up to five times in glutathione levels was observed (Blaszczyk et al. 1999; Matityahu et al. 2006). Compared to past accomplishments, transgenic tobacco plants expressing feedback-insensitive glutathione synthetase enzyme from *Streptococcus thermophilus* (*St*GCL-GS) indicated up to 12 μmol GSH/gFW, which was 20-fold higher content compared with control plants. Remarkably, the significantly elevated production of GSH does not appear to affect plant growth but instead augments plant resilience to abiotic stressors (Liedschulte et al. 2010). The transgenic tobaccos expressing *St*GCL-GS present a promising and cost-effective alternative for the production of GSH, as they can compete with yeast-based systems (Li et al. 2004). Moreover, experiments of transgenic tobacco plants expressing Arabidopsis active and inactive SERAT in the cytosol exhibited significant increases in the OAS, Cys, and glutathione. Specifically, active SERAT expression has resulted in a 2.3-fold increase in OAS, a 5-fold increase in cysteine, and a 1.7-fold increase in glutathione. In contrast, the inactive expression of SERAT has led to a 3.5-fold increase in OAS, a 30-fold increase in cysteine, and a 2.3-fold increase in glutathione (Wirtz et al. 2007). Consistent with the previous results, a recent study showed that the expression of inactive SERAT in the cytosol and plastid of tobacco led to up to a 7.8-fold increase in OAS, 23-fold increase in cysteine, and a 2.3-fold increase in glutathione, which was higher than that of in plants expressing active SERAT in the same subcellular localization. These findings suggest that the improved accumulation of cysteine in transgenic plants is due to the formation of cysteine synthase complex rather than enhanced SERAT

activity (Wirtz et al. 2023). A recent study reported the constitutive overexpression of the feedback-insensitive SERAT isoform from tobacco (*Nt*SAT4) under the control of 35s promoter in three subcellular compartments of *Brassica napus* using different transit peptides. The result showed a significant increase in the steady-state level of free cysteine, ranging from 2.5-fold to 3.5-fold, and a corresponding 2.2-fold to 5.3-fold elevation in GSH levels in leaves compared to non-transformed plants. In contrast to the findings of this research, the mitochondrial-targeted SERAT overexpressor indicated the most elevated levels of cysteine and glutathione, up to 3.5-fold and 5.3-fold, compared with wild-type plants.

Compared to prior investigations, the employed approach in the current study resulted in a significant upregulation of OAS, a recognized indicator of cysteine and glutathione biosynthesis. However, this increase in OAS levels did not correspond proportionally to the cysteine and glutathione pools, indicating a potential discrepancy between OAS accumulation and thiol production. Notably, prior overexpression strategies have indicated more substantial enhancements in either cysteine or glutathione content. These observations collectively suggest the possibility of accelerated turnover rates for either OAS or thiols in the cellular milieu, which may contribute to the maintenance of lower steady-state concentrations.

4.6.1 Anions in complemented transformants with cytosolic and mitochondrial *At*OAS-TL

OAS plays a crucial role in sulfur assimilation and serves as the carbon building block for cysteine synthesis (Hoefgen et al. 2008). Evidence obtained from studies on sulfur assimilation in enteric bacteria suggested a putative signaling role of *O*-acetyl serine (OAS). These bacteria utilize the contents of OAS to indicate their intracellular sulfur levels (Ostrowski et al. 1990; Ostrowski et al. 1991; Lynch et al. 1994). Besides, the utilization of OAS in plants led to an increase in the expression of genes associated with sulfur assimilation, such as *SULTR1;1* and *SULTR1;2* (Takahashi et al. 1997; Koprivova et al. 2000; Kopriva et al. 2002; Hesse et al. 2003; Maruyama-Nakashita et al. 2004), and sulfur deprivation resulted in OAS accumulation (Hirai et al. 2003; Maruyama-Nakashita et al. 2003; Nikiforova et al. 2003). On the other hand, there seems to be some ambiguity surrounding the potential use of OAS as a signaling compound, mainly based on the argument that OAS is restricted even for thiol synthesis (Neuenschwander et al. 1991; Kopriva et al. 1999; Harms et al. 2000; Koprivova et al. 2000; Tsakrak-

lides et al. 2002; Hesse et al. 2003). Furthermore, no overlap was observed in other studies between the OAS content and the expression *SULTR* family 1 (sulfate starvation-responsive gene) (Hopkins et al. 2005; Rouached et al. 2008). However, regardless of OAS's signaling role, increasing the OAS concentration within the cell requires a raise in sulfide level for the second step of cysteine synthesis, in which sulfide integrates into the carbon backbone *O*-acetylserine (OAS). According to the findings in this study, complemented *oastla* (*At*OAS-TL A^{S102N}), WT (*At*OAS-TL A^{S102N}), *oastlc* (*At*OAS-TL C^{S210N}), and WT (*At*OAS-TL C^{S210N}) plants exhibited an increase in the levels of OAS, cysteine, and glutathione. Therefore, it was anticipated that there would be a sulfide accumulation, as shown in the *astol1* mutant in rice (Sun et al. 2021).

However, upon conducting a thorough analysis of various anions, including sulfate, it was observed that the quantity of sulfate in the transformants and controls did not exhibit a significant difference. Although an analogous outcome was noted in transgenic tobacco plants overexpressing active and inactive Arabidopsis SERAT (Wirtz et al. 2007), contrasting outcomes were observed in the *astol1* mutant of rice (Sun et al. 2021). Nonetheless, the observed discrepancy between the expected sulfate accumulation and the observed unchanged sulfate levels in the transformants can be attributed to several factors, such as impaired sulfate transport mechanisms leading to reduced sulfate acquisition and subsequent failure to accumulate in the plant tissues (Takahashi 2019). Therefore, it is recommended that further investigation be conducted on the expression of genes involved in sulfate uptake and reduction. Additionally, alternative metabolic pathways could be activated to compensate for the reduced function of some enzymes in the sulfate assimilation pathway. These alternative pathways could involve redirecting sulfur flow or utilizing stored sulfur reserves, e.g., from sulfur-containing amino acids or intermediates from other metabolic pathways, enabling cysteine synthesis even in the absence of sulfate accumulation. These metabolites possess a wide range of functions, including serving as proteogenic amino acids such as cysteine and methionine, being derivatives of hormones such as sulfojasmonate and sulfated brassinosteroids, functioning as antioxidants such as Glutathione or secondary metabolites such as sulfoflavonoids, acting as signaling molecules such as phosphonucleotide, PAP (3'-phosphoadenosine 5'-phosphate), and hydrogen sulfide, and playing a role in the synthesis of secondary metabolites such as Glucosinolates and Sulfoflavonoids (Kopriva 2006; Gigolashvili et al. 2014; González-Morales et al. 2021). Thus, it would be beneficial to consider

transcriptomic or proteomic analyses to understand the mechanisms behind cysteine accumulation better and explore potential alternative pathways. These analytical methods provide valuable insights into the molecular mechanisms involved and may uncover promising targets for further investigation.

4.7 *At*OAS-TL A^{S102N} results in improved cadmium tolerance in Arabidopsis

Plants subjected to high levels of cadmium may encounter specific adverse effects such as stunted growth, impaired photosynthesis, root decay, leaf chlorosis, and leaf roll (Kabir et al. 2016; Rahman et al. 2017). In addition, cadmium toxicity can negatively impact gas exchange and transpiration rate, stomatal conductance, and protein metabolism (Wang et al. 2014; Rascio et al. 2008). In plants, phytochelatins (PCs) are well-defined heavy metal-binding ligands that tightly bind metal ions to form complexes and store them in vacuoles (Pinter et al. 2014; Joshi et al. 2016). The results of this study demonstrated that *oastla* and wild-type plants complemented with cytosolic *At*OAS-TL A^{S102N} contain higher amounts of OAS, cysteine, and glutathione. An indirect approach was utilized to assess the flux levels compared to steady-state levels by evaluating the effects of cadmium stress on the root growth of the transformants. Therefore, the root-growth measurement was conducted on transformants after five weeks of growing on ½ AT medium containing 100 μM $CdCl_2$.The result showed that although the root length of *oastla* (*At*OAS-TL A) reduced significantly under cadmium treatment, *oastla* (*At*OAS-TL A^{S102N}) depicted comparable root length in both cadmium treatment (+Cd) and control condition (Ctrl). The experiment results indicate that the transformants displayed a greater resistance to high concentrations of cadmium, which was attributed to a higher quantity of phytochelatins. This suggests an increased turnover of thiols, leading to a lower concentration of thiols in the respective transformants. However, complemented *serat1;1* and *a1;1* plants with either *At*OAS-TL A or *At*OAS-TL A^{S102N} displayed a significant decline in root length under cadmium treatment compared to the controls, indicating the critical role of functional endogenous SERAT to uninterrupted synthesis of OAS and thiols. According to these findings, the S102N in Arabidopsis transformants, which resulted in higher levels of OAS, cysteine, and glutathione through a stable CS complex, can enhance the ability to tolerate cadmium stress, thus offering a promising means to generate

heavy metal stress resilient plant varieties using this method. The obtained results align with the prior study in Arabidopsis (Dominguez-Solis et al. 2001), sorghum (Akbudak et al. 2019), and *Brassica napus* (Rajab et al. 2020).

5 | Supplement

5.1 Membranes used for the immunological detection of *in vitro* pull-down analysis

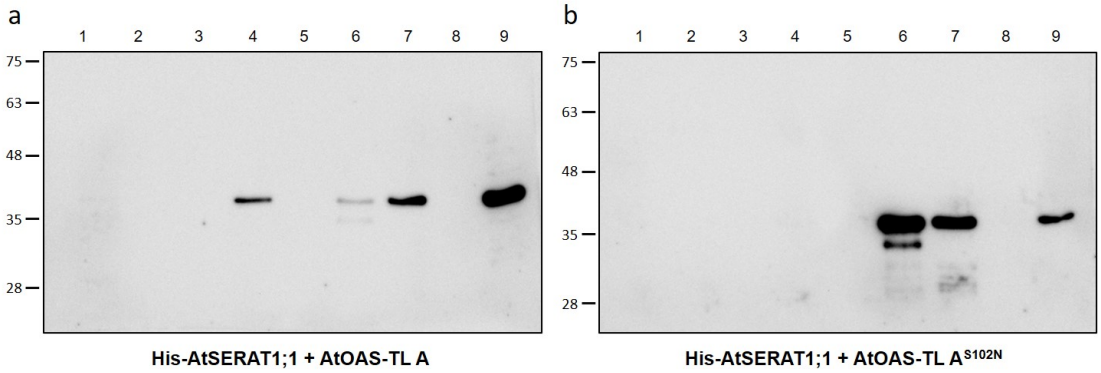

Figure S1: **In vitro pull-down analysis of the dissociation effect of OAS on CS complex consists of cytosolic *At*SERAT1;1 and cytosolic *At*OAS-TL A.** A pull-down analysis was conducted to study the impact of OAS on the dissociation of the CS complex containing *At*SERAT1;1 and **a)** *At*OAS-TL A and **b)** *At*OAS-TL A^{S102N}. First, each elution fraction, containing 2 μg, was loaded into an SDS-PAGE gel (2.4.3), followed by western blotting (2.4.4) and immunological detection (2.4.5) using a polyclonal antibody against the *At*OAS-TL C (1:1000), which can detect all three OAS-TL isoforms simultaneously. The experiment included various lanes containing different samples, including crude extracts and elutions, and washing buffers, with specific imidazole concentrations. Full description of the membrane in Fig. 3.1.

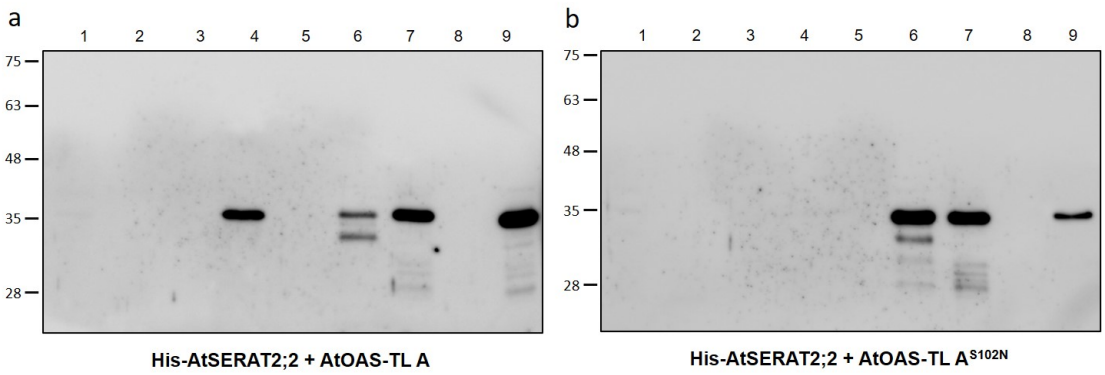

Figure S2: **In vitro pull-down analysis of the dissociation effect of OAS on CS complex consists of mitochondrial *At*SERAT2;2 and cytosolic *At*OAS-TL A.** A pull-down analysis was conducted to study the impact of OAS on the dissociation of the CS complex containing *At*SERAT2;2 and **a)** *At*OAS-TL A and **b)** *At*OAS-TL A^{S102N}. First, each elution fraction, containing 2 μg, was loaded into an SDS-PAGE gel (2.4.3), followed by western blotting (2.4.4) and immunological detection (2.4.5) using a polyclonal antibody against the *At*OAS-TL C (1:1000), which can detect all three OAS-TL isoforms simultaneously. The experiment included various lanes containing different samples, including crude extracts and elutions, and washing buffers, with specific imidazole concentrations. Full description of the membrane in Fig. 3.2.

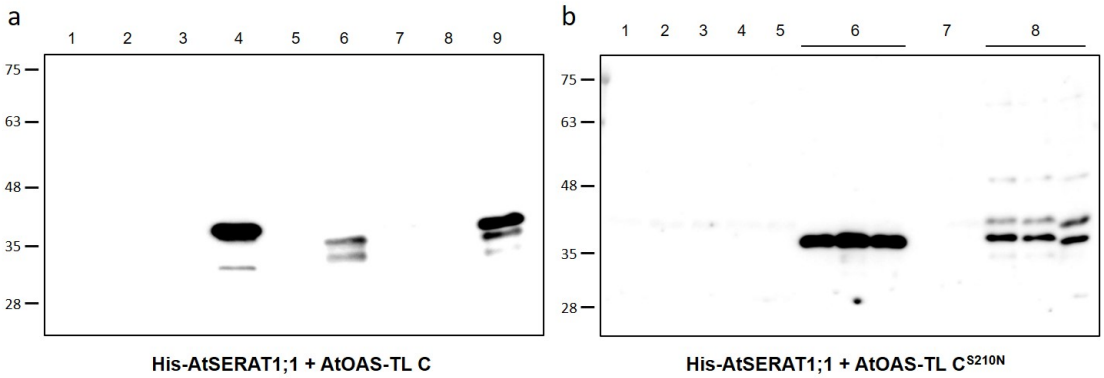

Figure S3: **In vitro pull-down analysis of the dissociation effect of OAS on CS complex consists of cytosolic *At*SERAT1;1 and mitochondrial *At*OAS-TL C.** A pull-down analysis was conducted to study the impact of OAS on the dissociation of the CS complex containing *At*SERAT1;1 and **a)** *At*OAS-TL C and **b)** *At*OAS-TL C^{S210N}. First, each elution fraction, containing 2 μg, was loaded into an SDS-PAGE gel (2.4.3), followed by western blotting (2.4.4) and immunological detection (2.4.5) using a polyclonal antibody against the *At*OAS-TL C (1:1000), which can detect all three OAS-TL isoforms simultaneously. The experiment included various lanes containing different samples, including crude extracts and elutions, and washing buffers, with specific imidazole concentrations. Full description of the membrane in Fig. 3.3.

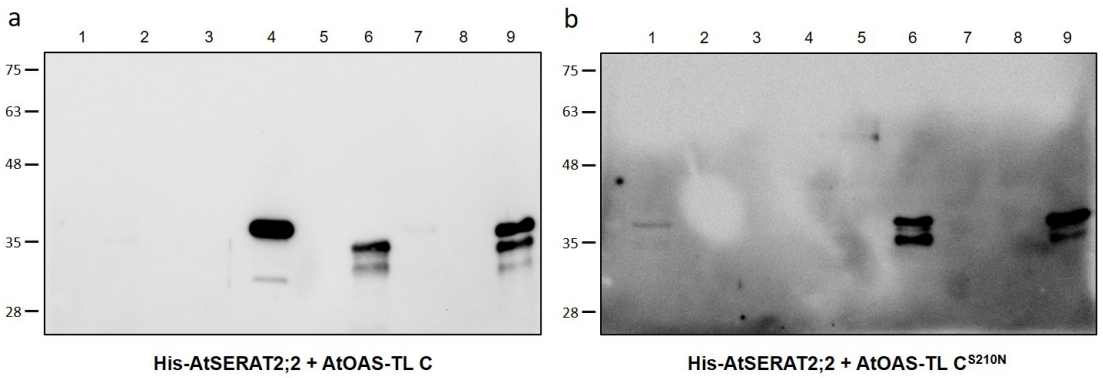

Figure S4: **In vitro pull-down analysis of the dissociation effect of OAS on CS complex consists of mitochondrial *At*SERAT2;2 and mitochondrial *At*OAS-TL C.** A pull-down analysis was conducted to study the impact of OAS on the dissociation of the CS complex containing *At*SERAT2;2 and **a)** *At*OAS-TL C and **b)** *At*OAS-TL C^{S210N}. First, each elution fraction, containing 2 μg, was loaded into an SDS-PAGE gel (2.4.3), followed by western blotting (2.4.4) and immunological detection (2.4.5) using a polyclonal antibody against the *At*OAS-TL C (1:1000), which can detect all three OAS-TL isoforms simultaneously. The experiment included various lanes containing different samples, including crude extracts and elutions, and washing buffers, with specific imidazole concentrations. Full description of the membrane in Fig. 3.4.

5.2 DNA gels

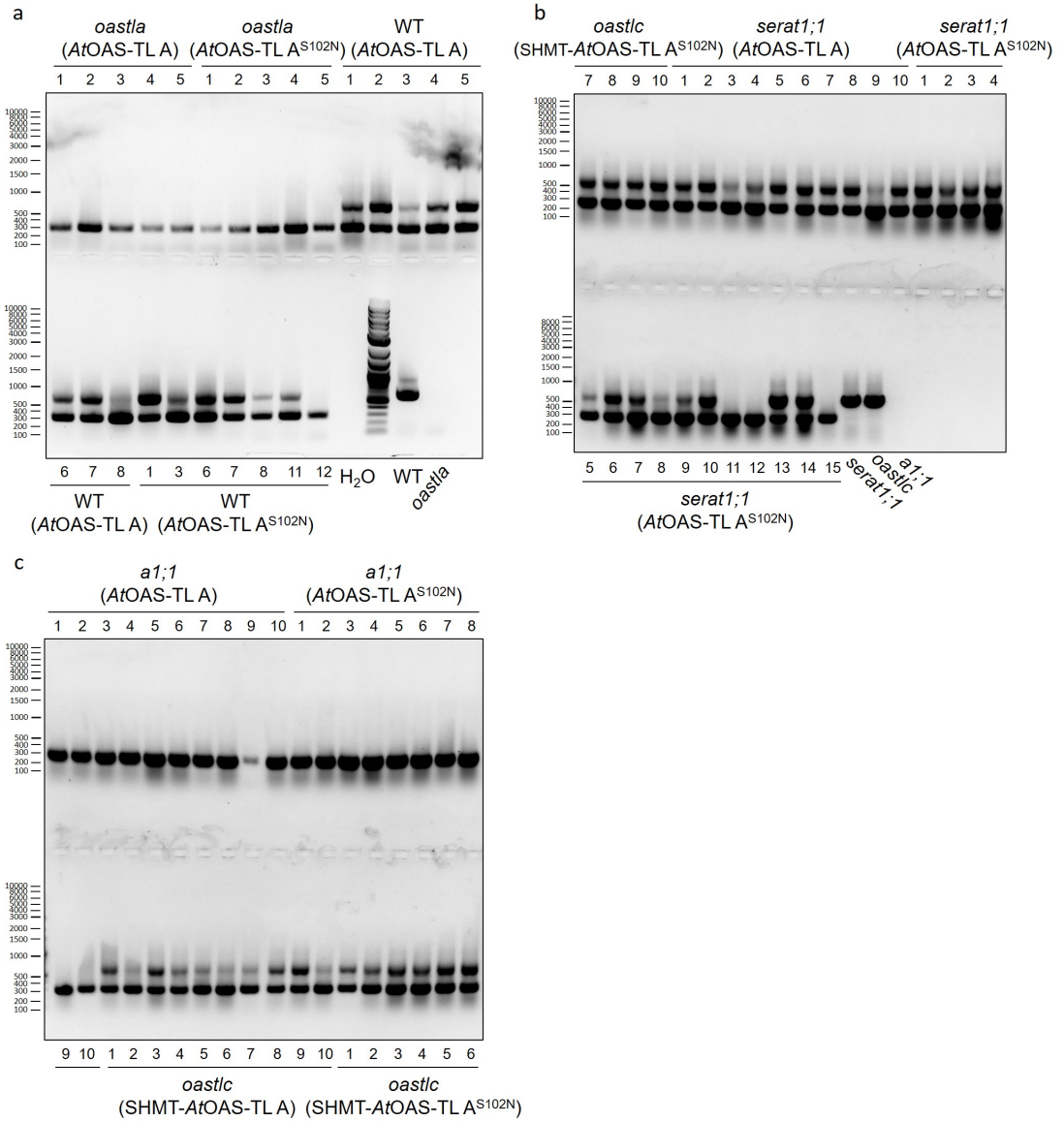

Figure S5: **Genotyping of T1 transformants to confirm the insertion.** Picture of DNA gels shown in Fig. 3.6. Confirmation of *At*OAS-TL A, *At*OAS-TL A^{S102N}, SHMT-*At*OAS-TL A, and SHMT-*At*OAS-TL A^{S102N} insertions into the genome of T1 transformants. **a)** Picture represents Fig. 3.6 a, **b)** Picture represents Fig. 3.6 b, **c)** Picture represents Fig. 3.6 c.

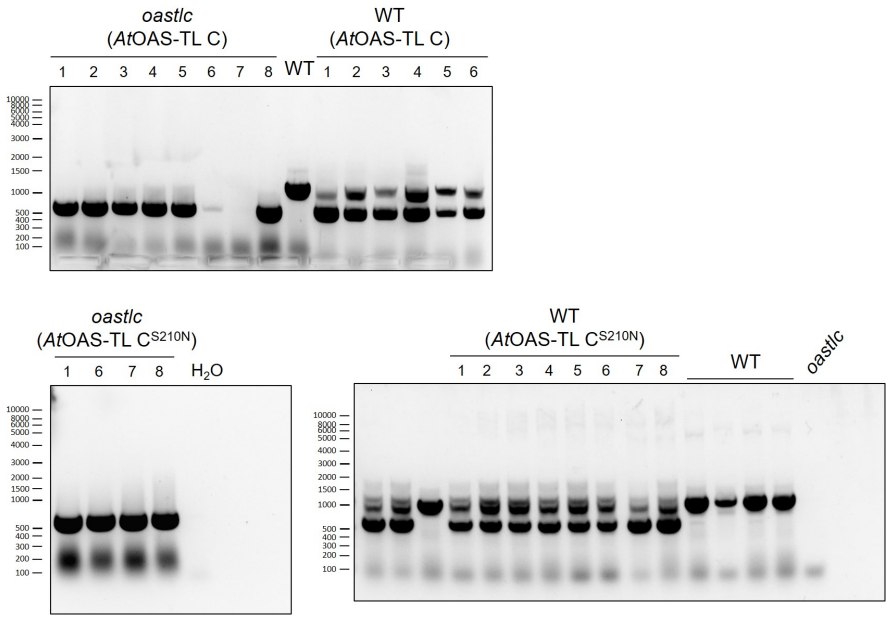

Figure S6: **Genotyping of T1 transformants to confirm the insertion.** Picture of DNA gels shown in Fig. 3.6 d. Confirmation of *At*OAS-TL C and *At*OAS-TL C^{S210N} insertions into the genome of T1 transformants.

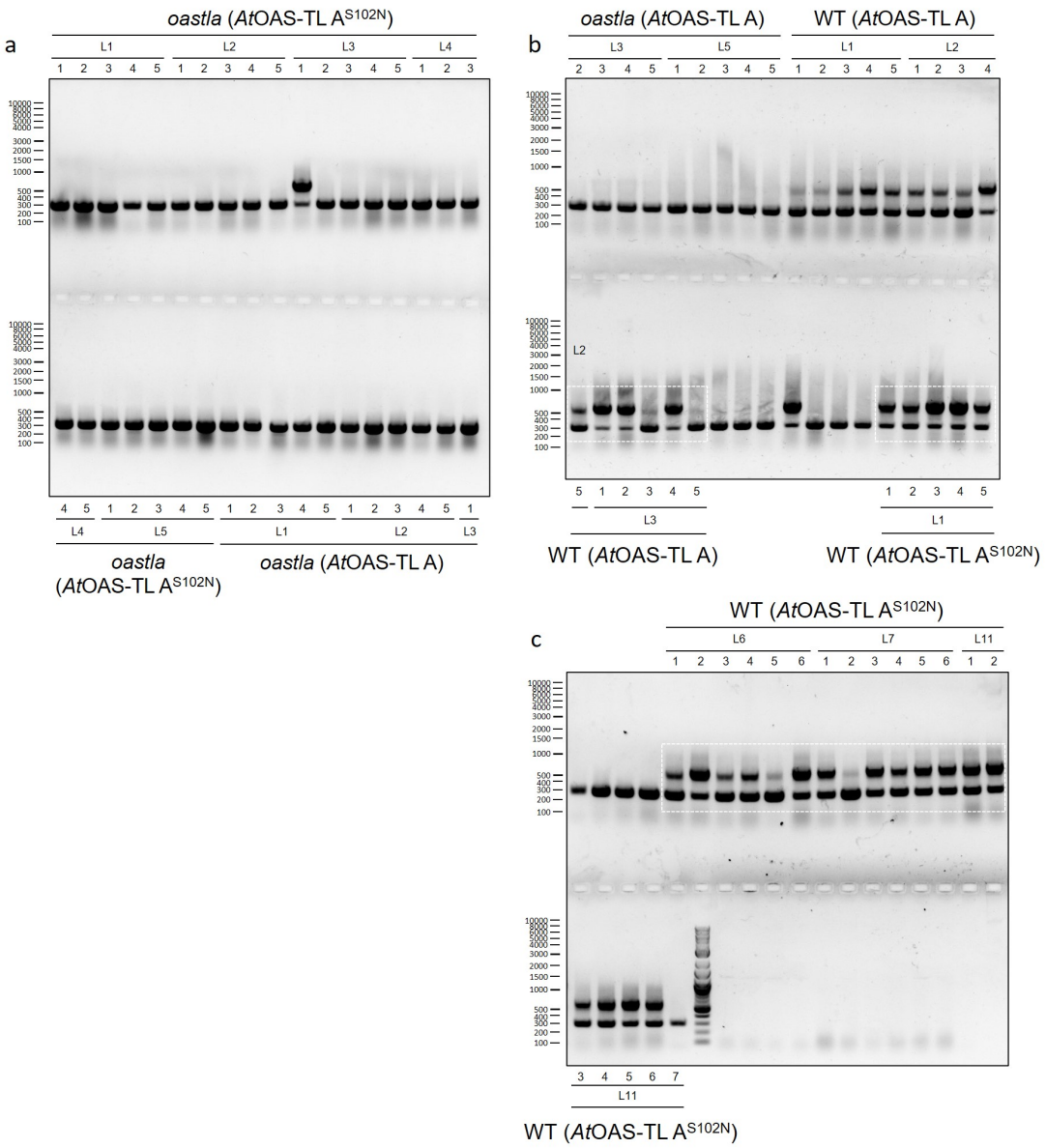

Figure S7: **Genotyping of T2 transformants to confirm the insertion.** Picture of DNA gels shown in Fig. 3.10. Confirmation of *At*OAS-TL A and *At*OAS-TL A^{S102N} insertions into the genome of T2 transformants. **a)** Picture represents Fig. 3.10 a, **b)** Picture represents Fig. 3.10 b and Fig. 3.10 c-left, **c)** Picture represents Fig. 3.10 c-middle and right. Areas with dashed border lines indicate part of the picture shown in Fig. 3.10.

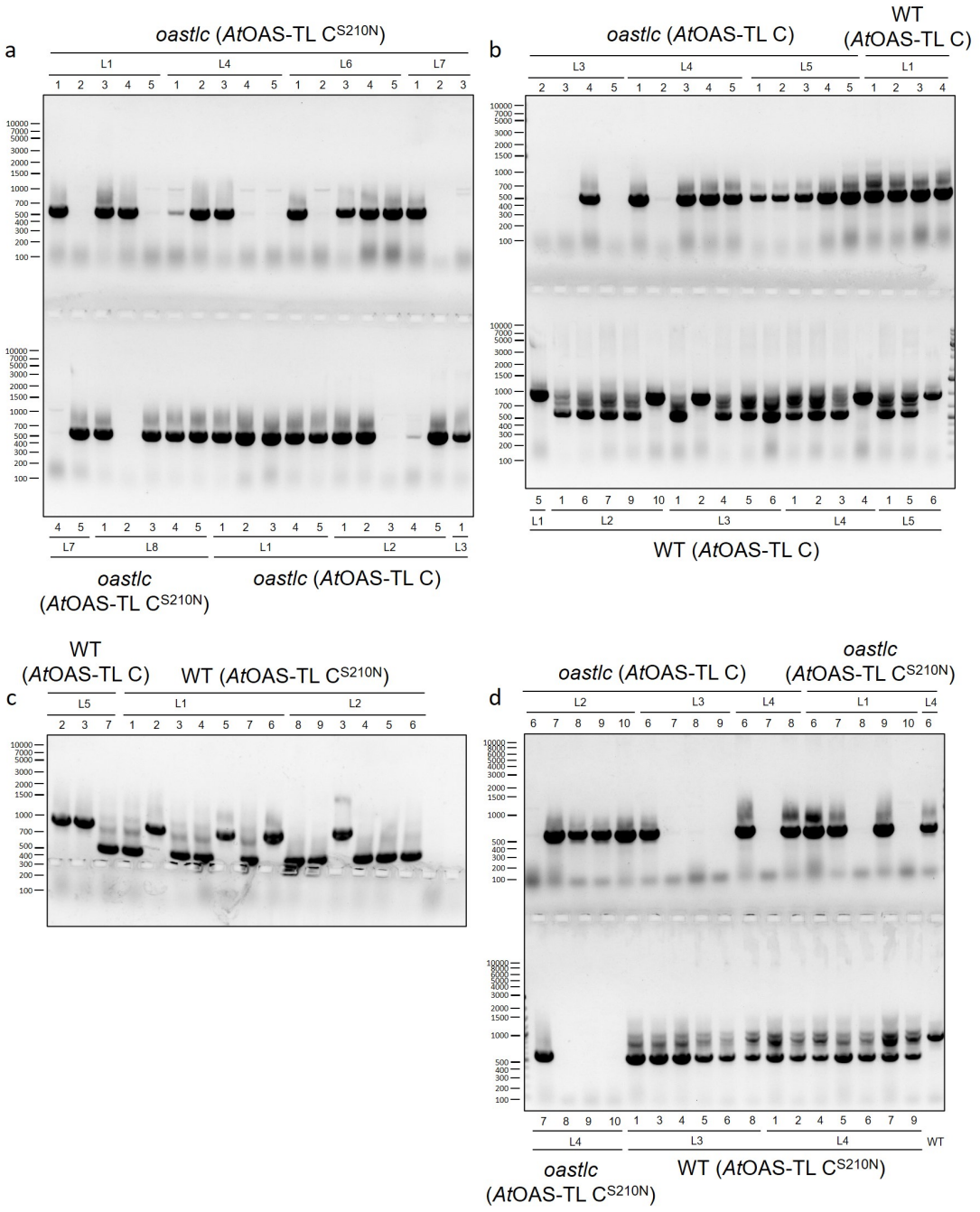

Figure S8: **Genotyping of T2 transformants to confirm the insertion.** Picture of DNA gels shown in Fig. 3.11. Confirmation of *At*OAS-TL C and *At*OAS-TL C^{S210N} insertions into the genome of T2 transformants. **a)** Picture represents Fig. 3.11 a, **b)** Picture represents Fig. 3.11 b, **c)** Picture represents Fig. 3.11 c, and **d)** Picture represents Fig. 3.11 d. Areas with dashed border lines indicate part of the picture shown in Fig. 3.11.

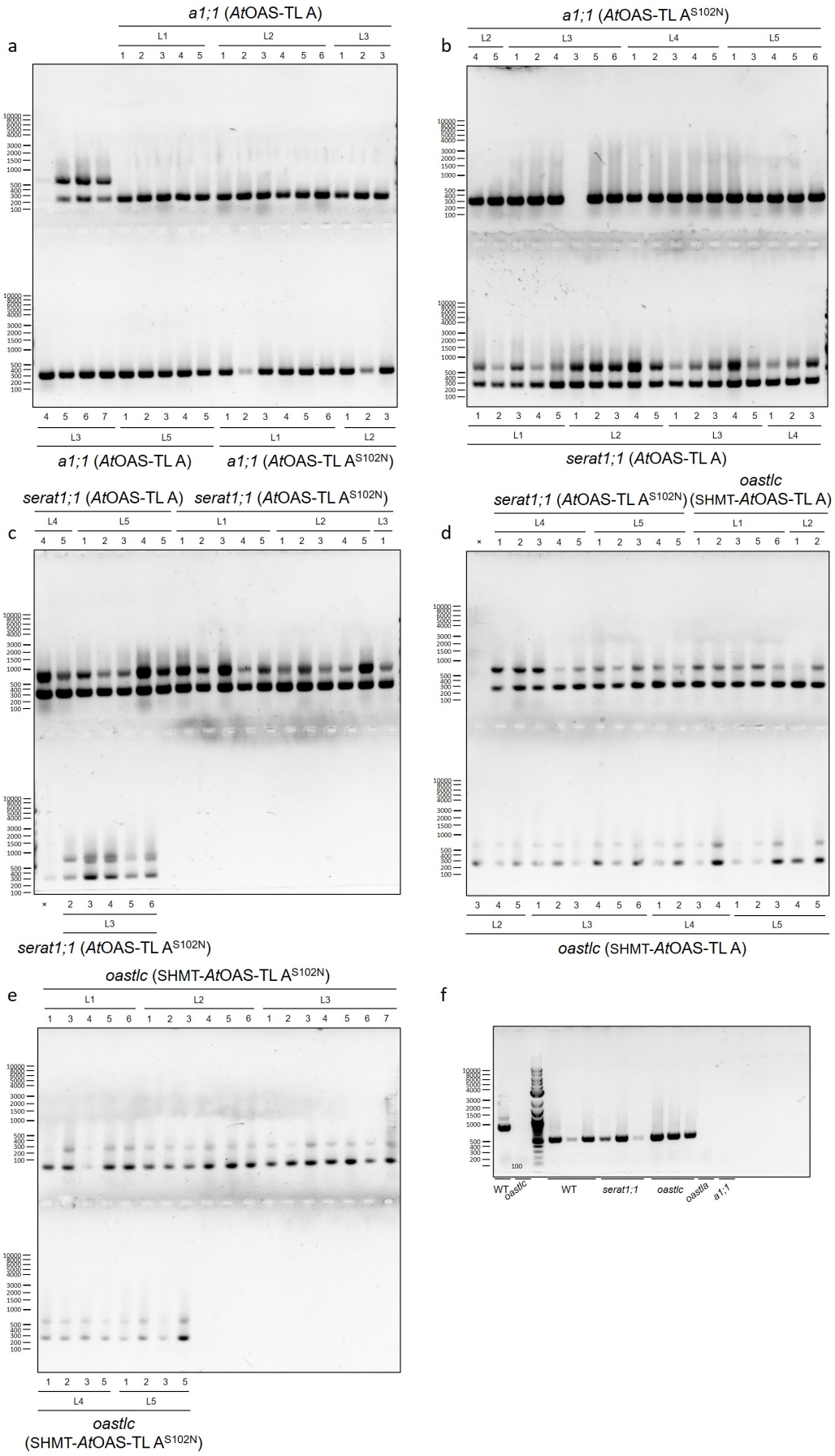

Figure S9: **Confirmation of insertion into the genome of T2 transformants by genotyping.**

Figure S9: Representative pictures of agarose gels detecting the presence of the transgene. To perform PCR (Table 2.11), DNA was extracted (2.3.1) from 6-week-old plants grown under short-day conditions on soil (2.5.2). Then, PCR was performed with 302+653 primer pairs (Table 2.10). **a)** and **b-upper part)** *a1;1* plants complemented with either *At*OAS-TL A or *At*OAS-TL A^{S102N} display smaller signal with 298bp related to the cDNA of *AtOAS-TL A*. **c-e)** *serat1;1*(*At*OAS-TL A), *serat1;1* (*At*OAS-TL A^{S102N}), *oastlc* (SHMT-*At*OAS-TL A), and *oastlc* (SHMT-*At*OAS-TL A^{S102N}) represent both smaller signal with 298bp and the bigger one with 600bp related to the cDNA and gDNA of *AtOAS-TL A*, respectively. **f)** All controls were used in the genotyping of T2 plants. WT and *oastlc* represented in the left side of the DNA-ladder were amplified with 325+922 primer pairs (Table 2.10) related to the gDNA of *AtOAS-TL C*. WT, *serat1;1*, *oastlc*, *oastla*, and *a1;1* represented in the right side of the DNA-ladder were amplified with 302+653 primer pairs (Table 2.10) related to the gDNA of *AtOAS-TL A*.

5.3 Membranes used for the immunological detection and amido black staining

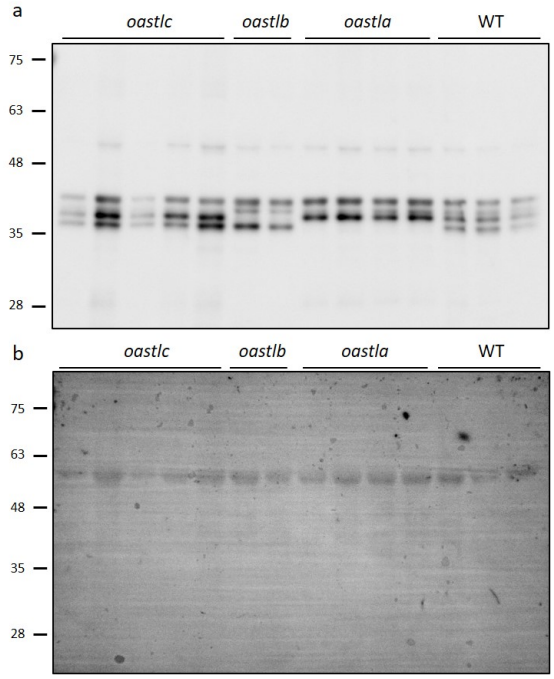

Figure S10: **Immunological detection of different *At*OAS-TL isoforms.** Pictures of membrane used for the immunological detection of Arabidopsis OAS-TL isoforms. Full description of the membrane in Fig. 3.13.

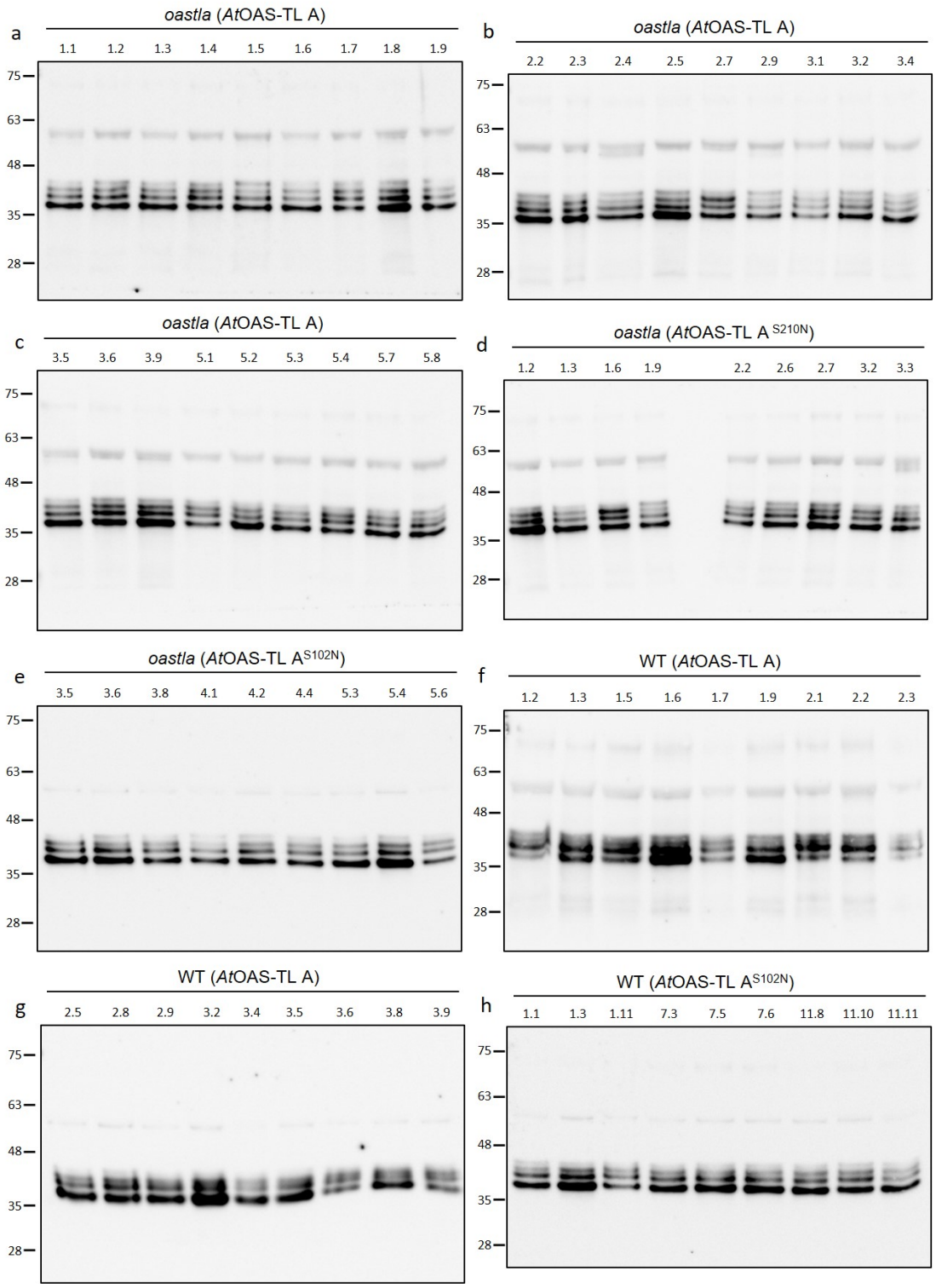

Figure S11: **Immunoblot analysis of *At*OAS-TL A protein in T2 plants.** Pictures of membrane used for the immunological detection of *At*OAS-TL A in T2 plants. Full description of the membrane in Fig. 3.14.

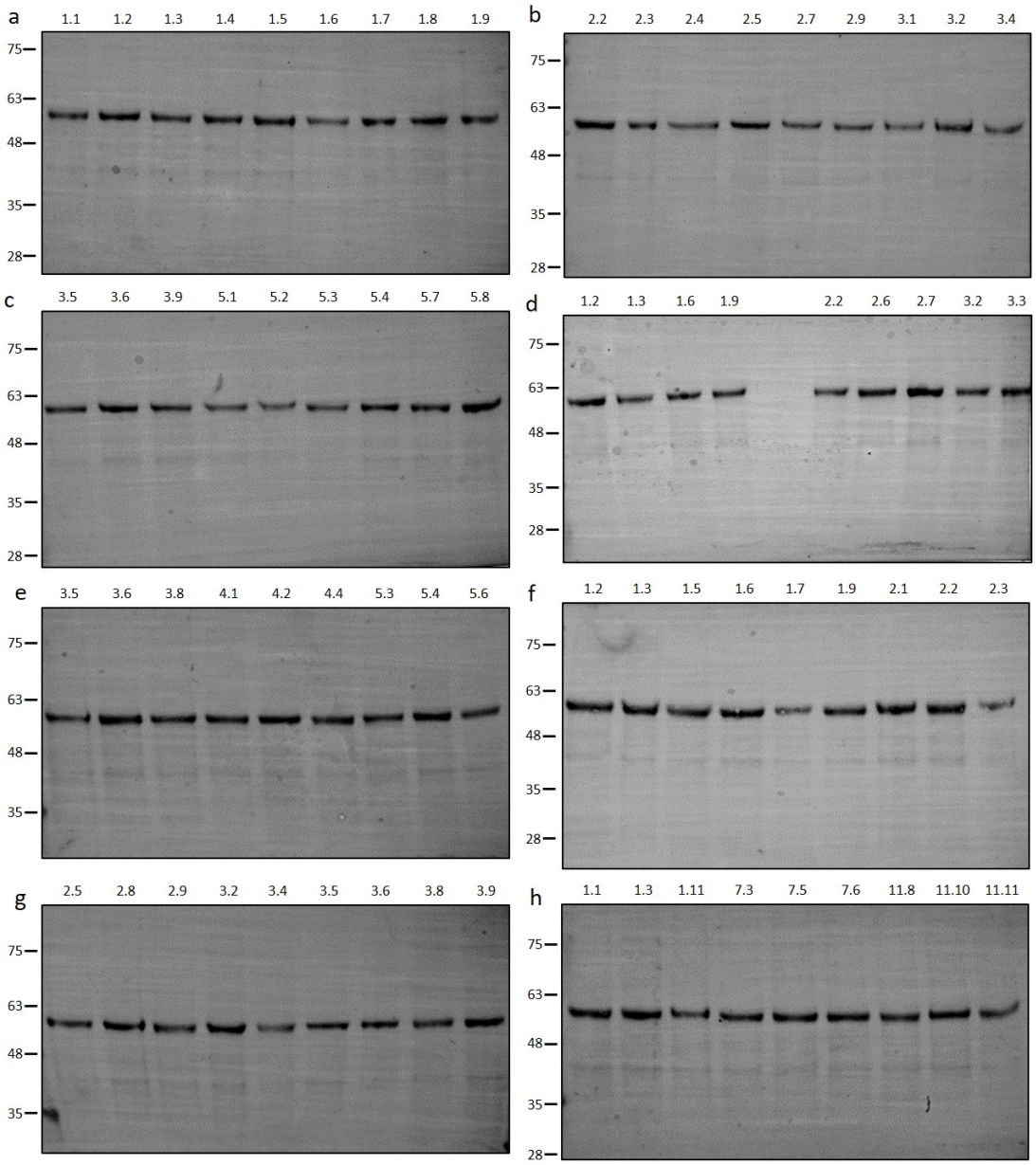

Figure S12: **Amido black staining of the membrane used for immunoblot analysis of *At*OAS-TL A proteins in T2 plants.** Picture of membrane used for amido black staining as loading control in Fig. 3.14.

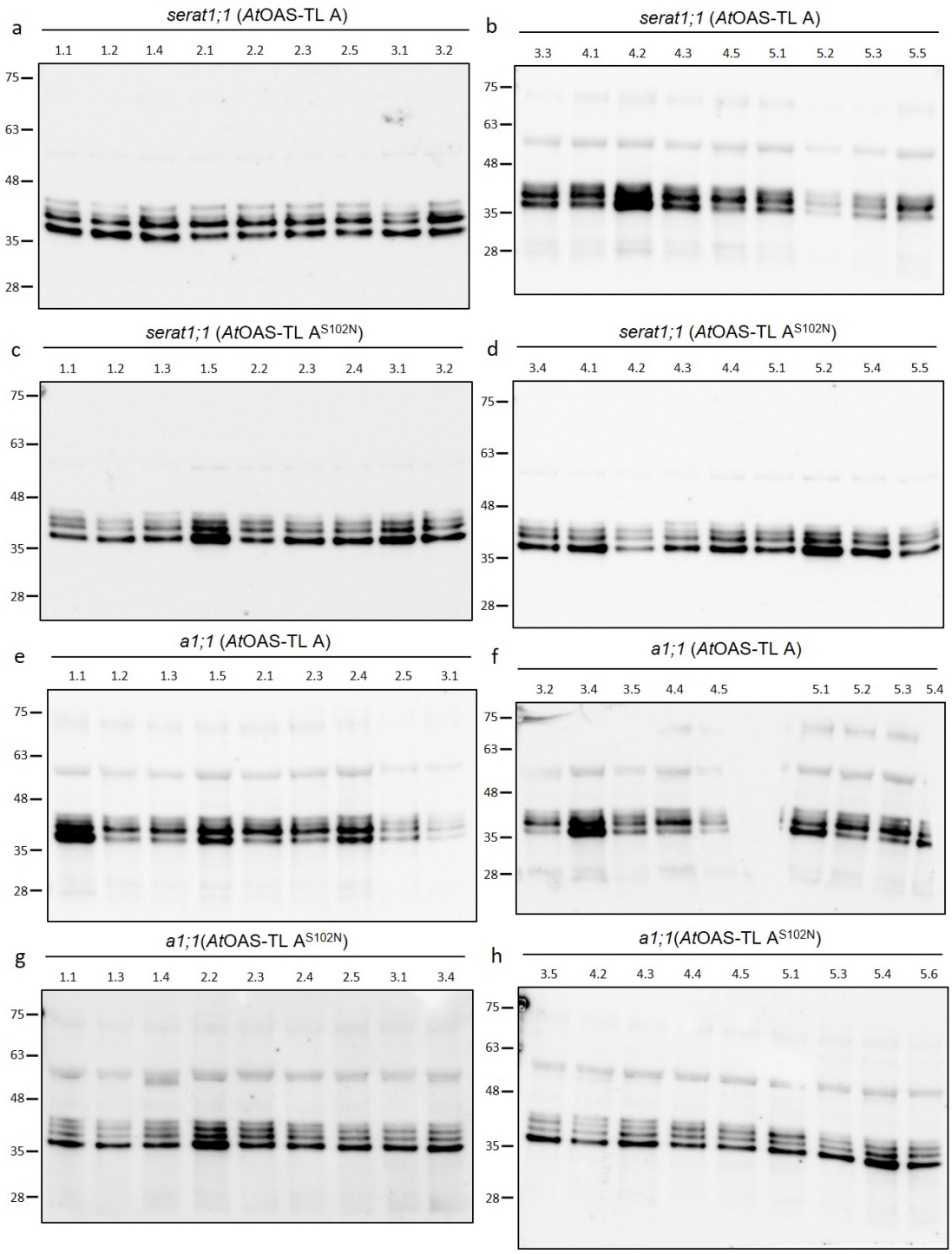

Figure S13: **Immunoblot analysis of *At*OAS-TL A protein in T2 plants.** Pictures of membrane used for the immunological detection of *At*OAS-TL A in T2 plants. Full description of the membrane in Fig. 3.15.

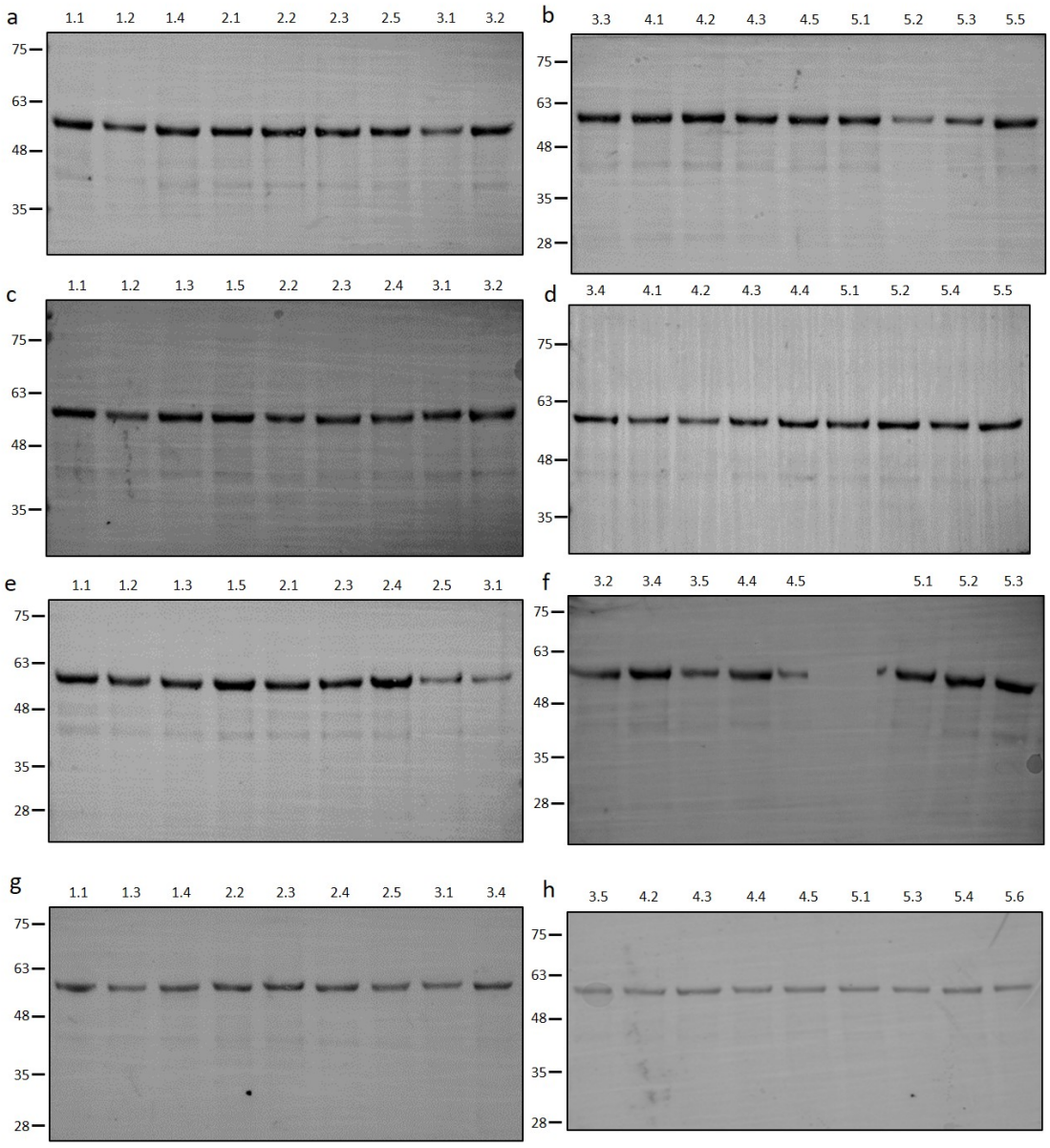

Figure S14: **Amido black staining of the membrane used for immunoblot analysis of *At*OAS-TL A proteins in T2 plants.** Picture of membrane used for amido black staining as loading control in Fig. 3.15.

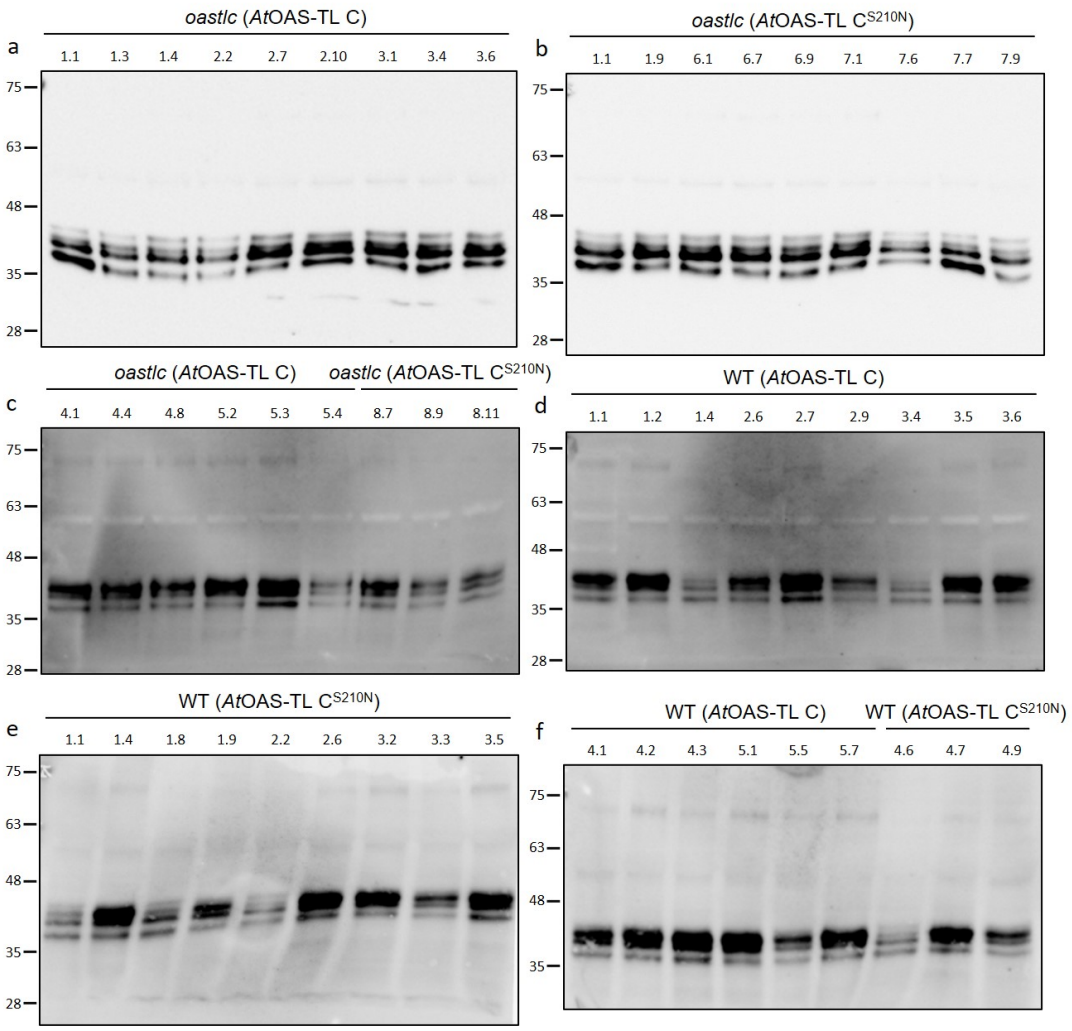

Figure S15: **Immunoblot analysis of *At*OAS-TL C protein in T2 plants.** Pictures of membrane used for the immunological detection of *At*OAS-TL C in T2 plants. Full description of the membrane in Fig. 3.16.

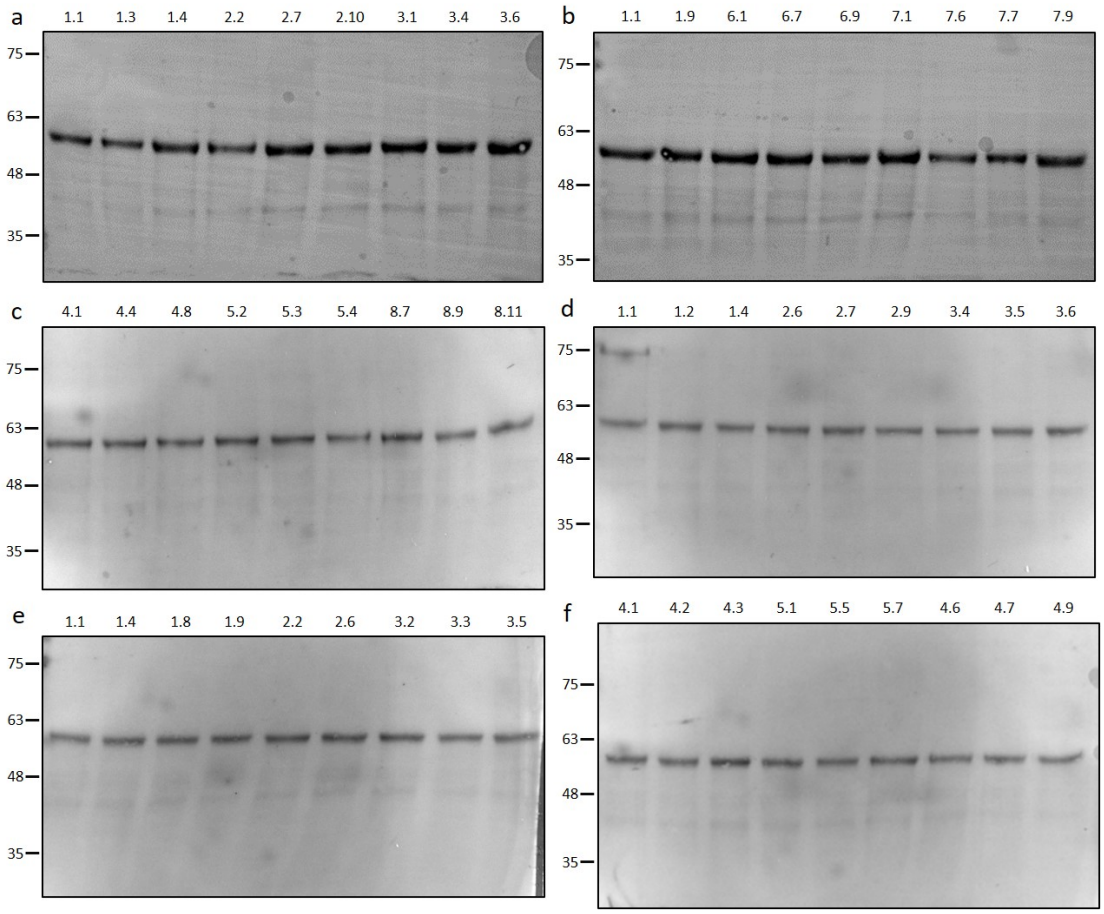

Figure S16: **Amido black staining of the membrane used for immunoblot analysis of *At*OAS-TL A proteins in T2 plants.** Picture of membrane used for amido black staining as loading control in Fig. 3.16.

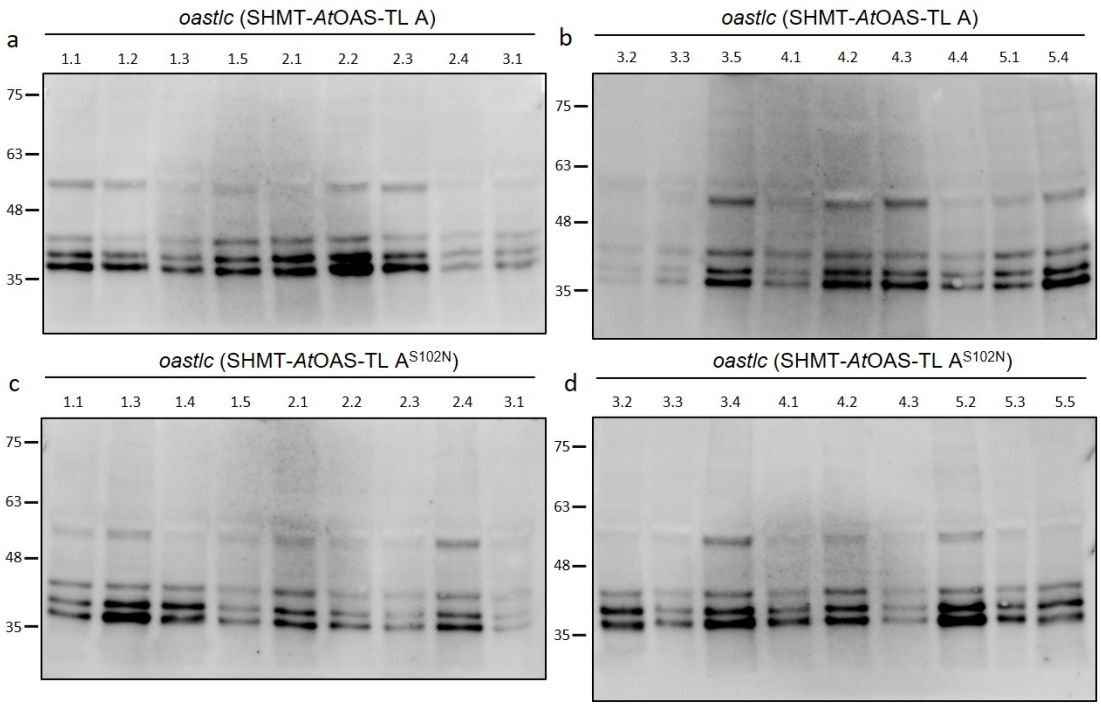

Figure S17: **Immunoblot analysis of *At*OAS-TL A protein in T2 plants.** Pictures of membrane used for the immunological detection of *At*OAS-TL A in T2 plants. Full description of the membrane in Fig. 3.17.

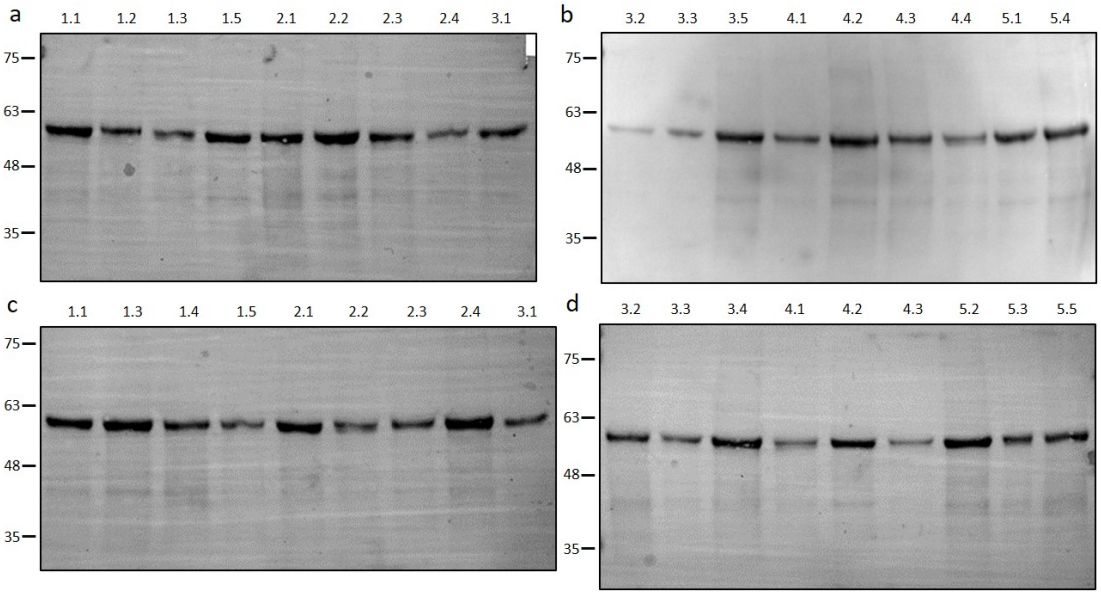

Figure S18: **Amido black staining of the membrane used for immunoblot analysis of *At*OAS-TL A proteins in T2 plants.** Picture of membrane used for amido black staining as loading control in Fig. 3.17.

5.4 Vector maps

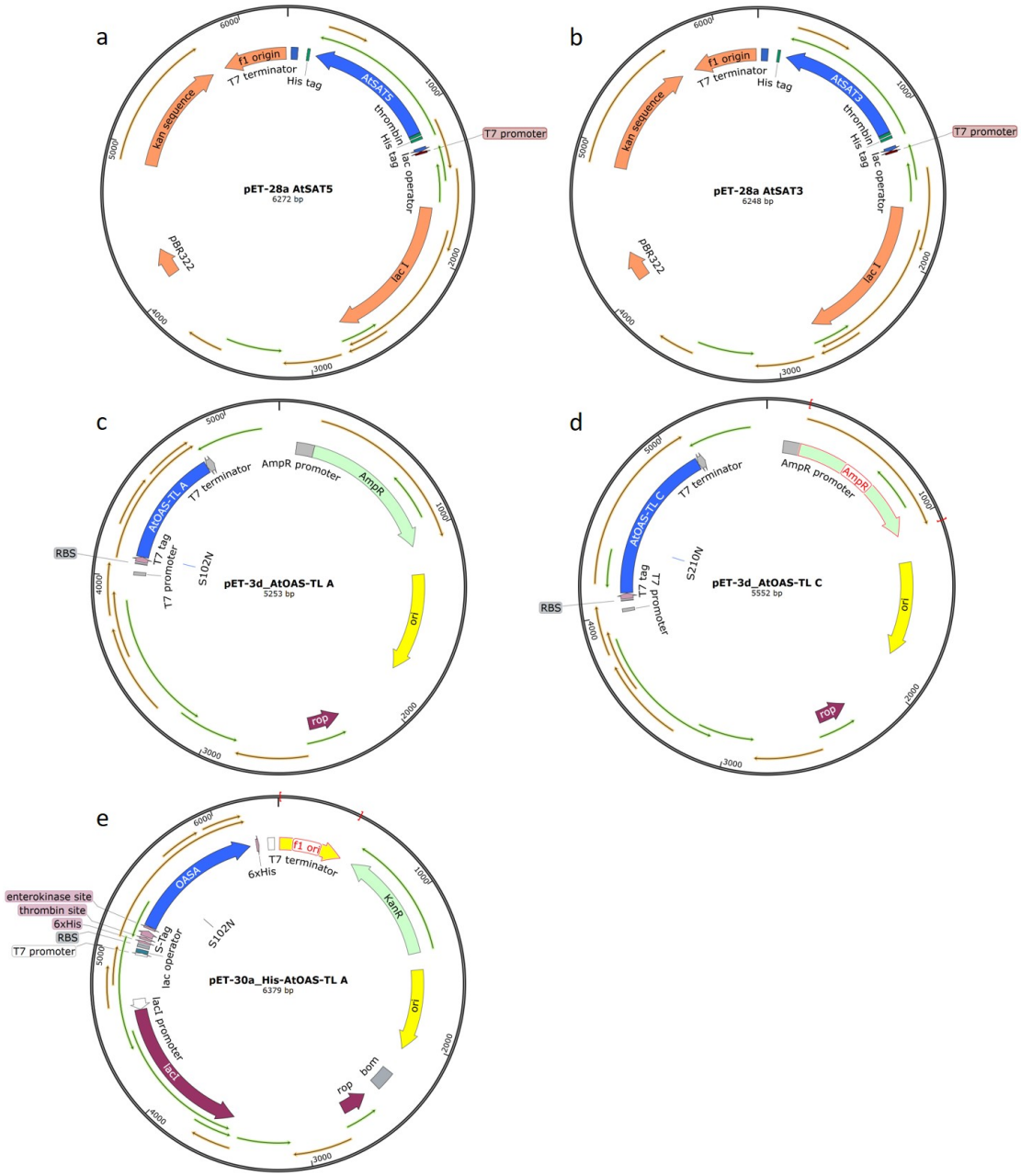

Figure S19: **Vector map of the construct used in this thesis**

Schematic illustration of regulatory elements and coding proteins (highlit arrows) in the used vectors in this study. **a)** pET-28a AtSAT5 (AtSERAT1;1) tagged in N-terminus with His-tag (3.1). **b)** pET-28a AtSAT3 (AtSERAT2;2) tagged in N-terminus with His-tag (3.1). **c)** pET-3d-*At*OAS-TL A/pET-3d-*At*OAS-TL A^{S102N} (3.1). **d)** pET-3d-*At*OAS-TL C/pET-3d *At*OAS-TL C^{S210N} (3.1). **e)** pET-30a-OAS-TL-A/pET-30a-OAS-TL A^{S102N} tagged in N-terminus with His-tag (3.6). Cloned ORFs are represented in blue.

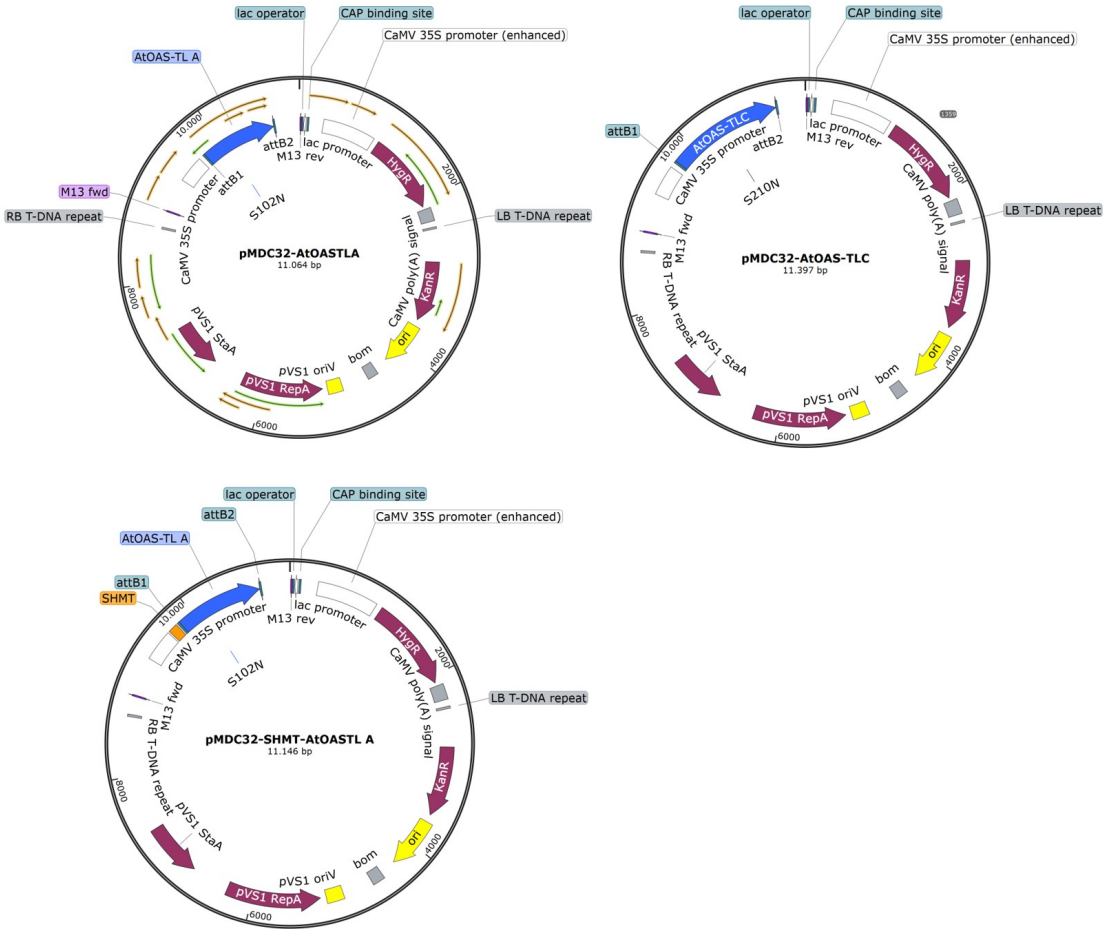

Figure S20: **Maps of pMDC vectors used in this thesis**

Schematic illustration of regulatory elements and coding proteins (highlight arrows) present in pMDC vectors used to transform plants (3.2). **a)** pMDC32-*At*OAS-TL A (GVO database 1794)/pMDC32-*At*OAS-TL A^{S102N} (GVO database 1795). **b)** pMDC32-*At*OAS-TL C (GVO database 2049)/pMDC32-*At*OAS-TL C^{S210N} (GVO database 2050). **c)** pMDC32-SHMT-*At*OAS-TL A (GVO database 2047)/pMDC32-SHMT-*At*OAS-TL A^{S102N} (GVO database 2048). Cloned ORFs are represented in blue.

5.5 Determination of anions in the leaves of T2 complemented plants

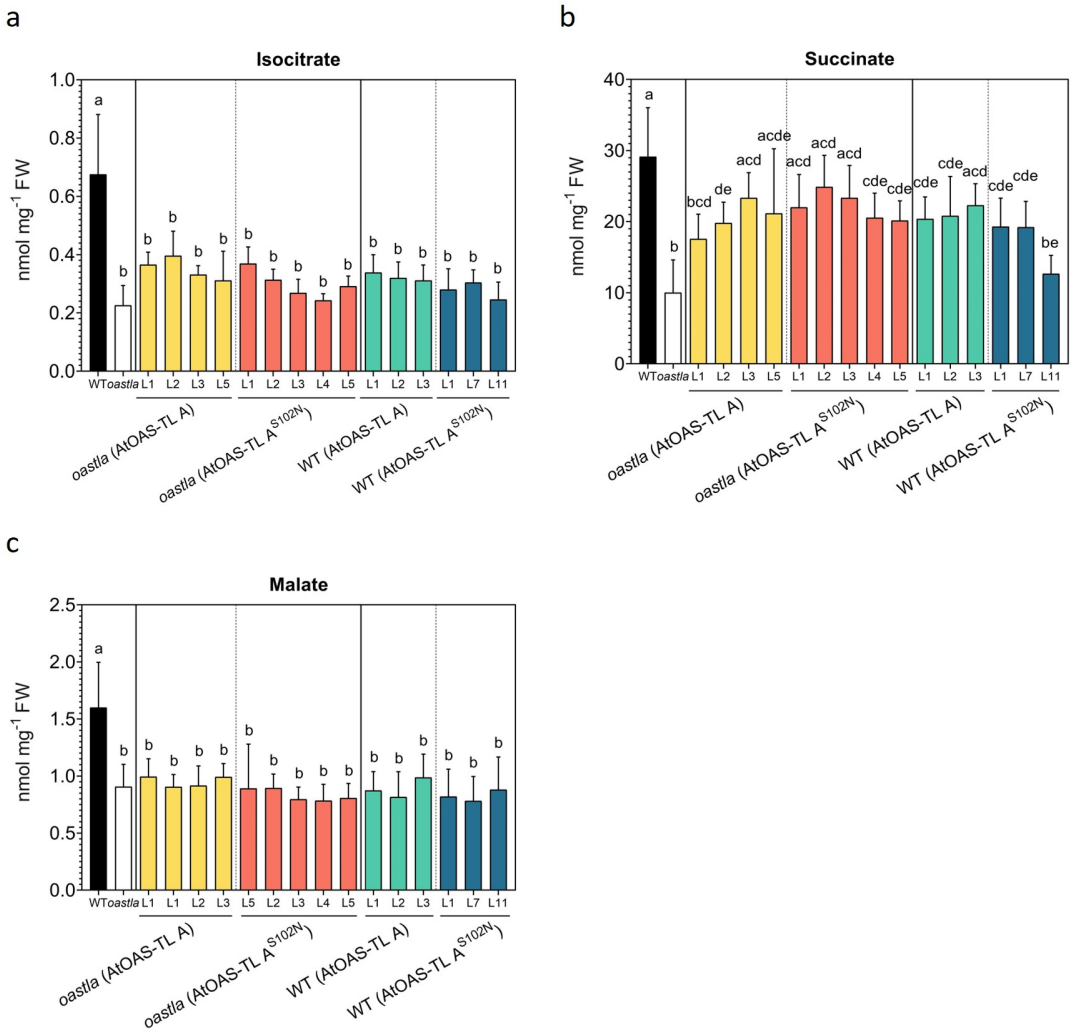

Figure S21: **Steady-state levels of anions in the leaves of complemented *oastla* and wild-type lines.** To analyze **a)** isocitrate, **b)** succinate, and **c)** malate, metabolites were extracted from the leaf tissue of six-week-old plants grown on soil under short-day conditions (2.5.2). The HCl extract was diluted 1:10 using ddH_2O; otherwise, the chloride ions from the HCl extract would overload the column and interfere with the run. Diluted samples were separated and quantified using HPLC. Data are shown as means ± SD, n=6-9 biological replicates; each biological replicate represents an individual plant. Different letters indicate significant differences ($p<0.05$) using one-way ANOVA followed by Tukey's test.

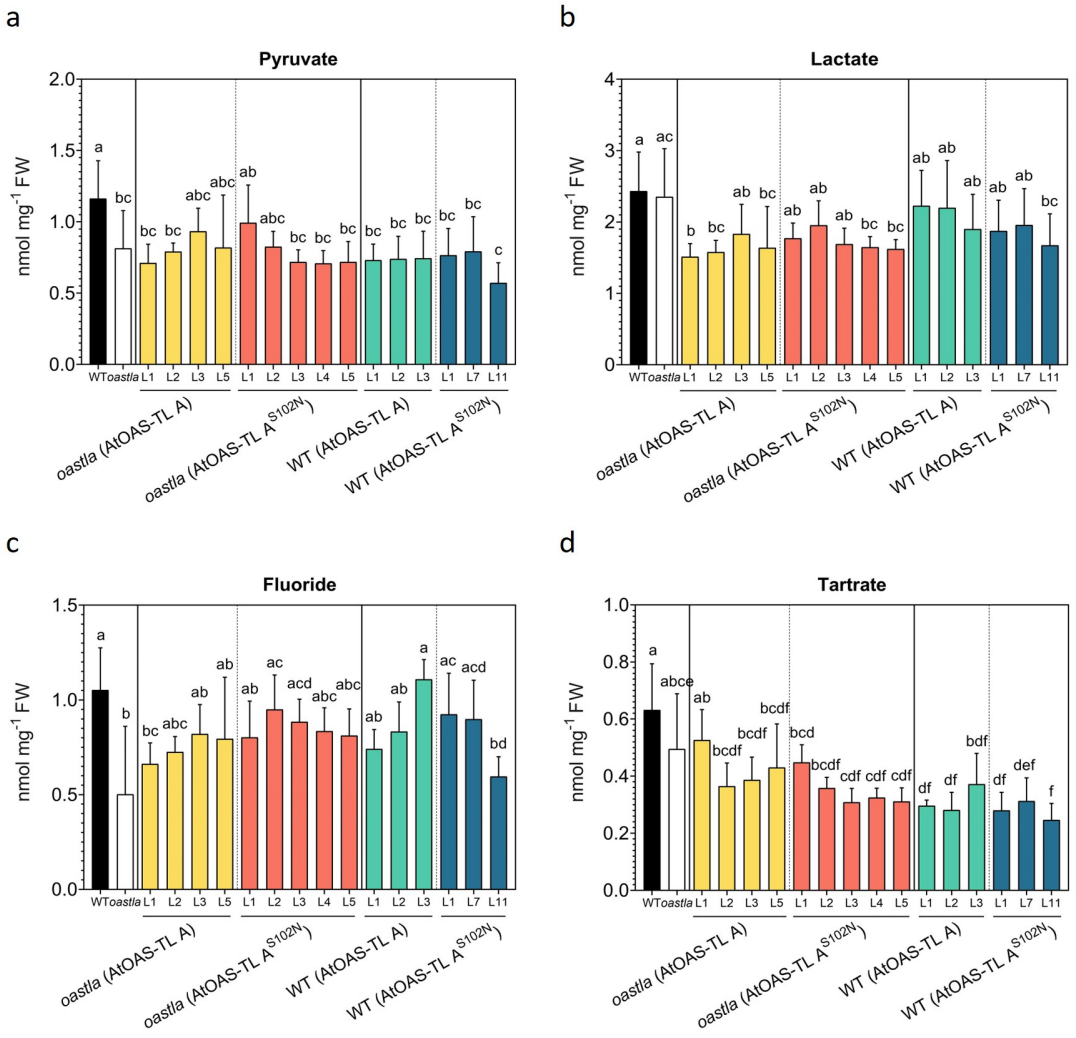

Figure S22: **Steady-state levels of anions in the leaves of complemented *oastla* and wild-type lines.** To analyze **a)** pyruvate, **b)** lactate, **c)** fluoride and **d)** tartrate, metabolites were extracted from the leaf tissue of six-week-old plants grown on soil under short-day conditions (2.5.2). The HCl extract was diluted 1:10 using ddH_2O; otherwise, the chloride ions from the HCl extract would overload the column and interfere with the run. Diluted samples were separated and quantified using HPLC. Data are shown as means ± SD, n=6-9 biological replicates; each biological replicate represents an individual plant. Different letters indicate significant differences ($p<0.05$) using one-way ANOVA followed by Tukey's test.

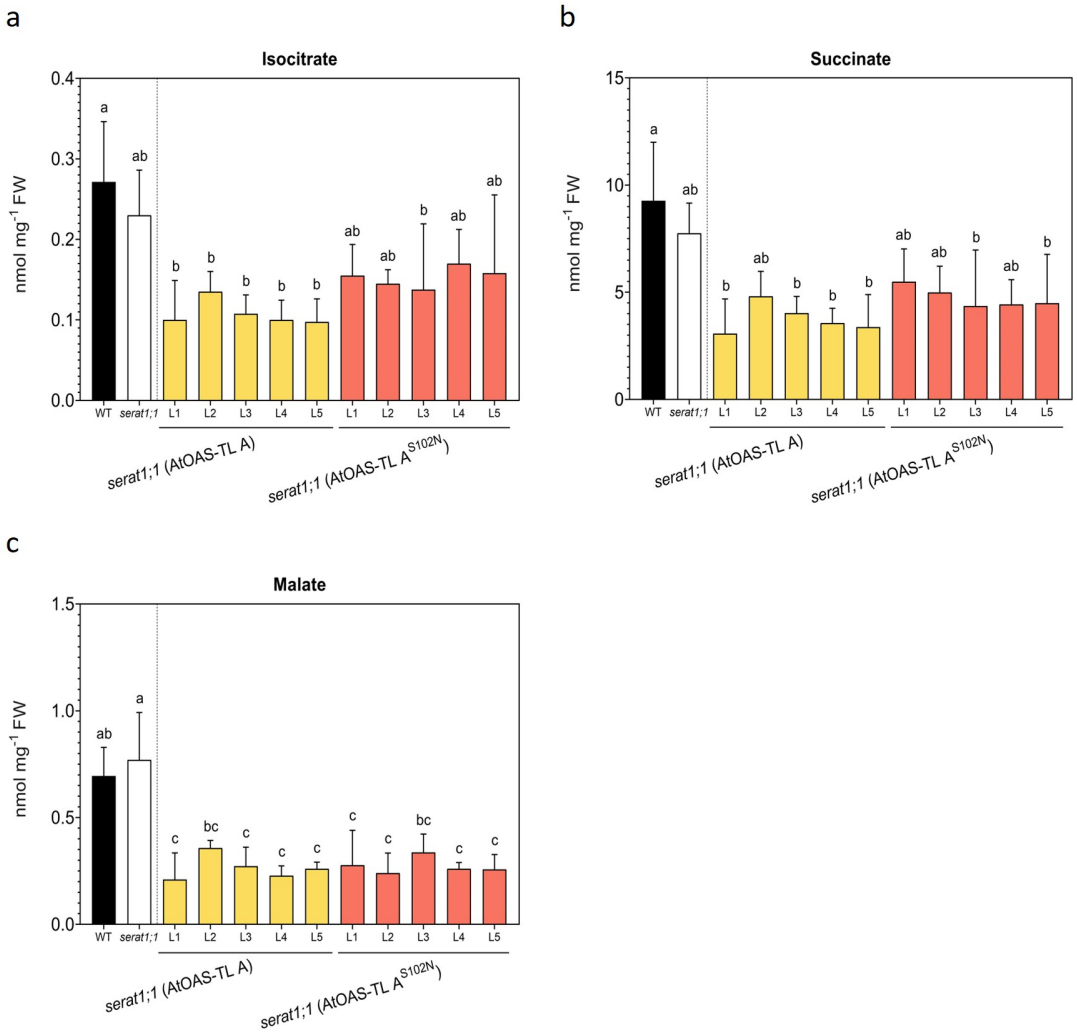

Figure S23: **Steady-state levels of anions in the leaves of complemented *serat1;1* lines.** To analyze **a)** isocitrate, **b)** succinate, and **c)** malate, metabolites were extracted from the leaf tissue of six-week-old plants grown on soil under short-day conditions (2.5.2). The HCl extract was diluted 1:10 using ddH_2O; otherwise, the chloride ions from the HCl extract would overload the column and interfere with the run. Diluted samples were separated and quantified using HPLC. Data are shown as means ± SD, n=3-5 biological replicates; each biological replicate represents an individual plant. Different letters indicate significant differences ($p<0.05$) using one-way ANOVA followed by Tukey's test.

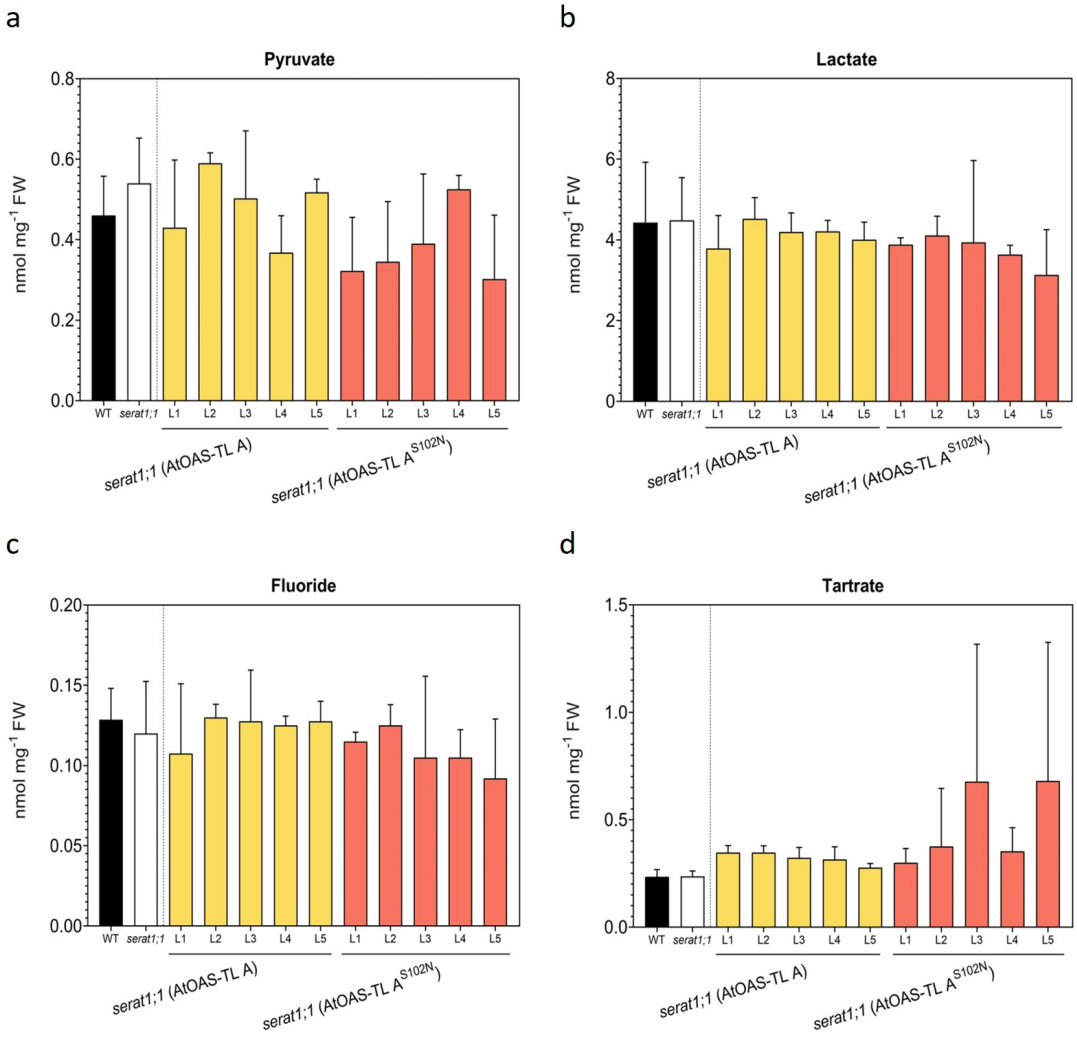

Figure S24: **Steady-state levels of anions in the leaves of complemented *serat1;1* lines.** To analyze **a)** pyruvate, **b)** lactate, **c)** fluoride and **d)** tartrate, metabolites were extracted from the leaf tissue of six-week-old plants grown on soil under short-day conditions (2.5.2). The HCl extract was diluted 1:10 using ddH_2O; otherwise, the chloride ions from the HCl extract would overload the column and interfere with the run. Diluted samples were separated and quantified using HPLC. Data are shown as means ± SD, n=3-5 biological replicates; each biological replicate represents an individual plant. Different letters indicate significant differences ($p<0.05$) using one-way ANOVA followed by Tukey's test.

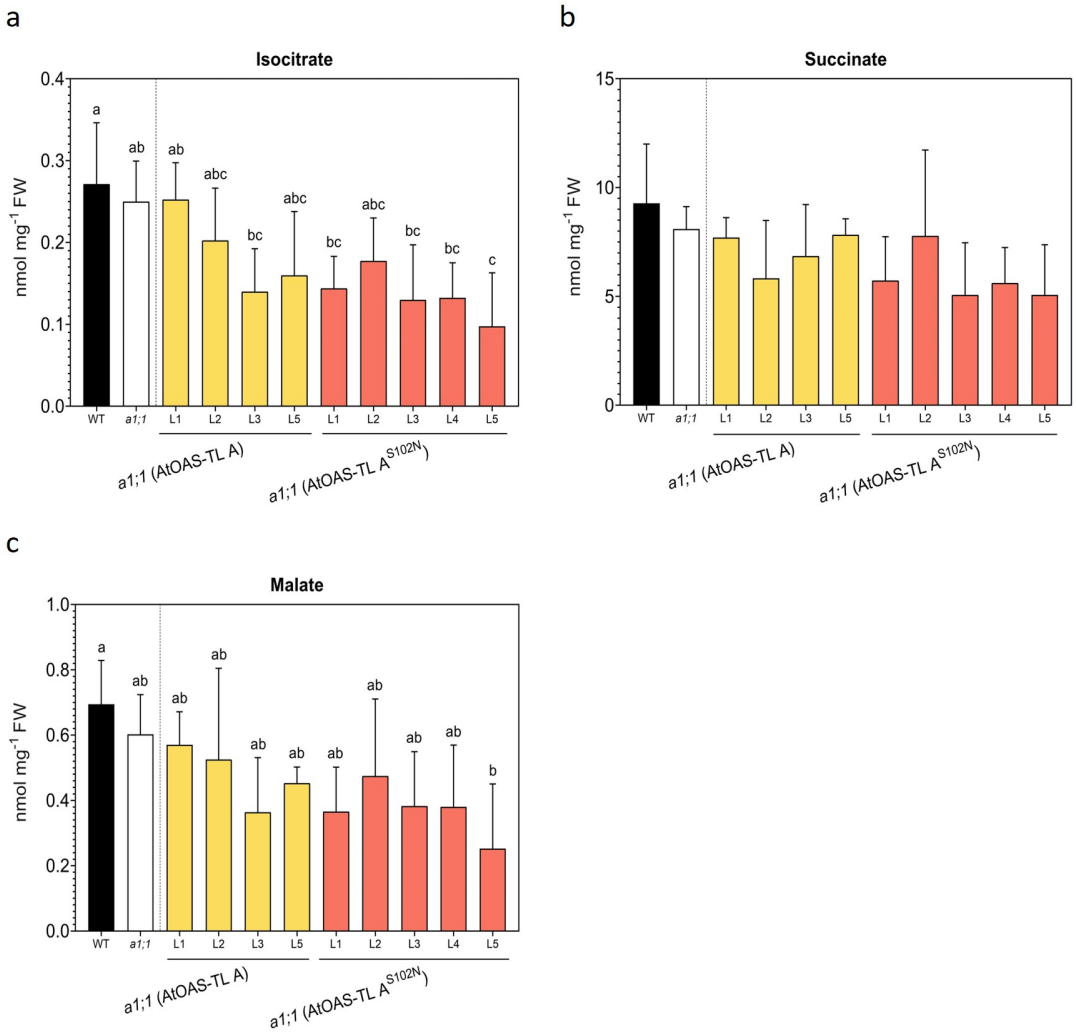

Figure S25: **Steady-state levels of anions in the leaves of complemented *a1;1* lines.** To analyze **a)** isocitrate, **b)** succinate, and **c)** malate, metabolites were extracted from the leaf tissue of six-week-old plants grown on soil under short-day conditions (2.5.2). The HCl extract was diluted 1:10 using ddH_2O; otherwise, the chloride ions from the HCl extract would overload the column and interfere with the run. Diluted samples were separated and quantified using HPLC. Data are shown as means ± SD, n=3-5 biological replicates; each biological replicate represents an individual plant. Different letters indicate significant differences ($p<0.05$) using one-way ANOVA followed by Tukey's test.

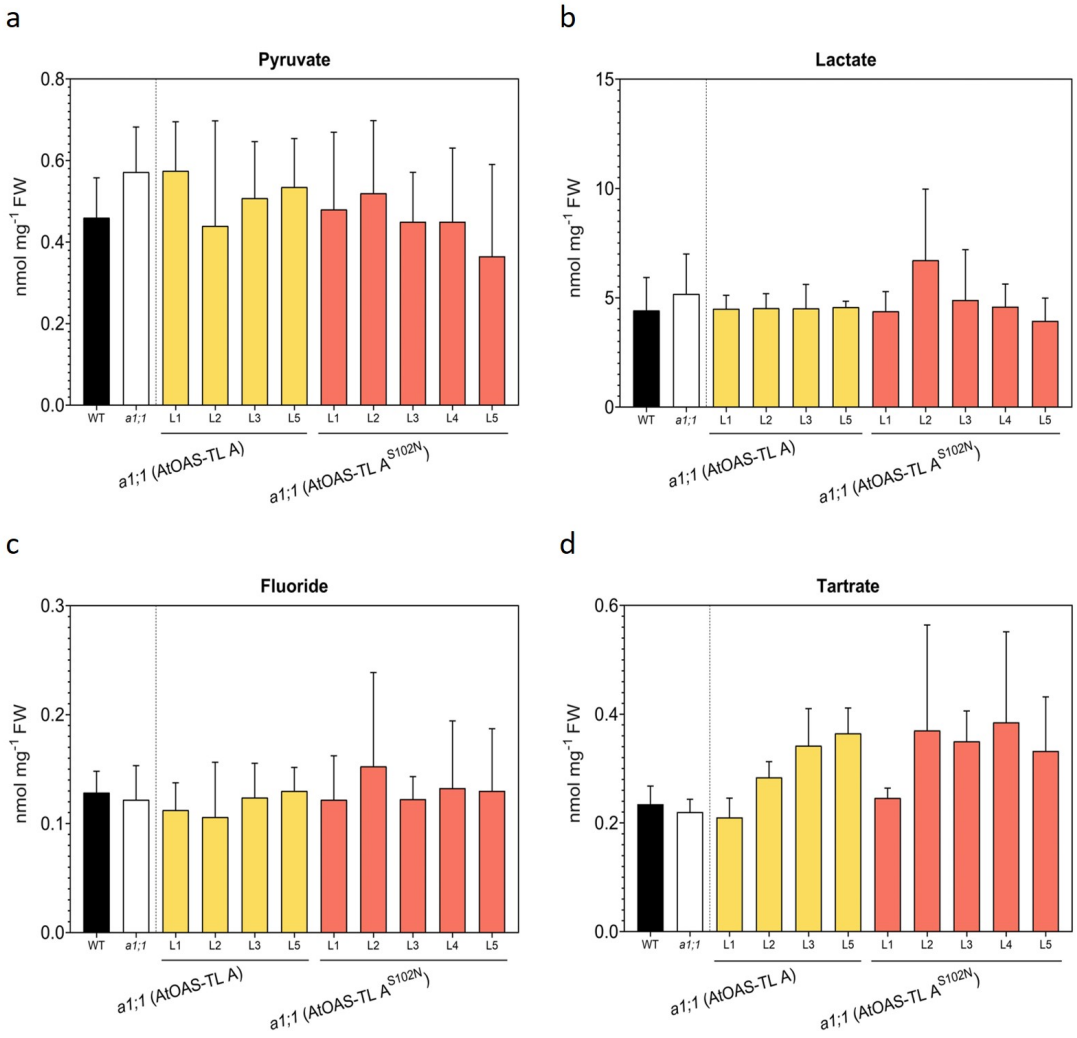

Figure S26: **Steady-state levels of anions in the leaves of complemented *a1;1* lines.** To analyze **a)** pyruvate, **b)** lactate, **c)** fluoride and **d)** tartrate, metabolites were extracted from the leaf tissue of six-week-old plants grown on soil under short-day conditions (2.5.2). The HCl extract was diluted 1:10 using ddH_2O; otherwise, the chloride ions from the HCl extract would overload the column and interfere with the run. Diluted samples were separated and quantified using HPLC. Data are shown as means ± SD, n=3-5 biological replicates; each biological replicate represents an individual plant. Different letters indicate significant differences ($p<0.05$) using one-way ANOVA followed by Tukey's test.

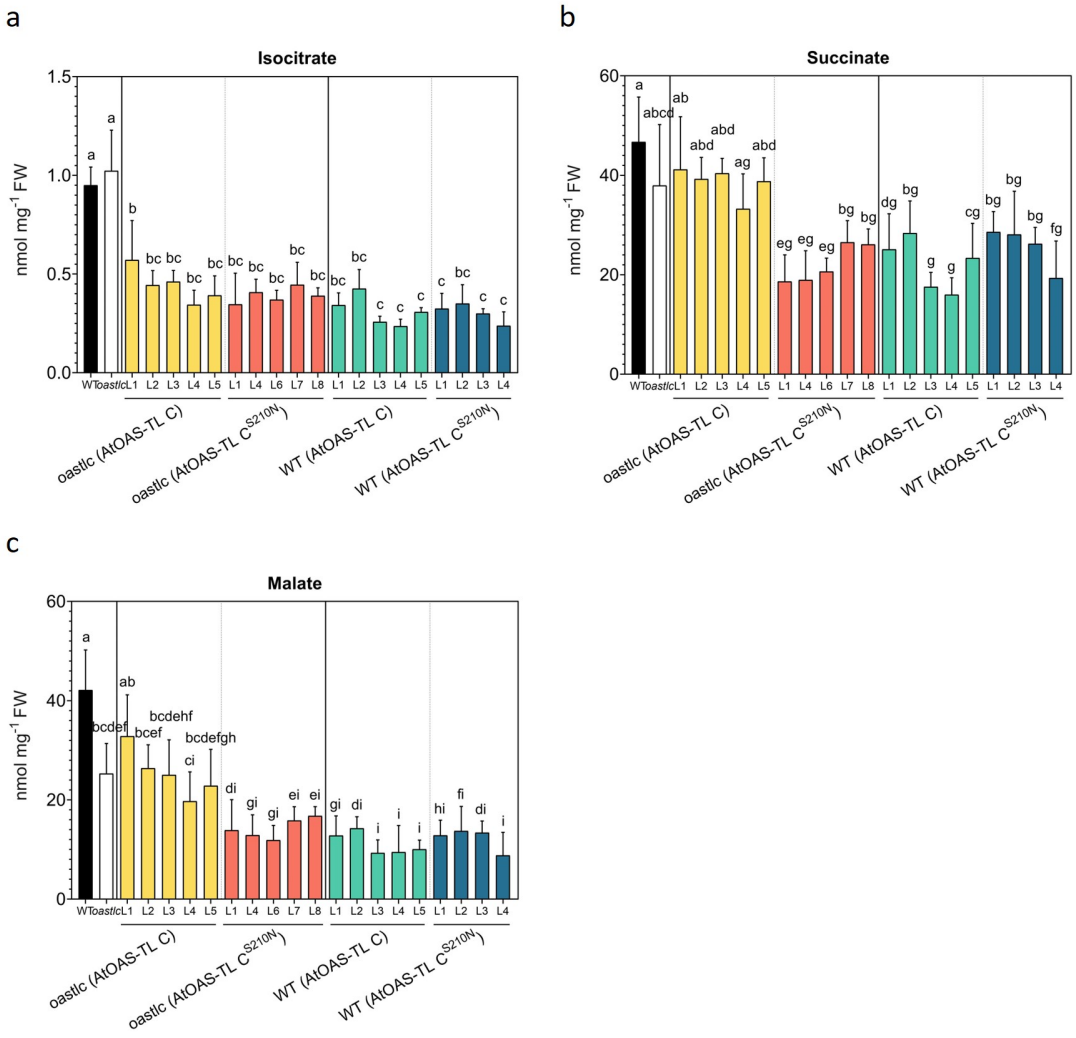

Figure S27: **Steady-state levels of anions in the leaves of complemented *oastlc* and wild-type lines.** To analyze **a)** isocitrate, **b)** succinate, and **c)** malate, metabolites were extracted from the leaf tissue of six-week-old plants grown on soil under short-day conditions (2.5.2). The HCl extract was diluted 1:10 using ddH_2O; otherwise, the chloride ions from the HCl extract would overload the column and interfere with the run. Diluted samples were separated and quantified using HPLC. Data are shown as means ± SD, n=4-5 biological replicates; each biological replicate represents an individual plant. Different letters indicate significant differences ($p<0.05$) using one-way ANOVA followed by Tukey's test.

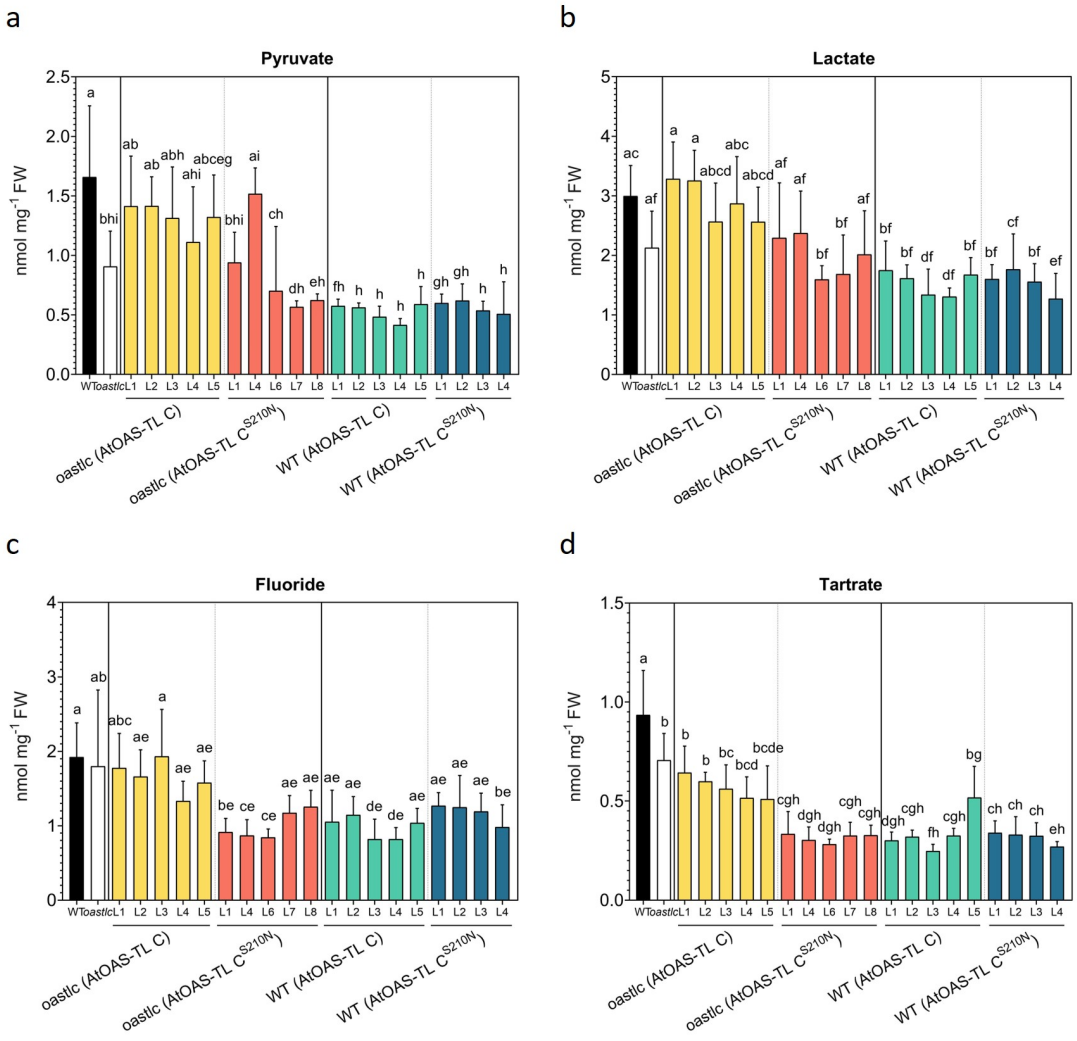

Figure S28: **Steady-state levels of anions in the leaves of complemented *oastlc* and wild-type lines.** To analyze **a)** pyruvate, **b)** lactate, **c)** fluoride and **d)** tartrate, metabolites were extracted from the leaf tissue of six-week-old plants grown on soil under short-day conditions (2.5.2). The HCl extract was diluted 1:10 using ddH_2O; otherwise, the chloride ions from the HCl extract would overload the column and interfere with the run. Diluted samples were separated and quantified using HPLC. Data are shown as means ± SD, n=4-5 biological replicates; each biological replicate represents an individual plant. Different letters indicate significant differences ($p<0.05$) using one-way ANOVA followed by Tukey's test.

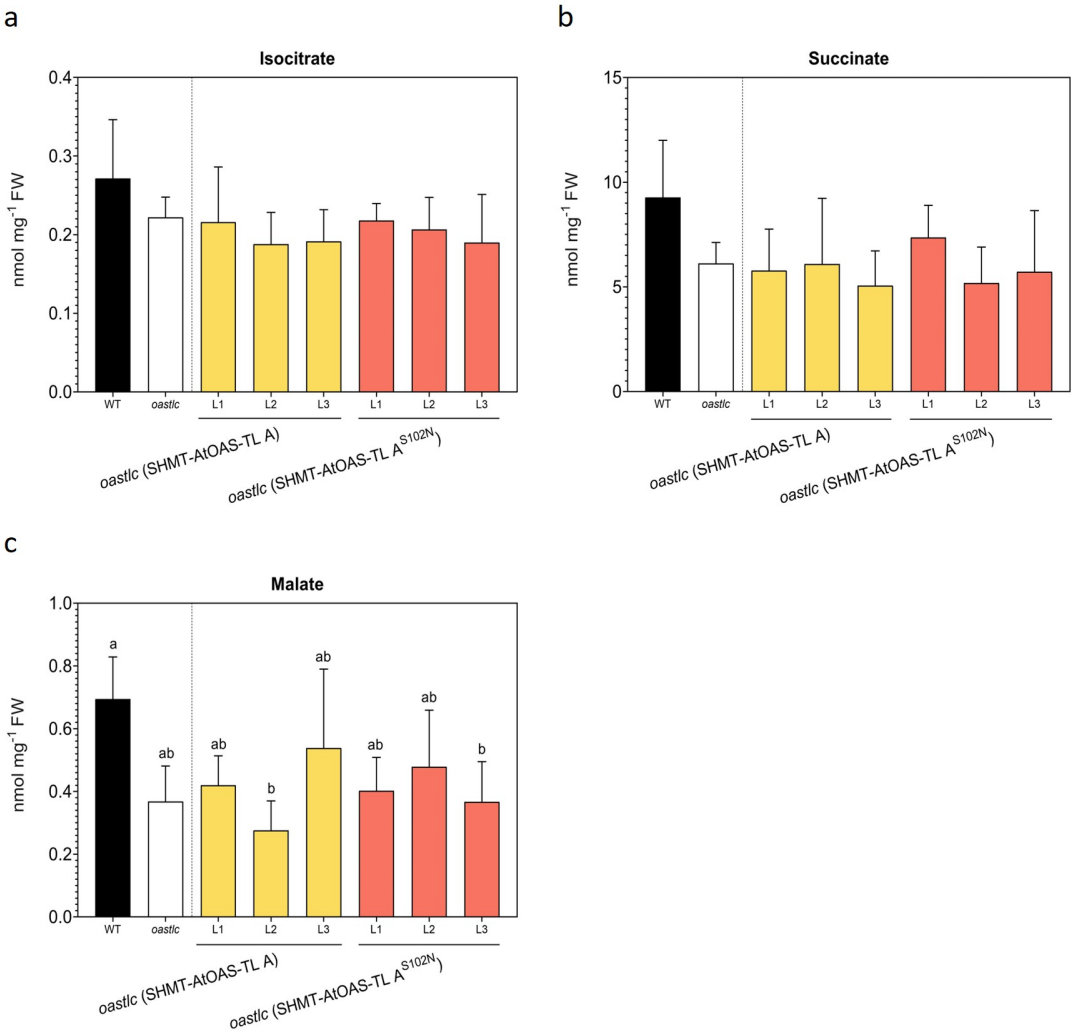

Figure S29: **Steady-state levels of anions in the leaves of complemented *oastlc* lines.** To analyze **a)** isocitrate, **b)** succinate, and **c)** malate, metabolites were extracted from the leaf tissue of six-week-old plants grown on soil under short-day conditions (2.5.2). The HCl extract was diluted 1:10 using ddH_2O; otherwise, the chloride ions from the HCl extract would overload the column and interfere with the run. Diluted samples were separated and quantified using HPLC. Data are shown as means ± SD, n=3-5 biological replicates; each biological replicate represents an individual plant. Different letters indicate significant differences ($p<0.05$) using one-way ANOVA followed by Tukey's test.

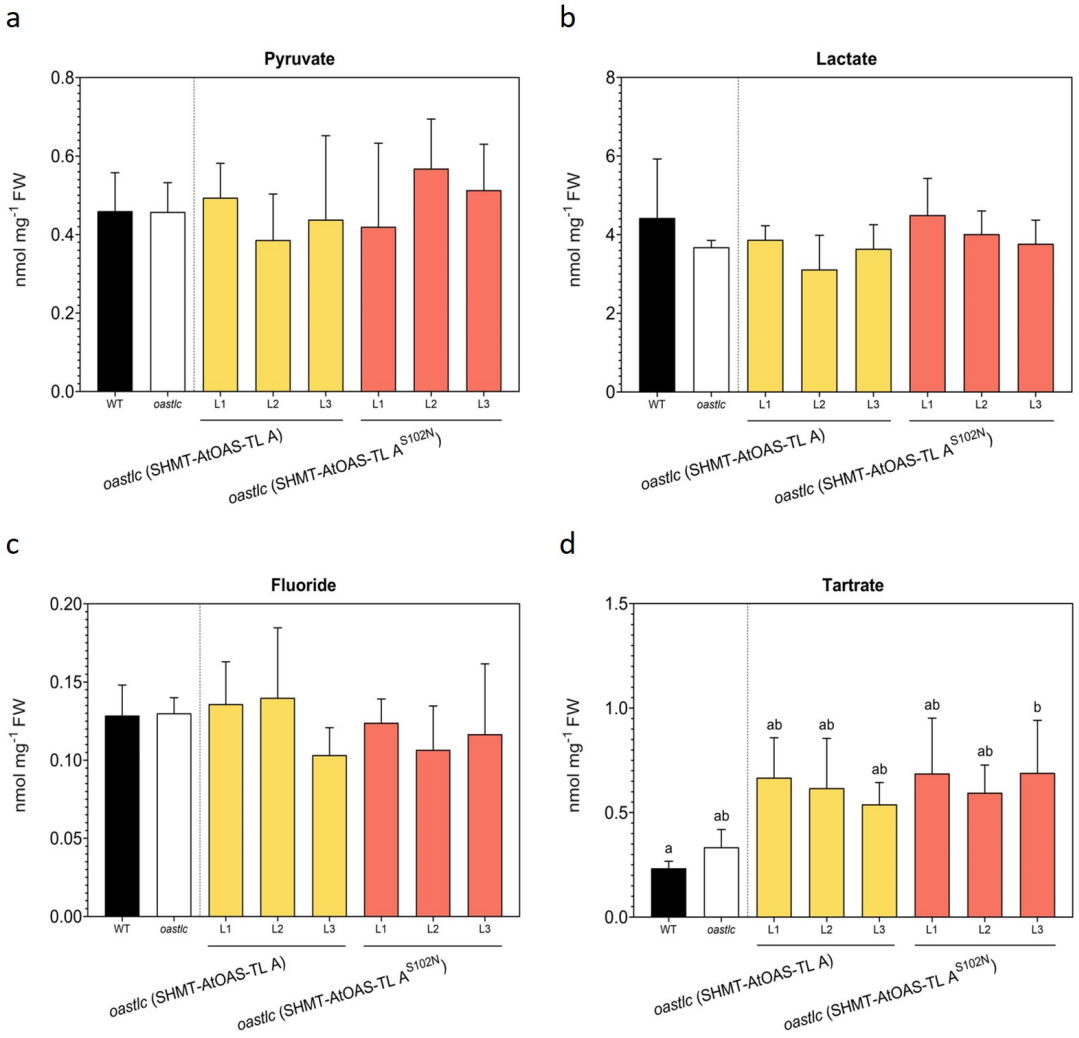

Figure S30: **Steady-state levels of anions in the leaves of complemented *oastlc* lines.** To analyze **a)** pyruvate, **b)** lactate, **c)** fluoride and **d)** tartrate, metabolites were extracted from the leaf tissue of six-week-old plants grown on soil under short-day conditions (2.5.2). The HCl extract was diluted 1:10 using ddH_2O; otherwise, the chloride ions from the HCl extract would overload the column and interfere with the run. Diluted samples were separated and quantified using HPLC. Data are shown as means ± SD, n=3-5 biological replicates; each biological replicate represents an individual plant. Different letters indicate significant differences ($p<0.05$) using one-way ANOVA followed by Tukey's test.

5.6 Determination of amino acids in the leaves of T2 complemented plants

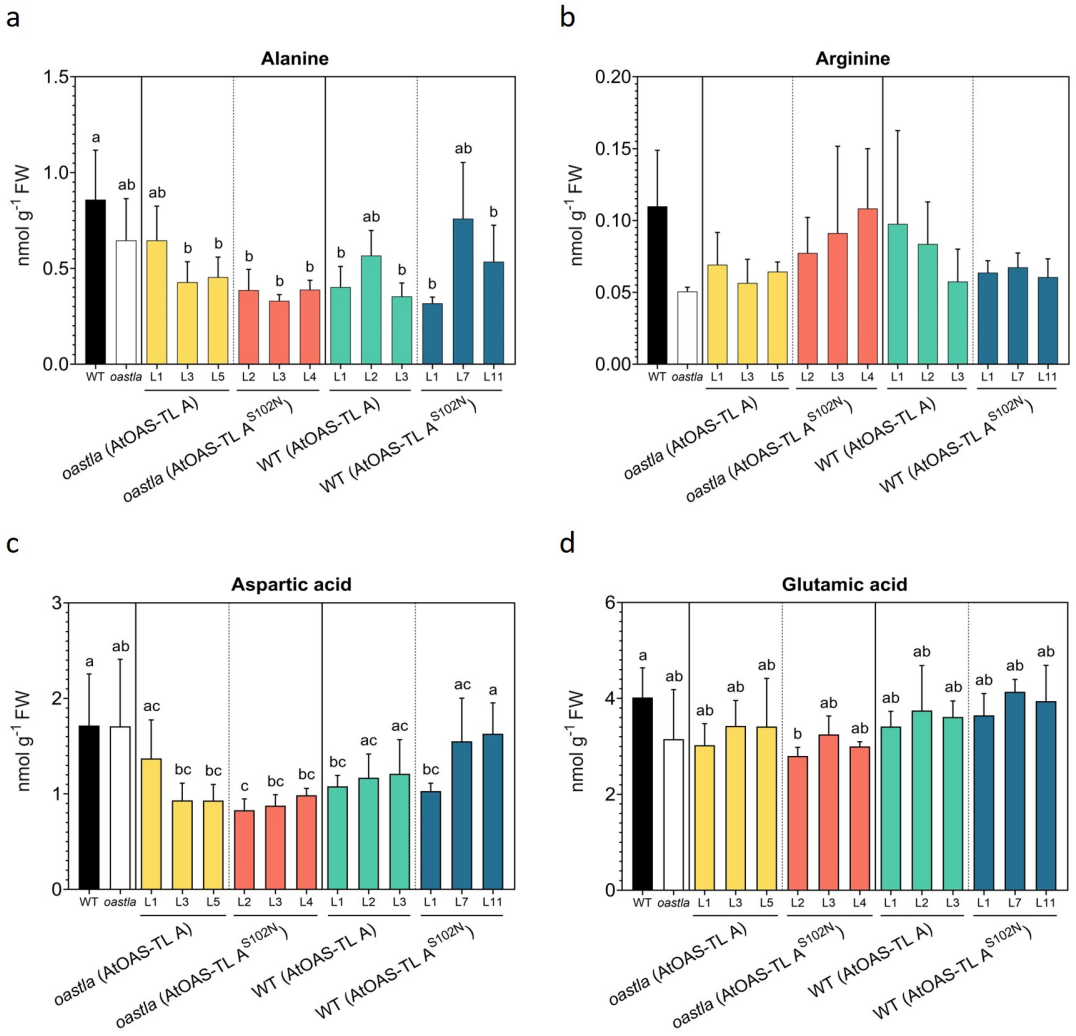

Figure S31: **Steady-state levels of amino acids in the leaves of complemented *oastla* and wild-type lines.** To analyze amino acids **a)** alanine, **b)** arginine, **d)** aspartic acid, and **e)** glutamic acid metabolites were extracted using 0.1 M HCl (2.6.1) from the leaf tissue of six-week-old plants grown on soil under short-day conditions (2.5.2). Then, the amino acids were derivatized using AccTaq (2.6.2). Derivatized samples were separated and quantified using HPLC. Data are shown as means ± SD, n=3-6 biological replicates; each biological replicate represents an individual plant. Different letters indicate significant differences ($p<0.05$) using one-way ANOVA followed by Tukey's test.

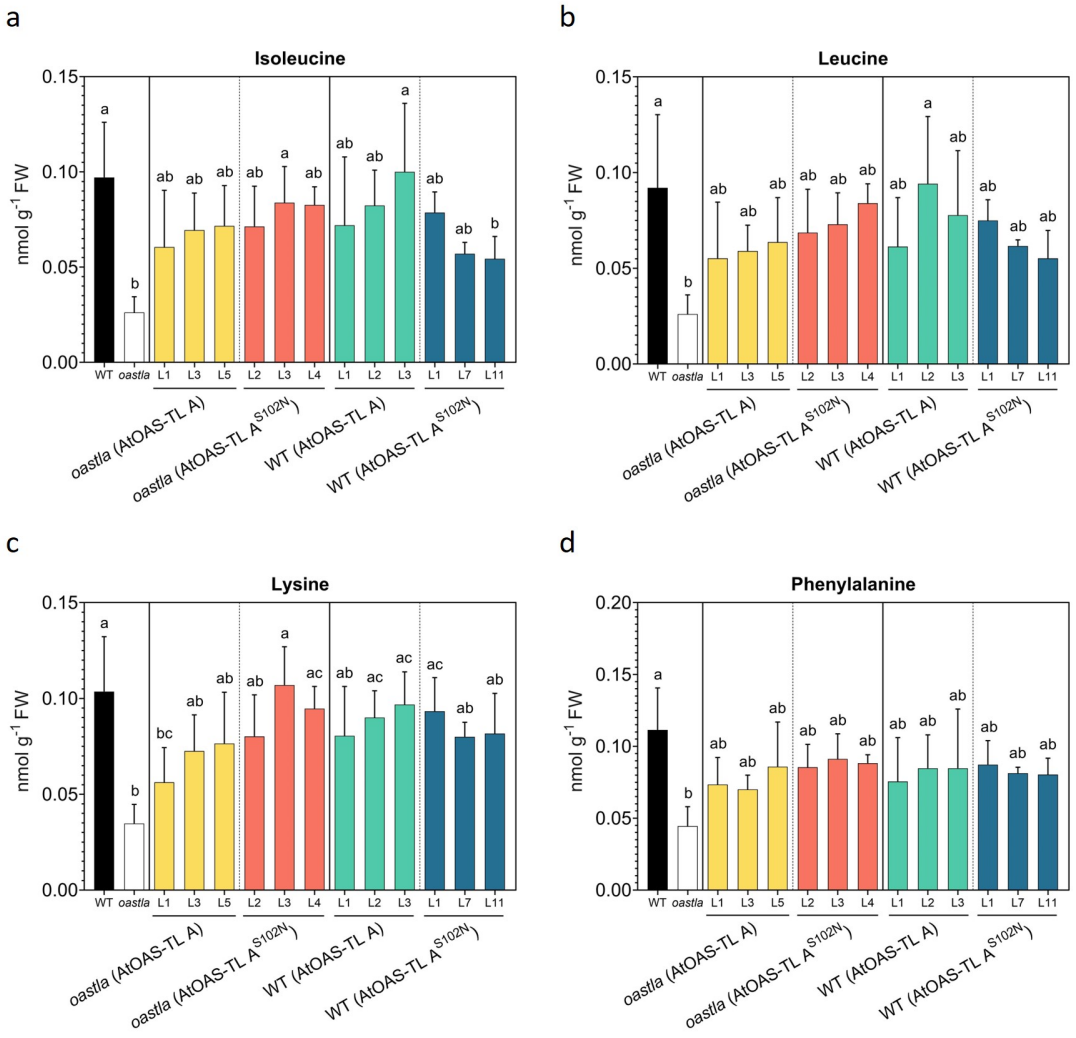

Figure S32: **Steady-state levels of amino acids in the leaves of complemented *oastla* and wild-type lines.** To analyze polar amino acids **a)** isoleucine, **b)** leucine, **c)** lysine, **d)** phenylalanine metabolites were extracted using 0.1 M HCl (2.6.1) from the leaf tissue of six-week-old plants grown on soil under short-day conditions (2.5.2). Then, the amino acids were derivatized using AccTaq (2.6.2). Derivatized samples were separated and quantified using HPLC. Data are shown as means ± SD, n=3-6 biological replicates; each biological replicate represents an individual plant. Different letters indicate significant differences ($p<0.05$) using one-way ANOVA followed by Tukey's test.

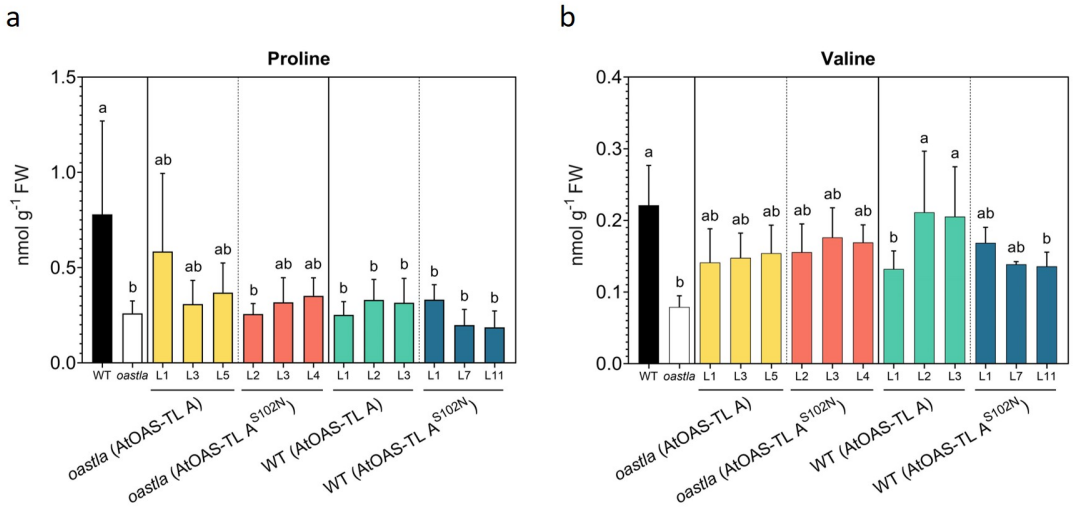

Figure S33: **Steady-state levels of amino acids in the leaves of complemented *oastla* and wild-type lines.** To analyze amino acids **a)** proline and **b)** valine, metabolites were extracted using 0.1 M HCl (2.6.1) from the leaf tissue of six-week-old plants grown on soil under short-day conditions (2.5.2). Then, the amino acids were derivatized using AccTaq (2.6.2). Derivatized samples were separated and quantified using HPLC. Data are shown as means ± SD, n=3-6 biological replicates; each biological replicate represents an individual plant. Different letters indicate significant differences ($p<0.05$) using one-way ANOVA followed by Tukey's test.

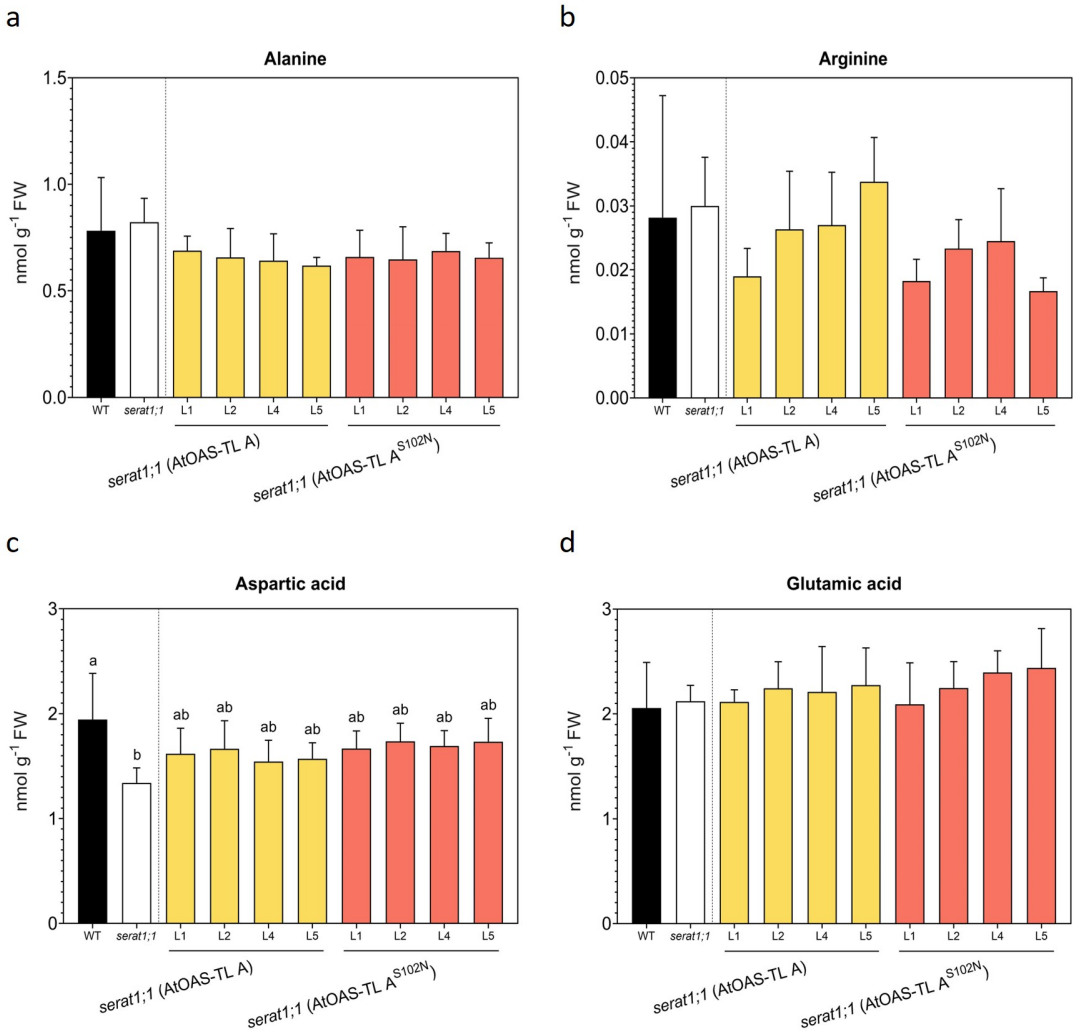

Figure S34: **Steady-state levels of amino acids in the leaves of complemented *serat1;1*.** To analyze amino acids **a)** alanine, **b)** arginine, **d)** aspartic acid, and **e)** glutamic acid metabolites were extracted using 0.1 M HCl (2.6.1) from the leaf tissue of six-week-old plants grown on soil under short-day conditions (2.5.2). Then, the amino acids were derivatized using AccTaq (2.6.2). Derivatized samples were separated and quantified using HPLC. Data are shown as means ± SD, n=3-6 biological replicates; each biological replicate represents an individual plant. Different letters indicate significant differences ($p<0.05$) using one-way ANOVA followed by Tukey's test.

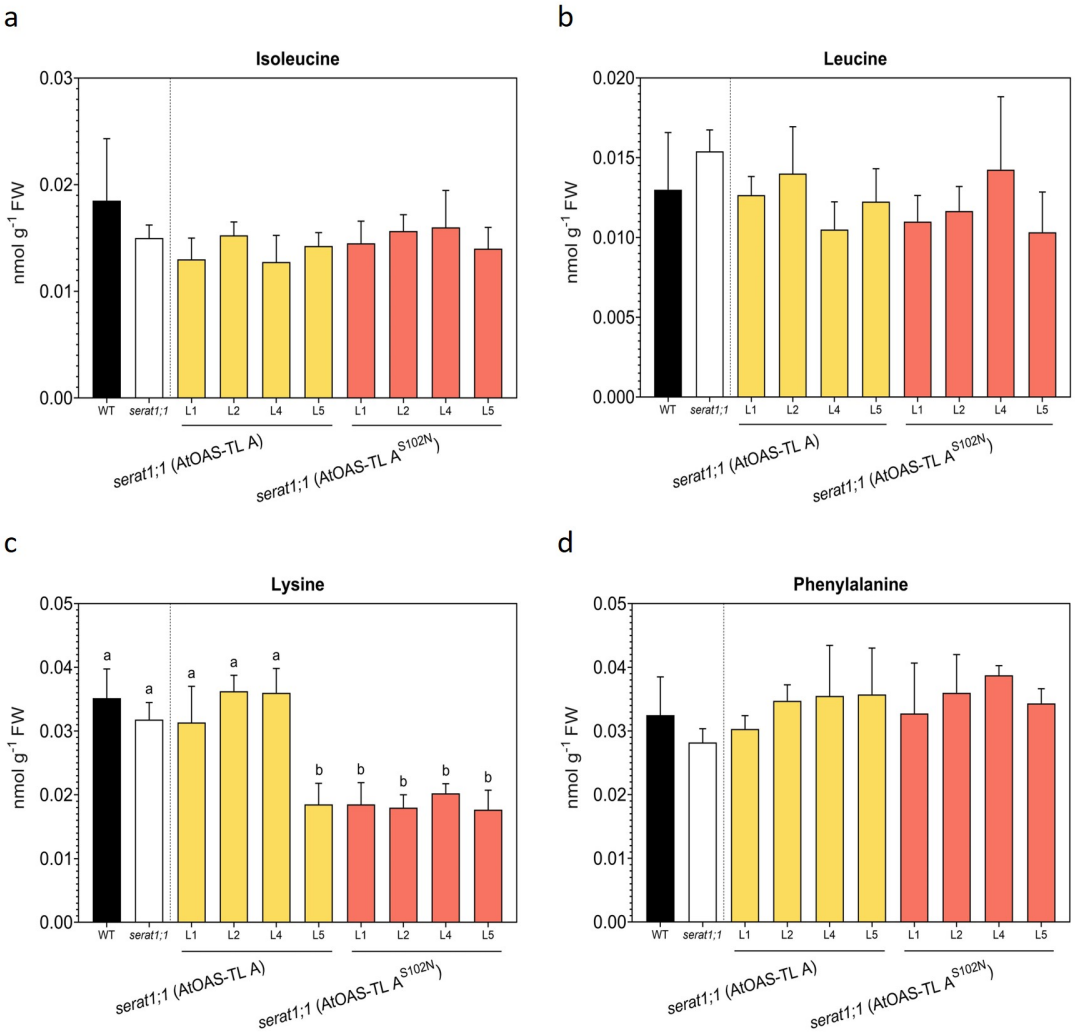

Figure S35: **Steady-state levels of amino acids in the leaves of complemented *serat1;1*.** To analyze polar amino acids **a)** isoleucine, **b)** leucine, **c)** lysine, **d)** phenylalanine metabolites were extracted using 0.1 M HCl (2.6.1) from the leaf tissue of six-week-old plants grown on soil under short-day conditions (2.5.2). Then, the amino acids were derivatized using AccTaq (2.6.2). Derivatized samples were separated and quantified using HPLC. Data are shown as means ± SD, n=3-6 biological replicates; each biological replicate represents an individual plant. Different letters indicate significant differences ($p<0.05$) using one-way ANOVA followed by Tukey's test.

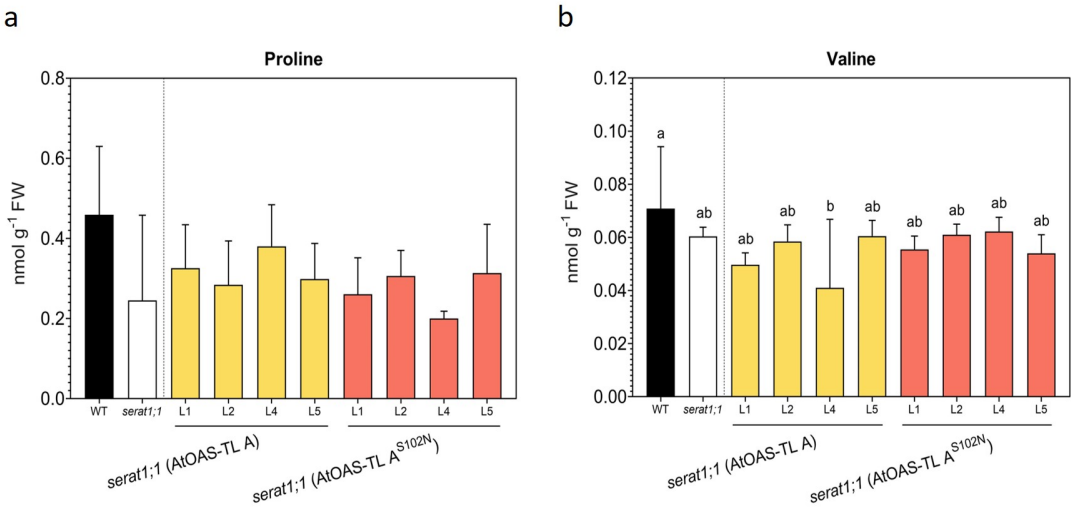

Figure S36: **Steady-state levels of amino acids in the leaves of complemented *serat1;1*.** To analyze amino acids **a)** proline and **b)** valine, metabolites were extracted using 0.1 M HCl (2.6.1) from the leaf tissue of six-week-old plants grown on soil under short-day conditions (2.5.2). Then, the amino acids were derivatized using AccTaq (2.6.2). Derivatized samples were separated and quantified using HPLC. Data are shown as means ± SD, n=3-6 biological replicates; each biological replicate represents an individual plant. Different letters indicate significant differences ($p<0.05$) using one-way ANOVA followed by Tukey's test.

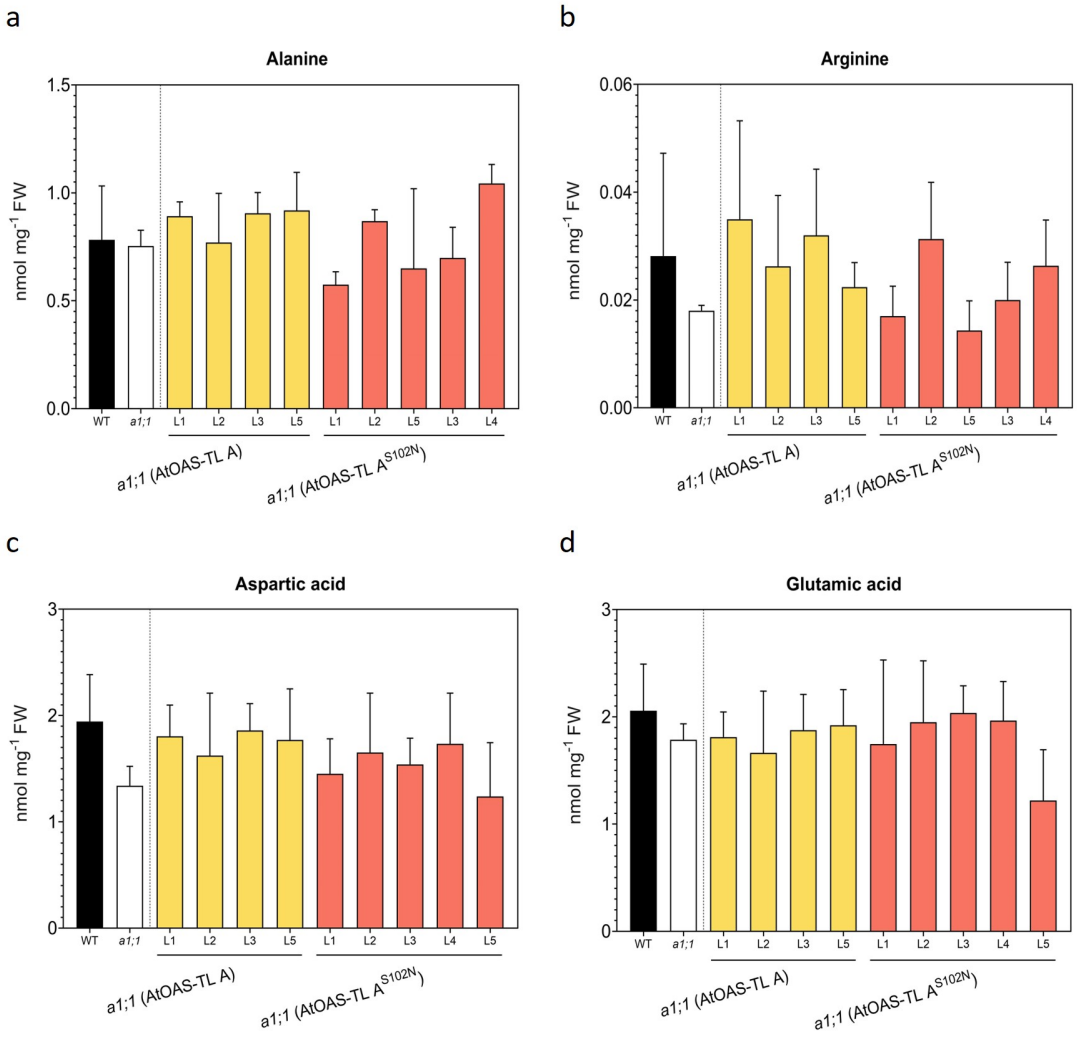

Figure S37: **Steady-state levels of amino acids in the leaves of complemented *a1;1*.** To analyze amino acids **a)** alanine, **b)** arginine, **d)** aspartic acid, and **e)** glutamic acid metabolites were extracted using 0.1 M HCl (2.6.1) from the leaf tissue of six-week-old plants grown on soil under short-day conditions (2.5.2). Then, the amino acids were derivatized using AccTaq (2.6.2). Derivatized samples were separated and quantified using HPLC. Data are shown as means ± SD, n=3-6 biological replicates; each biological replicate represents an individual plant. Different letters indicate significant differences ($p<0.05$) using one-way ANOVA followed by Tukey's test.

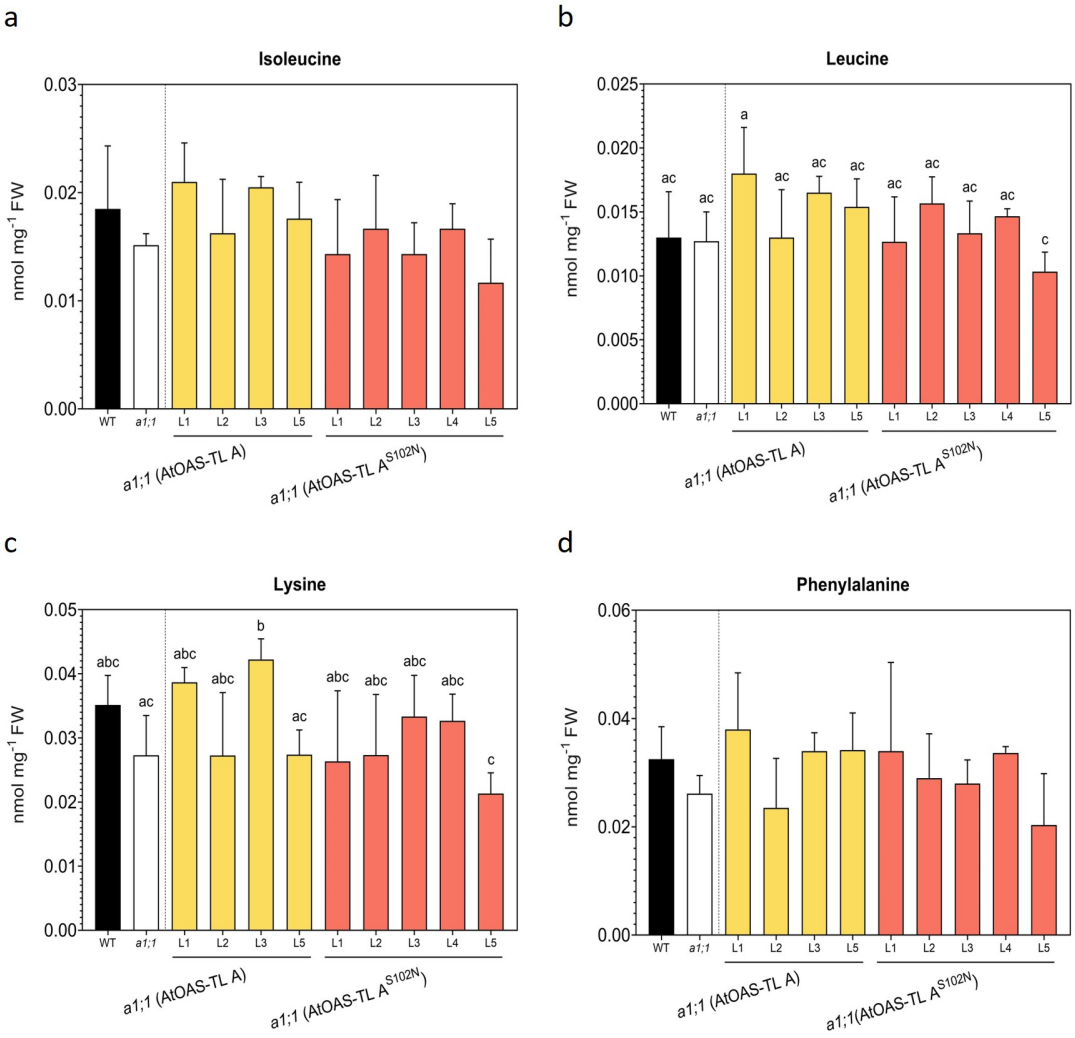

Figure S38: **Steady-state levels of amino acids in the leaves of complemented *a1;1*.** To analyze polar amino acids **a)** isoleucine, **b)** leucine, **c)** lysine, **d)** phenylalanine metabolites were extracted using 0.1 M HCl (2.6.1) from the leaf tissue of six-week-old plants grown on soil under short-day conditions (2.5.2). Then, the amino acids were derivatized using AccTaq (2.6.2). Derivatized samples were separated and quantified using HPLC. Data are shown as means ± SD, n=3-6 biological replicates; each biological replicate represents an individual plant. Different letters indicate significant differences ($p<0.05$) using one-way ANOVA followed by Tukey's test.

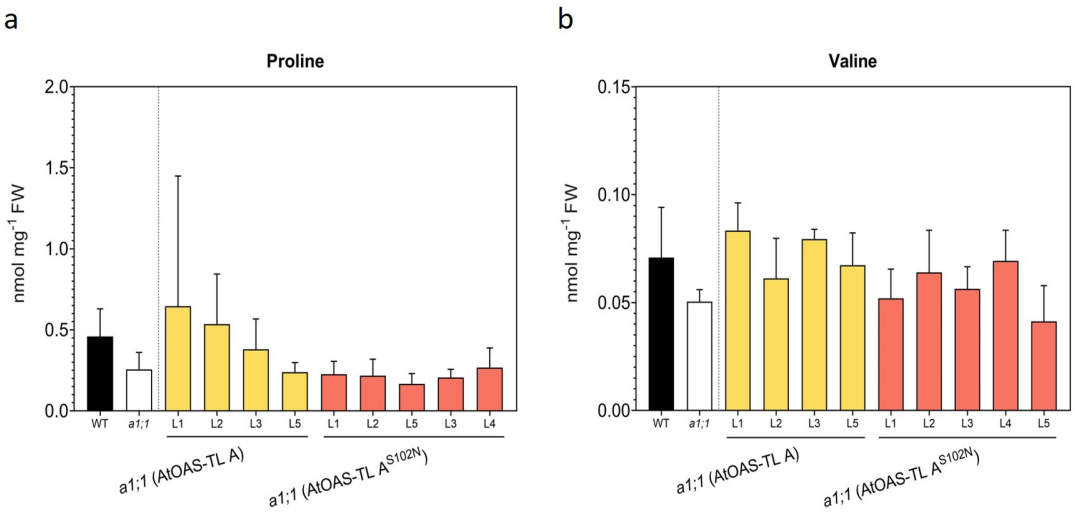

Figure S39: **Steady-state levels of amino acids in the leaves of complemented *a1;1*.** To analyze amino acids **a)** proline and **b)** valine, metabolites were extracted using 0.1 M HCl (2.6.1) from the leaf tissue of six-week-old plants grown on soil under short-day conditions (2.5.2). Then, the amino acids were derivatized using AccTaq (2.6.2). Derivatized samples were separated and quantified using HPLC. Data are shown as means ± SD, n=3-6 biological replicates; each biological replicate represents an individual plant. Different letters indicate significant differences ($p<0.05$) using one-way ANOVA followed by Tukey's test.

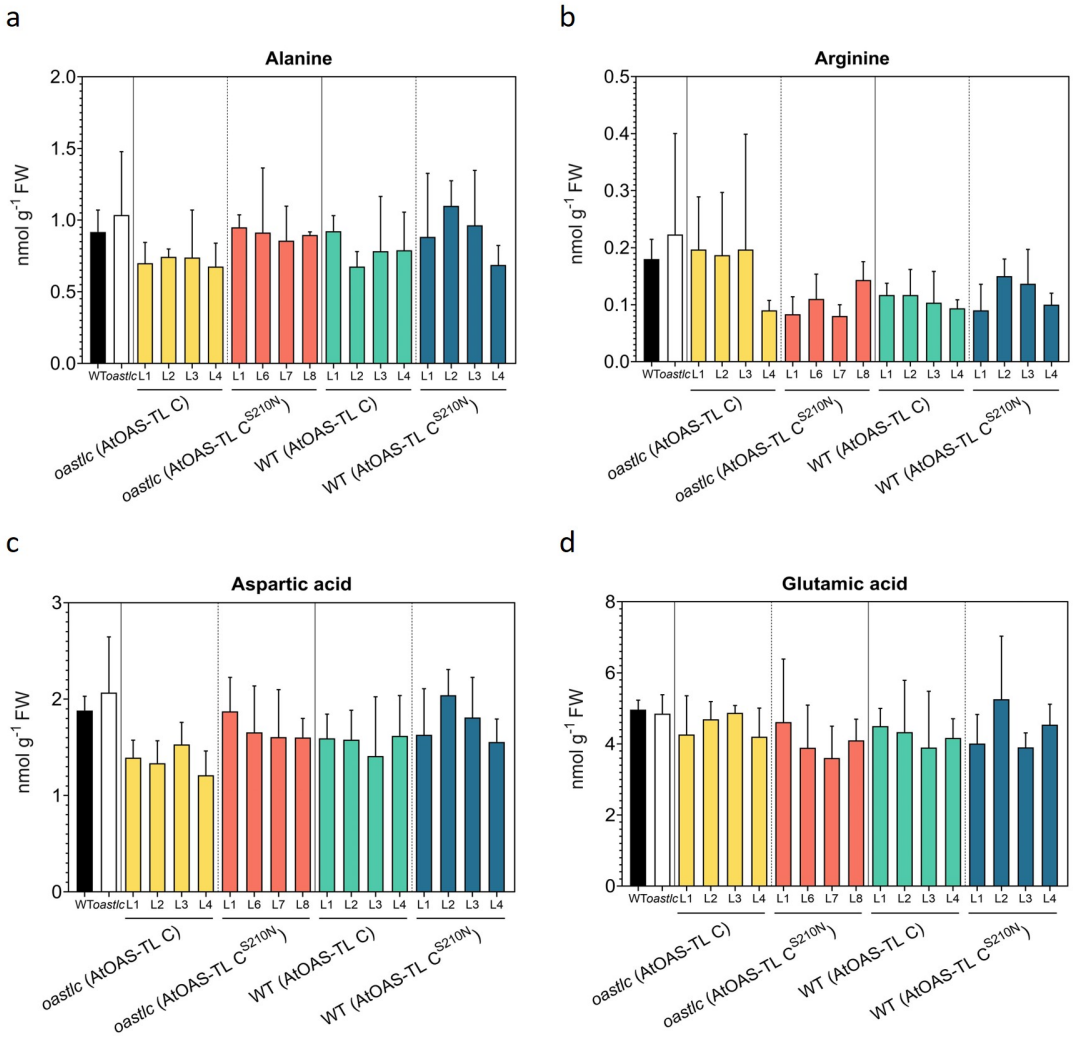

Figure S40: **Steady-state levels of amino acids in the leaves of complemented *oastlc* and wild-type lines.** To analyze amino acids **a)** alanine, **b)** arginine, **d)** aspartic acid, and **e)** glutamic acid metabolites were extracted using 0.1 M HCl (2.6.1) from the leaf tissue of six-week-old plants grown on soil under short-day conditions (2.5.2). Then, the amino acids were derivatized using AccTaq (2.6.2). Derivatized samples were separated and quantified using HPLC. Data are shown as means ± SD, n=3-6 biological replicates; each biological replicate represents an individual plant. Different letters indicate significant differences ($p<0.05$) using one-way ANOVA followed by Tukey's test.

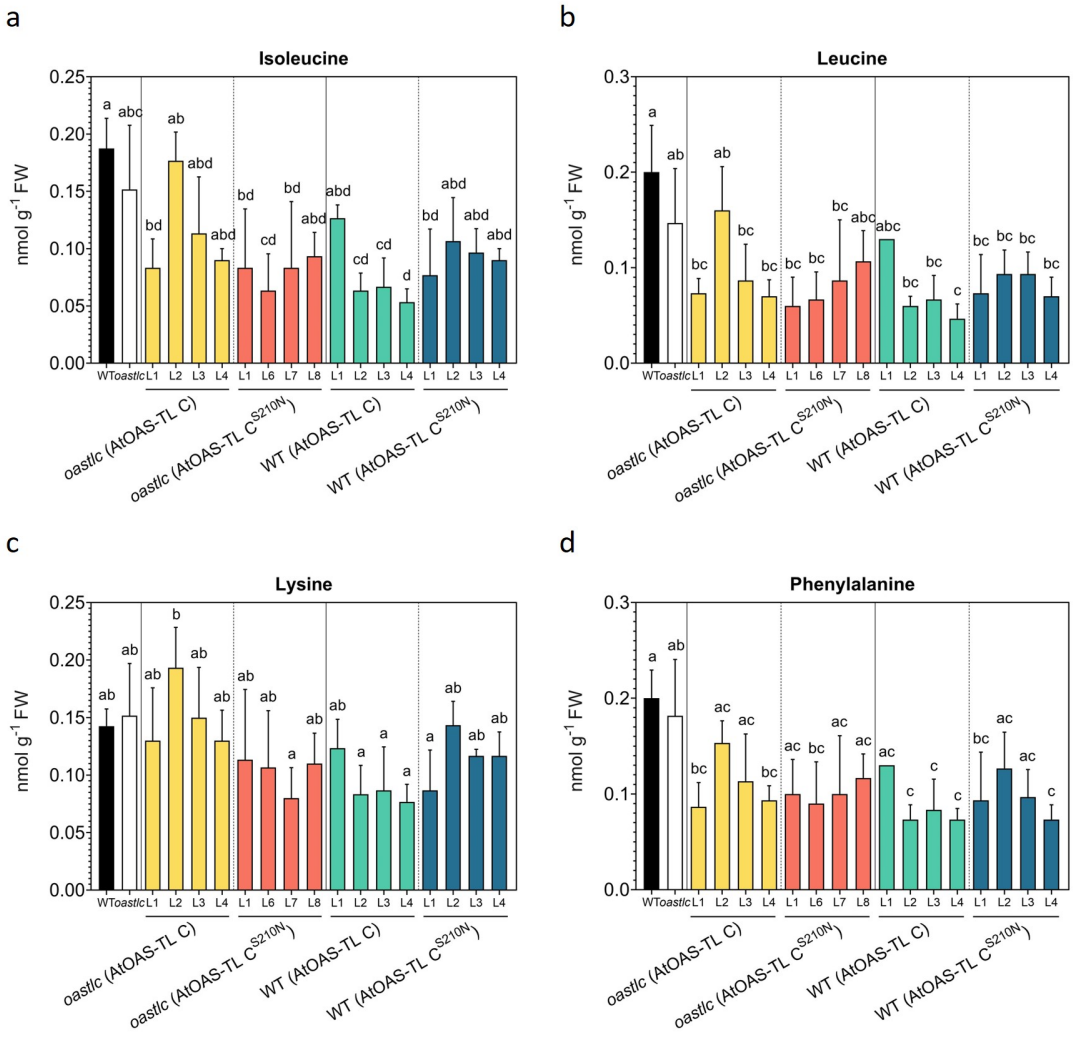

Figure S41: **Steady-state levels of amino acids in the leaves of complemented *oastlc* and wild-type lines.** To analyze polar amino acids **a)** isoleucine, **b)** leucine, **c)** lysine, **d)** phenylalanine metabolites were extracted using 0.1 M HCl (2.6.1) from the leaf tissue of six-week-old plants grown on soil under short-day conditions (2.5.2). Then, the amino acids were derivatized using AccTaq (2.6.2). Derivatized samples were separated and quantified using HPLC. Data are shown as means ± SD, n=3-6 biological replicates; each biological replicate represents an individual plant. Different letters indicate significant differences ($p<0.05$) using one-way ANOVA followed by Tukey's test.

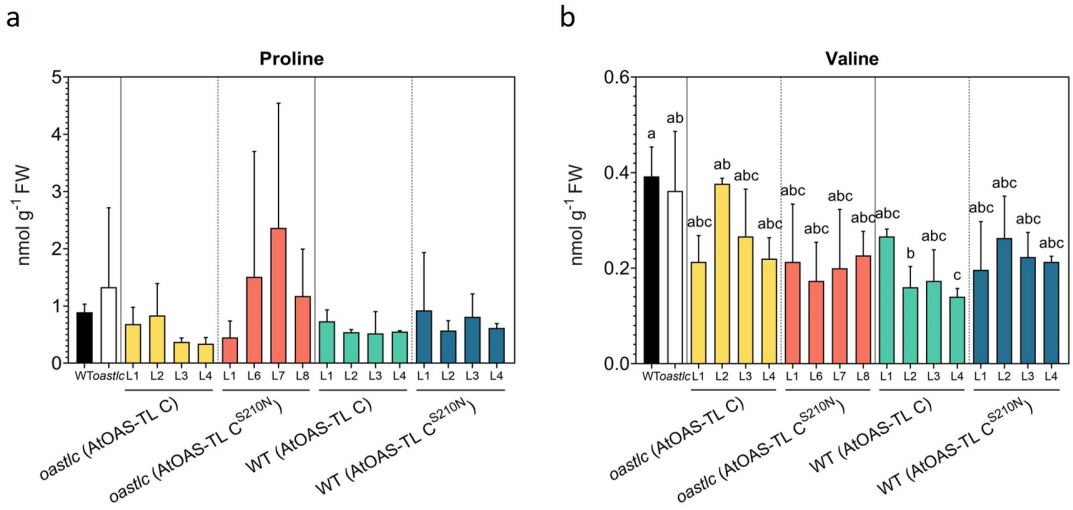

Figure S42: **Steady-state levels of amino acids in the leaves of complemented *oastlc* and wild-type lines.** To analyze amino acids **a)** proline and **b)** valine, metabolites were extracted using 0.1 M HCl (2.6.1) from the leaf tissue of six-week-old plants grown on soil under short-day conditions (2.5.2). Then, the amino acids were derivatized using AccTaq (2.6.2). Derivatized samples were separated and quantified using HPLC. Data are shown as means ± SD, n=3-6 biological replicates; each biological replicate represents an individual plant. Different letters indicate significant differences ($p<0.05$) using one-way ANOVA followed by Tukey's test.

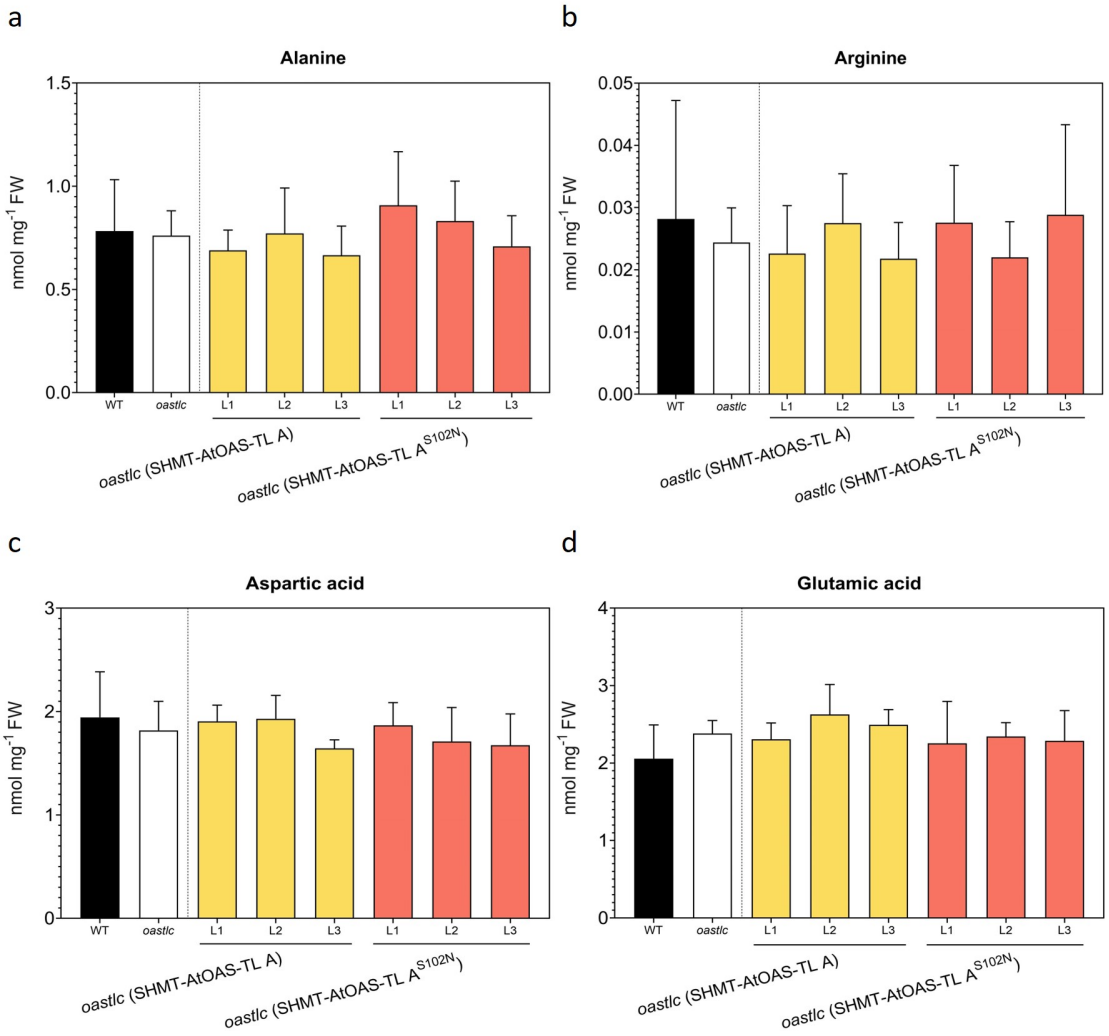

Figure S43: **Steady-state levels of amino acids in the leaves of complemented *oastlc*.** To analyze amino acids **a)** alanine, **b)** arginine, **d)** aspartic acid, and **e)** glutamic acid metabolites were extracted using 0.1 M HCl (2.6.1) from the leaf tissue of six-week-old plants grown on soil under short-day conditions (2.5.2). Then, the amino acids were derivatized using AccTaq (2.6.2). Derivatized samples were separated and quantified using HPLC. Data are shown as means ± SD, n=3-6 biological replicates; each biological replicate represents an individual plant. Different letters indicate significant differences ($p<0.05$) using one-way ANOVA followed by Tukey's test.

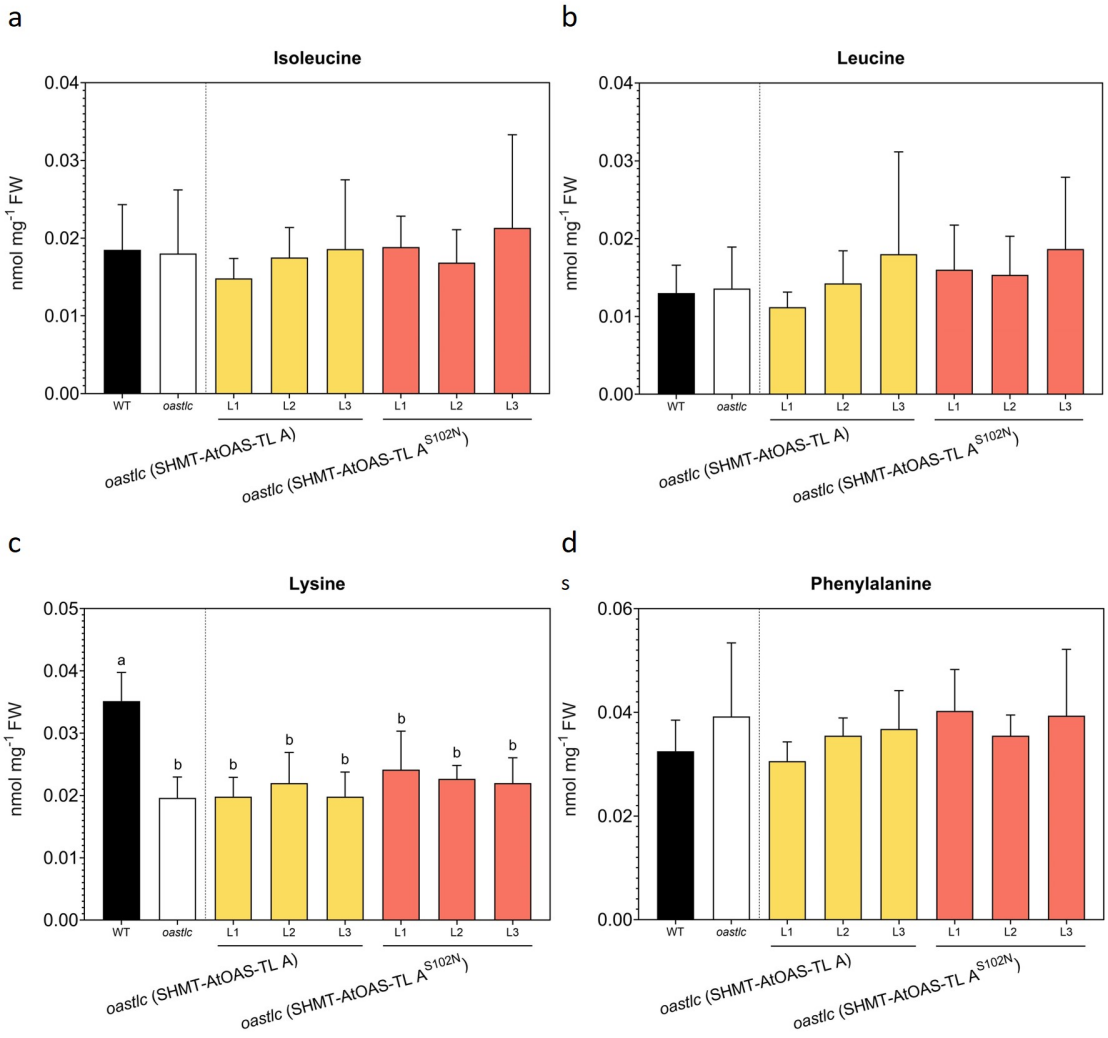

Figure S44: **Steady-state levels of amino acids in the leaves of complemented *oastlc*.** To analyze polar amino acids **a)** isoleucine, **b)** leucine, **c)** lysine, **d)** phenylalanine metabolites were extracted using 0.1 M HCl (2.6.1) from the leaf tissue of six-week-old plants grown on soil under short-day conditions (2.5.2). Then, the amino acids were derivatized using AccTaq (2.6.2). Derivatized samples were separated and quantified using HPLC. Data are shown as means ± SD, n=3-6 biological replicates; each biological replicate represents an individual plant. Different letters indicate significant differences ($p<0.05$) using one-way ANOVA followed by Tukey's test.

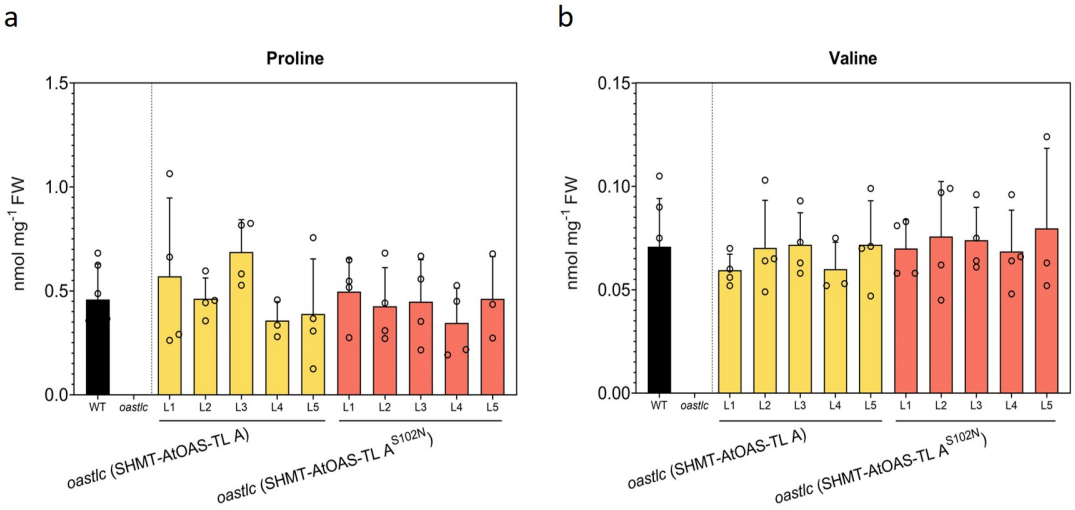

Figure S45: **Steady-state levels of amino acids in the leaves of complemented *oastlc*.** To analyze amino acids **a)** proline and **b)** valine, metabolites were extracted using 0.1 M HCl (2.6.1) from the leaf tissue of six-week-old plants grown on soil under short-day conditions (2.5.2). Then, the amino acids were derivatized using AccTaq (2.6.2). Derivatized samples were separated and quantified using HPLC. Data are shown as means ± SD, n=3-6 biological replicates; each biological replicate represents an individual plant. Different letters indicate significant differences ($p<0.05$) using one-way ANOVA followed by Tukey's test.

5.7 Cadmium treatment

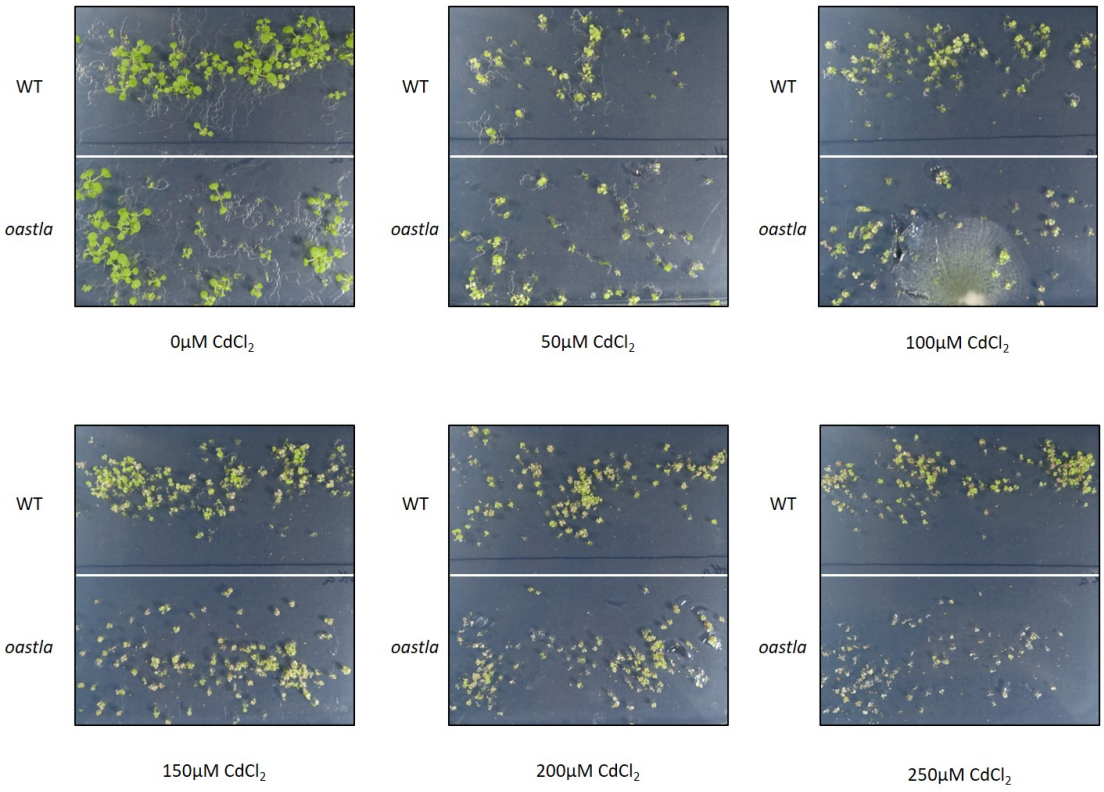

Figure S46: **The growth of *Arabidopsis thaliana* wild-type and *oastla* on AT medium supplemented with different concentrations of $CdCl_2$.** In order to determine the best concentration of cadmium for the 3.9 experiment, I grew wild-type and *oastla* seedlings on ½ AT media (Table 2.4) with varying amounts of $CdCl_2$ - 0, 50, 100, 150, 200, and 250 μM - for three weeks. Finally, 100 μM $CdCl_2$ was selected for further experimentation based on the growth of the seedlings.

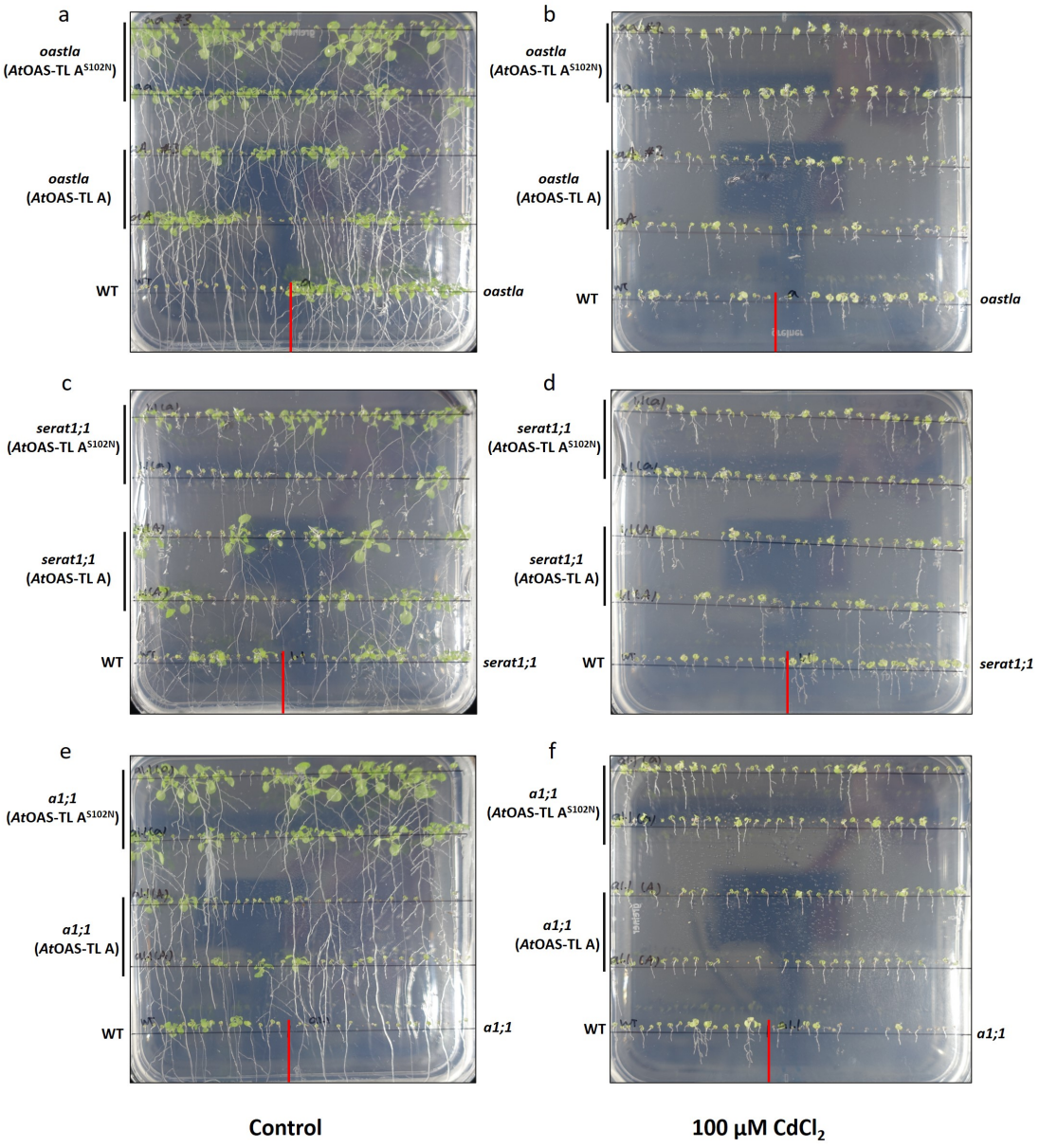

Figure S47: **Root growth of T2 transgenic plants under cadmium treatment.** T2 transformants consist of *oastla* (*At*OAS-TL A), *oastla* (*At*OAS-TL A^{S102N}), *serat1;1* (*At*OAS-TL A), *serat1;1* (*At*OAS-TL A^{S102N}), *a1;1* (*At*OAS-TL A), and *a1;1* (*At*OAS-TL A^{S102N}), as well as controls, were grown in AT media supplemented with 0 and 100 μM $CdCl_2$. After five weeks, the roots' length of seedlings was measured using Fiji (2.7) and compared against wild-type seedlings of the same age.

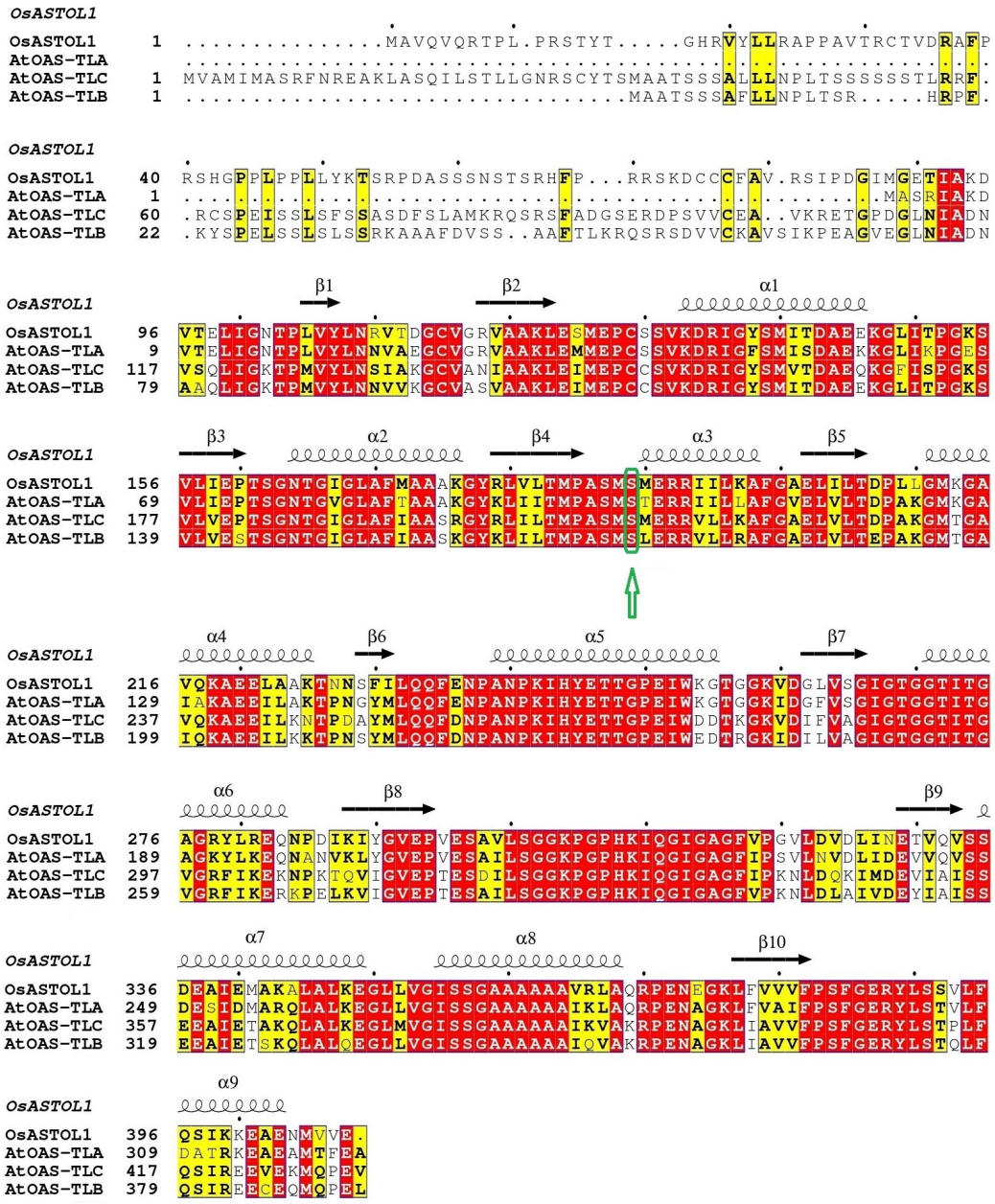

Figure S48: **Sequence alignment of cysteine synthase proteins.** Alignment of *Os*ASTOL1, *At*OAS-TL A, *At*OAS-TL C, and *At*OAS-TL B using ESPript (Gouet et al. 1999). Accession numbers for aligned sequences: *Os*ASTOL1 (XP_015620529), *At*OAS-TL A (NP_001190732), *At*OAS-TL C (NP_191535), *At*OAS-TL B (NP_001189745). The green box and arrow represent the mutation site. Red boxes with white letters represent strictly identical amino acids. Yellow boxes with bold black letters represent similar amino acids conserved among at least two sequences. Black squiggles with α sign and black arrows with β sign represent α-helical structures and β-sheet structures, respectively.

	*Os*ASTOL1	*At*OAS-TL A	*At*OAS-TL C	*At*OAS-TL B
*Os*ASTOL1	100%	80.69%	61.48%	64.49%
*At*OAS-TL A	80.69%	100%	70.19%	71.12%
*At*OAS-TL C	61.48%	70.19%	100%	79.74%
*At*OAS-TL B	64.49%	71.12%	79.74%	100%

Figure S49: **Percentage identity matrix of *Os*ASTOL1 and three *At*OAS-TL proteins.** The percentages of identity between *Os*ASTOL1, *At*OAS-TL A, *At*OAS-TL C, and *At*OAS-TL B proteins were generated using Uniprot. Accession numbers: *Os*ASTOL1 (XP_015620529), *At*OAS-TL A (NP_001190732), *At*OAS-TL C (NP_191535), *At*OAS-TL B (NP_001189745).

List of Abbreviations

γ-EC	γ-glutamylcysteine.
γ-GC	γ-glutamylcysteine
Acetyl-CoA	acetyl coenzyme A
APR	APS reductase
APS	adenosine 5'-phosphosulfate
ATPS	ATP sulfurylase
CS26	cysteine synthase 26
CS	cysteine synthase
CysC1	cysteine synthase C1
IPTG	Isopropyl ß-D-1-thiogalactopyranoside
OAS	*O*-acetylserine
OAS-TL	*O*-acetylserine (thiol)ly
RT	room temperature
SAT	serine acetyltransferase
S102N	Ser102Asn
S210N	Ser210Asn
SERAT	serine acetyltransferase
SHMT	serine hydroxymethyltransferase
SiR	sulfite reductase
SULTR	sulfate transporter
GSH	reduced glutathione
GSH1	γ-glutamylcysteine ligase
GSH2	glutathione synthetase

List of Figures

List of Tables

References

Akbudak, M AYDIN, ERTUGRUL Filiz, and SENEM Uylas (2019). "Identification of *O*-acetylserine (thiol) lyase (OASTL) genes in sorghum (*Sorghum bicolor*) and gene expression analysis under cadmium stress". In: *Molecular Biology Reports* 46.1, pp. 343–354.

Alvarez, CONSOLACION, LETICIA Calo, LUIS C Romero, IRENE Garcia, and CECILIA Gotor (2010). "An *O*-acetylserine (thiol) lyase homolog with L-cysteine desulfhydrase activity regulates cysteine homeostasis in Arabidopsis". In: *Plant Physiology* 152.2, pp. 656–669.

Arisi, ANA-CAROLINA M, GRAHAM Noctor, CHRISTINE H Foyer, and LISE Jouanin (1997). "Modification of thiol contents in poplars (*Populus tremula*× *Populus alba*) overexpressing enzymes involved in glutathione synthesis". In: *Planta* 203, pp. 362–372.

Awazuhara, MOTOKO, TORU Fujiwara, HIROAKI Hayashi, AKIKO Watanabe-Takahashi, HIDEKI Takahashi, and KAZUKI Saito (2005). "The function of SULTR2;1 sulfate transporter during seed development in *Arabidopsis thaliana*". In: *Physiologia Plantarum* 125.1, pp. 95–105.

Berkowitz, OLIVER, MARKUS Wirtz, ALEXANDER Wolf, JÜRGEN Kuhlmann, and RÜDIGER Hell (2002). "Use of biomolecular interaction analysis to elucidate the regulatory mechanism of the cysteine synthase complex from *Arabidopsis thaliana*". In: *Journal of Biological Chemistry* 277.34, pp. 30629–30634.

Bermúdez, MARIA ANGELES, MARIA ANGELES Páez-Ochoa, CECILIA Gotor, and LUIS C Romero (2010). "Arabidopsis S-sulfocysteine synthase activity is essential for chloroplast function and long-day light-dependent redox control". In: *The Plant Cell* 22.2, pp. 403–416.

Birke, HANNAH, STEFANIE J Müller, MICHAEL Rother, ANDREAS D Zimmer, SEBASTIAN NW Hoernstein, DIRK Wesenberg, MARKUS Wirtz, GERD-JOACHIM Krauss, RALF Reski, and RÜDIGER Hell (2012). "The relevance of compartmentation for cysteine synthesis in phototrophic organisms". In: *Protoplasma* 249.2, pp. 147–155.

Blaszczyk, ANNA, ROBERT Brodzik, and AGNIESZKA Sirko (1999). "Increased resistance to oxidative stress in transgenic tobacco plants overexpressing bacterial serine acetyltransferase". In: *The Plant Journal* 20.2, pp. 237–243.

Bogdanova, NATASCHA and RÜDIGER Hell (1997). "Cysteine synthesis in plants: protein-protein interactions of serine acetyltransferase from *Arabidopsis thaliana*". In: *The Plant Journal* 11.2, pp. 251–262.

Bonner, ERIC R, REBECCA E Cahoon, SARAH M Knapke, and JOSEPH M Jez (2005). "Molecular basis of cysteine biosynthesis in plants: structural and functional analysis of *O*-acetylserine sulfhydrylase from *Arabidopsis thaliana*". In: *Journal of Biological Chemistry* 280.46, pp. 38803–38813.

Bowen, CHARLES E, ELLI Rauscher, and LLOYD L Ingraham (1968). "The basicity of biotin". In: *Archives of Biochemistry and Biophysics* 125.3, pp. 865–872.

Bradford, MARION M (1976). "A rapid and sensitive method for the quantitation of microgram quantities of protein utilizing the principle of protein-dye binding". In: *Analytical Biochemistry* 72.1-2, pp. 248–254.

Brunold, CHRISTIAN and JEROME A Schiff (1976). "Studies of sulfate utilization of algae: 15. Enzymes of assimilatory sulfate reduction in euglena and their cellular localization". In: *Plant Physiology* 57.3, pp. 430–436.

Buchanan, BOB B and YVES Balmer (2005). "Redox regulation: a broadening horizon". In: *Annual Review of Plant Biology* 56, pp. 187–220.

Butt, ADRIAN D and JOHN B Ohlrogge (1991). "Acyl carrier protein is conjugated to glutathione in spinach seed". In: *Plant Physiology* 96.3, pp. 937–942.

Carmel-Harel, ORNA and GISELA Storz (2000). "Roles of the glutathione-and thioredoxin-dependent reduction systems in the *Escherichia coli* and *Saccharomyces cerevisiae* responses to oxidative stress". In: *Annual Reviews in Microbiology* 54.1, pp. 439–461.

Chen, ZHEN, PING-XIA Zhao, ZI-QING Miao, GUO-FENG Qi, ZHEN Wang, YANG Yuan, NISAR Ahmad, MIN-JIE Cao, RUEDIGER Hell, MARKUS Wirtz, et al. (2019). "SULTR3s function in chloroplast sulfate uptake and affect ABA biosynthesis and the stress response". In: *Plant Physiology* 180.1, pp. 593–604.

Clarkson, DT, MJ Hawkesford, and JC Davidian (1993). "Membrane and long-distance transport of sulfate". In: *Sulfur Nutrition and Sulfur Assimilation in Higher Plants: Fundamental, Environmental and Agricultural Aspects* 3, p. 19.

Clemens, STEPHAN and JIAN FENG Ma (2016). "Toxic heavy metal and metalloid accumulation in crop plants and foods". In: *Annual Review of Plant Biology* 67, pp. 489–512.

Clough, STEVEN J and ANDREW F Bent (1998). "Floral dip: a simplified method for Agrobacterium-mediated transformation of *Arabidopsis thaliana*". In: *The Plant Journal* 16.6, pp. 735–743.

Cobbett, CHRISTOPHER and PETER Goldsbrough (2002). "Phytochelatins and metallothioneins: roles in heavy metal detoxification and homeostasis". In: *Annual Review of Plant Biology* 53.1, pp. 159–182.

Cobbett, CHRISTOPHER S (2000). "Phytochelatins and their roles in heavy metal detoxification". In: *Plant Physiology* 123.3, pp. 825–832.

Cobbett, CHRISTOPHER S, MIKE J May, ROSS Howden, and BARBARA Rolls (1998). "The glutathione-deficient, cadmium-sensitive mutant, cad2–1, of *Arabidopsis thaliana* is deficient in γ-glutamylcysteine synthetase". In: *The Plant Journal* 16.1, pp. 73–78.

Cook, PF and WEDDING RT (1978). "Cysteine synthetase from *salmonella typhimurium* lt-2. aggregation, kinetic behavior and effect of modifiers". In: *Journal of Biological Chemistry* 253.1, pp. 7874–7879.

Crawford, NM (2000). "Nitrogen and sulfur". In: *Biochemistry and Molecular Biology of Plants*.

Creissen, GARY, JOHN Firmin, MICHAEL Fryer, BALDEEP Kular, NICOLA Leyland, HELEN Reynolds, GABRIELA Pastori, FLORENCE Wellburn, NEIL Baker, ALAN Wellburn, et al. (1999). "Elevated glutathione biosynthetic capacity in the chloroplasts of transgenic tobacco plants paradoxically causes increased oxidative stress". In: *The Plant Cell* 11.7, pp. 1277–1291.

Davidian, JEAN-CLAUDE and STANISLAV Kopriva (2010). "Regulation of sulfate uptake and assimilation—the same or not the same?" In: *Molecular Plant* 3.2, pp. 314–325.

Denk, DAGMAR and AUGUST Böck (1987). "L-cysteine biosynthesis in *Escherichia coli*: nucleotide sequence and expression of the serine acetyltransferase (cysE) gene from the wild-type and a cysteine-excreting mutant". In: *Microbiology* 133.3, pp. 515–525.

Dominguez-Solis, JOSE R, GLORIA Gutierrez-Alcala, LUIS C Romero, and CECILIA Gotor (2001). "The cytosolic *O*-acetylserine (thiol) lyase gene is regulated by heavy metals and can function in cadmium tolerance". In: *Journal of Biological Chemistry* 276.12, pp. 9297–9302.

Droux, MICHEL (2003). "Plant serine acetyltransferase: new insights for regulation of sulphur metabolism in plant cells". In: *Plant Physiology and Biochemistry* 41.6-7, pp. 619–627.

Droux, MICHEL (2004). "Sulfur assimilation and the role of sulfur in plant metabolism: a survey". In: *Photosynthesis Research* 79.3, pp. 331–348.

Droux, MICHEL, MARIE-LINE Ruffet, ROLAND Douce, and DOMINIQUE Job (1998). "Interactions between serine acetyltransferase and *O*-acetylserine (thiol) lyase in higher plants: Structural and kinetic properties of the free and bound enzymes". In: *European Journal of Biochemistry* 255.1, pp. 235–245.

DuBose, AMANDA J, STEPHEN T Lichtenstein, NARISU Narisu, LORI L Bonnycastle, AMY J Swift, PETER S Chines, and FRANCIS S Collins (2013). "Use of microarray hybrid capture and next-generation sequencing to identify the anatomy of a transgene". In: *Nucleic Acids Research* 41.6, e70–e70.

Edwards, K, C Johnstone, and C1 Thompson (1991). "A simple and rapid method for the preparation of plant genomic DNA for PCR analysis." In: *Nucleic Acids Research* 19.6, p. 1349.

El Kassis, ELIE, NICOLE Cathala, HATEM Rouached, PIERRE Fourcroy, PIERRE Berthomieu, NORMAN Terry, and JEAN-CLAUDE Davidian (2007). "Characterization of a selenate-resistant Arabidopsis mutant. Root growth as a potential target for selenate toxicity". In: *Plant Physiology* 143.3, pp. 1231–1241.

Feldman-Salit, ANNA, MARKUS Wirtz, RÜDIGER Hell, and REBECCA C Wade (2009). "A mechanistic model of the cysteine synthase complex". In: *Journal of Molecular Biology* 386.1, pp. 37–59.

Feldman-Salit, ANNA, MARKUS Wirtz, ESTHER D Lenherr, CHRISTIAN Throm, MICHAEL Hothorn, KLAUS Scheffzek, RÜDIGER Hell, and REBECCA C Wade (2012). "Allosterically gated enzyme dynamics in the cysteine synthase complex regulate cysteine biosynthesis in *Arabidopsis thaliana*". In: *Structure* 20.2, pp. 292–302.

Foyer, CHRISTINE H and GRAHAM Noctor (2009). "Redox regulation in photosynthetic organisms: signaling, acclimation, and practical implications". In: *Antioxidants and Redox Signaling* 11.4, pp. 861–905.

— (2011). "Ascorbate and glutathione: the heart of the redox hub". In: *Plant Physiology* 155.1, pp. 2–18.

Francois, JULIE A, SANGARALINGAM Kumaran, and JOSEPH M Jez (2006). "Structural basis for interaction of *O*-acetylserine sulfhydrylase and serine acetyltransferase in the Arabidopsis cysteine synthase complex". In: *The Plant Cell* 18.12, pp. 3647–3655.

Gadalla, MOATAZ M and SOLOMON H Snyder (2010). "Hydrogen sulfide as a gasotransmitter". In: *Journal of Neurochemistry* 113.1, pp. 14–26.

Gigolashvili, TAMARA and STANISLAV Kopriva (2014). "Transporters in plant sulfur metabolism". In: *Frontiers in Plant Science* 5, p. 442.

González-Morales, SUSANA, RAÚL CARLOS López-Sánchez, ANTONIO Juárez-Maldonado, ARMANDO Robledo-Olivo, and ADALBERTO Benavides-Mendoza (2021). "A transcriptomic and proteomic view of hydrogen sulfide signaling in plant abiotic stress". In: *Hydrogen Sulfide and Plant Acclimation to Abiotic Stresses*, pp. 161–186.

Gouet, PATRICE, EMMANUEL Courcelle, DAVID I Stuart, and F M√© toz (1999). "ESPript: analysis of multiple sequence alignments in PostScript." In: *Bioinformatics (Oxford, England)* 15.4, pp. 305–308.

Grill, ERWIN, SUSANNE Löffler, ERNST-L Winnacker, and MEINHART H Zenk (1989). "Phytochelatins, the heavy-metal-binding peptides of plants, are synthesized from glutathione by a specific γ-glutamylcysteine dipeptidyl transpeptidase (phytochelatin synthase)". In: *Proceedings of the National Academy of Sciences* 86.18, pp. 6838–6842.

Grill, ERWIN, ERNST-L Winnacker, and MEINHART H Zenk (1987). "Phytochelatins, a class of heavy-metal-binding peptides from plants, are functionally analogous to metallothioneins". In: *Proceedings of the National Academy of Sciences* 84.2, pp. 439–443.

Gushima, H, T Miya, K Murata, and A Kimura (1983). "Construction of glutathione-producing strains of *Escherichia coli* B by recombinant DNA techniques." In: *Journal of Applied Biochemistry* 5.1-2, pp. 43–52.

Ha, SUK-BONG, AARON P Smith, ROSS Howden, WENDY M Dietrich, SARAH Bugg, MATTHEW J O'Connell, PETER B Goldsbrough, and CHRISTOPHER S Cobbett (1999). "Phytochelatin synthase genes from Arabidopsis and the yeast *Schizosaccharomyces pombe*". In: *The Plant Cell* 11.6, pp. 1153–1163.

Haas, FLORIAN H, CORINNA Heeg, RAFAEL Queiroz, ANDREA Bauer, MARKUS Wirtz, and RÜDIGER Hell (2008). "Mitochondrial serine acetyltransferase functions as a pacemaker of cysteine synthesis in plant cells". In: *Plant Physiology* 148.2, pp. 1055–1067.

Harada, EMIKO, YONG-EUI Choi, ATSUNARI Tsuchisaka, HITOSHI Obata, and HIROSHI Sano (2001). "Transgenic tobacco plants expressing a rice cysteine synthase gene are tolerant to toxic levels of cadmium". In: *Journal of Plant Physiology* 158.5, pp. 655–661.

Harington, CHARLES ROBERT and THOMAS HOBSON Mead (1935). "Synthesis of glutathione". In: *Biochemical Journal* 29.7, p. 1602.

Harms, KARSTEN, PETER Von Ballmoos, CHRISTIAN Brunold, RAINER Höfgen, and HOLGER Hesse (2000). "Expression of a bacterial serine acetyltransferase in transgenic potato plants leads to increased levels of cysteine and glutathione". In: *The Plant Journal* 22.4, pp. 335–343.

Hartmann, TANJA, PETRA Hönicke, MARKUS Wirtz, RÜDIGER Hell, HEINZ Rennenberg, and STANISLAV Kopriva (2004). "Regulation of sulphate assimilation by glutathione in poplars (*Populus tremula*× *Populus alba*) of wild type and overexpressing γ-glutamylcysteine synthetase in the cytosol". In: *Journal of Experimental Botany* 55.398, pp. 837–845.

Hatzfeld, YVES, AKIKO Maruyama, AHLERT Schmidt, MASAAKI Noji, KIMIHARU Ishizawa, and KAZUKI Saito (2000). "β-Cyanoalanine synthase is a mitochondrial cysteine synthase-like protein in spinach and Arabidopsis". In: *Plant Physiology* 123.3, pp. 1163–1172.

Heeg, CORINNA, CORDULA Kruse, RICARDA Jost, MICHAEL Gutensohn, THOMAS Ruppert, MARKUS Wirtz, and RÜDIGER Hell (2008). "Analysis of the Arabidopsis *O*-acetylserine (thiol) lyase gene family demonstrates compartment-specific differences in the regulation of cysteine synthesis". In: *The Plant Cell* 20.1, pp. 168–185.

Hell, RÜDIGER and HELKE Hillebrand (2001). "Plant concepts for mineral acquisition and allocation". In: *Current Opinion in Biotechnology* 12.2, pp. 161–168.

Hell, RÜDIGER, RICARDA Jost, O Berkowitz, and M Wirtz (2002). "Molecular and biochemical analysis of the enzymes of cysteine biosynthesis in the plant *Arabidopsis thaliana*". In: *Amino Acids* 22.3, pp. 245–257.

Hell, RÜDIGER and MARKUS Wirtz (2008). "Metabolism of cysteine in plants and phototrophic bacteria". In: *Sulfur Metabolism in Phototrophic Organisms*. Springer, pp. 59–91.

— (2011). "Molecular biology, biochemistry and cellular physiology of cysteine metabolism in *Arabidopsis thaliana*". In: *The Arabidopsis Book/American Society of Plant Biologists* 9.

Hesse, HOLGER, NADINE Trachsel, MARIANNE Suter, STANISLAV Kopriva, PETER von Ballmoos, HEINZ Rennenberg, and CHRISTIAN Brunold (2003). "Effect of glucose on assimilatory sulphate reduction in *Arabidopsis thaliana* roots". In: *Journal of Experimental Botany* 54.388, pp. 1701–1709.

Hirai, MASAMI YOKOTA, TORU Fujiwara, MOTOKO Awazuhara, TOMOKO Kimura, MASAAKI Noji, and KAZUKI Saito (2003). "Global expression profiling of sulfur-starved Arabidop-

sis by DNA macroarray reveals the role of *O*-acetyl-l-serine as a general regulator of gene expression in response to sulfur nutrition". In: *The Plant Journal* 33.4, pp. 651–663.

Hoefgen, RAINER and VICTORIA J Nikiforova (2008). "Metabolomics integrated with transcriptomics: assessing systems response to sulfur-deficiency stress". In: *Physiologia Plantarum* 132.2, pp. 190–198.

Hopkins, LAURA, SAROJ Parmar, ANNA Błaszczyk, HOLGER Hesse, RAINER Hoefgen, and MALCOLM J Hawkesford (2005). "*O*-acetylserine and the regulation of expression of genes encoding components for sulfate uptake and assimilation in potato". In: *Plant Physiology* 138.1, pp. 433–440.

Huang, BIN, MATTHEW W Vetting, and STEVEN L Roderick (2005). "The active site of *O*-acetylserine sulfhydrylase is the anchor point for bienzyme complex formation with serine acetyltransferase". In: *Journal of Bacteriology* 187.9, pp. 3201–3205.

Ingham, DAVID J, SANDRA Beer, STEPHANIE Money, and GENEVIÈVE Hansen (2001). "Quantitative real-time PCR assay for determining transgene copy number in transformed plants". In: *Biotechniques* 31.1, pp. 132–140.

Ishii, S and R Miyajima (1989). "Glutathione manufacture by cultivation of Saccharomyces in a synthetic medium". In: *Jpn. Patent* 1, pp. 141–591.

Jones-Mortimer, MC, JF Wheldrake, and CA Pasternak (1968). "The control of sulphate reduction in *Escherichia coli* by *O*-acetyl-L-serine". In: *Biochemical Journal* 107.1, pp. 51–53.

Joshi, ROHIT, ASHWANI Pareek, and SNEH L Singla-Pareek (2016). "Plant metallothioneins: classification, distribution, function, and regulation". In: *Plant Metal Interaction*. Elsevier, pp. 239–261.

Jost, RICARDA, O Berkowitz, M Wirtz, L Hopkins, MJ Hawkesford, and R Hell (2000). "Genomic and functional characterization of the *oas* gene family encoding *O*-acetylserine (thiol) lyases, enzymes catalyzing the final step in cysteine biosynthesis in *Arabidopsis thaliana*". In: *Gene* 253.2, pp. 237–247.

Kabir, AHMAD H, MOHAMMAD M Hossain, MOST A Khatun, ABUL Mandal, and SYED A Haider (2016). "Role of silicon counteracting cadmium toxicity in alfalfa *(Medicago sativa* L.)" In: *Frontiers in Plant Science* 7, p. 1117.

Kataoka, TATSUHIKO, NAOMI Hayashi, TOMOYUKI Yamaya, and HIDEKI Takahashi (2004a). "Root-to-shoot transport of sulfate in Arabidopsis. Evidence for the role of SULTR3;5 as

a component of low-affinity sulfate transport system in the root vasculature". In: *Plant Physiology* 136.4, pp. 4198–4204.

Kataoka, TATSUHIKO, AKIKO Watanabe-Takahashi, NAOMI Hayashi, MIWA Ohnishi, TETSURO Mimura, PETER Buchner, MALCOLM J Hawkesford, TOMOYUKI Yamaya, and HIDEKI Takahashi (2004b). "Vacuolar sulfate transporters are essential determinants controlling internal distribution of sulfate in Arabidopsis". In: *The Plant Cell* 16.10, pp. 2693–2704.

Kawashima, CINTIA GOULART, OLIVER Berkowitz, RÜDIGER Hell, MASAAKI Noji, and KAZUKI Saito (2005). "Characterization and expression analysis of a serine acetyltransferase gene family involved in a key step of the sulfur assimilation pathway in Arabidopsis". In: *Plant Physiology* 137.1, pp. 220–230.

Khan, MUHAMMAD SAYYAR, FLORIAN HEINRICH Haas, ARMAN Allboje Samami, AMIN Moghaddas Gholami, ANDREA Bauer, KURT Fellenberg, MICHAEL Reichelt, ROBERT Hänsch, RALF R Mendel, ANDREAS J Meyer, et al. (2010). "Sulfite reductase defines a newly discovered bottleneck for assimilatory sulfate reduction and is essential for growth and development in *Arabidopsis thaliana*". In: *The Plant Cell* 22.4, pp. 1216–1231.

Kong, QINGRAN, MEILING Wu, YANJUN Huan, LI Zhang, HAIYAN Liu, GERELCHIMEG Bou, YIBO Luo, YANSHUANG Mu, and ZHONGHUA Liu (2009). "Transgene expression is associated with copy number and cytomegalovirus promoter methylation in transgenic pigs". In: *PLOS One* 4.8, e6679.

Kopriva, STANISLAV (2006). "Regulation of sulfate assimilation in Arabidopsis and beyond". In: *Annals of Botany* 97.4, pp. 479–495.

Kopriva, STANISLAV, REGULA Muheim, ANNA Koprivova, NADINE Trachsel, CINZIA Catalano, MARIANNE Suter, and CHRISTIAN Brunold (1999). "Light regulation of assimilatory sulphate reduction in *Arabidopsis thaliana*". In: *The Plant Journal* 20.1, pp. 37–44.

Kopriva, STANISLAV, MARIANNE Suter, PETER von Ballmoos, HOLGER Hesse, URS Krähenbühl, HEINZ Rennenberg, and CHRISTIAN Brunold (2002). "Interaction of sulfate assimilation with carbon and nitrogen metabolism in *Lemna minor*". In: *Plant Physiology* 130.3, pp. 1406–1413.

Koprivova, ANNA, MICHAEL Melzer, PETER von Ballmoos, THERESE Mandel, CHRISTIAN Brunold, and STANISLAV Kopriva (2001). "Assimilatory sulfate reduction in C3, C3-C4, and C4 species of Flaveria". In: *Plant Physiology* 127.2, pp. 543–550.

Koprivova, ANNA, MARIANNE Suter, ROEL OP den Camp, CHRISTIAN Brunold, and STANISLAV Kopriva (2000). "Regulation of sulfate assimilation by nitrogen in Arabidopsis". In: *Plant Physiology* 122.3, pp. 737–746.

Kredich, NICHOLAS M (2008). "Biosynthesis of cysteine". In: *EcoSal Plus* 3.1.

Kredich, NICHOLAS M, MICHAEL A Becker, and GORDON M Tomkins (1969). "Purification and characterization of cysteine synthetase, a bifunctional protein complex, from *Salmonella typhimurium*". In: *Journal of Biological Chemistry* 244.9, pp. 2428–2439.

Kredich, NICHOLAS M and GORDON M Tomkins (1966). "The enzymic synthesis of L-cysteine in *Escherichia coli* and *Salmonella typhimurium*". In: *Journal of Biological Chemistry* 241.21, pp. 4955–4965.

Kredich, NM (1996). *Biosynthesis of cysteine. ln Escherichia coli and Salmonella.*

Krueger, STEPHAN, ANNETTE Niehl, M CARMEN Lopez Martin, DIRK Steinhauser, ANDREA Donath, TATJANA Hildebrandt, LUIS C Romero, RAINER Hoefgen, CECILIA Gotor, and HOLGER Hesse (2009). "Analysis of cytosolic and plastidic serine acetyltransferase mutants and subcellular metabolite distributions suggests interplay of the cellular compartments for cysteine biosynthesis in Arabidopsis". In: *Plant, Cell and Environment* 32.4, pp. 349–367.

Kumaran, SANGARALINGAM, HANKUIL Yi, HARI B Krishnan, and JOSEPH M Jez (2009). "Assembly of the cysteine synthase complex and the regulatory role of protein-protein interactions". In: *Journal of Biological Chemistry* 284.15, pp. 10268–10275.

Lee, SANGMAN, DAVID Petros, JAE S Moon, TAE-SEOK Ko, PETER B Goldsbrough, and SCHUYLER S Korban (2003). "Higher levels of ectopic expression of Arabidopsis phytochelatin synthase do not lead to increased cadmium tolerance and accumulation". In: *Plant Physiology and Biochemistry* 41.10, pp. 903–910.

Leustek, THOMAS, MELINDA N Martin, JULIE-ANN Bick, and JOHN P Davies (2000). "Pathways and regulation of sulfur metabolism revealed through molecular and genetic studies". In: *Annual Review of Plant Biology* 51.1, pp. 141–165.

Li, YIN, GONGYUAN Wei, and JIAN Chen (2004). "Glutathione: a review on biotechnological production". In: *Applied Microbiology and Biotechnology* 66, pp. 233–242.

Li, YUJING, OM PARKASH Dankher, LAURA Carreira, AARON P Smith, and RICHARD B Meagher (2006). "The shoot-specific expression of γ-glutamylcysteine synthetase directs the

long-distance transport of thiol-peptides to roots conferring tolerance to mercury and arsenic". In: *Plant Physiology* 141.1, pp. 288–298.

Liedschulte, VERENA, ANDREAS Wachter, AN Zhigang, and THOMAS Rausch (2010). "Exploiting plants for glutathione (GSH) production: uncoupling GSH synthesis from cellular controls results in unprecedented GSH accumulation". In: *Plant Biotechnology Journal* 8.7, pp. 807–820.

Liszewska, F and A Sirko (2003). "Analysis of transgenic tobacco lines expressing bacterial cysK gene encoding *O*-acetylserine (thiol) lyase A". In: *Sulphur Transport and Assimilation in Plants. Regulation, Interaction and Signaling. Leiden: Backhuys Publishers*, pp. 269–271.

— (2005). "Identification and characteristics of tobacco clones encoding an organellar isoform of serine acetyltransferase and a cytosolic isoform of cysteine synthase". In: *Biological Letters* 42.2 Spec. Vol.

Liszewska, FRANTZ, ANNA Błaszczyk, and AGNIESZKA Sirko (2001). "Modification of non-protein thiols contents in transgenic tobacco plants producing bacterial enzymes of cysteine biosynthesis pathway." In: *Acta Biochimica Polonica* 48.3, pp. 647–656.

López-Martín, M CARMEN, MANUEL Becana, LUIS C Romero, and CECILIA Gotor (2008). "Knocking out cytosolic cysteine synthesis compromises the antioxidant capacity of the cytosol to maintain discrete concentrations of hydrogen peroxide in Arabidopsis". In: *Plant Physiology* 147.2, pp. 562–572.

Lunn, JOHN E, MICHEL Droux, JACQUELINE Martin, and ROLAND Douce (1990). "Localization of ATP sulfurylase and *O*-acetylserine (thiol) lyase in spinach leaves". In: *Plant Physiology* 94.3, pp. 1345–1352.

Lynch, AS, R Tyrrell, SJ Smerdon, GS Briggs, and AJ Wilkinson (1994). "Characterization of the CysB protein of *Klebsiella aerogenes*: direct evidence that *N*-acetylserine rather than *O*-acetylserine serves as the inducer of the cysteine regulon". In: *Biochemical Journal* 299.1, pp. 129–136.

Maruyama-Nakashita, AKIKO, ERI Inoue, AKIKO Watanabe-Takahashi, TOMOYUKI Yamaya, and HIDEKI Takahashi (2003). "Transcriptome profiling of sulfur-responsive genes in Arabidopsis reveals global effects of sulfur nutrition on multiple metabolic pathways". In: *Plant Physiology* 132.2, pp. 597–605.

Maruyama-Nakashita, AKIKO, YUMIKO Nakamura, TOMOYUKI Yamaya, and HIDEKI Takahashi (2004). "Regulation of high-affinity sulphate transporters in plants: towards systematic analysis of sulphur signalling and regulation". In: *Journal of Experimental Botany* 55.404, pp. 1843–1849.

Matityahu, I, L Kachan, I Bar Ilan, and R Amir (2006). "Transgenic tobacco plants overexpressing the Met25 gene of *Saccharomyces cerevisiae* exhibit enhanced levels of cysteine and glutathione and increased tolerance to oxidative stress". In: *Amino Acids* 30, pp. 185–194.

Meister, ALTON (1988). "Glutathione metabolism and its selective modification." In: *Journal of Biological Chemistry* 263.33, pp. 17205–17208.

— (1994). "Glutathione-ascorbic acid antioxidant system in animals". In: *Journal of Biological Chemistry* 269.13, pp. 9397–9400.

Meister, ALTON and MARY E Anderson (1983). "Glutathione". In: *Annual Review of Biochemistry* 52.1, pp. 711–760.

Mildvan, ALBERT S, MICHAEL C Scrutton, and MERTON F Utter (1966). "Pyruvate carboxylase: VII. A possible role for tightly bound manganese". In: *Journal of Biological Chemistry* 241.15, pp. 3488–3498.

Mullineaux, PHILIP M and THOMAS Rausch (2005). "Glutathione, photosynthesis and the redox regulation of stress-responsive gene expression". In: *Photosynthesis Research* 86.3, pp. 459–474.

Murata, KOUSAKU, TOYOFUMI Miya, HIROSHI Gushima, and AKIRA Kimura (1983). "Cloning and amplification of a gene for glutathione synthetase in *Escherichia coli* B". In: *Agricultural and Biological Chemistry* 47.6, pp. 1381–1383.

Murata, KOUSAKU, KEIKO Tani, JYOJI Kato, and ICHIRO Chibata (1981). "Glutathione production by immobilized *Saccharomyces cerevisiae* cells containing an ATP regeneration system". In: *European Journal of Applied Microbiology and Biotechnology* 11, pp. 72–77.

Neuenschwander, URS, MARIANNE Suter, and CHRISTIAN Brunold (1991). "Regulation of sulfate assimilation by light and *O*-acetyl-l-serine in *Lemna minor* L." In: *Plant Physiology* 97.1, pp. 253–258.

Nikiforova, VICTORIA, JENS Freitag, STEFAN Kempa, MONIKA Adamik, HOLGER Hesse, and RAINER Hoefgen (2003). "Transcriptome analysis of sulfur depletion in *Arabidopsis*

thaliana: interlacing of biosynthetic pathways provides response specificity". In: *The Plant Journal* 33.4, pp. 633–650.

Noctor, GRAHAM, ANA-CAROLINA M Arisi, LISE Jouanin, and CHRISTINE H Foyer (1998a). "Manipulation of glutathione and amino acid biosynthesis in the chloroplast". In: *Plant Physiology* 118.2, pp. 471–482.

Noctor, GRAHAM and CHRISTINE H Foyer (1998b). "Ascorbate and glutathione: keeping active oxygen under control". In: *Annual Review of Plant Biology* 49.1, pp. 249–279.

Noctor, GRAHAM, LEONARDO Gomez, HÉLÈNE Vanacker, and CHRISTINE H Foyer (2002). "Interactions between biosynthesis, compartmentation and transport in the control of glutathione homeostasis and signalling". In: *Journal of Experimental Botany* 53.372, pp. 1283–1304.

Noctor, GRAHAM, AMNA Mhamdi, SEJIR Chaouch, YI Han, JENNY Neukermans, BELEN Marquez-Garcia, GUILLAUME Queval, and CHRISTINE H Foyer (2012). "Glutathione in plants: an integrated overview". In: *Plant, Cell and Environment* 35.2, pp. 454–484.

Noctor, GRAHAM, MICHAEL Strohm, LISE Jouanin, KARL-JOSEF Kunert, CHRISTINE HELEN Foyer, and HEINZ Rennenberg (1996). "Synthesis of glutathione in leaves of transgenic poplar overexpressing γ-glutamylcysteine synthetase". In: *Plant Physiology* 112.3, pp. 1071–1078.

Noji, M and K Saito (2002). "Molecular and biochemical analysis of serine acetyltransferase and cysteine synthase towards sulfur metabolic engineering in plants". In: *Amino Acids* 22, pp. 231–243.

Noji, MASAAKI, KENJI Inoue, NOBUHITO Kimura, ATSUKO Gouda, and KAZUKI Saito (1998). "Isoform-dependent differences in feedback regulation and subcellular localization of serine acetyltransferase involved in cysteine biosynthesis from *Arabidopsis thaliana*". In: *Journal of Biological Chemistry* 273.49, pp. 32739–32745.

Norici, ALESSANDRA, RÜDIGER Hell, and MARIO Giordano (2005). "Sulfur and primary production in aquatic environments: an ecological perspective". In: *Photosynthesis Research* 86.3, pp. 409–417.

Ohtake, YASUYUKI, KUNIHIKO Watanabe, HIDETOSHI Tezuka, TOMOO Ogata, SEIZOU Yabuuchi, KOUSAKU Murata, and AKIRA Kimura (1988). "The Expression of the γ-glutamylcysteine synthetase gene of *Escherichia coli* B in *Saccharomyces cerevisiae*". In: *Agricultural and Biological Chemistry* 52.11, pp. 2753–2762.

Ohtake, YASUYUKI, KUNIHIKO Watanabe, HIDETOSHI Tezuka, TOMOO Ogata, SEIZOU Yabuuchi, KOUSAKU Murata, and AKIRA Kimura (1989). "Expression of the glutathione synthetase gene of *Escherichia coli* B in *Saccharomyces cerevisiae*". In: *Journal of Fermentation and Bioengineering* 68.6, pp. 390–394.

Ostrowski, J and NM Kredich (1990). "*In vitro* interactions of CysB protein with the cysJIH promoter of *Salmonella typhimurium*: inhibitory effects of sulfide". In: *Journal of Bacteriology* 172.2, pp. 779–785.

Ostrowski, JACEK and NICHOLAS M Kredich (1991). "Negative autoregulation of cysB in *Salmonella typhimurium*: *in vitro* interactions of CysB protein with the cysB promoter". In: *Journal of Bacteriology* 173.7, pp. 2212–2218.

Palmiter, RICHARD D and RALPH L Brinster (1986). "Germ-line transformation of mice". In: *Annual Review of Genetics* 20.1, pp. 465–499.

Pasternak, MACIEJ, BENSON Lim, MARKUS Wirtz, RÜDIGER Hell, CHRISTOPHER S Cobbett, and ANDREAS J Meyer (2008). "Restricting glutathione biosynthesis to the cytosol is sufficient for normal plant development". In: *The Plant Journal* 53.6, pp. 999–1012.

Patron, NICOLA J, DION G Durnford, and STANISLAV Kopriva (2008). "Sulfate assimilation in eukaryotes: fusions, relocations and lateral transfers". In: *BMC Evolutionary Biology* 8.1, pp. 1–14.

Penninckx, MICHEL (2000). "A short review on the role of glutathione in the response of yeasts to nutritional, environmental, and oxidative stresses". In: *Enzyme and Microbial Technology* 26.9-10, pp. 737–742.

Penninckx, MICHEL J (2002). "An overview on glutathione in *Saccharomyces* versus non-conventional yeasts". In: *FEMS Yeast Research* 2.3, pp. 295–305.

Penninckx, MICHEL J and MARC T Elskens (1993). "Metabolism and functions of glutathione in micro-organisms". In: *Advances in Microbial Physiology* 34, pp. 239–301.

Peterson, ANNITA G and DAVID J Oliver (2006). "Leaf-targeted phytochelatin synthase in *Arabidopsis thaliana*". In: *Plant Physiology and Biochemistry* 44.11-12, pp. 885–892.

Picault, N, AC Cazalé, A Beyly, S Cuiné, P Carrier, DT Luu, C Forestier, and G Peltier (2006). "Chloroplast targeting of phytochelatin synthase in Arabidopsis: effects on heavy metal tolerance and accumulation". In: *Biochimie* 88.11, pp. 1743–1750.

Pinter, TYLER BJ and MARTIN J Stillman (2014). "The zinc balance: competitive zinc metalation of carbonic anhydrase and metallothionein 1A". In: *Biochemistry* 53.39, pp. 6276–6285.

Pye, VALERIE E, ANDREW P Tingey, ROBERT L Robson, and PETER CE Moody (2004). "The structure and mechanism of serine acetyltransferase from *Escherichia coli*". In: *Journal of Biological Chemistry* 279.39, pp. 40729–40736.

Queval, GUILLAUME, DOROTHÉE Thominet, HÉLÈNE Vanacker, MYROSLAWA Miginiac-Maslow, BERTRAND Gakière, and GRAHAM Noctor (2009). "H_2O_2-activated up-regulation of glutathione in Arabidopsis involves induction of genes encoding enzymes involved in cysteine synthesis in the chloroplast". In: *Molecular Plant* 2.2, pp. 344–356.

Rabeh, WAEL M and PAUL F Cook (2004). "Structure and mechanism of *O*-acetylserine sulfhydrylase". In: *Journal of Biological Chemistry* 279.26, pp. 26803–26806.

Rahman, MOHAMMAD FARHADUR, ANUBRATA Ghosal, MOHAMMAD FIROZ Alam, and AHMAD HUMAYAN Kabir (2017). "Remediation of cadmium toxicity in field peas (*Pisum sativum* L.) through exogenous silicon". In: *Ecotoxicology and Environmental Safety* 135, pp. 165–172.

Rajab, HALA, MUHAMMAD SAYYAR Khan, MARKUS Wirtz, MARIO Malagoli, FARIHA Qahar, and RÜDIGER Hell (2020). "Sulfur metabolic engineering enhances cadmium stress tolerance and root to shoot iron translocation in *Brassica napus* L". In: *Plant Physiology and Biochemistry* 152, pp. 32–43.

Rascio, NICOLETTA, FRANCESCA Dalla Vecchia, NICOLETTA La Rocca, ROBERTO Barbato, CRISTINA Pagliano, MARCO Raviolo, CRISTINA Gonnelli, and ROBERTO Gabbrielli (2008). "Metal accumulation and damage in rice (*cv.* Vialone nano) seedlings exposed to cadmium". In: *Environmental and Experimental Botany* 62.3, pp. 267–278.

Rea, PHILIP A, OLENA K Vatamaniuk, and DANIEL J Rigden (2004). "Weeds, worms, and more. Papain's long-lost cousin, phytochelatin synthase". In: *Plant Physiology* 136.1, pp. 2463–2474.

Rennenberg, HEINZ (1980). "Glutathione metabolism and possible biological roles in higher plants". In: *Phytochemistry* 21.12, pp. 2771–2781.

Richman, PG and A Meister (1975). "Regulation of γ-glutamyl-cysteine synthetase by non-allosteric feedback inhibition by glutathione." In: *Journal of Biological Chemistry* 250.4, pp. 1422–1426.

Rolland, NORBERT, MICHEL Droux, and ROLAND Douce (1992). "Subcellular distribution of *O*-acetylserine (thiol) lyase in cauliflower (*Brassica oleracea* L.) inflorescence". In: *Plant Physiology* 98.3, pp. 927–935.

Rouached, HATEM, MARKUS Wirtz, REMI Alary, RUDIGER Hell, A BULAK Arpat, JEAN-CLAUDE Davidian, PIERRE Fourcroy, and PIERRE Berthomieu (2008). "Differential regulation of the expression of two high-affinity sulfate transporters, SULTR1.1 and SULTR1.2, in Arabidopsis". In: *Plant Physiology* 147.2, pp. 897–911.

Ruffet, MARIE-LINE, MICHEL Droux, and ROLAND Douce (1994). "Purification and kinetic properties of serine acetyltransferase free of *O*-acetylserine (thiol) lyase from spinach chloroplasts". In: *Plant Physiology* 104.2, pp. 597–604.

Ruffet, MARIE-LINE, MICHEL Lebrun, MICHEL Droux, and ROLAND Douce (1995). "Subcellular distribution of serine acetyltransferase from *Pisum sativum* and characterization of an *Arabidopsis thaliana* putative cytosolic isoform". In: *European Journal of Biochemistry* 227.1-2, pp. 500–509.

Saito, KAZUKI (2000). "Regulation of sulfate transport and synthesis of sulfur-containing amino acids". In: *Current Opinion in Plant Biology* 3.3, pp. 188–195.

— (2004). "Sulfur assimilatory metabolism. The long and smelling road". In: *Plant Physiology* 136.1, pp. 2443–2450.

Saito, KAZUKI, MAKOTO Kurosawa, KAZUYO Tatsuguchi, YOSHIKO Takagi, and ISAMU Murakoshi (1994). "Modulation of cysteine biosynthesis in chloroplasts of transgenic tobacco overexpressing cysteine synthase [*O*-acetylserine (thiol)-Iyase]". In: *Plant Physiology* 106.3, pp. 887–895.

Shibagaki, NAKAKO, ALAN Rose, JEFFREY P McDermott, TORU Fujiwara, HIROAKI Hayashi, TADAKATSU Yoneyama, and JOHN P Davies (2002). "Selenate-resistant mutants of *Arabidopsis thaliana* identify Sultr1;2, a sulfate transporter required for efficient transport of sulfate into roots". In: *The Plant Journal* 29.4, pp. 475–486.

Sigel, HELMUT, DONALD B McCormick, ROLF Griesser, BERNHARD Prijs, and LEMUEL DARY Wright (1969). "Metal ion complexes with biotin and biotin derivatives. Participation of sulfur in the orientation of divalent cations". In: *Biochemistry* 8.7, pp. 2687–2695.

Sirko, AGNIESZKA, ANNA Błaszczyk, and FRANTZ Liszewska (2004). "Overproduction of SAT and/or OASTL in transgenic plants: a survey of effects". In: *Journal of Experimental Botany* 55.404, pp. 1881–1888.

Smith, FRANK W, MALCOLM J Hawkesford, PAUL M Ealing, DAVID T Clarkson, PETER J Vanden Berg, ANN R Belcher, and ANDREW GS Warrilow (1997). "Regulation of expression of a cDNA from barley roots encoding a high affinity sulphate transporter". In: *The Plant Journal* 12.4, pp. 875–884.

Song, WON-YONG, JIYOUNG Park, DAVID G Mendoza-Cózatl, MARIANNE Suter-Grotemeyer, DONGHWAN Shim, STEFAN Hörtensteiner, MARKUS Geisler, BARBARA Weder, PHILIP A Rea, DORIS Rentsch, et al. (2010). "Arsenic tolerance in Arabidopsis is mediated by two ABCC-type phytochelatin transporters". In: *Proceedings of the National Academy of Sciences* 107.49, pp. 21187–21192.

Song, WON-YONG, TOMOHIRO Yamaki, NAOKI Yamaji, DONGHWI Ko, KI-HONG Jung, MIHO Fujii-Kashino, GYNHEUNG An, ENRICO Martinoia, YOUNGSOOK Lee, and JIAN FENG Ma (2014). "A rice ABC transporter, *Os*ABCC1, reduces arsenic accumulation in the grain". In: *Proceedings of the National Academy of Sciences* 111.44, pp. 15699–15704.

Sun, SHENG-KAI, XUEJIE Xu, ZHONG Tang, ZHU Tang, XIN-YUAN Huang, MARKUS Wirtz, RÜDIGER Hell, and FANG-JIE Zhao (2021). "A molecular switch in sulfur metabolism to reduce arsenic and enrich selenium in rice grain". In: *Nature Communications* 12.1, pp. 1–14.

Takahashi, HIDEKI (2010). "Regulation of sulfate transport and assimilation in plants". In: *International Review of Cell and Molecular Biology* 281, pp. 129–159.

— (2019). "Sulfate transport systems in plants: functional diversity and molecular mechanisms underlying regulatory coordination". In: *Journal of Experimental Botany* 70.16, pp. 4075–4087.

Takahashi, HIDEKI, STANISLAV Kopriva, MARIO Giordano, KAZUKI Saito, and RÜDIGER Hell (2011). "Sulfur assimilation in photosynthetic organisms: molecular functions and regulations of transporters and assimilatory enzymes". In: *Annual Review of Plant Biology* 62, pp. 157–184.

Takahashi, HIDEKI, AKIKO Watanabe-Takahashi, FRANK W Smith, MECHTELD Blake-Kalff, MALCOLM J Hawkesford, and KAZUKI Saito (2000). "The roles of three functional sulphate transporters involved in uptake and translocation of sulphate in *Arabidopsis thaliana*". In: *The Plant Journal* 23.2, pp. 171–182.

Takahashi, HIDEKI, MAMI Yamazaki, NORIKO Sasakura, AKIKO Watanabe, THOMAS Leustek, JANICE DE ALMEIDA Engler, GILBERT Engler, MARC Van Montagu, and KAZUKI Saito

(1997). “Regulation of sulfur assimilation in higher plants: a sulfate transporter induced in sulfate-starved roots plays a central role in *Arabidopsis thaliana*”. In: *Proceedings of the National Academy of Sciences* 94.20, pp. 11102–11107.

Tsakraklides, GEORGE, MELINDA Martin, RADHIKA Chalam, MITCHELL C Tarczynski, AHLERT Schmidt, and THOMAS Leustek (2002). “Sulfate reduction is increased in transgenic *Arabidopsis thaliana* expressing 5-adenylylsulfate reductase from *Pseudomonas aeruginosa*”. In: *The Plant Journal* 32.6, pp. 879–889.

Wachter, ANDREAS, SEBASTIAN Wolf, HEIKE Steininger, JOCHEN Bogs, and THOMAS Rausch (2005). “Differential targeting of GSH1 and GSH2 is achieved by multiple transcription initiation: implications for the compartmentation of glutathione biosynthesis in the *Brassicaceae*”. In: *The Plant Journal* 41.1, pp. 15–30.

Wang, SHANSHAN (2018). “The redox regulation of cysteine biosynthesis in the plastids of *Arabidopsis thaliana*”. In: *Doctoral thesis-Heidelberg University*.

Wang, YUWEN, XIAOHAN Jiang, KANG Li, MIN Wu, RUFENG Zhang, LU Zhang, and GUOXIANG Chen (2014). “Photosynthetic responses of *Oryza sativa* L. seedlings to cadmium stress: physiological, biochemical and ultrastructural analyses”. In: *Biometals* 27, pp. 389–401.

Watanabe, MUTSUMI, MIYAKO Kusano, AKIRA Oikawa, ATSUSHI Fukushima, MASAAKI Noji, and KAZUKI Saito (2008a). “Physiological roles of the β-substituted alanine synthase gene family in Arabidopsis”. In: *Plant Physiology* 146.1, pp. 310–320.

Watanabe, MUTSUMI, KEIICHI Mochida, TOMOHIKO Kato, SATOSHI Tabata, NAOKO Yoshimoto, MASAAKI Noji, and KAZUKI Saito (2008b). “Comparative genomics and reverse genetics analysis reveal indispensable functions of the serine acetyltransferase gene family in Arabidopsis”. In: *The Plant Cell* 20.9, pp. 2484–2496.

Watanabe, MUTSUMI, TAKAYUKI Tohge, ALISDAIR R Fernie, and RAINER Hoefgen (2018). “The effect of single and multiple SERAT mutants on serine and sulfur metabolism”. In: *Frontiers in Plant Science* 9, p. 702.

Wirtz, M and R Hell (2003). “Comparative biochemical characterization of OAS-TL isoforms from *Arabidopsis thaliana*”. In: *Sulfur Transport and Assimilation in Plants: Regulation, Interaction, Signaling, J.-C. Davidian, D. Grill, LJ De Kok, I. Stulen, M. J. Hawkesford, E. Schnug and H. Rennenberg, eds (Leiden, The Netherlands: Backhuys)*, pp. 355–357.

Wirtz, MARKUS, OLIVER Berkowitz, MICHEL Droux, and RÜDIGER Hell (2001). “The cysteine synthase complex from plants: mitochondrial serine acetyltransferase from *Arabidopsis*

thaliana carries a bifunctional domain for catalysis and protein–protein interaction". In: *European Journal of Biochemistry* 268.3, pp. 686–693.

Wirtz, MARKUS, HANNAH Birke, CORINNA Heeg, CHRISTOPHER Müller, FABIAN Hosp, CHRISTIAN Throm, STEPHAN König, ANNA Feldman-Salit, KARSTEN Rippe, GABRIELE Petersen, et al. (2010). "Structure and function of the hetero-oligomeric cysteine synthase complex in plants". In: *Journal of Biological Chemistry* 285.43, pp. 32810–32817.

Wirtz, MARKUS, MICHEL Droux, and RÜDIGER Hell (2004). "*O*-acetylserine (thiol) lyase: an enigmatic enzyme of plant cysteine biosynthesis revisited in *Arabidopsis thaliana*". In: *Journal of Experimental Botany* 55.404, pp. 1785–1798.

Wirtz, MARKUS and RÜDIGER Hell (2006). "Functional analysis of the cysteine synthase protein complex from plants: structural, biochemical and regulatory properties". In: *Journal of Plant Physiology* 163.3, pp. 273–286.

Wirtz, MARKUS and RUDIGER Hell (2007). "Dominant-negative modification reveals the regulatory function of the multimeric cysteine synthase protein complex in transgenic tobacco". In: *The Plant Cell* 19.2, pp. 625–639.

Wirtz, MARKUS, WIEBKE Leemhuis, and RUEDIGER Hell (2023). "Dynamic association of the plastid localized cysteine synthase complex is vital for efficient cysteine production, photosynthesis, and granal thylakoid formation in transgenic tobacco". In: *Journal of Experimental Botany* 74.11, pp. 3379–3394.

Yamaguchi, CHISATO, NAOKO Ohkama-Ohtsu, TAKURO Shinano, and AKIKO Maruyama-Nakashita (2017). "Plants prioritize phytochelatin synthesis during cadmium exposure even under reduced sulfate uptake caused by the disruption of SULTR1;2". In: *Plant Signaling and Behavior* 12.5, e1325053.

Yamaguchi, YUBE, TATSUO Nakamura, TOMONOBU Kusano, and HIROSHI Sano (2000). "Three Arabidopsis genes encoding proteins with differential activities for cysteine synthase and β-cyanoalanine synthase". In: *Plant and Cell Physiology* 41.4, pp. 465–476.

Yang, JIAN, MING-XING Gao, HAN Hu, XIAO-MENG Ding, HONG-WEI Lin, LEI Wang, JI-MING Xu, CHUAN-ZAO Mao, FANG-JIE Zhao, and ZHONG-CHANG Wu (2016). "*Os*CLT1, a CRT-like transporter 1, is required for glutathione homeostasis and arsenic tolerance in rice". In: *New Phytologist* 211.2, pp. 658–670.

Yoshimoto, NAOKO, ERI Inoue, KAZUKI Saito, TOMOYUKI Yamaya, and HIDEKI Takahashi (2003). "Phloem-localizing sulfate transporter, Sultr1;3, mediates re-distribution of sulfur from source to sink organs in Arabidopsis". In: *Plant Physiology* 131.4, pp. 1511–1517.

Yoshimoto, NAOKO, HIDEKI Takahashi, FRANK W Smith, TOMOYUKI Yamaya, and KAZUKI Saito (2002). "Two distinct high-affinity sulfate transporters with different inducibilities mediate uptake of sulfate in Arabidopsis roots". In: *The Plant Journal* 29.4, pp. 465–473.

Youssefian, SHOHAB, MICHIMI Nakamura, EMIN Orudgev, and NORIAKI Kondo (2001). "Increased cysteine biosynthesis capacity of transgenic tobacco overexpressing an *O*-acetylserine (thiol) lyase modifies plant responses to oxidative stress". In: *Plant Physiology* 126.3, pp. 1001–1011.

Youssefian, SHOHAB, MICHIMI Nakamura, and HIROSHI Sano (1993). "Tobacco plants transformed with the *O*-acetylserine (thiol) lyase gene of wheat are resistant to toxic levels of hydrogen sulphide gas". In: *The Plant Journal* 4.5, pp. 759–769.

Zhu, YONG LIANG, ELIZABETH AH Pilon-Smits, ALICE S Tarun, STEFAN U Weber, LISE Jouanin, and NORMAN Terry (1999). "Cadmium tolerance and accumulation in Indian mustard is enhanced by overexpressing γ-glutamylcysteine synthetase". In: *Plant Physiology* 121.4, pp. 1169–1177.

Zimmermann, P, M Hirsch-Hoffmann, L Hennig, and GW Genevestigator (2004). "Arabidopsis microarray database and analysis toolbox (vol 136, pg 2621, 2004)". In: *Plant Physiology* 136.4, pp. 4335–4335.

Declaration

I declare that I am the sole author of this submitted dissertation and that I did not make use of any sources or help apart from those specifically referred to. Experimental data or material collected from or produced by other persons is made easily identifiable.

I also declare that I did not apply for permission to enter the examination procedure at another institution and that the dissertation is neither presented to any other faculty, nor used in its current or any other form in another examination.

City, Date	**Sara Haghani**

Acknowledgments

I express my sincere gratitude to Prof. Dr. Rüdiger Hell for granting me the opportunity to pursue my doctoral studies under his esteemed guidance. His mentorship and support have been invaluable throughout the research process, providing me with insightful feedback and direction that has helped the outcome of this thesis.

I sincerely thank Dr. Markus Wirtz for his invaluable ideas, tremendous assistance in conducting the research, dedicated and consistent discussions, and critical suggestions throughout my PhD study.

I sincerely appreciate my advisory committee members, Prof. Dr. Thomas Rausch and Prof. Dr. Michael Wink, for their annual meetings and for offering invaluable scientific advice and thought-provoking questions that greatly enriched our discussions.

I thank Dr. Gernot Poschet and the Metabolomics Core Technology Platform (MCTP) team, who supported me with metabolite analyses, especially Dr. Michael Büttner, who taught and helped me analyze the anion data.

I extend my heartfelt gratitude to our outstanding Postdocs, Dr. Shengkai Sun and Dr. Xiaodi Gong, whose dedication and expertise have elevated our group's scientific and collaborative standards. Dr. Sun's invaluable contributions to the theoretical and practical aspects of OAS-TL mutations in rice and Arabidopsis have significantly advanced my research, and I sincerely appreciate his generous support.

I would like to thank my colleagues, Wiebke Leemhuis, Marlena Pozoga, and Dr. Laura Armbruster, for their collaboration, friendship, and shared laughter that made our time productive and enjoyable. Additionally, I want to express my appreciation to the diligent and hard-working students I had the honor to supervise, Lenard Kreis, Nadja Wunsch, and Klara Diester, for their dedicated efforts, which greatly contributed to the success of my work.

I sincerely appreciate Olga Keberlein's technical expertise and diligent efforts that have elevated the quality and efficiency of my work. I appreciate Eva-Maria Lorenz, with whom I had the honor of working for a short time; however, her kindness and helpfulness have left a lasting impression. I also thank Birgit Maresch and the administration team for their invaluable support, Michael Schilbach, our skilled gardener, for his dedicated efforts and contributions, and Michael Kraft, the technician, for his exceptional skill and prompt assistance in

efficiently fixing the broken machines.

Finally, I would like to express my profound appreciation to my devoted parents and supportive siblings. Last, I express my heartfelt gratitude to my spouse, Javad Mirzaaghaei, whose encouragement and unwavering support have been crucial in completing this demanding endeavor.